



PH.D. THESIS:

TRACE GAS EVOLUTION IN THE PRESENT AND PAST ATMOSPHERE

By:

MALTE NORDMANN WINTHER

ACADEMIC SUPERVISOR: PROF. THOMAS BLUNIER



THIS THESIS HAS BEEN SUBMITTED TO THE PHD SCHOOL OF SCIENCE,
FACULTY OF SCIENCE, UNIVERSITY OF COPENHAGEN, DENMARK, ON DECEMBER 14th, 2016

Abstract

Nitrous oxide (N_2O) is a very important trace greenhouse gas in the atmosphere. With an increasing atmospheric concentration of 327 ppb at present, and a warming potential 300 times that of CO_2 , the significance of N_2O has been rapidly increasing since the 1950s. It is generally known that N_2O primarily originates from microbial production in terrestrial and aquatic ecosystems. In this thesis I present measurements of the intramolecular distribution of ^{15}N in N_2O given as site preference (difference in abundance of the isotopomers), $\delta^{15}\text{N}^{bulk}$ (average abundance of the isotopomers), and measurements of $\delta^{18}\text{O}-\text{N}_2\text{O}$. The isotopes of N_2O are used in investigations of both the specific reactions pathways influencing N_2O emissions and the general evolution of N_2O .

In Part II, I presents continuous incubation experiments with the two primary microbial communities responsible for N_2O production. The two microbial communities have been studied numerous times, but to the best of our knowledge never continuously. Continuous measurements of the microbial evolution of N_2O is possible due to the recent instrument development of a cavity ringdown spectroscopy-based analyzer, which allows for continuous position dependent ^{15}N measurements.

Continuous incubation experiments are presented with nitrifying bacteria *Nitrosomonas mobilis* revealing strong indications of N_2O production from different chemical reactions. The measurements revealed a three step site preference pattern in the range of nitrification and denitrification and we therefore suggest that *Nitrosomonas mobilis* is of the bacterial community nitrifier denitrification. The experiments furthermore revealed the bacterial potential for cyclic use of the most abundant substrate rather than the most energy efficient.

Continuous incubation experiments with denitrifying bacteria are also presented with *Pseudomonas fluorescens* (producing and reducing N_2O) and *Pseudomonas chlororaphis* (only producing N_2O). Measurements revealed a clear transient pattern of KNO_3 to N_2O and KNO_3 to N_2O to N_2 for the two bacterial species, respectively. A Rayleigh type distillation model modified for isotopomers and simultaneous reduction, allowed for determination of isotopic fractionation values during both production and reduction of N_2O , comparable to previous studies.

In Part III, I present measurements of ice core samples analyzed for isotopes of N_2O . Ice samples from three time periods of the Holocene and one from the glacial were selected and measured for isotopic composition of N_2O using isotope ratio mass spectrometry. The analysis resulted in isotopic variations comparable with previous findings of site preference,

$\delta^{15}\text{N}^{bulk}$, and $\delta^{18}\text{O}-\text{N}_2\text{O}$. Source identification analysis using the isotopic composition resulted in a discussion of the primary source region being nitrification in aquatic ecosystems, while inclusion of the stratospheric sink effect leads to heavy depletion in all isotopes, hence shifting the primary source region towards denitrification in terrestrial ecosystems.

In Part IV, I present N_2O measurements from field studies performed 1) on the Arctic tundra and 2) on an inclined temperate slope. 1) Previous studies has shown that large amounts of N_2O is being emitted after thawing of permafrost. We investigated a downslope site covering a moisture gradient area in the arctic tundra. Moss-covered sites revealed high nitrification potential, low nitrate levels, and emission of denitrification marked N_2O . The natural nitrogen cycle in the arctic is therefore hypothesized to reduce the atmospheric N_2O concentration by denitrification, which contrasts the opening nitrogen cycle in temperate and tropical areas. 2) On an inclined temperate slope N_2O emission variations were investigated on a mesoscale range. A temperate changing interface with oxic nitrification enhancing conditions upslope and anoxic denitrification enhancing conditions downslope was discovered with high N_2O production.

Resumé

Dinitrogenoxid (N_2O) er en meget vigtig spor-drivhusgas i atmosfæren. På grund af den stadigt voksende atmosfæriske koncentration, fra de nuværende 327 ppb, samt et varme potentiale 300 gange større end det for CO_2 , har betydningen af N_2O været kraftigt voksende siden 1950'erne. Det er generelt anerkendt, at N_2O primært bliver dannet igennem mikrobakteriel produktion i enten jordbaserede eller vandbaserede økosystemer. I denne afhandling præsenterer jeg målinger af den intramolekulære fordeling af ^{15}N i N_2O givet som "site preference" (forskellen i isotopomer-hyppighed), $\delta^{15}N^{bulk}$ (den gennemsnitlige isotopomer-hyppighed), samt målinger af $\delta^{18}O-N_2O$. Isotoperne af N_2O er brugt i forskningsundersøgelser af de specifikke reaktioner der er involveret i udledningen af N_2O samt af den generelle udvikling af N_2O .

I del II, præsenterer jeg kontinuerte inkubationsforsøg med de to bakterie stammer der primært er ansvarlig for produktionen af N_2O . De to bakterie stammer er tidligere blevet studeret utallige gange, men til vores bedste overbevisning er deres kontinuerte udvikling aldrig blevet studeret. Kontinuerte målinger af den bakterielle udvikling af N_2O er muliggjort på grund af vores seneste udvikling af et "cavity ringdown spectroscopy" baseret instrument, der tillader kontinuerte positionsafhængige målinger af ^{15}N .

Kontinuerte inkubationsforsøg med den nitrificerende bakterie *Nitrosomonas mobilis*, afslørede en stærk indikation af N_2O produktion fra forskellige kemiske reaktioner. Målingerne afsører et tre-trins "site preference" mønster i intervallet for nitrifikation og denitrifikation. Vi foreslår derfor at *Nitrosomonas mobilis* er af den bakterie familie med betegnelsen nitrifikant denitrifikant. Eksperimenterne afsører yderligere, at bakterierne har potentialet til periodisk at skifte mellem den mest tilstedeværende substrat frem for den mest energy effektive.

Kontinuerte inkubations forsøg blev udført med de to denitrificerende bakterie kulturer *Pseudomonas fluorescens* (både producerer og reducerer N_2O) og *Pseudomonas chlororaphis* (producerer kun N_2O). Målingerne afslører tydeligt overgangen henholdsvis fra KNO_3 til N_2O samt fra KNO_3 til N_2O og videre til N_2 for de to bakterie kulturer. Ved at modificere en Rayleigh fraktionerings model således at den tager højde for isotopomerer og reduktion samtidig med produktion, er det gjort muligt at bestemme isotop fraktionerings værdier der er sammenlignelige med tidligere studier, både for produktion og reduktion af N_2O .

I del III, præsenterer jeg målinger af N_2O isotoperne fra iskerneprøver. Iskerneprøver fra tre tidsperioder i den sidste mellemistid (Holocene), og en fra den sidste istid blev valgt til

måling af isotop sammensætningen ved brug af "isotope ratio mass spectrometry". Analysen resulterede i sammenlignelige variationer i isotop værdierne i forhold til tidligere undersøgelser af "site preference", $\delta^{15}\text{N}^{bulk}$, og $\delta^{18}\text{O}-\text{N}_2\text{O}$. På baggrund af de målte isotop forhold, resulterede en kilde identifikations analyse i en diskussion om, at den primære udskildning af N_2O skulle være fra nitrifikation i vandbaserede økosystemer. Inddragelse af teorien om stratosfærisk nedbrydning, medfører en kraftig formindskelse af alle isotoperne, hvilket medfører at det primære oprindelses område blev rykket hen imod denitrifikation fra jordbaserede økosystemer.

I del IV, præsenterer jeg N_2O målinger fra feltstudier udført på 1) den arktiske tundra, og på 2) en skrænt i den tempererede zone. 1) Tidligere studier har vist, at der udsendes store mængder N_2O når permafrost tør. Vi undersøgte en nedadgående skrænt med en fugtigheds gradient på den arktiske tundra. Mos tildækkede områder afslørede et højt potentiale for nitrifikation, lave nitrat niveauer, samt udskildning af N_2O markeret fra denitrifikation. Vi har derfor en hypotese om, at den naturlige nitrogen cyklus i arktiske egne reducerer den atmosfæriske koncentration af N_2O . Dette modstrider den åbne nitrogen cyklus der er fundet i de tropiske og tempererede egne. 2) På en skrænt i den tempererede zone, undersøgte vi udskildningen af N_2O på et mesoskale område. Vi fandt en skrænt med en kraftig udskildning af N_2O , på tidlig ændrende grænseflade mellem oxygen-holdig, nitrifikant forstærkende forhold op ad skrænten, og anoxiske, denitrifikant forstærkende forhold ned af skrænten.

Acknowledgements

There are many people whom I owe a special thank for helping me making this project a success. First of all I want to thank my supervisor, Thomas Blunier, for your guidance, advices, and for always having your door open for me to stop by and discuss the issues at hand. I am very happy that I walked into your office four and a half years ago and that you introduced me to ice core science as a laboratory work research field. I would secondly like to thank Søren Christensen, for your many discussions on microbial activities and for your support during our collaboration. I would like to thank David Balslev-Harder for your guidance, support, comments, and for our many fruitful discussions.

I would like to thank Thomas Röckmann for your guidance and support during my stay at IMAU, Utrecht. I feel very fortunate that I got the opportunity to work in your lab, with so many nice people. A special thank also to Carina, without your help my stay would not have been the same. Also thanks to Markella and Celia for your discussions and guidance in the lab. Thomas Reerink, Leo, and Marianne, I am very thankful for you letting me into your homes.

As already said by many before me, working at the Centre for Ice and Climate is like working with a second family. I have only great memories from working at the Centre and I am thankful to everybody who is and/or has been at the Centre for the past years. Alex, Andreas, and Nanna, thank you for being such great office mates. Kaitlin and Hans-Christian, a special thanks to you for, among other things, helping me with my english in this thesis. I would like to thank everybody from the gaslab Gabriela, Sindhu, Diana, Corentin, Jonas, Kirstin and everybody else who have been part of the lab. I have really enjoyed working with all of you. A special thanks to Corentin for your many lunch and coffee talks, and for always being there to help and making the long days feel shorter. I would also like to thank J.P., Trevor, and Dorte for giving me the opportunity to go the new EGRIP ice coring camp. I had an awesome time on the ice, and it is something I will never forget. Therefore also a special thank to everybody who was in camp and/or in Kanger with me. I have not written the names of all who deserves a thank you, but that is simply to avoid forgetting some of you. But you have all made my years as a PhD student, to something special.

Finally I would like to give a special thank to my entire family and my friends, without your support and understanding I would not be where I am today. Last but definitely

not least, I would like to thank, Lisbeth my girlfriend, without your love, patience, and encouragement I could not have performed like I have done.

Contents

I	Introduction	1
1	General Introduction	3
1.1	Nitrous Oxide	3
1.1.1	Isotopomers of Nitrous oxide	4
1.1.2	Sources	6
1.1.3	Sink	8
1.1.4	Historical overview	9
2	Instrumental theory	11
2.1	Cavity Ringdown Spectroscopy	11
2.1.1	”Leak reduced” pump	13
2.2	Isotope Ratio Mass Spectrometry	14
3	Calibration and corrections	16
3.1	Concentration-dependent correction	16
3.2	Oxygen-dependent correction	21
3.3	Standard gases	24
3.3.1	CIC-MPI version I	25
3.3.2	CIC-MPI version II	27
II	Microbial evolution	29
4	Introduction - part II	31
4.1	Incubation setup	33

5	Nitrifying bacterial production of nitrous oxide isotopomers	37
5.1	Introduction	37
5.2	Method	40
5.2.1	Instrumentation	40
5.2.2	Pure bacterial cultures	41
5.2.3	Incubation experiment	41
5.2.4	Data calibration and correction	43
5.3	Results	44
5.4	Discussion	48
5.4.1	Production rate	48
5.4.2	A changing site preference	48
5.4.3	Oxygen isotope as reaction indicator	51
5.5	Conclusion	53
6	Continuous measurements of nitrous oxide isotopomers during incubation experiments	55
6.1	Introduction	57
6.2	Method	59
6.2.1	Instrumentation	59
6.2.2	Correction of CRDS concentration dependence	60
6.2.3	Calibration gases	62
6.2.4	Pure bacterial cultures	63
6.2.5	Determination of isotopic fractionation	64
6.3	Results	68
6.3.1	<i>Pseudomonas chlororaphis</i>	68
6.3.2	<i>Pseudomonas fluorescens</i>	69
6.4	Discussion	73
6.4.1	Comparison to previous studies	75
6.5	Conclusions	77
6.6	Author contribution	77
6.7	Acknowledgements	77
6.8	Supporting material	78
6.8.1	Oxygen dependence	78
6.8.2	<i>Pseudomonas chlororaphis</i>	80
6.8.3	<i>Pseudomonas fluorescens</i>	83

III	Past atmosphere	87
7	Introduction - part III	89
7.1	A short introduction to ice cores as climate archives	89
7.2	NEEM	90
8	Measurements of N₂O isotopomers from NEEM ice core	91
8.1	Introduction	91
8.2	Method	92
8.2.1	Instrumentation	92
8.2.2	NEEM samples	95
8.2.3	Correction of IRMS size dependence	96
8.2.4	Isotopic calibration	97
8.2.5	Statistical correction	98
8.3	Results	100
8.4	Discussion	102
8.4.1	Determination of possible source	102
8.4.2	Stability of isotopic composition	105
8.5	Conclusion	107
8.6	Author contribution	108
8.7	Acknowledgements	108
8.8	Supporting material	109
IV	Present atmosphere	111
9	Introduction - part IV	113
10	Fast production of nitrate in the Arctic leads to lower emission of green- house gas N₂O	115
10.1	Introduction	117
10.2	Experiment	118
10.3	Results and Discussion	119
10.4	Author contribution	123
10.5	Supporting material	124
10.5.1	Materials and Methods	124
10.5.2	Results	126

11 Huge N₂O emission from drained organic soil is related to seasonally mobile oxic-anoxic interface	131
11.1 Introduction	133
11.2 Materials and Method	134
11.2.1 The site	134
11.2.2 N ₂ O flux measurements	134
11.2.3 Potential activity of processes forming N ₂ O	135
11.3 Results	136
11.3.1 Field N ₂ O fluxes	136
11.3.2 Soil air N ₂ O	140
11.3.3 N ₂ O isotopomer site preference	140
11.3.4 Coupling of nitrification and denitrification	142
11.4 Discussion	142
11.4.1 Field fluxes	142
11.4.2 Soil air N ₂ O	145
11.4.3 Microbial processes producing N ₂ O	145
11.4.4 Coupling of nitrification and denitrification	145
11.5 Conclusion	146
11.6 Author contribution	146
Conclusions and Outlook	149
Bibliography	154

Part I

Introduction

General Introduction

This PhD thesis is a study of Nitrous oxide. This first part of my thesis serves as a brief review of well established knowledge concerning Nitrous oxide, including the molecular structure, sources, sinks and historical evolution. Here I also include a general introduction to the measuring techniques used to perform experiments presented in the remaining parts of this thesis.

1.1 Nitrous Oxide

Nitrous oxide (N_2O) is a naturally produced trace gas in the atmosphere on Earth which due to its warming potential per molecule 300 times that of CO_2 has a great significance for life on Earth. N_2O has an atmospheric lifetime of 118-131 years leading to a homogeneous tropospheric distribution and an almost invisible annual cycle (Ciais et al., 2013). N_2O consist of two Nitrogen atoms and one Oxygen atom. The three atoms are positioned in a linear structure with the Oxygen atom at one terminal position and the two Nitrogen atoms at the central and the other terminal position. The exact molecular structure of N_2O depends on the intramolecular distribution of the available stable isotopes of each atom. Two elements of the same atom (e.g. Nitrogen (N)) can be distinguished by a difference in the number of neutrons, and therefore a difference in the atomic mass. Two

Table 1.1: *Stable isotopes of Nitrogen and Oxygen. Values refer to the specific mean global abundance.*(Leuenberger et al., 1998)

Element	Isotopic abundance [%]		
Nitrogen	^{14}N : 99.63	^{15}N : 0.37	
Oxygen	^{16}O : 99.759	^{18}O : 0.204	^{17}O : 0.037

such molecules are defined as the isotopes of a given atom. Isotopes are further divided into stable and unstable isotopes, depending on whether the isotope naturally experiences a radioactive decay causing it to split into another isotope. Both Nitrogen and Oxygen are stable isotopes and are therefore possible to trace over time. Table 1.1 shows the natural abundance of the five stable isotopes of Nitrogen (^{14}N and ^{15}N) and Oxygen (^{16}O , ^{17}O , and ^{18}O). Nitrous oxide, being a linear three-atom molecule, exists in 12 different isotopic molecular species, all of which have a different natural abundance. The most common isotopic molecular species of N_2O are $^{14}\text{N}-^{14}\text{N}-^{16}\text{O}$, followed by $^{14}\text{N}-^{15}\text{N}-^{16}\text{O}$, $^{15}\text{N}-^{14}\text{N}-^{16}\text{O}$, $^{14}\text{N}-^{14}\text{N}-^{18}\text{O}$, and $^{14}\text{N}-^{14}\text{N}-^{17}\text{O}$.

The ability to trace molecules of stable isotopes over time leads to the ability to track the source and sink of the individual molecule. Back-tracking molecules and the chemical reactions altering these molecules is discerned by measurement of the isotopic ratio. The isotopic ratio (or isotopic molar concentration ratio) is a measure of the ratio between two molecules of different abundance, e.g. the ratio between $^{14}\text{N}-^{14}\text{N}-^{16}\text{O}$ (more abundant molar concentration (x_m)) and $^{15}\text{N}-^{15}\text{N}-^{18}\text{O}$ (less abundant molar concentration (x_l)) as shown in equation 1.1.

$$R_{x_l/x_m} = \frac{x_l}{x_m} \quad (1.1)$$

The generally small isotopic ratios are difficult to interpret as absolute values and conversions to delta-values are therefore preferred. Delta-values are a measure of the deviation between the calculated isotopic ratio of the sample and a reference ratio based on internationally recognized standard measurements. The delta-values are often given in per mil (‰) because of the very small numbers. (Leuenberger et al., 1998)

$$\delta R_{sample} = \frac{R_{sample}}{R_{ref}} - 1 \quad (1.2)$$

The reference ratios used for experiments presented in this thesis are provided by the International Atomic Energy Agency (IAEA). The accepted absolute isotope ratios used for ^{18}O are VSMOW (Vienna Standard Mean Ocean Water), and AIR- N_2 (atmospheric nitrogen) for ^{15}N .

1.1.1 Isotopomers of Nitrous oxide

The five most common isotopic molecular species of N_2O can be divided up into isotopomers and isotopologues of N_2O . The isotopomers of N_2O are defined as the group of molecules constructed from the same isotopes, and are only distinguished by the allocation of the isotopes (Hellerstein and Neese, 1999). The isotopes of N_2O are therefore $^{14}\text{N}-^{15}\text{N}-^{16}\text{O}$ and $^{15}\text{N}-^{14}\text{N}-^{16}\text{O}$. The isotopologues of N_2O are defined as molecules distinguished by the isotopic

composition (Hellerstein and Neese, 1999), e.g. ^{14}N - ^{14}N - ^{16}O , ^{14}N - ^{14}N - ^{17}O , and ^{14}N - ^{14}N - ^{18}O . The primary focus of this thesis is the isotopic composition of N_2O . The most interesting N_2O molecules are the most abundant isotopic compositions which are the isotopomers and ^{14}N - ^{14}N - ^{16}O . The latter is primarily used as a reference in the calculations of the absolute isotopic ratio, and also in Chapter 8 for the calculation of the estimated N_2O concentration. The isotopomers of N_2O can be distinguished by the allocation of the heavy Nitrogen atom (^{15}N), because the ^{15}N atom either can be at the central or at the terminal position of the molecule. Experimental methods to measure the intramolecular distribution of ^{15}N using mass spectrometry was discovered by Brenninkmeijer and Röckmann (1999), and lead to naming of the two nitrogen positions in N_2O . Since then two different terminologies have been presented first by Yoshida and Toyoda (2000) and later by Kaiser et al. (2002). The terminology presented by Yoshida and Toyoda (2000) is used throughout this thesis. Therefore ^{15}N positioned on the central position is referred to as alpha (α), while ^{15}N at the terminal position is referred to as beta (β).

Throughout the thesis, measurements of the two isotopomers are presented in delta-values calculated as shown in Eq. 1.3 and Eq. 1.4, for $\delta^{15}\text{N}^\alpha$ and $\delta^{15}\text{N}^\beta$, respectively.

$$\delta^{15}\text{N}^\alpha = \frac{{}^{15}\text{R}_{sample}^\alpha}{{}^{15}\text{R}_{std}^\alpha} - 1 \quad \text{with} \quad {}^{15}\text{R}^\alpha = \frac{[{}^{14}\text{N}^{15}\text{N}^{16}\text{O}]}{[{}^{14}\text{N}^{14}\text{N}^{16}\text{O}]} \quad (1.3)$$

$$\delta^{15}\text{N}^\beta = \frac{{}^{15}\text{R}_{sample}^\beta}{{}^{15}\text{R}_{std}^\beta} - 1 \quad \text{with} \quad {}^{15}\text{R}^\beta = \frac{[{}^{15}\text{N}^{14}\text{N}^{16}\text{O}]}{[{}^{14}\text{N}^{14}\text{N}^{16}\text{O}]} \quad (1.4)$$

Investigations of the intramolecular distribution of ^{15}N from different sources of N_2O lead to the definition of two important quantities, namely the ^{15}N - site preference (SP) and the ^{15}N -bulk ($\delta^{15}\text{N}^{bulk}$) (Toyoda and Yoshida, 1999; Toyoda et al., 2008). The bulk nitrogen isotope ratio is given as the average of the two isotopomer isotope ratios (Eq. 1.5)(Toyoda and Yoshida, 1999).

$$\delta^{15}\text{N}^{bulk} = \frac{\delta^{15}\text{N}^\alpha + \delta^{15}\text{N}^\beta}{2} \quad (1.5)$$

Measurements of N_2O emitted from tropical forests soils was found to be enriched in $\delta^{15}\text{N}$ compared to N_2O emitted from agricultural soils (Pérez et al., 2000; Perez et al., 2001). Perez et al. (2001) suggested that measurements of the intramolecular distribution of ^{15}N could be used to distinguish sources of N_2O . This hypothesis was confirmed through multiple experiments with different air samples (Park et al. (2011) and others therein). The $\delta^{15}\text{N}^{bulk}$ and $\delta^{18}\text{O}$ (N_2O) have the disadvantage that both quantities depend on the historical isotope fractionations and isotopic ratios, which have occurred to the molecule prior to N_2O formation. The SP, on the other hand, is only dependent on the reaction leading to N_2O formation, hence the formation of N-N bond and cleavage of N-O bond (Toyoda et al.,

2008). The site preference is defined as the difference between the two isotopomers (Eq. 1.6)(Toyoda et al., 2008).

$$SP = \delta^{15}\text{N}^{\alpha} - \delta^{15}\text{N}^{\beta} \quad (1.6)$$

Park et al. (2011) reviewed a number of studies presenting measurements of SP from different terrestrial environments and from pure bacterial nitrification, denitrification, and nitrifier denitrification. This review highlights the current, well established understanding that SP can be used to discriminate N_2O produced via different microbial productions. Multiple experiments agree that N_2O produced via nitrification results in SP values in the range of 11 ‰ to 46 ‰, whereas N_2O produced via denitrification results in a general depletion in $\delta^{15}\text{N}^{\alpha}$ leading to $SP \leq 10$ ‰. The SP has therefore proved to be a significant tool in distinguishing sources of N_2O , though complicated by production via nitrifier denitrification, which have shown SP values similar to SP resulting from denitrification (Park et al., 2011). A combined investigation of both quantities ($\delta^{15}\text{N}^{bulk}$ and SP) in the analysis of N_2O production and reduction is therefore favored, especially in combination with $\delta^{18}\text{O}$ (N_2O) measurements. Field experiments by Schilt et al. (2014) have shown that oceanic sources and terrestrial sources have significantly different isotopic signatures for $\delta^{15}\text{N}^{bulk}$ and $\delta^{18}\text{O}$ (N_2O) with oceanic-produced N_2O enriched in both quantities relative to terrestrial-produced N_2O .

1.1.2 Sources

N_2O is produced from both natural sources and anthropogenic sources. It is generally accepted that the primary sources of N_2O are microbial production in terrestrial and aquatic ecosystems, via nitrification and denitrification (see part II). The present day best estimation of the natural production ratio between terrestrial and aquatic ecosystems shows that terrestrial sources are responsible for 63 % and the aquatic ecosystems are responsible for 37 % (Ciais et al., 2013; Schilt et al., 2014). In Table 1.2 a list of the natural and anthropogenic sources of N_2O for year 2006 and an average from the 1990s are shown.

The anthropogenic source of N_2O has rapidly increased since the beginning of the industrial era. For production of N_2O , the primary anthropogenic influence has been agriculture. Expansion of agricultural land areas, combined with an increased use of fertilizers, has led to an increased production of crops needed to feed the increasing population of humans on Earth. The downside of expanding agriculture is that fertilizers consist to a large degree of Nitrogen-minerals, which leads to an increased production of N_2O from microbial production. Therefore the anthropogenic increase in N_2O emission stems from fertilized agricultural soils (Mosier et al. (1998); Sutka and Ostrom (2006); Forster et al. (2007); Opdyke et al. (2009); Ciais et al. (2013) and references therein). The contribution from

abiotic production of N_2O to the global budget has not yet been clearly estimated, though investigations have shown that a number of reactions, with intermediates from nitrification, leads to N_2O production (Heil et al., 2014).

Table 1.2: *The N_2O budget for the year 2006, and the 1990s compared to AR4. Unit: [TgN (N_2O) yr^{-1}] (Ciais et al., 2013). This Table is a slightly modified version of the one presented in the IPCC Fifth Assesments Report (Ciais et al., 2013).*

	2006	1990s
Anthropogenic sources		
Fossil fuel combustion and industrial processes	0.7 (0.2-1.8)	0.7 (0.2-1.8)
Agriculture	4.1 (1.7-4.8)	3.7 (1.7-4.8)
Biomass and biofuel burning	0.7 (0.2-1.0)	0.7 (0.2-1.0)
Human excreta	0.2 (0.1-0.3)	0.2 (0.1-0.3)
Rivers, estuaries, coastal zones	0.6 (0.1-2.9)	0.6 (0.1-2.9)
Atmospheric deposition on land	0.4 (0.3-0.9)	0.4 (0.3-0.9)
Atmospheric deposition on ocean	0.2 (0.1-0.4)	0.2 (0.1-0.4)
Surface sink	-0.01 (0- -1)	-0.01 (0- -1)
Total anthropogenic sources	6.9 (2.7-11.1)	6.5 (2.7-11.1)
Natural sources		
Soils under natural vegetation	6.6 (3.3-9.0)	6.6 (3.3-9.0)
Oceans	3.8 (1.8-9.4)	3.8 (1.8-9.4)
Atmospheric chemistry	0.6 (0.3-1.2)	0.6 (0.3-1.2)
Total natural sources	11.0 (5.4-19.6)	11.0 (5.4-19.6)
Total emission	17.9 (8.1-30.7)	17.5 (8.1-30.7)

1.1.3 Sink

Once emitted from the near surface sources the known reactions leading to a sink of N_2O are constricted to three well defined chemical loss reactions in the stratosphere. The primary reaction leading to stratospheric sink of N_2O is ultraviolet (UV) photolysis via the chemical reactions shown in reaction 1.7, where $h\nu$ is the energy of the light reacting with the molecule and $O(^1D)$ is Oxygen in an excited state (Wingen and Finlayson-Pitts, 1998; Röckmann et al., 2001).



It is widely accepted that the N_2O photolysis reaction in the stratosphere is responsible for 90 % of the total global N_2O sink, with the largest (by far) contributing UV range being between 195 nm and 205 nm (Röckmann et al., 2001; Kaiser et al., 2002, 2003; McLinden et al., 2003). Due to spatial variations, such as altitude and latitude, the range of maximum photolysis changes within the range of 281 nm to 230 nm (Kaiser et al., 2003). On either sides of this UV range, photolysis is restricted due to protection from O_2 . Yung and Miller (1997) proposed that N_2O in the stratosphere experienced isotopic fractionation via the photolysis reaction (Eq. 1.7) leading to enrichment of $\delta^{15}N$ and $\delta^{18}O$ (N_2O) and to a considerably different fractionation of the two isotopomers. This theory was later verified by Röckmann et al. (2001) and others. Röckmann et al. (2001) performed experiments on laboratory photolysis and compared the results to measurements of the stratospheric fractionation. This comparison confirmed that UV photolysis in the stratosphere is the primary cause of isotopic enrichment, with a significantly different fractionation of the two isotopomers. The study determined the stratospheric fractionation constants of $17.1 \text{ ‰} \pm 1.6$ for $\delta^{15}N$, $14.0 \text{ ‰} \pm 2.0$ for $\delta^{18}O$ (N_2O), $21.3 \text{ ‰} \pm 1.5$ for $\delta^{15}N^\alpha$, and $12.9 \text{ ‰} \pm 2.4$ for $\delta^{15}N^\beta$, respectively. The last 10% of the stratospheric sink has been found to be from N_2O reacting with $O(^1D)$ (Eq. 1.8 and Eq. 1.9), where reaction 1.8 is believed to be contributing 6 % to the stratospheric sink while reaction 1.9 is responsible for 4 % (Röckmann et al., 2001).



Reaction 1.9 has a huge effect and a very significant role in general climate change and atmospheric chemistry, despite only contributing 6 % to the stratospheric sink. The oxidation of N_2O leads to production of Nitric oxide (NO), and has been found to be the largest natural source in the stratosphere. In the stratosphere, NO has a major role in the destruction of Ozone (O_3), where two chemical reactions destroy O_3 by oxidation with NO

to NO_2 , followed by a second oxidation reaction in which NO_2 reacts with O and create NO and O_2 (Wingen and Finlayson-Pitts, 1998). Therefore, O_3 is destroyed with NO as catalyst and N_2O has therefore been found the single most important ozone-depleting substance (Ravishankara et al., 2009)

1.1.4 Historical overview

Measurements from the Antarctic European Project for Ice Coring in Antarctica (EPICA) Dome C ice core has revealed that atmospheric N_2O concentrations has been within 200 ppb to 300 ppb over the past 800,000 years before year 2000 (b2k), with the highest interglacial mean around 400,000 years before present (Fig. 1.1A) (Loulergue et al., 2007; Schilt et al., 2009). In comparison, measurements from the North Greenland Ice Core project (NGRIP) ice core showed variations in a similar range of concentrations through the past 117,560 years b2k (Fig. 1.1B) (Flückiger et al., 2004; Schilt et al., 2010, 2013; Veres et al., 2013). Both of these ice cores from Antarctica and Greenland reveal N_2O concentration variations that are consistent with climate and millennial-scale variations of similar temporal scale as the methane (CH_4) records. The N_2O concentrations had been relatively stable since the onset of the present interglacial period (the Holocene), until the beginning of the industrial era as shown in Fig. 1.1C. Atmospheric N_2O concentrations has increased with an average annual increase of $0.73 \text{ ppb} \pm 0.03$ over the past three decades (Ciais et al., 2013) and show no sign of slowing down.

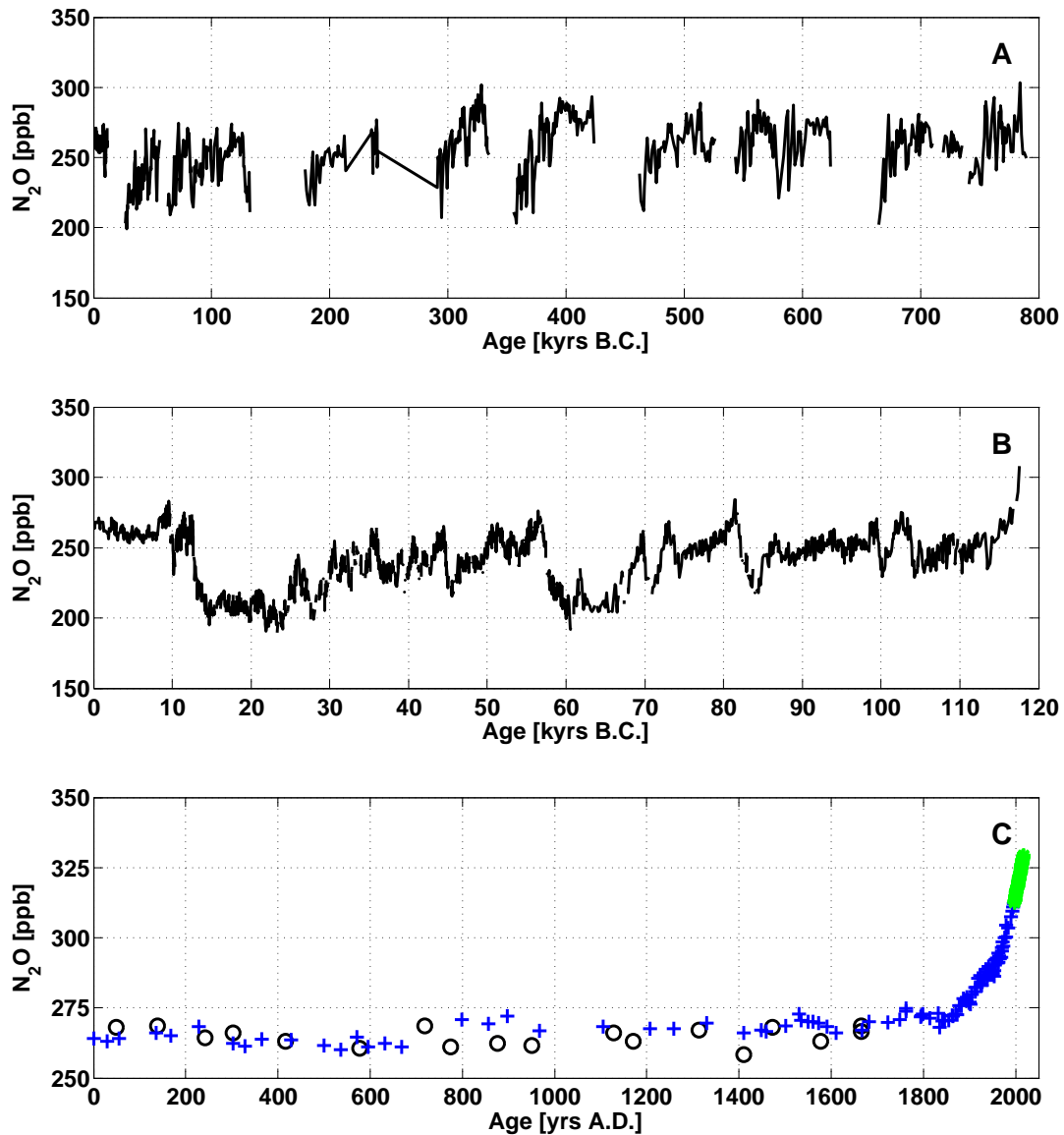


Figure 1.1: N_2O evolution since year 800 kyrs b2k until November 2016. Figure A: EPICA Dome C record covering past 800 kyrs before present (Loulergue et al., 2007; Schilt et al., 2009). Figure B show a merged record covering the years 117.56 kyrs b2k until year 0. The record is a merged record of the Dome C record (Flückiger et al., 2002) and the NGRIP record (Flückiger et al., 2004; Schilt et al., 2010, 2013; Veres et al., 2013). Figure C shows a merged record from the resent 2016 years AD. The record consists of data from the Dome C record (Flückiger et al., 2002), Law Dome ice core and firn record (MacFarling Meure et al., 2006), and present day measurements show Nitrous Oxide data from the NOAA/ESRL halocarbons in situ program (NOAA, 2016). Values are average values calculated from measurements at Barrow, Alaska, USA, South Pole, Antarctica, and Mauna Loa, Hawaii, USA.

During the work presented in this dissertation, three instruments were used to measure the isotopomers of N_2O , namely the prototype of the Picarro G5101-i analyzer (in the following named G5101i-CIC), the Picarro G5313-i analyzer (in the following named G5313i-CIC), and a continuous-flow isotope ratio mass spectrometer (IRMS). The two Picarro analyzers are based on Cavity ringdown spectroscopy, whereas the IRMS is based on mass-spectrometry. In this chapter, a short introduction is given to the principles involved. The theory describing the principles of cavity ringdown spectroscopy (section 2.1) is based on Balslev-Clausen (2011) and references therein. The theory describing the principles of isotope ratio mass spectrometry is based on the Reutenauer (2016).

2.1 Cavity Ringdown Spectroscopy

The gas phase molar concentration of simple gas molecules can be measured using laser absorption spectroscopy. When light travels a distance z through a uniform gas filled volume, the input light intensity I_0 will decrease due to absorption by the molecules. The transmitted light intensity can be described by Beer-Lambert's law for optical absorption. Beer-Lambert's law states that the transmitted light intensity I_T drops exponentially with distance z traveled through the gas as:

$$I_T = I_0 e^{-\alpha(\lambda) \cdot z} \quad (2.1)$$

where $\alpha(\lambda)$ is the absorption coefficient and depends on the gas composition. The range of wavelengths (λ) at which a given molecule will absorb light is determined by the transition energy between quantum mechanical energy states of the molecule. The energy states depend, among other things, on the atomic masses and the binding forces between the atoms in the molecule. This is why different molecules absorb light with different spectra and why isotope composition can be distinguished through absorption spectroscopy.

For simple molecules, the spectrum of the absorption coefficient can be expressed as a sum of absorption lines, corresponding to transitions between pairs of quantum mechanical energy states i and j . Each molecular absorption line, has four distinctive features, namely the line position ν_{ij} , line intensity $S_{ij}(T)$, line shape $g(\nu)$, and the line width $\Delta\nu$ (usually proportional to the total pressure when greater than 100 mbar). The line shape can generally be expressed as a normalized non-dimensional function, with different profiles depending on the transition. Often the Voigt or Galatry profile is used. When measuring at low sub-atmospheric pressure (< 300 mBar) the absorption lines becomes narrower and individual absorption lines become resolvable. When individual lines are measurable, it becomes possible to quantify the volumetric concentration n of the intended molecule (or isotopologue). This is done, by measurements of the line area, $A_{\text{line}} = \int \alpha(\nu) d\nu = nS_{ij}(T) \int g(\nu) d\nu = 1$. The molar concentration x can then be found by measurement of the temperature T and total pressure p as $x = n/n_{\text{total}} = n \cdot p / (k_B \cdot T)$.

Measurements of trace gases performed with most spectrometers are limited by the sensitivity of the analyzers. The development of Cavity Ringdown Spectroscopy (CRDS) has greatly enhanced the sensitivity of optical analyzers, and therefore the opportunity for measurements of low concentration gases and less abundant isotopologues in particular. CRDS is based on the absorption principle as conventional absorption spectroscopy, but has a significantly enhanced optical path length. The effective path length in CRDS instruments can be multiple kilometers, due to the confined path defined by the high reflective mirrors (each reflects 99.99 %) placed in a closed path configuration, called an optical cavity. A standing wave will be generated in the cavity, when light entering the cavity oscillates in tune with the light which has already circulated within the cavity. When a standing wave is generated, light intensity inside the cavity become so large, that light can be detected on the transmission side of the cavity, despite the large reflectivity of the mirrors.

A photo detector sitting outside one of the mirrors, while the laser beam circulates inside the cavity, will detect the small amount of light leaking out. This detection of the escaping (loss) light produces a signal proportional to the intensity of light inside the cavity. If the light source is turned off, a "ringdown"-event will occur, as an exponentially decay of the light intensity inside the cavity, as also measured by the photo detector. This decay is finite also in the case of an empty cavity, due to the lack of perfect reflection from the mirrors. The decay time is inverse proportional to the intra-cavity losses (including mirrors). In a gas filled cavity, the gas molecules inside the cavity absorb the circulating light like conventional absorption spectroscopy. The additional losses from molecular absorption leads to decreased ring-down times. The loss is proportional to the concentration of the gas, and likewise is the

inverse of the ring-down time. Analysis of the difference between the empty and gas filled cavity ring-down times provide concentration measurements, which are independent of the input laser intensity. Fast CRDS instruments provide continuous measurements of the gas concentration, at sub second data intervals.

2.1.1 "Leak reduced" pump

One of the great advantages of the applied CRDS analyzer is that it has high precision temperature and pressure controls inside the cavity, and that the measuring technique is non destructive to the gas matrix. The non destructiveness of CRDS allows for continuous incubation measurements, as presented in part II of this dissertation. One critical issue for continuous incubation measurements is that the leak rate of the analyzer and the setup must be minimized. A four headed diaphragm pump (KNF, N84.4 ANDC) is build into the Picarro analyzers, but this pump was not found to be sufficiently leak tight, especially for the incubation experiments. A custom modified leak reduced pump was made as described below and placed downstream, outside the analyzer.

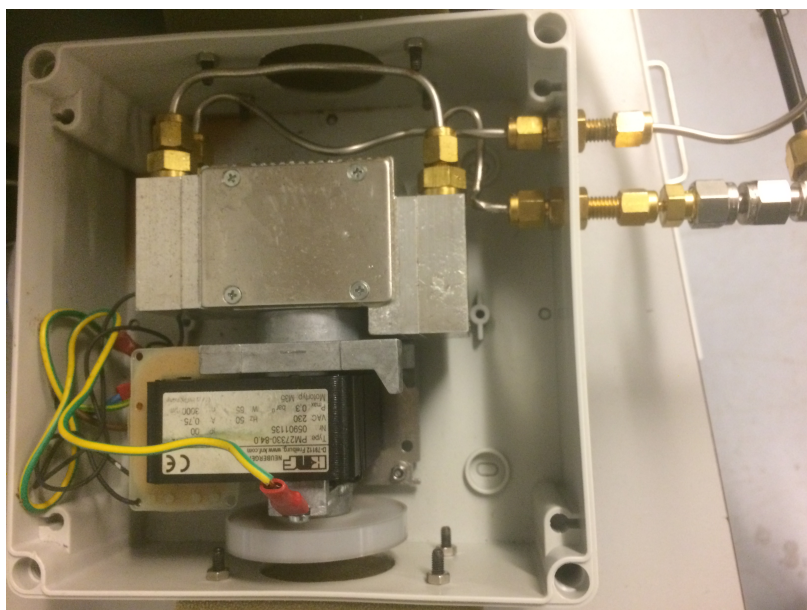


Figure 2.1: *Picture of the "leak reduced" diaphragm pump used with the CRDS analyzers, instead of the build-in pump.*

A commercially available mini diaphragm vacuum pump (KNF, N84.4 ANE) was purchased, stripped from plastic tubing and connectors before the head plates were removed. Vacuum grease (Dow corning brand High vacuum grease, silicone lubricant, Midland, Michigan, USA) was applied to the O-rings positioned between the head plates and the elastic di-

aphragm, before the head plates were reconnected to the diaphragm casing. New compression fittings (Swagelok) and tubing were mounted on the inlet and outlet, before all metal joints and the membrane were sealed with vacuum sealant (Celvaseal high vacuum leak sealant, Myers vacuum repair service, Inc., Kittanning, PA 16201, USA).

2.2 Isotope Ratio Mass Spectrometry

Measurements of gas samples are conventionally done with Mass Spectrometry (MS) or with specialized Isotope Ratio Mass Spectrometry (IRMS) for measurements of the gas isotopes. Mass spectrometry is basically a measurement technique of the mass-to-charge ratio (m/z) of the molecules in a given gas sample.

The sample of interest is introduced into the ion source, where the molecules are ionized before they are accelerated through focusing plates. Due to the ionization and the acceleration, the molecules are charged with kinetic energy (E_{kin}) once leaving the ion source. The kinetic energy of each individual molecule is described, using Newtons second law of motion, as a function of the molecular mass (m), the velocity (v) of the molecule, and as a function of the difference in voltage (V) used to accelerate the molecule and the charge (q) of the molecule.

$$E_{kin} = \frac{1}{2} \cdot m \cdot v^2 = V \cdot q \quad (2.2)$$

Once the ionized molecule reaches the magnet, it will experience a deflection by the magnetic field caused by the strong magnet. The equation for the radius of the curvature given by the magnetic field (see equation 2.3) is an equation dependent on the molecular mass, difference in voltage, charge, and magnet field (B) applied to the molecule.

$$r = \sqrt{\frac{2 \cdot m \cdot V}{q \cdot B^2}} \quad (2.3)$$

Since all molecules in a sample are influenced by the same charge, voltage difference and magnetic field, the curvature of the deflection depends solely on the mass of the molecule. The different molecules will therefore be curved according to their mass, with the heavier molecules having the largest radius and the light molecules having the smallest radius. The deflected ionized molecules are then trapped in the designated Faraday cups, in which the ionized molecules are neutralized by a flow of electrons. This neutralization result in an electric current, which in the amplifier is transformed into pulses. The resulting pulses are measured as signal intensity over a given time interval. Finally, the area is calculated as the integral between the sample curve and background curve (see Fig. 2.2). The areas are

then used to calculate the isotope ratios using the conventional calculation techniques as described by Kaiser and Röckmann (2008).

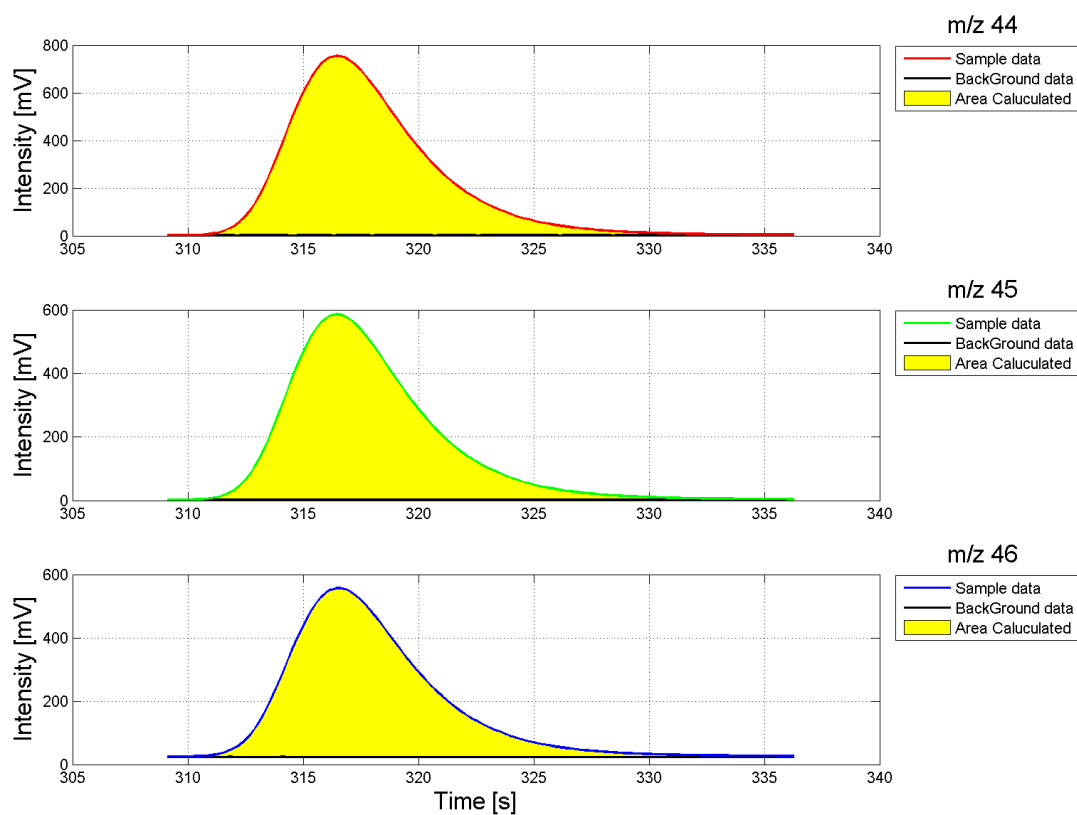


Figure 2.2: *Example plots of the integration measurements for m/z 44, 45, and 46 from measurements of the standard NAT332 (used at the Institute for Marine and Atmospheric research Utrecht in The Netherlands (IMAU)).*

Calibration and corrections

3.1 Concentration-dependent correction

Isotope measurements made with the G5101i-CIC and G5131i-CIC analyzers are dependent on concentration, which needs to be taken into account in the analysis of the measurements. The dependence originates from a rippled baseline rather than a smooth baseline (Fig. 3.1). The ^{14}N - ^{15}N - ^{16}O and ^{15}N - ^{14}N - ^{16}O peaks (from here on referred to as peak10 and peak11, respectively). Baseline ripples are created because of the periodic optical effect (etalon) that

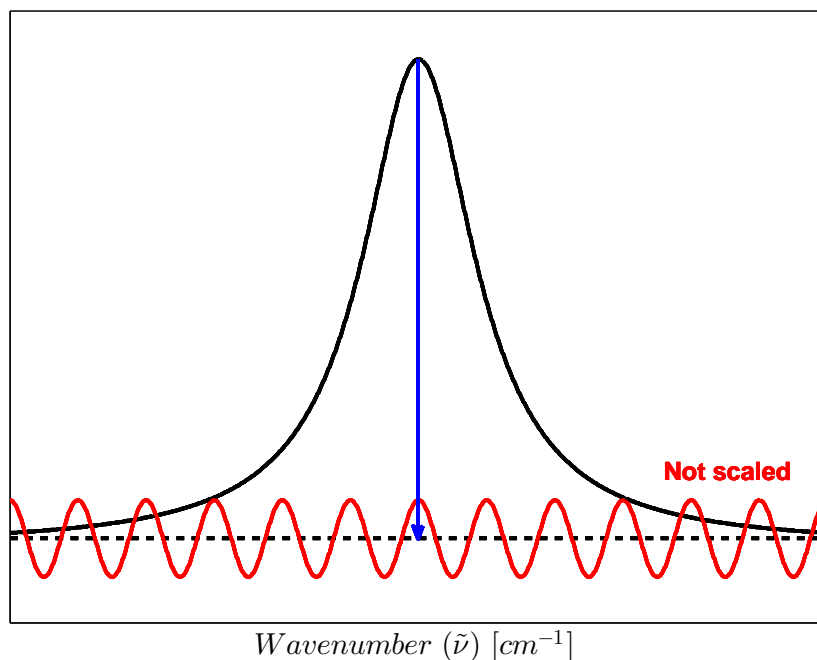


Figure 3.1: *Demonstrative baseline ripple offset. The solid black line is a Lorentz line shape calculated with standard normal distribution. The dashed line is the normal baseline. The solid red line is a rippled baseline. The peak height is shown with the blue arrow.*

is created when the light beam undergoes multiple reflections between the mirrors inside the cavity. The resulting ripples can appear both in and out of phase, leading to a spectral shift and therefore leading to resulting offset in absorption intensity. The ripples are therefore

the cause of a concentration dependent error in the isotope measurements and therefore δ -values. Since the baseline ripples have a larger relative impact at lower concentrations, the concentration dependence on the δ -values is therefore $\pm 1/\text{concentration}$.

The setup used for concentration-dependent experiments is made as an automatic increasing/ decreasing N_2O concentration setup. The setup (Fig. 3.2) consist of two parts, namely 1) the N_2O part and 2) the synthetic air part.

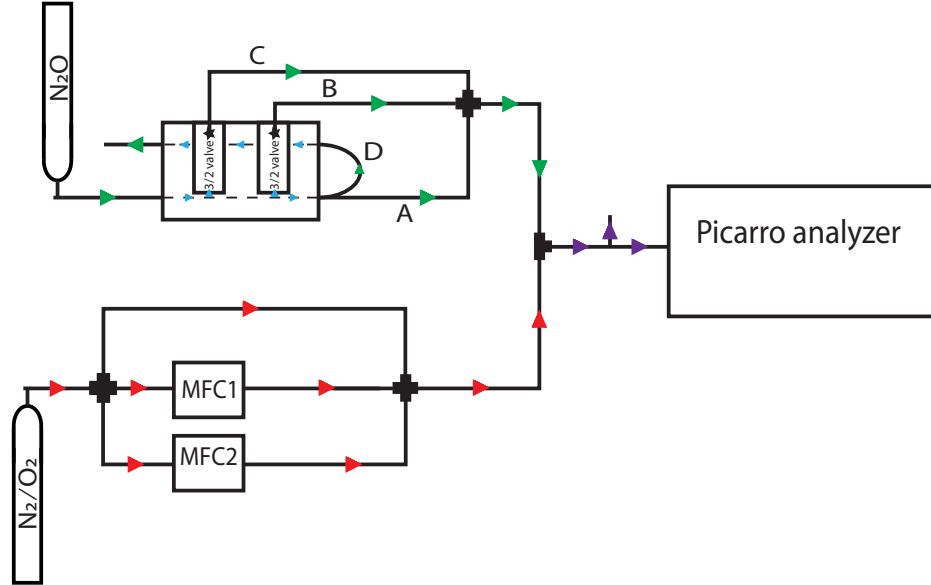


Figure 3.2: Schematic of the setup used for the concentration-dependent measurements.

Table 3.1: Capillary specifications as used in the CDC measurements using G5101i-CIC. The capillary specifications and the flow were calculated to match the specific N_2O concentration.

Capillary	ID (μm)	OD(μm)	Length (m)	Flow (mL/min)	N_2O (ppm)
A	5	150	2.45	0.0000027	0.268
B	5	150	0.72	0.00001	0.875
C	5	150	0.29	0.00002	2.216
D	50	-	0.79	0.08699	8699

Table 3.2: Capillary specifications as used in the CDC measurements using G5131i-CIC. The capillary specifications and the flow were calculated to match the specific N_2O concentration.

Capillary	ID (μm)	OD(μm)	Length (m)	Flow (mL/min)	N_2O (ppm)
A	5	150	2.56	0.0000027	0.268
B	5	150	2.10	0.0000033	0.326
C	5	150	0.72	0.00001	0.950
D	50	-	0.79	0.08699	8699

1) The N_2O part consists of a pure N_2O (100 % N_2O , purity 99.999 %) gas (green arrows), which is connected to four glass capillaries labeled A,B,C and D via a mounting plate (blue arrows indicate flow through mounting plate). A constant flow of 0.0000027 cc/min is flowing through Capillary "A". Capillary "B" and "C" are connected to the rest of the setup via two 3-port solenoid valves (SMC SY113-SGZD-M3-Q) which in turn can be switched on leading to an additional flow of N_2O . Capillary "D" is a vent for the overflow of N_2O . The capillary specifications were slightly modified for measurements performed with the G5131i-CIC analyser (Table 3.2) compared to those measured with the G5101i-CIC analyser (Table 3.1), to better reach the specifications of the individual analyzers.

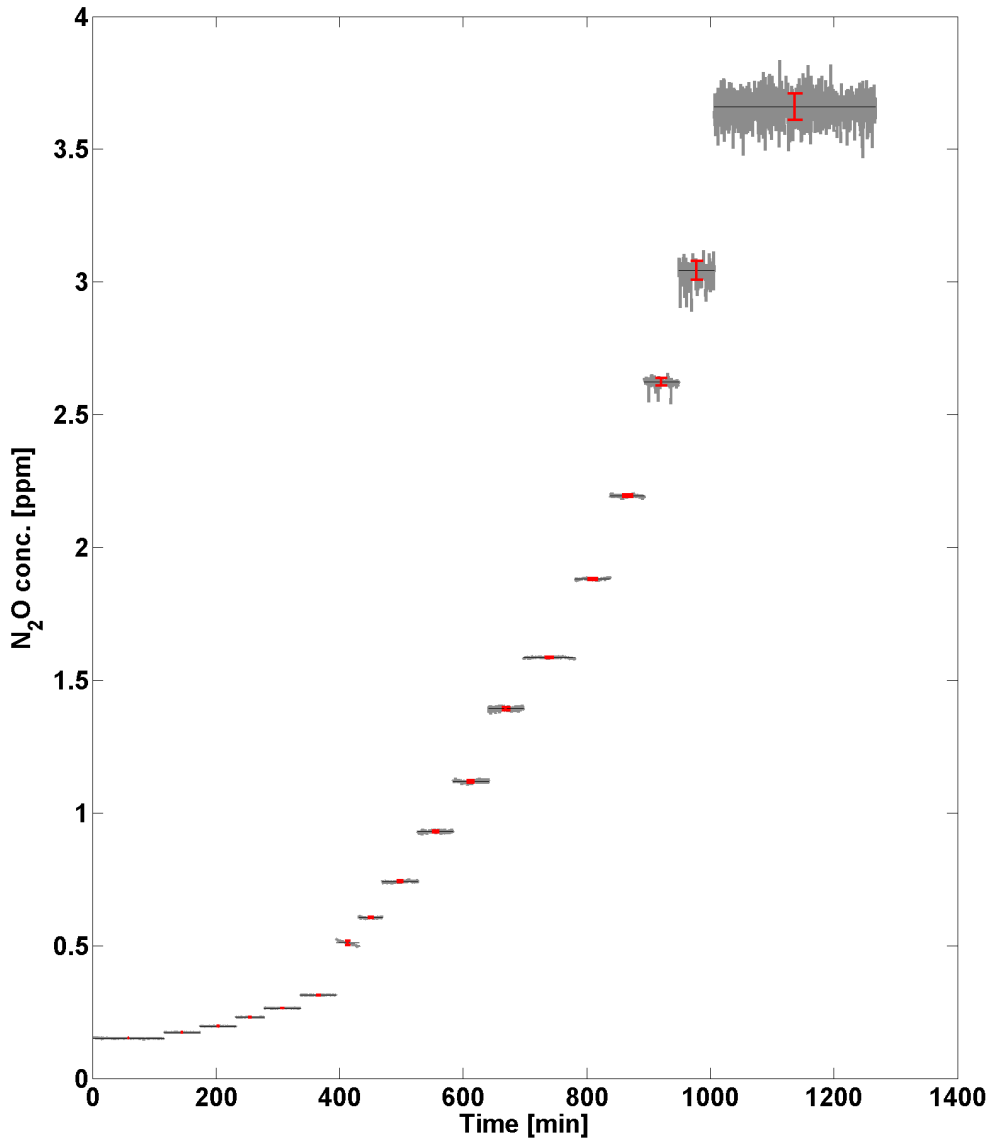


Figure 3.3: Raw N_2O measurements from dilution experiment using G5101i-CIC - gradually mixing of a pure N_2O gas (100 % N_2O , purity 99.999 %) and synthetic gas (20.1 % O_2 and 79.9 % N_2 , and approximately 15ppb N_2O , purity 99.999 %).

2) The synthetic air part consist of a synthetic air (79.9 % N₂, 20.1 % O₂, and approximately 15ppb N₂O, purity 99.999 %) gas bottle connected through three stainless steel 1/8” tubes connected via a 1/8” cross to two mass flow controllers (MFC) and one pressure gauge (as shown with red arrows in Figure 3.2). The pressure gauge is installed to ensure a constant flow of 24 cc/min, while the two MFC’s are installed to control the addition of synthetic air to a rate of 2 cc/min, 6 cc/min, 10 cc/min, 15 cc/min, 20 cc/min, or 25 cc/min, respectively. Downstream from the MFC’s and the electric valves, the flow of N₂O is mixed with the flow of synthetic air (purple arrows), before it is measured with the analyser.

The measurements are performed as a dilution experiment in which the pure N₂O gas is gradually diluted over 18 steps. In the first step 0.000027 cc/min of N₂O is mixed with 49 cc/min synthetic air, leading to a N₂O concentration of approximately 150 ppb. After 120 minutes of continuous measurements the N₂O concentration is gradually increased, either by reducing the flow of synthetic air or by increasing the flow of N₂O. An example of this in turn increase in N₂O concentration is shown in Fig. 3.3.

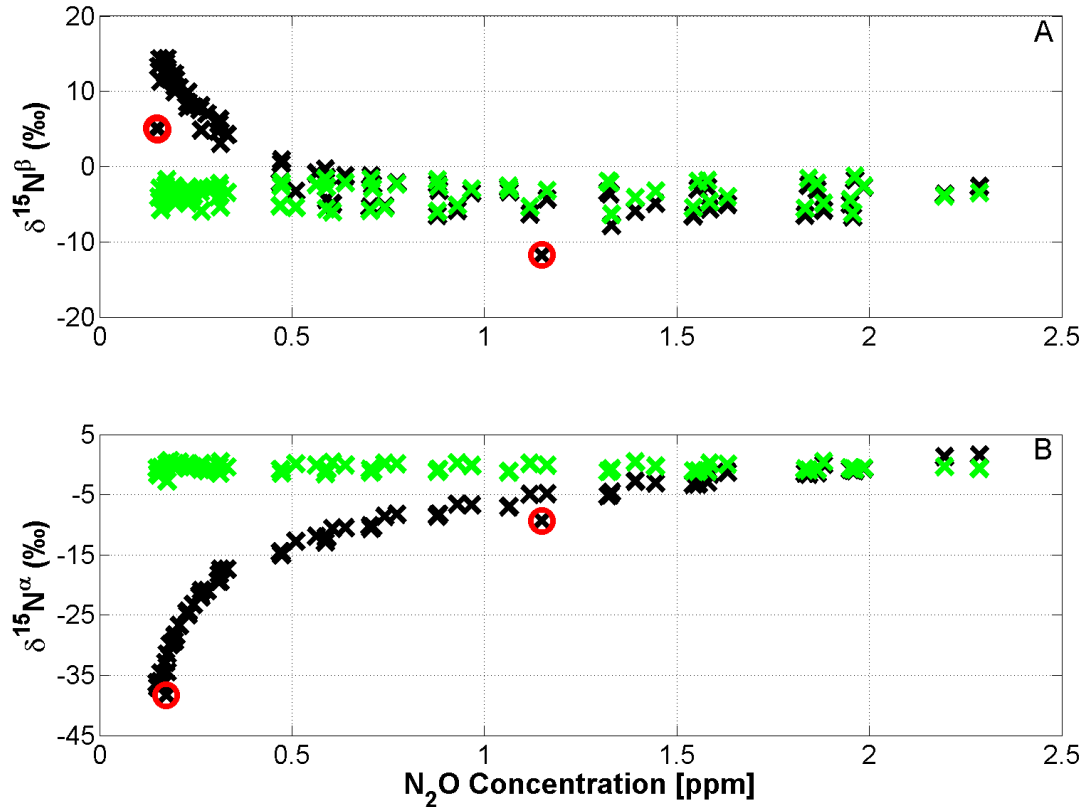


Figure 3.4: The concentration-dependent correction (CDC) using G5101i-CIC for (A) $\delta^{15}N^{\beta}$ and (B) $\delta^{15}N^{\alpha}$ respectively. In both figures, the raw data are presented in black, the CDC data is plotted in green, and the outliers are marked with red circles.

The raw isotopomer measurements were fitted with a cubic spline smoothing function (CSS-function) (Brumback and Rice, 1998). The best fit of these CSS-functions is found using a smoothing parameter of $p = 0.999$ in a regression analysis. For G5101i-CIC, four outliers were identified to be outside the 2σ boundary and removed from the data set (red circles in Fig. 3.4), while two outliers were identified outside the 2σ boundary for the experiment with G5131i-CIC (red circles in Fig. 3.5). After these outliers were removed, the best fit was found again and the concentration-dependent correction (CDC) was applied as shown with the green crosses in Fig. 3.4 and 3.5 for measurements performed using G5101i-CIC and G5131i-CIC, respectively.

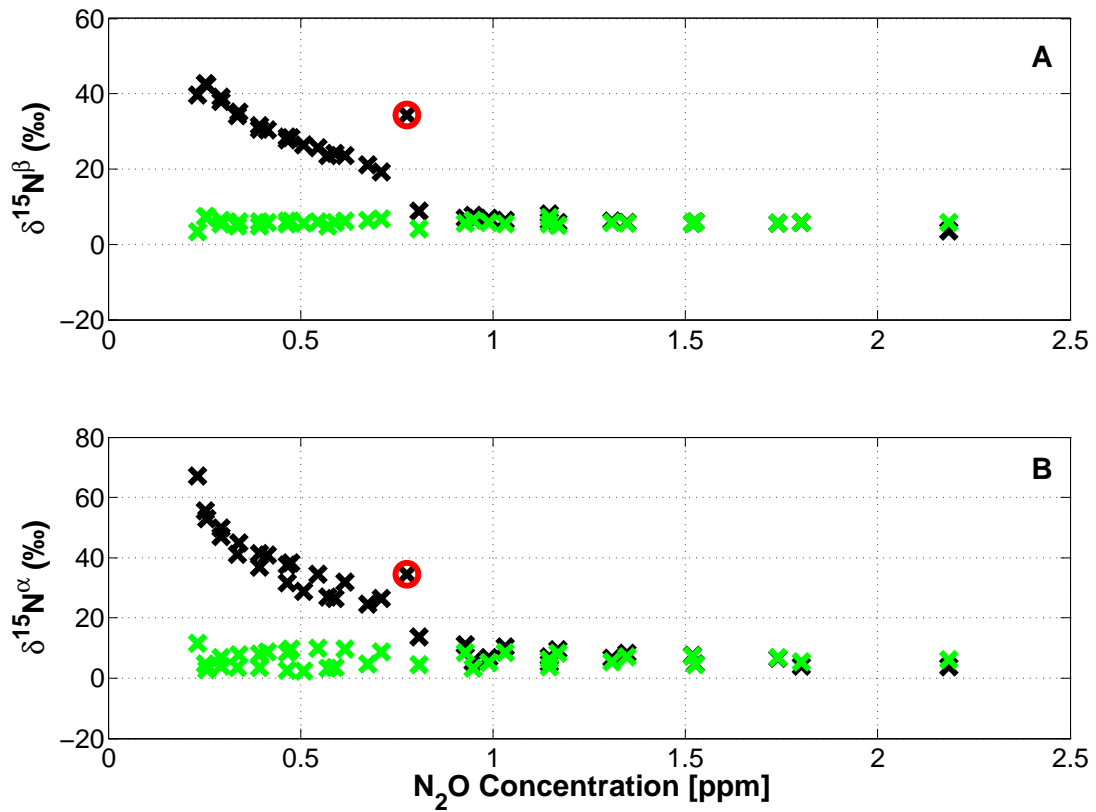


Figure 3.5: The concentration-dependent correction (CDC) using G5131i-CIC for (A) $\delta^{15}N^{\beta}$ and (B) $\delta^{15}N^{\alpha}$ respectively. In both figures, the raw data are presented in black, the CDC data is plotted in green, and the outliers are marked with red circles.

The isotopomer values measured using the G5101i-CIC analyzer are actually measurements of the ratio42 and ratio43. Ratio42 is the raw fitted peak-heights of the $^{14}N^{15}N^{16}O$ peak versus $^{14}N^{14}N^{16}O$ peak and is a measure for $\delta^{15}N^{\alpha}$. Similarly ratio43 is the raw fitted peak-heights of the $^{15}N^{14}N^{16}O$ peak versus $^{14}N^{14}N^{16}O$ peak. Ratio42 and ratio43 are linear proportional to the isotopomers $\delta^{15}N^{\alpha}$ and $\delta^{15}N^{\beta}$ respectively. The isotopomer concentration

is depending on the bulk concentration. We expected that concentration corrections directly on the δ -values would result in incorrect corrections, due to mingling between scaling and offset. To investigate this hypothesis were the above described CDC calculations performed directly on Ratio42 and Ratio43 simultaneously with CDC calculations on the $\delta^{15}\text{N}^\alpha$ and $\delta^{15}\text{N}^\beta$. CDC calculations on the ratio's and on the δ -values resulted in identical corrections. For simplicity, only the concentration dependent-correction directly on the δ -values are presented here.

3.2 Oxygen-dependent correction

Isotope measurements have proven to be sensitive to the oxygen (O_2) mixing ratio in the gas matrix (Erler et al., 2015). A sensitivity analysis has therefore been applied using two different methods depending on the analyser in use (G5101i-CIC or G5131i-CIC).

The following experiment and results are performed using G5101i-CIC.

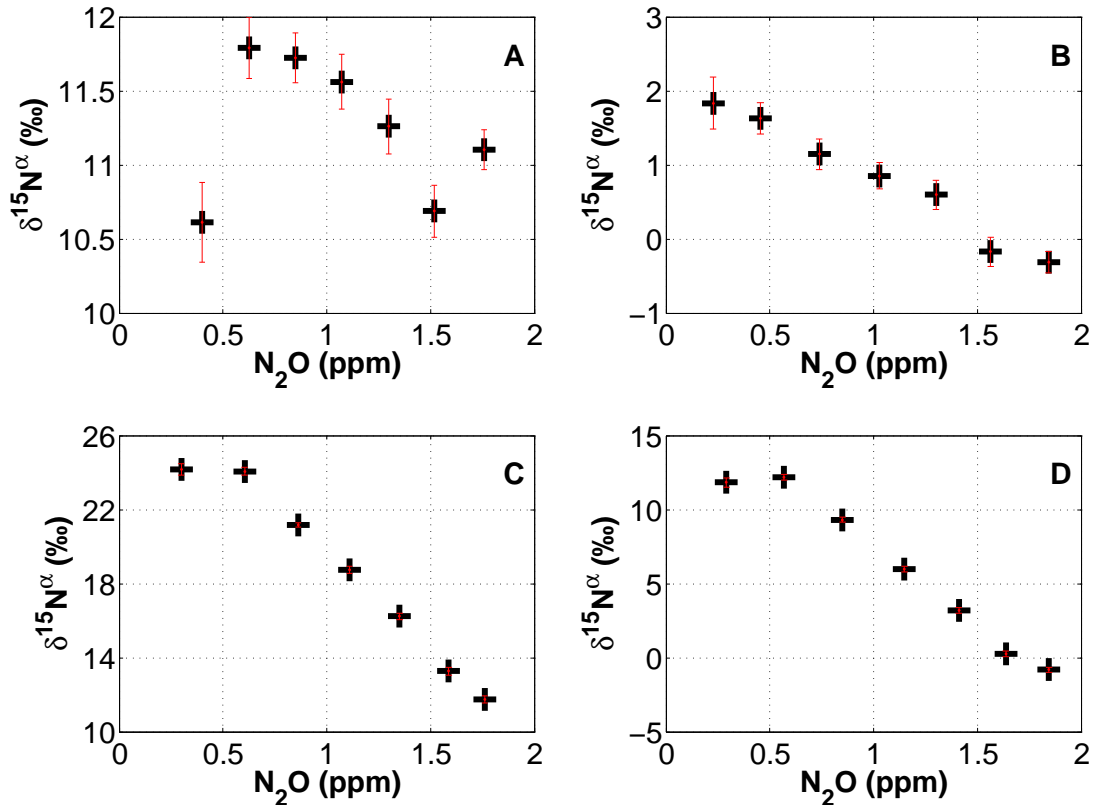


Figure 3.6: Measurements used for the oxygen dependence experiment. All data have been corrected using CDC, as described in Sec. 3.1

The oxygen dependence using the G5101i-CIC analyzer was explored through dilution experiments of the two standard gases (CIC-MPI-I and CIC-MPI-II). Each of the standard gases were diluted in seven steps in order to have a sufficient range of measurements between approximately 1.8 ppm and 0.3 ppm. Fig. 3.6 shows the results from four dilution experiments with CIC-MPI-II (Fig. 3.6A and 3.6C) and with CIC-MPI-I (Fig. 3.6B and 3.6D), respectively. In the experiment shown in Fig. 3.6A and 3.6B, a synthetic air (79.9 % N₂, 20.1 % O₂, and approximately 15 ppb N₂O, purity 99.999 %) was used as the diluting gas. In the experiments shown in Fig. 3.6C and 3.6D, a nitrogen gas (purity 99.999 % N₂) was used as the diluting gas.

The dilution of the standard gases was performed with manual adjustment of the flow. Therefore, the resulting N₂O concentrations is not identical for the two experiments with the same reference gas. The N₂O concentration of the pure standard gases is also different. The average N₂O concentration of the four experiments at each step is calculated and used in the following calculations and comparisons of the oxygen dependence.

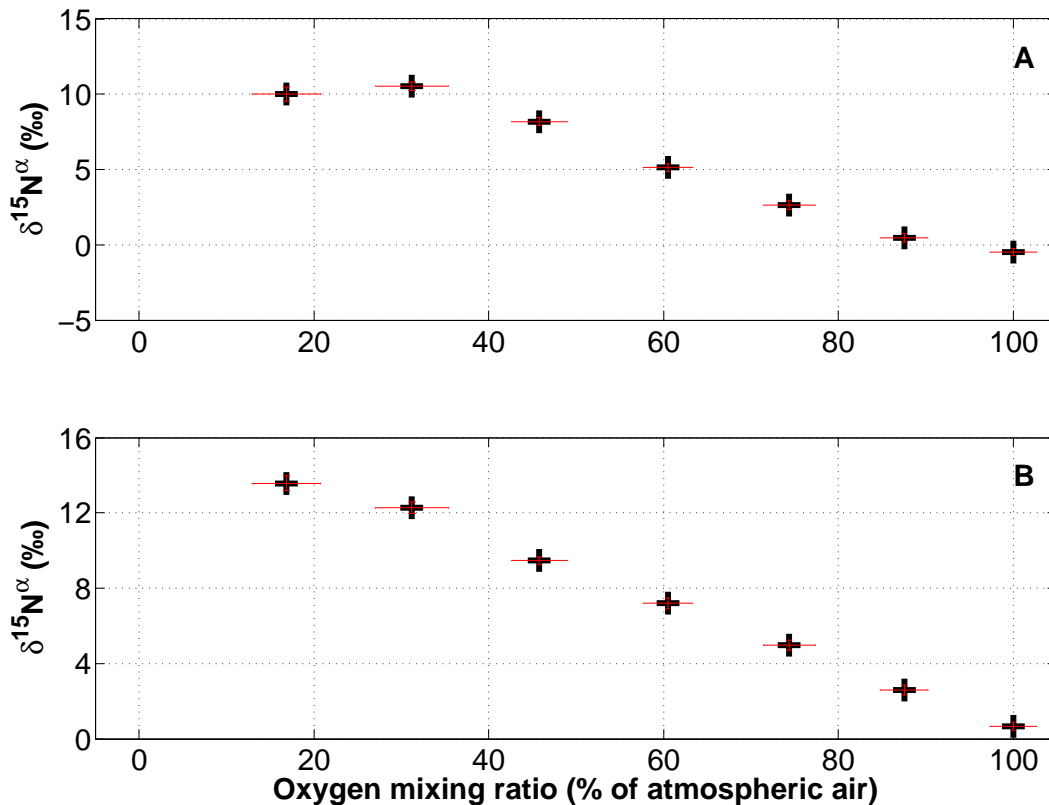


Figure 3.7: *Difference between measurements using synthetic air and nitrogen gas as dilution gas. Experiment with A) CIC-MPI-I and B) CIC-MPI-II.*

When synthetic air is used as the diluting gas approximately the same O_2 concentration is found throughout the experiments. After applying the CDC, the isotope measurements should (ideally) be constant throughout the experiments. This is not exactly the case in the presented experiments, though all corrected data points are within the standard deviation (1σ) of the average. The experiments with N_2 as the diluting gas present a decreasing O_2 concentration as more N_2 is introduced. The highest measured concentration is a measurement of pure standard gas in which the O_2 concentration is equal to that of the atmospheric mixing ratio (21 %). In the following calculations the N_2O concentrations are converted into O_2 mixing ratios (OMR), which is the relative oxygen concentration compared to that of atmospheric air (21 %).

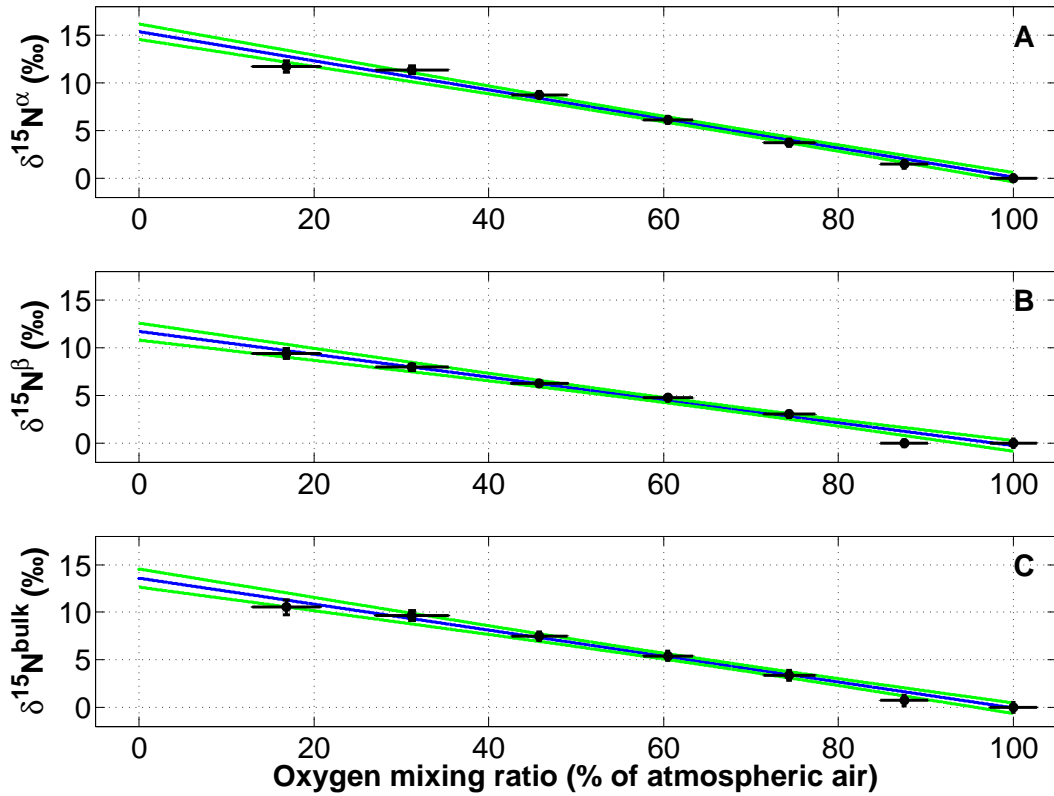


Figure 3.8: Final O_2 dependence on A) $\delta^{15}N^\alpha$, B) $\delta^{15}N^\beta$, and C) $\delta^{15}N^{bulk}$. Monte Carlo simulation of the linear relation between measurements (blue line), and the standard error at all concentrations (green lines). Mean O_2 dependence of the two experiments with CIC-MPI-I and CIC-MPI-II (black sign), and the resulting standard error (black error-bar).

Figure 3.7 shows the O_2 dependence of the $\delta^{15}N^\alpha$ measurements from each of the two standard gases. The O_2 dependence is found by subtracting measurements performed with

synthetic air from those performed with a pure N₂ gas. The results are therefore the relative difference between measurements performed with and without decreasing O₂ concentration. Each of the sub-figures (3.7A and 3.7B) are O₂ dependence experiments used in the final O₂ dependence correction analysis. Similar analysis is made for $\delta^{15}\text{N}^\beta$. Fig. 3.8A, 3.8B, and 3.8C show the final O₂ dependence on $\delta^{15}\text{N}^\alpha$, $\delta^{15}\text{N}^\beta$, and $\delta^{15}\text{N}^{bulk}$, respectively.

The final O₂ dependence between the O₂ mixing ratio and the δ -value, was found to fit a linear correlation with a coefficient of determination (R^2) of 0.984, 0.978, and 0.987 for $\delta^{15}\text{N}^\alpha$, $\delta^{15}\text{N}^\beta$, and $\delta^{15}\text{N}^{bulk}$, respectively. Equation 3.1, 3.2, and 3.3 show the resulting O₂ dependence correction equations for $\delta^{15}\text{N}^\alpha$, $\delta^{15}\text{N}^\beta$, and $\delta^{15}\text{N}^{bulk}$, respectively.

$$\delta^{15}N_{ODC}^\alpha = -0.1534 \cdot OMR + 15.269 \quad (3.1)$$

$$\delta^{15}N_{ODC}^\beta = -0.1210 \cdot OMR + 11.662 \quad (3.2)$$

$$\delta^{15}N_{ODC}^{bulk} = -0.1372 \cdot OMR + 13.465 \quad (3.3)$$

A linear O₂ dependence correction equation for $\delta^{15}\text{N}^{bulk}$ has previously been found by Erler et al. (2015). The relation found by Erler et al. (2015) is:

$$\delta^{15}N_{ODC}^{bulk} = -0.11 \cdot OMR + 11.36 \quad (3.4)$$

An O₂ mixing ratio of 0 % would result in an offset in $\delta^{15}\text{N}^{bulk}$ of 13.465 ‰. This relation would result in a difference of 2.1 ‰ compared to that found in Eq. 3.3. Taking the uncertainty of the Monte Carlo simulation and the uncertainty of our measurements of δ -values into account, this offset would be clearly within the 1-sigma uncertainty. Another likely explanation for the offset between the two equations is that the experiments were performed with different analyzers. The interlaboratory assessment of nitrous oxide isotopomer analysis shown by Mohn et al. (2014) shows a clear difference, even between measurements of the same standard gas depending on the analyzer. The equations presented here are therefore robust and trustworthy even though they are not based on a direct O₂ dependence experiment, but rather an indirect experiment of the O₂ dependence.

3.3 Standard gases

During the work presented in this thesis, two standard gases were used at all times to calibrate the measurements versus an internationally accepted standard reference, namely the atmospheric nitrogen (AIR-N₂) for $\delta^{15}\text{N}$ measurements and the Vienna Standard Mean Ocean Water (VSMOW) for $\delta^{18}\text{O}$ measurements. The standard gases used in the presented

work are based on standard gases MPI-I and MPI-II, provided by J. Kaiser at University of East Anglia (UEA), Norwich, United Kingdom. The two MPI standard gases are originally pure N₂O standard gases with a known isotopic composition as described by Kaiser (2002). Table 3.3 show the original isotopic composition as measured by J. Kaiser.

Table 3.3: *Original measurements of standard gas MPI-1 and MPI-2 (personal communication with J. Kaiser). The listed values are mean-values and standard deviations (σ).*

Std. gas	$\delta^{15}\text{N}^{bulk}$ (‰)	$\delta^{15}\text{N}^{\alpha}$ (‰)	$\delta^{15}\text{N}^{\beta}$ (‰)	$\delta^{18}\text{O}$ (‰)
MPI-I	1.0 ± 0.03	0.7 ± 0.9	1.3 ± 0.9	38.5 ± 0.22
MPI-II	-1.78 ± 0.03	12.4 ± 0.04	-15.9 ± 0.9	40.47 ± 0.22

Using a Picarro CRDS analyzer does not allow measurements of pure N₂O gases. The standard gases (MPI) were therefore diluted with a synthetic air mixture (20.1 % O₂ and 79.9 % N₂, purity 99.999 %), in our laboratory. This dilution resulted in two new standard gases, referred to as CIC-MPI standard gases.

3.3.1 CIC-MPI version I

The first batch of the standard gases CIC-MPI-1 and CIC-MPI-2 was used for the pure denitrifying bacterial experiments (part II), and the measurements performed on Disko island (chapter 10). These gases were mixed and originally used for the experiments described by Balslev-Clausen (2011).

Chapter 6 present measurements of the two standard gases (CIC-MPI-1 and CIC-MPI-2), as the average measurement from three laboratories: Tokyo Institute of Technology in Japan (Tokyo-Tech), Institute for Marine and Atmospheric research Utrecht in The Netherlands (IMAU), and Centre for Ice and Climate, Niels Bohr Institute, University of Copenhagen, Denmark (CIC). Table 3.4 show the same average measurements and additionally the results from each laboratory. The measurements from CIC were all done with the prototype of the G5101i-CIC analyzer. Measurements of CIC-MPI-1, at Tokyo-Tech, resulted in an average N₂O concentration offset by 80 ppb, compared to the concentrations measured at IMAU and CIC. We can not explain this offset, but the primary focus is on the isotopes, which are nicely correlated. It should also be noted that the measurements performed at IMAU are not calibrated for concentration, while the isotopes are calibrated against AIR-N₂ and VSMOW.

Table 3.4: *Measurements of standard gases CIC-MPI-1 and CIC-MPI-2, diluted MPI-1 and MPI-2 gases respectively. The listed values are shown for each laboratory, the combined mean-values, and combined standard deviations (σ) of measurements performed at Tokyo-Tech ($n = 3$), IMAU ($n = 22$), and CIC ($n=4$).*

Std. gas	Institute	[N ₂ O] (ppb)	$\delta^{15}\text{N}^{bulk}$ (‰)	$\delta^{15}\text{N}^{\alpha}$ (‰)	$\delta^{15}\text{N}^{\beta}$ (‰)
CIC-MPI-1					
	Tokyo-Tech	1828.9 ± 4.9	1.34 ± 0.17	1.44 ± 0.09	1.24 ± 0.35
	IMAU	1919.3 ± 21.0	1.08 ± 0.10	2.31 ± 0.25	-0.15 ± 0.33
	CIC	1918.4 ± 2.3	2.62 ± 1.77	0.29 ± 2.44	4.95 ± 2.37
	Mean	1909.8 ± 29.3	1.32 ± 0.82	1.94 ± 0.87	0.70 ± 1.42
CIC-MPI-2					
	Tokyo-Tech	1840.2 ± 32.1	-1.30 ± 0.06	12.79 ± 0.22	-15.41 ± 0.24
	IMAU	1865.9 ± 16.0	-1.68 ± 0.10	11.80 ± 0.37	-15.16 ± 0.46
	CIC	1827.2 ± 1.8	-0.15 ± 1.78	12.58 ± 2.51	-12.89 ± 2.35
	Mean	1857.9 ± 19.2	-1.43 ± 0.82	12.01 ± 1.06	-14.87 ± 1.13

Compared to the measurements presented in Table 3.4, the two standard gases were additionally measured with the G5131i-CIC analyzer (Table 3.5). The G5131i-CIC analyzer is also capable of measuring $\delta^{18}\text{O}$ in the standard gases (see chapter 2). The four measure-

Table 3.5: *Measurements of standard gases CIC-MPI-1 performed using the G5131i-CIC analyzer. The listed values are combined mean-values and combined standard deviations (σ) of measurements performed at CIC ($n = 4$).*

Laboratory	[N ₂ O] (ppb)	$\delta^{15}\text{N}^{bulk}$ (‰)	$\delta^{15}\text{N}^{\alpha}$ (‰)	$\delta^{15}\text{N}^{\beta}$ (‰)	$\delta^{18}\text{O}$ (‰)
CIC-MPI-1	1893.3 ± 4.2	1.82 ± 3.73	2.08 ± 4.15	1.50 ± 3.88	39.10 ± 3.06
CIC-MPI-2	1804.0 ± 2.3	-1.60 ± 2.96	12.12 ± 3.45	15.34 ± 3.25	40.57 ± 2.08

ments of CIC-MPI-1 and CIC-MPI-2 performed on the G5131i-CIC analyzer were used to 1) calibrate the new standard gases (CIC-MPI-1.2 and CIC-MPI-2.2) and 2) work as standard gases for the measurements performed with the analyzer.

3.3.2 CIC-MPI version II

A second batch of the CIC-MPI standard gases was mixed, since the first set of standard gases were previously used. The second batch was only used as standard gas with the G5131i-CIC analyzer.

The idea with the standard gases is that they have the same isotopic composition as the original MPI-gases. This is ensured by diluting the MPI-gas with synthetic air (20.1 % O₂ and 79.9 % N₂) of purity 99.9999 % to such a degree that the final N₂O concentration is in the measuring range of the analyzer. Prior to mixing, the synthetic air gas was measured to ensure the purity with respect to the concentration of N₂O. The concentration of N₂O was measured to be a few ‰ and is therefore treated as being 0 ppb due to the uncertainty of the analyzer at these low concentration levels.

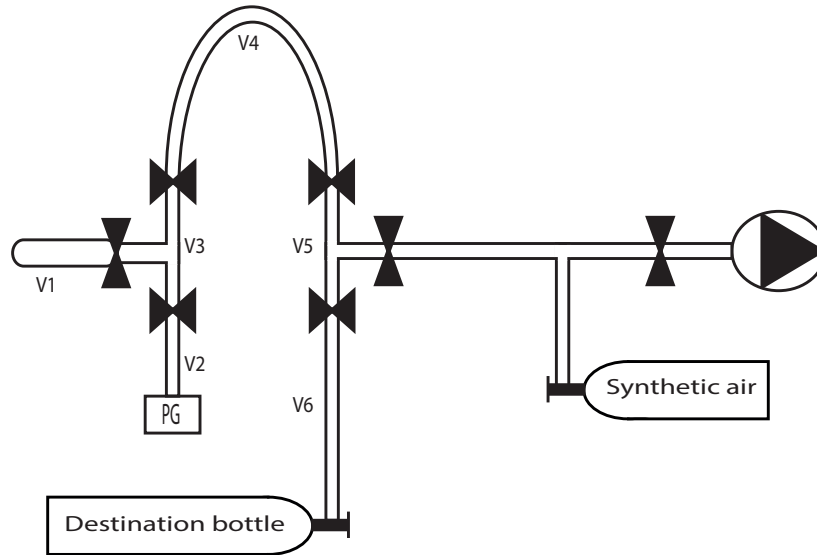


Figure 3.9: Schematic of the setup used for the mixing of new standard gases, CIC-MPI-1.2 and CIC-MPI-2.2.

The mixing was done using the setup as shown in Fig. 3.9, which consists of 6 volumes (V1-V6), a pressure gauge (PG), a rough pump, a vacuum pump, the synthetic air gas bottle (50 L at 200 bar overpressure), and an empty 10 L gas cylinder. The original MPI-gases were

Table 3.6: Measured volume sizes, from the setup used for mixing of new standard gases.

Name	V1	V2	V3	V4	V5	V6
Volume (mL)	5.56	9.2	7.68	5.44	3.8	2

stored in a glass-vial with two valves in line to keep the gas sealed from the outside air. The V1 volume is the volume centering the connection between the glass-vial and the setup.

The six volumes (shown in Fig. 3.9 and Table 3.6), were measured and calculated prior to mixing. It was thereafter possible to calculate the pressure required to mix the standard gasses to the desired concentration of N₂O.

The mixing of each of the two standard gases was done in four steps.

1. Creating a vacuum in the entire setup.
2. Introducing the pure MPI-gas into the setup through V1.
3. Expanding the gas in volume V1+V2+V3+V4, trapping 0.85 mL in V4 and freezing the gas using liquid nitrogen (LN2).
4. Transferring the MPI-gas from V4 to the new standard bottle and topping the bottle up with 50 bar of synthetic air.

The 0.85 mL pure MPI-gas should, in theory, lead to an approximate N₂O concentration of 1700 ppb in each of the two new CIC-MPI standard gases. The standard gases were measured both at IMAU and at CIC (Table 3.7 and Table 3.8). At IMAU the two standard gases were measured a total of 26 times using the IRMS analyzer. At CIC the standard gases were continuously measured 4 times for approximately 90 minutes using the G5131i-CIC analyzer.

Table 3.7: *Measurements of standard gas CIC-MPI-1.2. The listed values are from IMAU (n=26), CIC (n=4), and the combined mean-values and combined standard deviations (σ).*

Laboratory	[N ₂ O] (ppb)	$\delta^{15}\text{N}^{bulk}$ (‰)	$\delta^{15}\text{N}^{\alpha}$ (‰)	$\delta^{15}\text{N}^{\beta}$ (‰)	$\delta^{18}\text{O}$ (‰)
IMAU	1737.5 ± 9.5	2.65 ± 0.10	3.27 ± 0.40	2.04 ± 0.53	42.74 ± 0.23
CIC	1705.3 ± 3.1	2.48 ± 2.74	1.19 ± 3.32	3.78 ± 3.08	44.52 ± 1.95
Mean	1733.2 ± 8.9	2.63 ± 1.00	2.99 ± 1.27	2.27 ± 1.23	42.98 ± 0.74

Table 3.8: *Measurements of standard gas CIC-MPI-2.2. The listed values are from IMAU (n=26), CIC (n=4), and the combined mean-values and combined standard deviations (σ).*

Laboratory	[N ₂ O] (ppb)	$\delta^{15}\text{N}^{bulk}$ (‰)	$\delta^{15}\text{N}^{\alpha}$ (‰)	$\delta^{15}\text{N}^{\beta}$ (‰)	$\delta^{18}\text{O}$ (‰)
IMAU	1567.4 ± 10.3	-0.42 ± 0.12	12.41 ± 0.34	-13.26 ± 0.44	44.02 ± 0.31
CIC	1537.9 ± 2.21	-1.04 ± 2.74	11.87 ± 3.28	-13.95 ± 3.09	44.03 ± 1.99
Mean	1563.5 ± 9.6	-0.50 ± 1.01	12.34 ± 1.24	-13.35 ± 1.20	44.02 ± 0.78

Part II

Microbial evolution

Introduction - part II

Since the 1950's, it has been known that N_2O stems from biological sources in soils and oceans, but presently we lack an understanding of the role and pathways of production and reduction. The determination (in the 1970's) of the relationship between the destruction of Ozone (O_3) and the increased concentration of N_2O in the atmosphere and the stratosphere (Crutzen, 1972, 1974; Johnston, 1972), led to a rapidly increasing interest and investigation of the sources of N_2O , and also the complexity of the microbial pathways (Bremner, 1997). Studies have since established that the primary source of N_2O is via microbial production pathways of the catabolic nitrogen cycle in terrestrial and marine environments. Multiple studies have investigated all parts of the processes involved in the evolution of N_2O to comprehend and elucidate the very complex network of N_2O producing microorganisms (Stein (2011); Schreiber et al. (2012), and references therein).

It is generally accepted that the two microbial processes of *nitrification* (or *ammonia oxidizing bacteria*) and *denitrification* are the two primary natural metabolisms producing N_2O emitted to the atmosphere, from both terrestrial and oceanic environments. Figure 4.1 shows an illustration of the complexity of the production pathways responsible for the production and on-site reduction of N_2O as first presented by Schreiber et al. (2012) and later by Hu et al. (2015) in a slightly modified version. The illustration clearly presents the complexity of the production of NO and N_2O , since most pathways of the catabolic nitrogen cycle are capable of producing both molecules. The illustration includes microbial denitrification, microbial autotrophic nitrification (ammonia oxidizing bacteria (AOB)), ammonia oxidizing archaea (AOA), nitrite oxidizing bacteria (NOB)), bacteria producing dissimilatory nitrate reduction to ammonium (DNRA), and anaerobic ammonia oxidizers (anammox) (Stein, 2011; Chandran et al., 2011; Schreiber et al., 2012; Hu et al., 2015). Other well established processes producing N_2O , are nitrifier denitrification, and chemodenitrification. Nitrifier denitrification is identified as a nitrification process, but the microorganism has

the enzymes for catalyzing as the conventional nitrification first followed by denitrification (Wrage et al., 2001). Nitrifier denitrification oxidizes ammonia (NH_3) to nitrite (NO_2^-), followed by a reduction of nitrite ultimately to N_2 (Wrage et al., 2001). Rather than the biological processes of denitrification, chemodenitrification is a chemical decomposition of the intermediate states of the nitrification process (Bremner, 1997; Wrage et al., 2001).

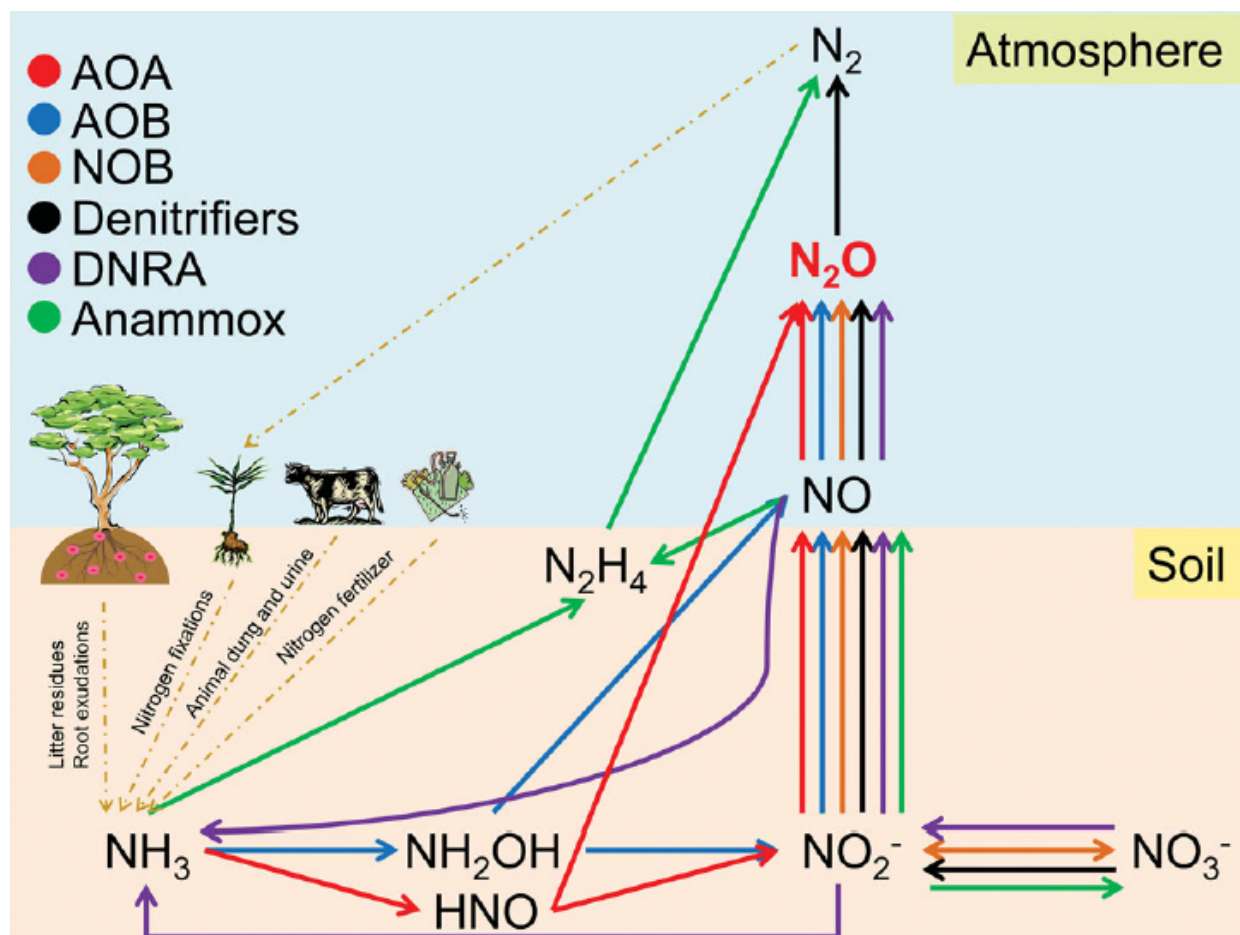


Figure 4.1: Illustrative outline of the microbial processes mainly involved in the evolution of N_2O . Representation of figure presented by Hu et al. (2015).

Due to this great complexity, the focus of this work will be purely on the two primary microbial pathways of nitrification and denitrification. In order to obtain a better understanding of the processes and pathways involved in the production and reduction of N_2O , continuous measurements of the evolution of N_2O produced from both pure denitrifying bacterial cultures and pure nitrifying bacterial cultures have been performed as incubation experiments. The results from these incubation experiments are presented in Chapter 5 and 6 for nitrification and denitrification experiments, respectively.

4.1 Incubation setup

The setup used for the incubation experiments with the nitrifying and denitrifying bacterial cultures, is shortly described in chapter 6. In the following section a more detailed explanation of the incubation setup is given.

The conventional method for measuring bacterial production and reduction of N_2O is by incubating a bacterial media in a sealed chamber, and taking out discrete gas samples a number of times. These discrete samples are then measured by IRMS or similar measurement techniques. In the incubation experiments presented in chapter 6 and 5, the idea was to use the CRDS analyzer to measure the evolution of the bacterial production continuously.

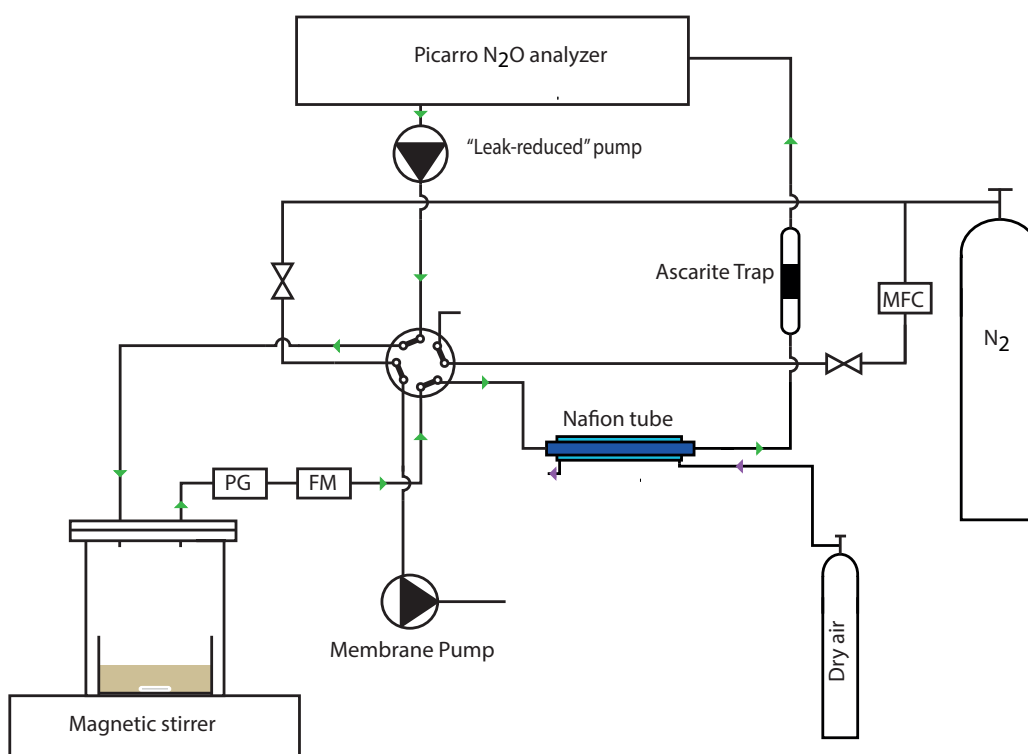


Figure 4.2: Schematic of the incubation setup as used in the measuring-mode during the denitrification experiments. The green arrows show the gas flow direction for flushing the analyzer. The purple arrows show the direction of the purge gas.

The incubation setup is, in its most simple form, a closed loop with 1/8" ss tubing between the CRDS analyzer and the chamber (change depending on the experiment) in which the bacterial solution is placed. Though, as previously stated, the internal pump is not leak tight to a satisfying degree, and the leak reduced pump therefore needs to be connected

downstream from the analyzer. Since the bacteria are in a liquid solution, a significant water vapor evaporation is expected. To hinder water vapor from entering the cavity of the CRDS analyzer and condensing on the mirrors, a nafion unit is placed upstream from the analyzer. The nafion unit consists of a nafion membrane inside a 1/8" ss tube. In either end, the nafion membrane is connected to a glass capillary which is connecting the nafion unit to a 1/8" ss tube. Furthermore, a dry technical air gas (Teknisk luft, lab line

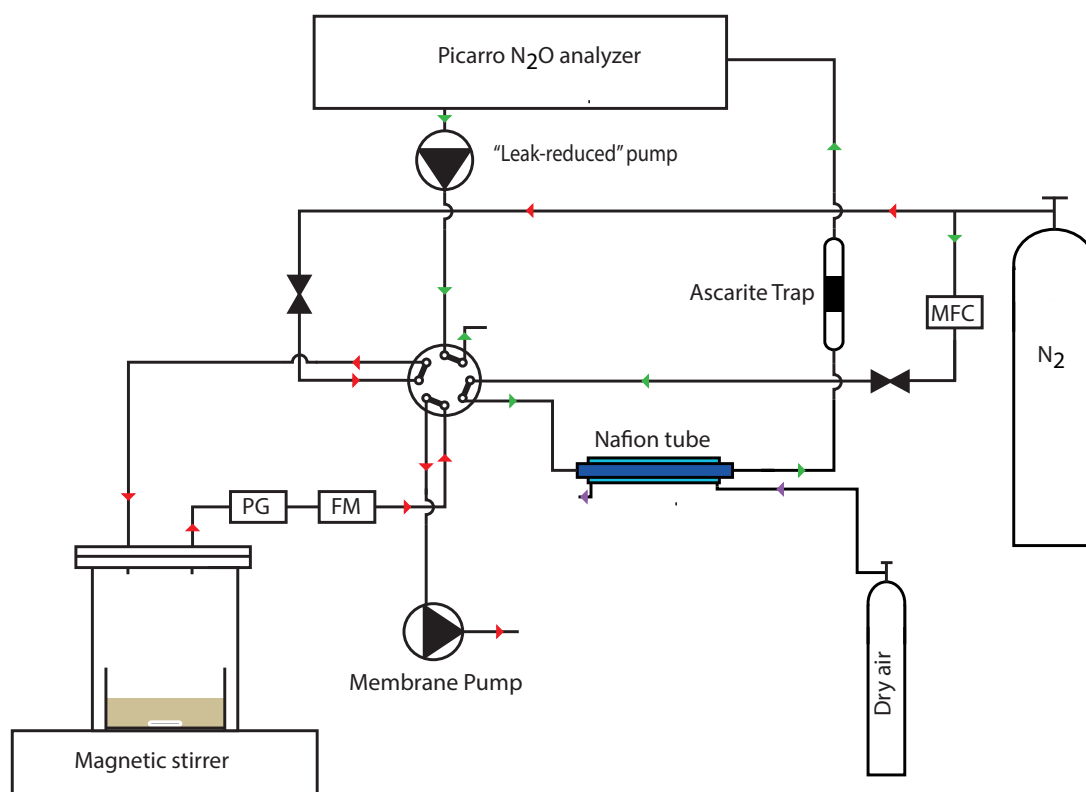


Figure 4.3: *Schematic of the incubation setup as used in flushing-mode during the denitrification setup. The green arrows show the gas flow direction for flushing the analyzer. The red arrows point in the direction of the gas flow for flushing the bacterial chamber. The purple arrows show the direction of the purge gas.*

5.0, Air Liquide, Denmark) is used as a purge gas for the nafion unit. To clean the gas for potential CO_2 contamination, an ascarite trap is installed between the nafion unit and the analyzer. The ascarite trap consists of sodium hydroxide (NaOH) flakes placed in a glass tube with magnesium perchlorate ($\text{Mg}(\text{ClO}_4)_2$) on either side. The NaOH undergoes a chemical reaction with CO_2 , leading to production of Na_2CO_3 and H_2O . The produced H_2O is removed again by the $\text{Mg}(\text{ClO}_4)_2$. A pressure gauge (PG) and a flow-meter (FM) is installed, downstream from the bacterial chamber, to monitor the pressure outside the

cavity and for possible detection of an unforeseen clogging in the setup.

The incubation setup is constructed in such a way that once the bacterial solution is placed in the incubation chamber, the entire setup can be flushed and thereby ensure identical starting conditions (same N_2O concentration and same isotopic composition) for all replicate experiments. The incubation setup therefore consists of both a measuring-mode (Fig. 4.2) and a flushing-mode (Fig. 4.3). Flushing the setup is automatically performed by activating an 8-port valve connected to the incubation setup. The flushing setup furthermore consists of a membrane pump, two electric valves (3 Port Solenoid Valve, SMC pneumatics, Part name: SMC SY113-SGZD-M3-Q), a mass flow controller (MFC), and additionally a flushing gas (F-gas) connected to the setup (see Fig. 4.2 and 4.3). The setup is constructed

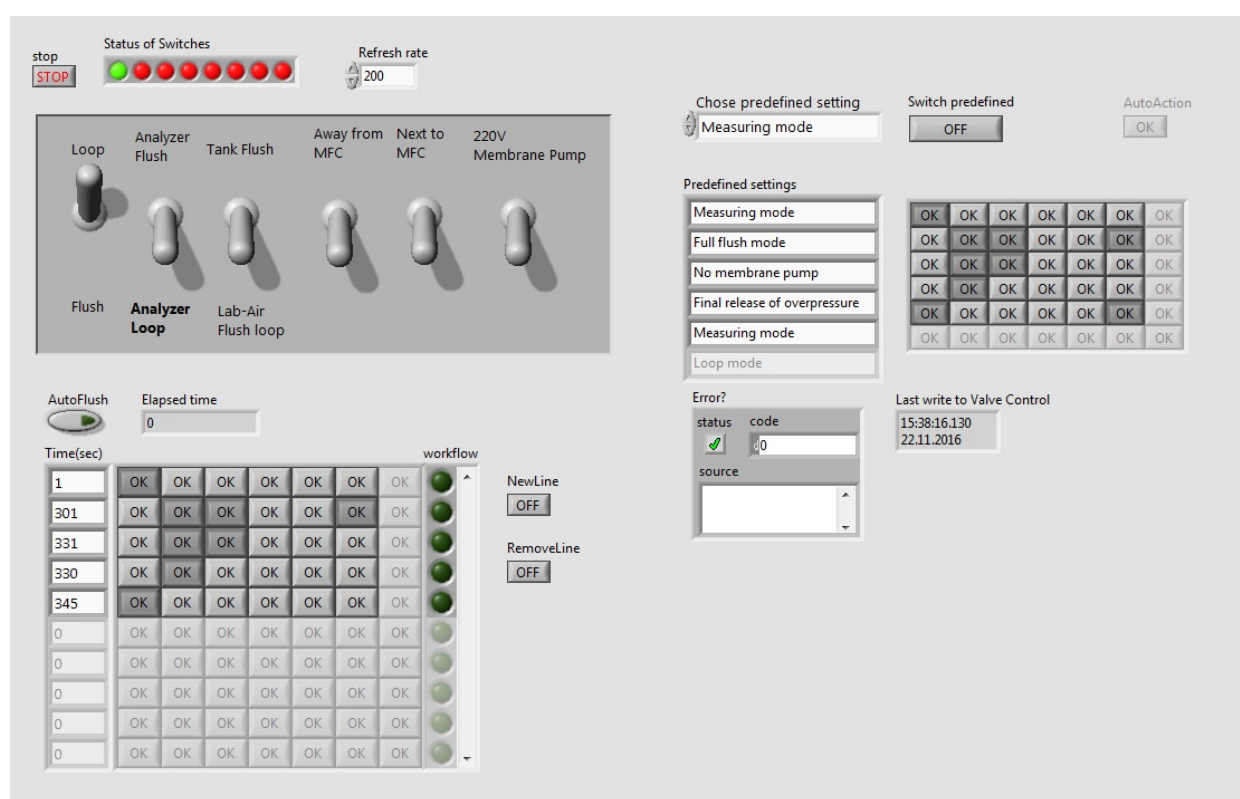


Figure 4.4: Labview script used for automatic control of the incubation flush.

so that the CRDS analyzer and the bacterial chamber can be flushed separately, allowing different flushing procedures for the CRDS analyzer and the bacterial chamber. Both flushing procedures are controlled via a labview script (see Fig. 4.4). The complete flushing sequence lasts 345 seconds, of which the incubation flush sequence is divided into 4 steps. 1) 0-300 seconds: the incubation chamber is flushed with the F-gas while the membrane pump is installed downstream and directs the gas to vent. 2) 300-330 seconds: incubation chamber is flushed with the F-gas. A slight overpressure builds up since the membrane pump

is disconnected. 3) 330-345 seconds: the electric valve is closed and the pressure in the incubation chamber decreases to ambient pressure. 4) After 345 seconds: The 8-port valve switches to incubation mode with approximately atmospheric pressure in the entire setup. During the incubation experiments with the denitrifying bacteria, the bacterial chamber is a 1 L glass chamber. To ensure optimal evaporation from the liquid solution, the chamber is placed on top of a magnetic stirrer, and a magnetic pin is placed in the bacterial solution. The F-gas used is pure N₂ (purity 99.9999 %), since the denitrifying bacteria only perform under anaerobic conditions.

Nitrifying bacterial production of nitrous oxide isotopomers

5.1 Introduction

The first step in the catabolic part of the nitrogen cycle is known as *nitrification*. Nitrification is defined by Stuart Chapin III et al. (2002) as "the process by which NH_4^+ is oxidized to NO_2^- and subsequently to NO_3^- ". The general definition of nitrification is divided into two distinguishable consortia of nitrifiers, namely autotrophic nitrification and heterotrophic nitrification. Heterotrophic nitrification is a biochemical oxidation of ammonium, using organic carbon as an energy source and for supply of carbon. Heterotrophic nitrifiers are mostly seen in soils with low pH-levels, high levels of dissolved oxygen, and/or ecosystems with low nitrogen availability (Wrage et al., 2001; Stuart Chapin III et al., 2002; Stein and Yung, 2003; Schreiber et al., 2012). The heterotrophic nitrification is generally more common for fungi-reactions, and the heterotrophic nitrifiers are believed to have a limited significance to the overall natural nitrification (Belser, 1979; Bremner, 1997). The heterotrophic nitrifying bacteria are (in some cases) known both to be nitrifying and denitrifying, and is therefore adding to the complexity of the natural N_2O production scheme (Wrage et al., 2001; Zhang et al., 2015). Autotrophic nitrification is described as two chemoautotrophic bacteria using energy yield from ammonium oxidation and nitrite oxidation as an energy source in production of nitrate from ammonium (Fig. 5.1). These two chemoautotrophic bacteria are defined as *ammonia oxidation bacteria (AOB)*, *nitrite oxidation bacteria (NOB)*, depending on whether the bacteria uses ammonia or nitrite to obtain energy (Belser, 1979; Bremner, 1997; Wrage et al., 2001; Stuart Chapin III et al., 2002). The autotrophic nitrification bacteria are believed to have the largest role of nitrification in natural present day soils, with the exception of forest soils as first pointed out by Schimel et al. (1984). The AOB are the primary nitrifiers, even though it is believed to be the rate

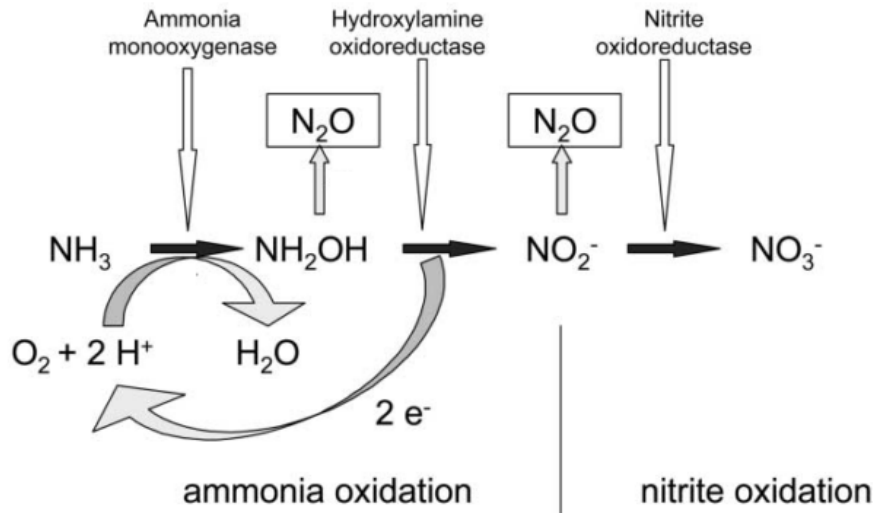


Figure 5.1: Outline of the autotrophic nitrification pathways in a slightly modified version compared to the one presented by Wrage et al. (2001).

limiting process during nitrification, because the electrons needed for oxidation of ammonia is derived from the oxidation of nitrite, and because a build up of nitrite is only rarely found naturally. The ammonia oxidation process is a two step reaction (Fig. 5.1), in which ammonia monooxygenase (AMO) is used to catalyze the first part, NH_3 to NH_2OH . The second part is the oxidation of NH_2OH to NO_2^- , during which hydroxylamine oxidoreductase (HAO) helps catalyzing the oxidation, which possibly leads to the production of N_2O through an enzymatic reaction with nitric oxide. The NOB are a bacterial community which oxidize NO_2^- to NO_3^- with the nitrite oxidoreductase enzyme as a catalyst. The second nitrifying producer of N_2O is via nitrifier denitrification (Fig. 5.1). Nitrifier denitrification is a group of AOB which additionally has the denitrifying enzymes responsible for in-turn production of NO , N_2O , and finally N_2 . (Ritchie and Nicholas, 1972; Otte et al., 1999; Wrage et al., 2001; Stuart Chapin III et al., 2002; Schreiber et al., 2012; Hu et al., 2015)

Pure nitrifying bacterial cultures and specifically chemoautotrophic bacteria are known to be slow producers of N_2O , for two essential reasons. 1) Chemoautotrophic nitrifiers use inorganic material as the energy source, though the very limited availability of sources (with low reduction potential) results in a slow growth or even no growth. The Chemoautotrophic nitrifiers have an additional energy source in the crucial enzyme hydroxylamine oxidoreductase (HAO). HAO has the ability to oxidize NH_2OH to HNO_2 from two simultaneously appearing reactions. The two reactions are only occurring simultaneously because HAO has the ability to create an electron flow in both the forward and backward direction. If the two electrons do not flow simultaneously, N_2O or NO is produced from HNO (Igarashi et al.,

1997). 2) Production of N_2O is a by-product of the nitrification process, and only a fraction of the primary production of NO_2^- is expected to lead to the N_2O produced. A qualitative analysis of the bacterial production of NO_2^- and N_2O , performed with a batch of bacteria, indicated that the expected production of N_2O was on the order of 0.25 % of the expected NO_2^- production (personal communication with S. Christensen). The bacterial batch used for the qualitative analysis was mixed like the cultures in the presented experiment (as described in section 5.2.2) and cultivated for 14 days with measurements performed once a day. Sutka et al. (2003); Sutka and Ostrom (2006) present incubation experiments in which ammonia oxidation bacteria are incubated 6 days prior to when headspace sample measurements are performed. We therefore aimed for incubation experiments lasting between one and two weeks.

The limitations caused by the slow process (lack of "easy" electrons) and the generally limited N_2O production, combined with a desire to keep the continuous measurements relatively short, led to an investigation for optimization of the expected N_2O productivity from different conditions. Nitrification is, generally speaking, an aerobic process in which oxygen is used as the electron acceptor. Different producers of N_2O (and even different species of nitrifiers) have been proven to have different pathways and to have different dependencies on the available oxygen level. Figure 5.2A shows the oxygen dependence for AOB, nitrifier denitrification, Heterotrophic denitrification, and the total N_2O production as presented by Hu et al. (2015). Hu et al. (2015) demonstrate how denitrification, nitrifier denitrification, and the total N_2O production generally decreases with increasing oxygen availability. An increasing oxygen availability results on the other hand in an increasing N_2O production from AOB. Interestingly, the ideal oxygen availability for N_2O production from nitrifier denitrification was found to be in the range of 0.5 % and 3 % O_2 . The highest contribution of total N_2O emission from the three bacterial species was found in anaerobe environments (no O_2).

Hu et al. (2015) (and authors therein) show how the pH has a strong influence on the production ratio of nitrification (and denitrification) and also on the N_2 versus N_2O ratio (see Fig. 5.2B). Studies with AOB, Heterotrophic denitrification, and the total N_2O production have been found to have a negative correlation with the production rate and $\text{N}_2/\text{N}_2\text{O}$ production ratio with an increasing pH within the range of a normal agricultural soil pH from 5 to 8. Only experiments with nitrifier denitrification bacteria have shown a positive correlation which an increasing pH. Unfortunately we did not realize this matter until after the presented measurements were accomplished, and now corrected adjustment of the pH in the media has been performed.

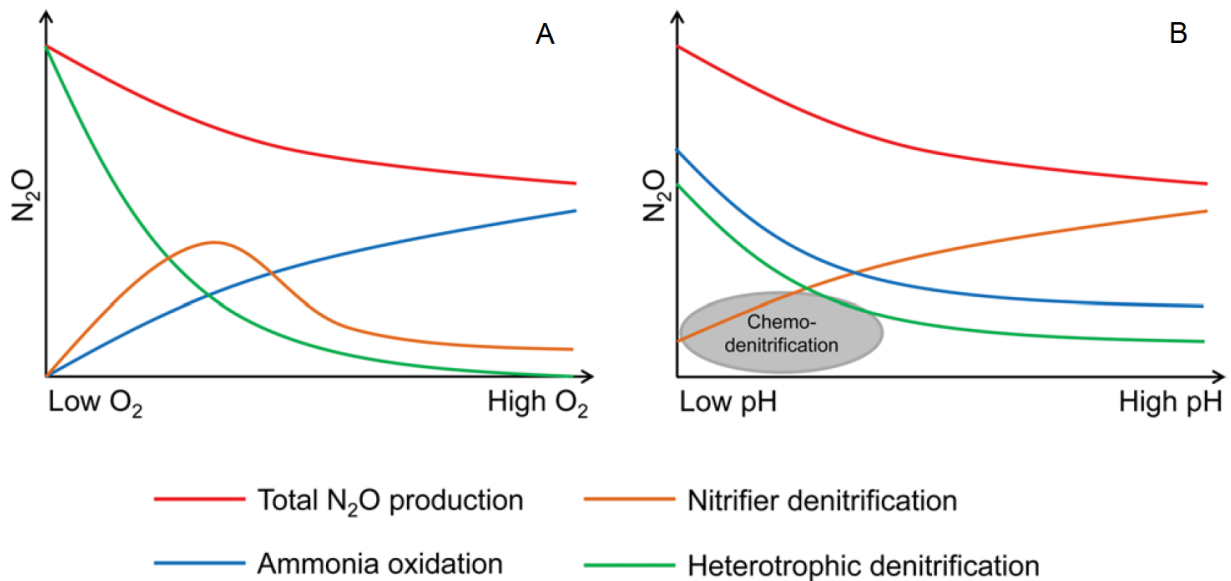


Figure 5.2: *Dependence of the total N_2O production on the oxygen level and the pH-level, for ammonia oxidation, nitrifier denitrification and heterotrophic denitrification. Representation of figure presented by Hu et al. (2015).*

5.2 Method

The scope of this study was to investigate the isotopic evolution of N_2O produced from pure nitrifying bacteria via continuous measurements during incubation experiments. Using a single nitrifying bacterial culture we determined SP during production and discovered a clear transition in SP from two different biological reactions.

5.2.1 Instrumentation

Continuously evolving N_2O production from incubated nitrifying bacteria was measured using the Picarro G5131-i CRDS analyzer (Picarro, Santa Clara, California, USA) (in the following named G5131i-CIC). The G5131i-CIC analyzer measures the concentration and isotopic composition of N_2O in the introduced gas using the non-destructive analysis method of CRDS (see section 2.1) and is therefore highly suitable for incubation experiments. Measurements are performed in the wavelength region between 2195.7 cm^{-1} and 2196.3 cm^{-1} , which allows for distinct measurements of $^{15}N^\alpha$, $^{15}N^\beta$, and $N_2^{18}O$. The official performance specifications were promised to give optimal measurements within the measuring range of 300 ppb to 1500 ppb. Over the experimental measuring period, the typical measured precision averaged over 10 minutes was 0.37 ppb, 3.75 ‰, and 2.85 ‰ for N_2O concentration, N_2O isotopomers, and $N_2^{18}O$, respectively.

The presented experiments were designed to secure continuous measurements of the complete evolution and validation of the resulting measurements. We increased the accuracy of the measurements by installing the leak-reduced pump (2.1) downstream from the G5131i-CIC analyzer. Thereby we decreased the leak rate in the incubation setup, hence the leak rate was measured to be approximately 1 ppb h^{-1} . We deliberately kept the total pressure in the incubation system above ambient. The leaking out from the system will to some degree hinder N_2O leaking into the system and mixing with the bacterial produced N_2O signal.

5.2.2 Pure bacterial cultures

The most studied species of ammonia oxidation bacteria (AOB) belongs to the family named *Nitrosomonas* and *Nitrosococcus*, but to our knowledge no continuous measurements have been performed on a pure nitrifying bacterial culture. The presented continuous incubation experiments were performed with the ammonia oxidation bacteria named *Nitrosomonas mobilis* NC2. *Nitrosomonas mobilis* is a Gram-negative bacteria and belongs to the family with the most studied AOB culture of *Nitrosomonas europaea*, which has been studied a number of times for multiple characteristics including the resulting SP from incubation experiments (Wrage et al., 2001; Sutka et al., 2003; Sutka and Ostrom, 2006) (and others). The culture batch used in the continuous incubation experiments was grown from cultures in stock at the Department of Plant and Environmental Science, Microbial Ecology and Biotechnology, University of Copenhagen.

The cultures were mixed with, and incubated in, 200 mL of growth medium. An 800 mL growth medium batch of liquid solution consists of 0.5 g $(\text{NH}_4)_2\text{SO}_4$, 0.2 g KH_2PO_4 , 20 mg $\text{CaCl}_2 \cdot 2\text{H}_2\text{O}$, 40 mg $\text{MgSO}_4 \cdot 7\text{H}_2\text{O}$, 3.8 mg FeNaEDTA , and 1 mL of a 100 mL trace element solution of 0.01 g $\text{NaMoO}_4 \cdot 2\text{H}_2\text{O}$, 0.2 g MnCl_2 , 0.0002 g $\text{CoCl}_2 \cdot 6\text{H}_2\text{O}$, 0.01 g $\text{ZnSO}_4 \cdot 7\text{H}_2\text{O}$, 0.02 g $\text{CuSO}_4 \cdot 5\text{H}_2\text{O}$. The medium was pH adjusted to approximately 7.5 using 10M NaOH, before 50 mL of medium solution was poured into 117 mL serum bottles and autoclaved. 0.5 mL of 1.26 g NaHCO_3 / 100 mL was added through a sterile filter.

5.2.3 Incubation experiment

The continuous incubation experiments were performed with the incubation setup as presented in a simplified schematic in Fig. 5.3 and described in detail in section 4.1. The incubation setup was slightly modified (compared to the setup used for denitrification experiments), because the glass chamber was replaced by a 250mL stainless steel chamber (4

cm inner diameter and 19.9 cm inner length) and the magnetic stirrer was removed from the setup. The incubation setup was estimated to have a total volume of approximately 325 mL, including the 250 mL chamber, 700 cm 1/8" ss tubing, 150 cm 1/16" tubing, the ascarite trap, the nafion unit, and the cavity in the G5131i-CIC analyzer. The F-gas used for the nitrifying bacterial experiments, was a synthetic air mixture (20.1 % O₂ and 79.9 % N₂, purity 99.999 %) since nitrifying bacteria are most active under aerobic conditions. The concentration of N₂O present in the F-gas was measured prior to each individual experiment. The initial N₂O concentration in experiment #1 was 10 ppb, while the initial N₂O concentration was 330 ppb in experiment #2. This change in starting concentration is believed not to have any influence on the experiment since all gases used were of the same purity, and since measurements from concentrations lower than 200 ppb were discarded from experiment #1 due to the instability of the analyzer when measuring at low concentrations.

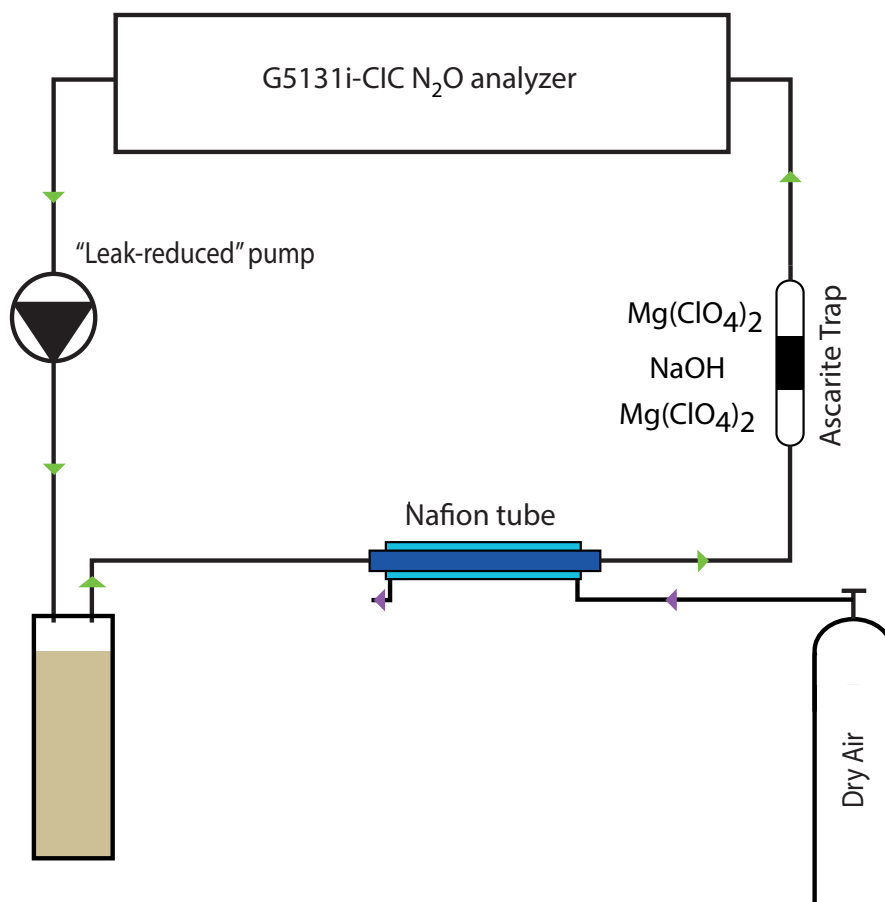


Figure 5.3: *Simplified schematic of the modified incubation setup. The green and the purple arrows show the flow direction of the measuring gas and the purge gas, respectively.*

In the presented experiments, two bacterial solutions of 40 mL of medium mixed with 1 mL of *Nitrosomonas mobilis* culture were used (C1a and C1b respectively). The bacterial solutions were mixed in a sealed 117 mL glass flask with one month separation and stored at room temperature (25 °C) before use, to secure similar conditions for both bacterial solutions. After 14 days of static incubation, 1 mL of gas was taken from the headspace of solution C1a using a syringe. The C1a gas was measured directly with a gas chromatograph (SRI 8610C), to ensure production of N₂O prior to incubation, because of living bacteria in the batch. The second solution (C1b) was used for the incubation experiments. For these experiments 7 mL of bacterial solution was extracted from C1b, mixed with 200 mL of medium and stirred before being poured into the incubation chamber. Once the newly mixed bacterial batch was placed in the incubation setup, the setup was flushed using the described method (section 4.1), before continuous measurements of the incubated nitrifying bacterial N₂O evolution started.

5.2.4 Data calibration and correction

The continuously measured evolution of nitrification produced N₂O was calibrated with respect to the isotopes using the four working standards (see section 3.3). Measurements of the four working standards were performed prior to, and in extension to, the nitrifying bacterial incubation experiments. The two sets of standard CIC-MPI gases (CIC-MPI-1, CIC-MPI-2 and CIC-MPI-1.2, CIC-MPI-2.2) are all anchored to atmospheric N₂, and they were all measured four times with the G5131i-CIC analyzer. Additionally, CIC-MPI-1 and CIC-MPI-2 were measured with the G5101i-CIC analyzer, measurements which are included in the statistical analysis. The standard gases were all measured at both the Centre for Ice and Climate (CIC), University of Copenhagen, Denmark, and at the Institute for Marine and Atmospheric research Utrecht (IMAU) in the Netherlands. The standard gases CIC-MPI-1 and CIC-MPI-2 were additionally measured at the Tokyo Institute of Technology (Tokyo-Tech) in Japan. The average and combined standard deviation of the N₂O concentration and isotopic composition are specified in Table 5.1 for the four standards.

Measurements performed with the G5131i-CIC analyzer experienced an isotopic offset caused by baseline ripples in the cavity of the analyzer. As shown in section 3.1, this isotopic offset is dependent on the concentration of the measured gas, hence a correction of the CRDS concentration dependence is required for the true isotopic signature of the sample to be known. The correction applied to the presented bacterial nitrification measurements is presented in section 3.1. All measurements were performed with a synthetic air mixture (20.1 % O₂ and 79.9 % N₂, purity 99.999 %) and the O₂ mixing ratio was therefore always at 100 % of the

Table 5.1: *Measurements of the four CIC-MPI standard gases. The listed values for CIC-MPI-1 and CIC-MPI-2 are mean-values and standard deviation (σ) from measurements at CIC only. The listed values for CIC-MPI-1.2 and CIC-MPI-2.2 are the mean-values and combined standard deviations (σ) of measurements performed at CIC and IMAU.*

Std. gas	[N ₂ O] (ppb)	$\delta^{15}\text{N}^{bulk}$ (‰)	$\delta^{15}\text{N}^{\alpha}$ (‰)	$\delta^{15}\text{N}^{\beta}$ (‰)	$\delta^{18}\text{O}$ (‰)
CIC-MPI-1	1893.3 ± 4.2	1.82 ± 3.73	2.08 ± 4.15	1.50 ± 3.88	39.10 ± 3.06
CIC-MPI-2	1804.0 ± 2.3	-1.60 ± 2.96	12.12 ± 3.45	15.34 ± 3.25	40.57 ± 2.08
CIC-MPI-1.2	1733.2 ± 8.9	2.63 ± 1.00	2.99 ± 1.27	2.27 ± 1.23	42.98 ± 0.74
CIC-MPI-2.2	1563.5 ± 9.6	-0.50 ± 1.01	12.34 ± 1.24	-13.35 ± 1.20	44.02 ± 0.78

atmospheric air (e.g. 21 ‰) and no oxygen-dependent correction is therefore needed.

5.3 Results

The experiments with the ammonia oxidation bacteria (*Nitrosomonas mobilis*) resulted in measurements from two temporal stages of the original bacterial batch. The incubation experiments with each of the two bacterial batches were continuously measured for concentration and isotopic composition of N₂O using the G5131i-CIC analyzer. Figure 5.4 shows the continuous evolution of N₂O for the first and second batches in green and blue, respectively. Both bacterial evolutions have the same overall characteristics, with a rapid increase followed by a decreasing production rate. For the first batch, the rapid increase is longer while the production rate ends up being significantly lower than for the second batch. The decreased production rate is believed to be due to a clogged ascarite trap which was discovered after approximately 100 hours. The clogged ascarite trap is also the reason why the measurements of the first batch was stopped after only 121.4 hours. The second batch was stopped after 235 hours because we ran out of purge gas for the nafion unit, which could have caused severe damage to the analyzer if the experiment continued. The average N₂O production rate over the entire incubation is calculated to be 1.14 ppb per hour per 100 mL (volume) and 0.60 ppb per hour per 100 mL (volume) for the first and second experiments, respectively.

Figure 5.5 shows the continuous evolution of the isotopic composition of N₂O for the first batch. Both isotopomers (Fig. 5.5A and 5.5B) experience an increasing production rate for the first 60 hours, after which the the production rate slows down a little and seems to be oscillating from this point on. The continuous evolution of $\delta^{18}\text{O}$ -N₂O (Fig. 5.5C) indicates

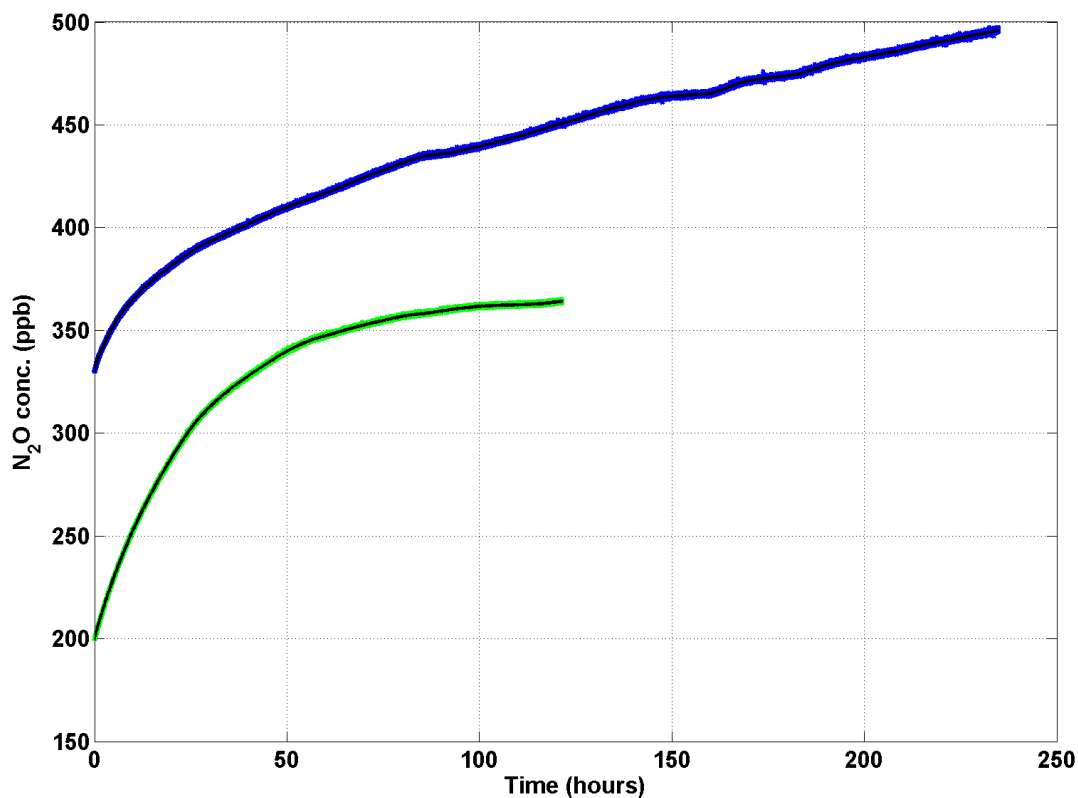


Figure 5.4: *The continuous N_2O concentration evolution from incubation of a *Nitrosomonas mobilis* solution. The first batch measured is in green. The second batch measured is in blue. The 5 minutes running mean is plotted in black.*

a very rapid enrichment of 60 ‰ within the first 23 hours, followed by a depletion of 0.0075 ‰/h resulting in an average of $48.09 \text{ ‰} \pm 4.76$. The $\delta^{15}N^{bulk}$ signal (Fig. 5.5D) results in a gradual enrichment from $-38.79 \text{ ‰} \pm 3.87$ to $-5.55 \text{ ‰} \pm 2.93$. The SP (Fig. 5.5E) resulted in a more stable signal. The SP start out at $39.29 \text{ ‰} \pm 5.00$ and experienced a slow depletion over the following 121.4 hours, leading to an average SP over the full incubation period of $34.91 \text{ ‰} \pm 4.69$.

Figure 5.6 shows the continuous evolution of the isotopic composition of N_2O from the second batch. The second batch was made from the same original solution as the first batch, only the second batch was made 11 days later than the first. Figure 5.6A and 5.6B show the evolution of the two isotopomers. The isotopic signature has a similar pattern for the two isotopomers for the first 115 hours. First a relatively short rapid decrease, followed by a roughly constant level. The $\delta^{15}N^{\alpha}$ value is thereafter increasing for approximately 25 hours while $\delta^{15}N^{\beta}$ decreases (with a slower rate) for the rest of the experiment. The $\delta^{15}N^{\alpha}$ stabilizes after 147 hours and is continuous at this constant level throughout the experiment. The synchronized yet different pattern of the two isotopomers resulted in an approximately

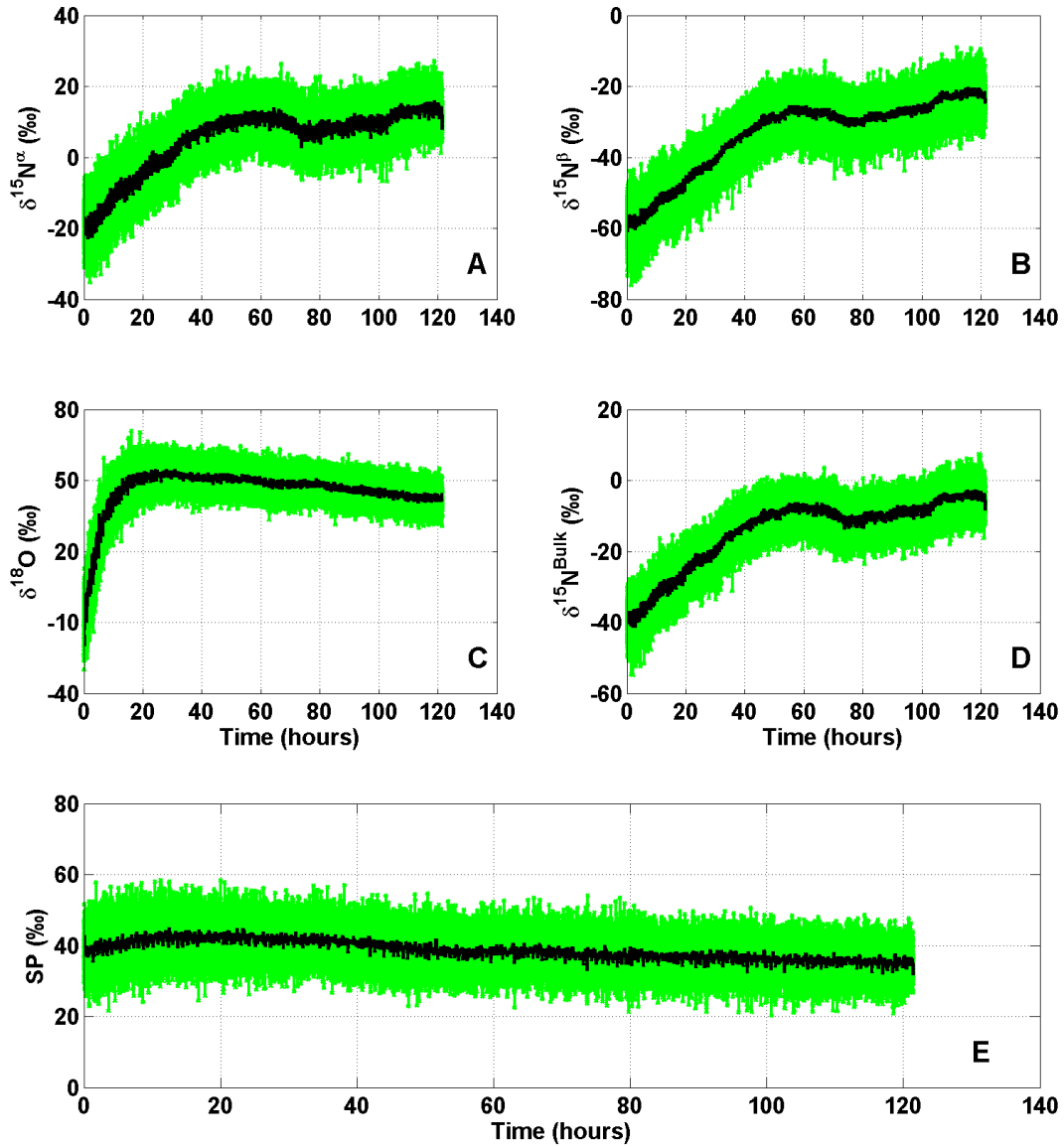


Figure 5.5: The continuously accumulated isotopic signature from the first batch of incubated *Nitrosomonas mobilis* bacteria. The five sub-figures present A) $\delta^{15}N^{\alpha}$, B) $\delta^{15}N^{\beta}$, C) $\delta^{18}O$ - N_2O , D) $\delta^{15}N^{bulk}$, and E) SP. In all sub-figures the high resolution CRDS data is shown in green, and five minutes running average in black.

constant $\delta^{15}N^{bulk}$ signal (Fig. 5.6D), that was only intercepted by a bump after 147 hours and the clear decrease in the beginning of the experiment. This resulted in an average $\delta^{15}N^{bulk} = -76.50 \text{ ‰} \pm 10.63$ for the first 147 hours followed by an average $\delta^{15}N^{bulk} = -75.02 \text{ ‰} \pm 3.92$ for the last 60 hours. The isotopomer signal resulted in a three step evolution for SP (Fig. 5.6E). 1) An approximately constant SP signature at $1.74 \text{ ‰} \pm 4.74 \text{ ‰}$, with the 5 minutes running mean starting at 5 ‰ and slowly decreasing to -4.5 ‰ . 2) A shift in SP with increasing SP from hour 115 to hour 193. 3) An approximately constant SP

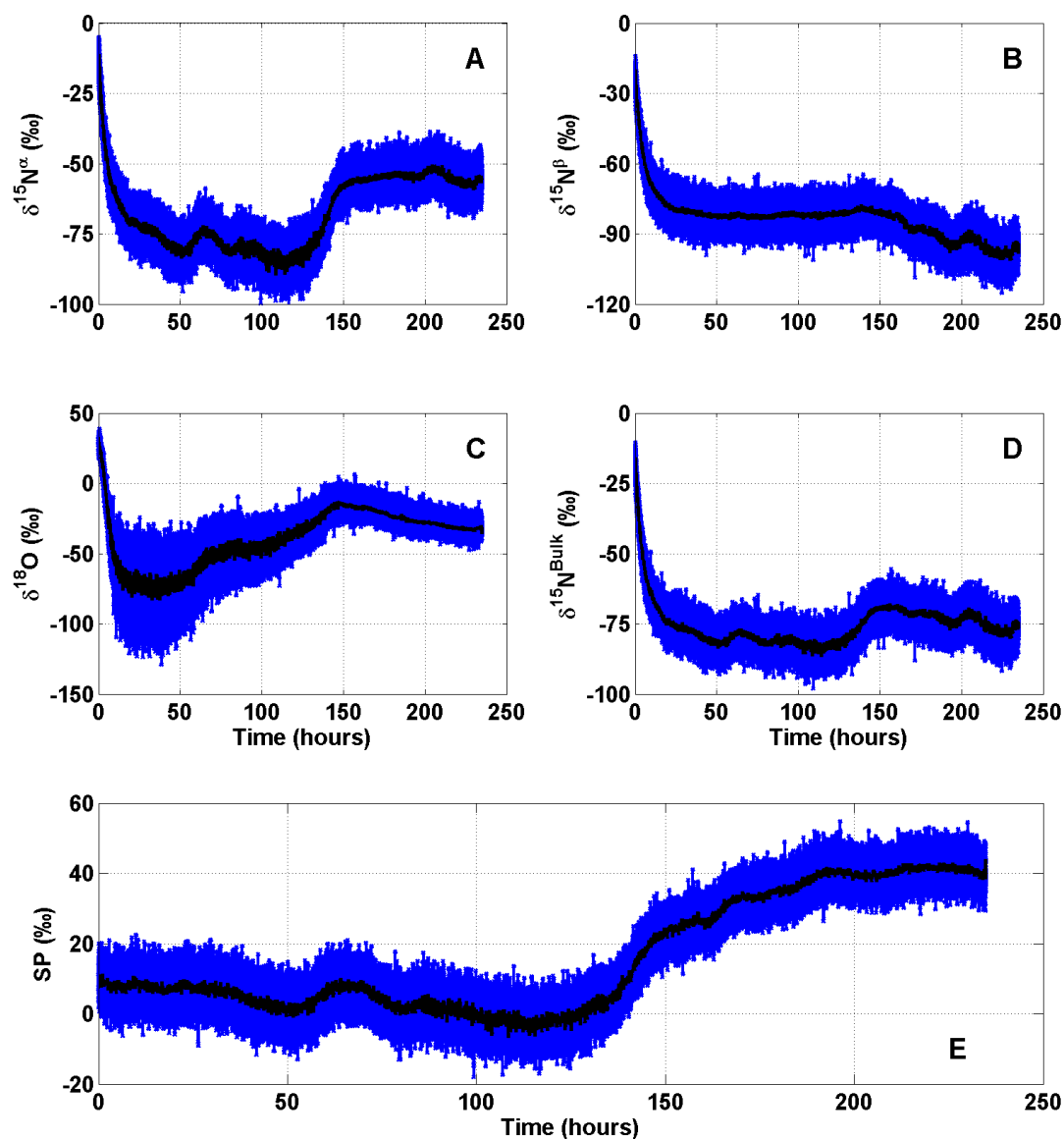


Figure 5.6: *The continuously accumulated isotopic signature from the second batch of incubated Nitrosomonas mobilis bacteria. The five sub-figures present A) $\delta^{15}N^{\alpha}$, B) $\delta^{15}N^{\beta}$, C) $\delta^{18}O-N_2O$, D) $\delta^{15}N^{bulk}$, and E) SP. In all sub-figures the high resolution CRDS data is shown in blue, and five minutes running average in black.*

signature at $39.25 \text{ ‰} \pm 3.28 \text{ ‰}$. The $\delta^{18}O-N_2O$ signal (Fig. 5.6C) generally has a very large uncertainty, though investigation of the 5 minutes running mean indicate a potential 3 step signature change. 1) Hour 19 - 54: a relatively constant level at $-72.06 \text{ ‰} \pm 3.18$. 2) Hour 69-147: A steady increasing trend with potential isotope fractionation. 3) Hour 147 and onward: A slowly depleting $\delta^{18}O-N_2O$ level with an average declination of 0.24 ‰/h .

5.4 Discussion

5.4.1 Production rate

N₂O produced from ammonia oxidation bacteria is expected to be a very slow process because of the restrictions caused by the limited energy sources and N₂O only being a by-product. The incubation experiments presented in this chapter, were expected to last for somewhere between one and two weeks because of a very slow N₂O production rate from the *Nitrosomonas mobilis* bacteria. It was intended to run the incubation experiments up to a N₂O concentration of 1500 ppb, the upper limit of the measuring range of the analyzer. Because of a clogged ascarite trap the incubation time for the first batch was only 121.4 hours with an accumulated concentration of 363.96 ppb. The second batch was continuously measured in the incubation setup for 235 hours, but had to be stopped at 496.52 ppb because of missing purge gas for the nafion unit. On average, the two batches of *Nitrosomonas mobilis* bacteria had a N₂O production rate of 1.14 ppb/h per 100 mL and 0.60 ppb/h per 100 mL, respectively. Sutka and Ostrom (2006) presented incubation experiments of the ammonia oxidation bacteria, *Nitrosomonas europaea*. In those incubation experiments, Sutka and Ostrom (2006) incubated the bacterial solution for 6 days before four headspace samples were taken from the serum bottles and measured. On average the four headspace samples measured 2.825 μ M or 124.34 ppb N₂O, which results in an average N₂O production rate of approximately 0.62 ppb/h per 100 mL, given the 139.5 mL headspace of the used serum bottles. The results from Sutka and Ostrom (2006) were therefore in the same range as what was measured from the presented experiments.

5.4.2 A changing site preference

Park et al. (2011) combined SP measurements from many studies of both nitrification, denitrification, and nitrifier denitrification experiments. Their review lead to the general conclusion that the different bacterial groups can be distinguished from the isotopic composition of the produced N₂O. Multiple studies of pure bacterial cultures and soil incubation experiments have shown that N₂O produced from nitrification results in SP values from 11 ‰ (in pure bacterial cultures (Sutka et al., 2004)) to 46 ‰ (in unfertilized temperate arable soils (Cardenas et al., 2007)). As also explained in chapter 6, N₂O emitted from denitrifying bacterial production has resulted in SP values ≤ 2 ‰. Finally, N₂O produced from nitrifier denitrification has been found to have SP values similar to those measured from denitrification (Toyoda et al., 2005; Sutka and Ostrom, 2006).

The first incubation experiment with *Nitrosomonas mobilis* showed an average SP of $34.91 \text{ ‰} \pm 4.69$. The SP value of this nitrifier is in line with previous findings, which clearly indicates the producing bacteria being from the nitrifying bacteria family. It should be taken into consideration that the actual N_2O production started prior to the presented measurements, and that the full evolution is therefore not presented. Likewise is it noteworthy that the production rate found during this experiment was 57 % higher than the average production rate measured by Sutka and Ostrom (2006), even though the production rate over the first 30 hours was significantly higher than the overall average production rate.

The second incubation experiment showed a partly different isotopic signal. The accumulated SP measured over the first 115 hours, was found to be $1.74 \text{ ‰} \pm 4.74 \text{ ‰}$. In comparison, the accumulated SP was measured over the last 60 hours found to be $39.25 \text{ ‰} \pm 3.28 \text{ ‰}$. This clear difference in isotopic signature suggests a change in the N_2O producing reaction. Beaumont et al. (2002, 2004) wrote how the enzyme nitrite reductase (NirK) is a widespread enzyme throughout the ammonia oxidation bacterial community. The presence of NirK would allow the bacterial community to "remove" NO_2^- from the solution, by production of NO and N_2O , and thereby would be in the group of nitrifier denitrification bacteria. This would furthermore detoxify the solution for the nitrifying bacterial enzymes, hence leading to ammonia oxidation. This is only possible because it was discovered that nitrifier denitrification can happen under aerobic conditions (Shaw et al., 2006). The *Nitrosomonas mobilis* bacterial solution from which the incubated batch was made, was 11 days older than the bacterial solution used for the first batch. Other than this, the two bacterial batches were identical with the same amount of medium used. It can therefore be assumed that the bacterial solution used for the second batch included active NirK enzymes. It can furthermore be assumed that neither the bacterial solution nor the medium was clean from NO_2^- . It is therefore hypothesized that the presented incubation experiment can be divided into 1) nitrifier denitrification, 2) transition zone, and 3) nitrification, as indicated in Fig. 5.7. 1) The low SP values found during the first 115 hours of the incubation is a signal of nitrifier denitrification produced N_2O . This suggested nitrifier denitrification would "clean" the solution for NO_2^- , while producing NO, N_2O , and finally N_2 . 2) The ammonia oxidation bacterial enzymes gradually overtake the production of N_2O in the solution, while the NirK enzymes gradually stop or significantly decrease production. 3) After 193 hours the ammonia oxidation bacteria become the primary producer of N_2O in the system, and N_2O is produced as a by-product from the oxidation of NH_2OH .

Wunderlin et al. (2012) studied the N_2O production in biological wastewater treatment under both nitrifying and denitrifying conditions and discovered indications that high NH_4^+

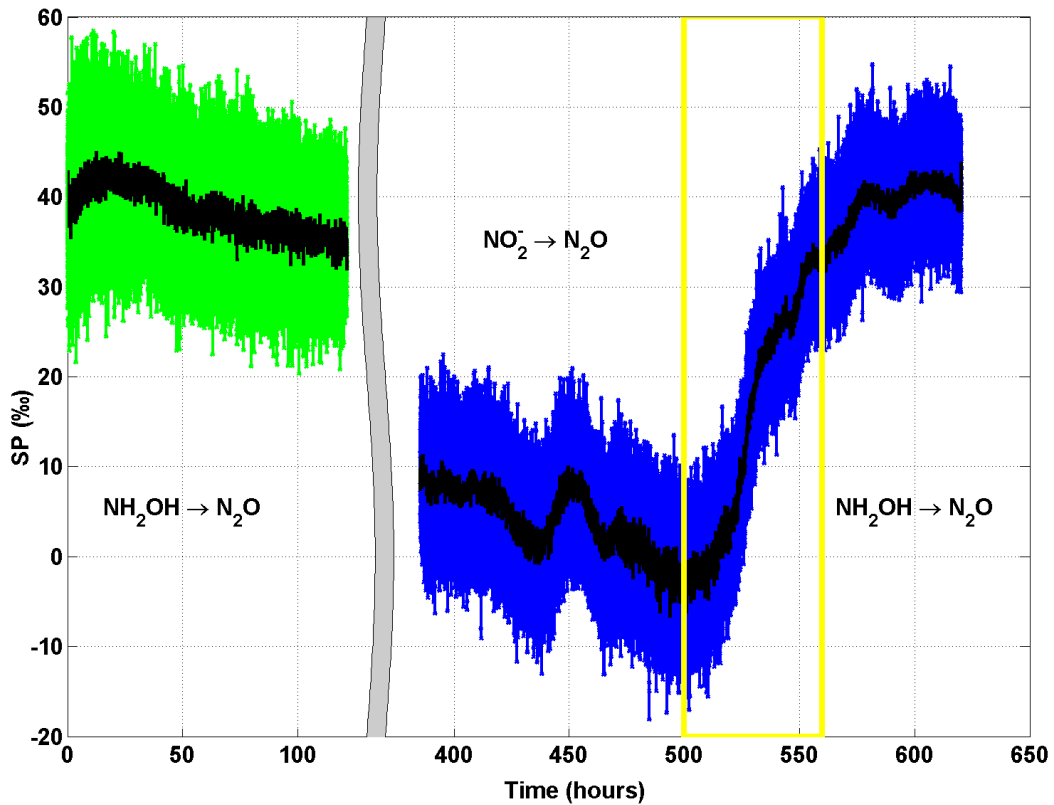


Figure 5.7: Combined SP record from the two incubation experiments. Green profile is the first incubation experiment. Blue profile is the second incubation experiment. Yellow box indicates the transition period. The suggested primary N_2O producing reaction is written in the respective sections.

combined with low NO_2^- increases N_2O production from AOB while high NO_2^- levels combined with low NH_4^+ levels increases N_2O production from nitrifier denitrification. Wunderlin et al. (2013) found similar results and showed distinct experiments with NO_2^- reduction and NH_3 oxidation, due to nitrifier denitrification and AOB respectively. The experiments presented by Wunderlin et al. (2013) resulted in average $\delta^{15}N^{bulk} = -63.82 \text{ ‰} \pm 6.97$ and $SP = -1.86 \text{ ‰} \pm 1.42$ for NO_2^- oxidation and $\delta^{15}N^{bulk} = -69.23 \text{ ‰} \pm 5.81$ and $SP = 28.16 \text{ ‰} \pm 2.23$ for experiments interpreted to stem from between 75% and 100 % NH_2OH oxidation. A similar isotopic signal of the two resulting reactions was presented by Peng et al. (2014). SP values resulting from the presented experiments are therefore in line with SP values presented by Wunderlin et al. (2013); Peng et al. (2014) and support the hypothesis of a temporally changing primary N_2O producer.

The $\delta^{15}N^{bulk}$ values are on the other hand partly indicating different signals. The presented $\delta^{15}N^{bulk}$ signal resulted in an increasing trend from $-38.79 \text{ ‰} \pm 3.87$ to $-5.55 \text{ ‰} \pm 2.93$ in the

first experiment. The second experiment resulted in significantly depleted $\delta^{15}\text{N}^{bulk}$ signal of $-76.50 \text{ ‰} \pm 10.63$ for the first 147 hours and $-75.02 \text{ ‰} \pm 3.92$ during the potential NH_3 oxidation in the end of the experiment. The second experiment is therefore in line with the results presented by Wunderlin et al. (2013); Peng et al. (2014) whereas the first experiment show significantly enriched $\delta^{15}\text{N}^{bulk}$ values. The strong depletion of $\delta^{15}\text{N}^{bulk}$ is similar to the bulk fractionation effect as presented in chapter 6. That $\delta^{15}\text{N}^{bulk}$ presented in this study is more heavily depleted than the $\delta^{15}\text{N}^{bulk}$ produced from denitrification and is hypothesized to be due to different bacterial species leading to slightly different values. N_2O produced through both nitrifier denitrification and denitrification are believed to be the result of the same sequence of reactions starting with NO_2^- . We therefore hypothesize that the strongly depleted $\delta^{15}\text{N}^{bulk}$ originates from the same processes as indicated in chapter 6, hence 1) a difference in production rates, and 2) mass-dependent fractionation associated with nitrous oxide reductase. This would imply the reduction rate of N_2O being significantly smaller than the net production, since we do not observe a decreased net production rate of in the second incubation experiment.

5.4.3 Oxygen isotope as reaction indicator

Combining continuous N_2O isotopomer measurements with measurements of $\delta^{18}\text{O}-\text{N}_2\text{O}$ over the same bacterial N_2O evolution should in principle allow for improved evaluation of the processes involved. The isotopomers indicated a three step evolution of the merged experiments (Fig. 5.7) while the $\delta^{18}\text{O}-\text{N}_2\text{O}$ signal indicates a four step evolution.

Sutka et al. (2003, 2004) presented incubation experiments in which nitrifying bacteria *Nitrosomonas europaea* was cultivated for 3 days with either NH_2OH or NO_2^- as the substrate, which resulted in N_2O production from AOB and nitrifier denitrification, respectively. The incubation experiments with AOB resulted in $\delta^{18}\text{O}-\text{N}_2\text{O}$ values of $26.5 \text{ ‰} \pm 6.3$ while experiments with nitrifier denitrification resulted in $\delta^{18}\text{O}-\text{N}_2\text{O}$ values of $8.8 \text{ ‰} \pm 1.4$ (Sutka et al., 2003, 2004). Sutka et al. (2003, 2004) showed experiments with four different trace element solutions resulting in a general trend that enrichment in SP appears synchronous with enrichment of $\delta^{18}\text{O}-\text{N}_2\text{O}$. Assuming this synchronous enrichment applies to all nitrifying AOBs, allows for verification that the average $\delta^{18}\text{O}-\text{N}_2\text{O}$ values of $48.09 \text{ ‰} \pm 4.76$ measured during the first experiment stems from NH_2OH oxidation (green profile in Fig. 5.8).

From the evaluation of SP it is hypothesized that the second experiment indicates N_2O from NO_2^- reduction during the first 115 hours followed by a transition period and finally a period with N_2O originating from NH_3 oxidation during the last 60 hours. The $\delta^{18}\text{O}-\text{N}_2\text{O}$

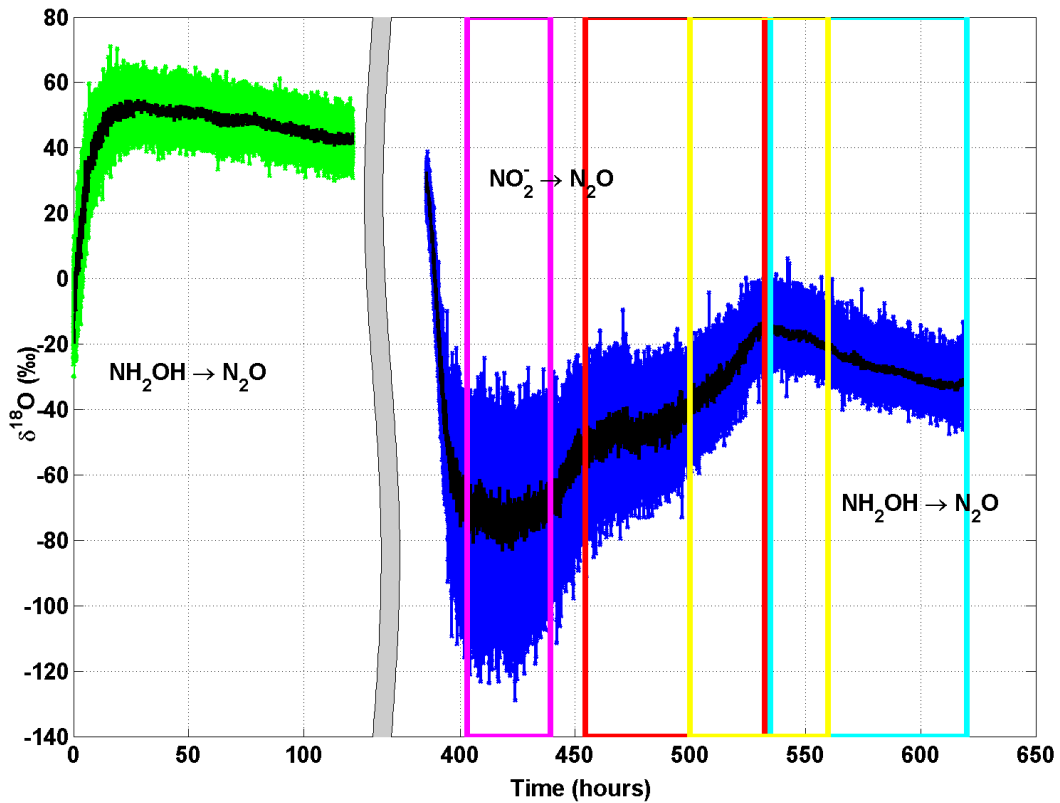


Figure 5.8: Combined $\delta^{18}\text{O}\text{-N}_2\text{O}$ record from the two incubation experiments. Green profile is the first incubation experiment. Blue profile is the second incubation experiment. Yellow box indicates the transition period between the two N_2O producing reactions. The suggested primary N_2O producing reaction is written in the respective sections. Magenta, red, and cyan boxes indicate the three sections in discussion.

signal during the second experiment resulted in the following three step pattern.

1) A constant $\delta^{18}\text{O}\text{-N}_2\text{O}$ level of $-72.06 \text{‰} \pm 3.18$ continues while N_2O production primarily originates from NO_2^- reduction (magenta box in Fig. 5.8). The strongly depleted $\delta^{18}\text{O}\text{-N}_2\text{O}$ values are hypothesized to be due to mass dependent fractionation of N_2O to N_2 (as explained in chapter 6). Mass dependent fractionation of N_2O to N_2 would additionally lead to enrichment in $\delta^{18}\text{O}\text{-H}_2\text{O}$. Sigman et al. (2001) and Casciotti et al. (2002, 2007) investigated the evolution of $\delta^{18}\text{O}$ from NO_3^- and NO_2^- to N_2O and have not found $\delta^{18}\text{O}$ signals as depleted as those presented here. because Sigman et al. (2001) and Casciotti et al. (2002, 2007) used denitrifying bacteria lacking an active N_2O reductase (enzyme), the effect of mass dependent fractionation was not investigated. In addition, it is hypothesized that the working nitrite reductase (NiR) is of the heme-type. Ye et al. (1991) investigated denitrifying bacterial N_2O production and describe how different nitrite reductase enzymes

(heme-type NiR or copper-type NiR) result in significantly different oxygen exchange with H₂O during NO₂⁻ reduction with a relatively large exchange found from organisms with heme-type NiRs. The working NiR enzyme in *Nitrosomonas mobilis* has unfortunately not been determined, though the NiR enzymes are hypothesized to be of the heme-type because of the large depletion in δ¹⁸O-N₂O.

2) A gradually increasing δ¹⁸O-N₂O signal following what appears to be Rayleigh fractionation (red box in Fig. 5.8). It is hypothesized that AOB enzymes are activated resulting in NO₂⁻ production. NO₂⁻ is hypothesized to be enriched in δ¹⁸O-NO₂⁻ due to production of NO₂⁻ via a reaction between NH₂OH and H₂O enriched in δ¹⁸O. Production of enriched NO₂⁻ leads to gradual enrichment of δ¹⁸O-N₂O. The constant net N₂O production rate is hypothesized (Fig. 5.4) to indicate that either NH₃⁻ oxidation or NO₂⁻ reduction is favored as primary reaction which would imply that the second step is a transition between the two primary reactions.

3) The δ¹⁸O-N₂O signal indicates a shift in reactions after 147 hours followed by a constant depleting signal (cyan box in Fig. 5.8). The offset between the section in discussion and the average δ¹⁸O-N₂O values of 48.09 ‰ measured during the first experiment is hypothesized to originate from the changing δ¹⁸O-H₂O composition, and NH₂OH oxidation is therefore hypothesized to be the primary N₂O producing reaction from hour 147. The synthetic air bottle used in the second experiment was unfortunately not measured and the original isotopic composition is therefore unknown. It is therefore possible that the generally depleted δ¹⁸O-H₂O signal during the second experiment compared to the first experiment is to some degree due to a change in isotopic composition of O₂ in the synthetic air used as the F-gas.

5.5 Conclusion

Continuous incubation experiments have successfully been performed with N₂O producing ammonia oxidation bacteria, *Nitrosomonas mobilis*. The first experiment showed continuous SP values (SP = 34.91 ‰ ± 4.69) within the expected range for nitrification and continuously increasing enrichment of δ¹⁵N^{bulk}. The second experiment is hypothesized to show the transition between nitrifier denitrification (SP = 1.74 ‰ ± 4.74 and δ¹⁵N^{bulk} = -76.50 ‰ ± 10.63) followed by nitrification (SP = 39.25 ‰ ± 3.28 and δ¹⁵N^{bulk} = -75.02 ‰ ± 3.92). The continuously increasing δ¹⁵N^{bulk} in the first experiment is hypothesized to be a result of the direct kinetic isotope effect, whereas the strongly depleted δ¹⁵N^{bulk} signal during the second experiment is hypothesized to stem from mass dependent fractionation of N₂O. Analysis of the oxygen signal show δ¹⁸O-N₂O values during the first experiments in

line with previously presented results from AOB N_2O production. The second experiment was interpreted as a signal of changing primary N_2O producing reaction between NH_2OH oxidation and NO_2^- reduction, hence *Nitrosomonas mobilis* is a nitrifier denitrification bacteria. We additionally suggest the existence of heme-type NiR enzyme and mass-dependent fractionation being responsible for the large depletion during the second experiment. The experiments unfortunately lack a complete continuous evolution and additional incubation experiments combined with measurements of isotopic compositions of the substrate and the F-gas should be performed for verification of the hypothesis.

Continuous measurements of nitrous oxide isotopomers during incubation experiments

Malte Winther¹, David Balslev-Harder^{1,2}, Søren Christensen³,
Anders Priemé^{4,5}, Bo Elberling⁵, Eric Crosson⁶, and Thomas Blunier¹

1. Centre for Ice and Climate, Niels Bohr Institute, University of Copenhagen, Denmark
2. DFM - Danish National Metrology Institute, Kgs. Lyngby, Denmark
3. Section for Terrestrial Ecology, Department of Biology, University of Copenhagen, Denmark
4. Section for Microbiology, Department of Biology, University of Copenhagen, Denmark
5. Center for Permafrost, Department of Geosciences and Natural Resource Management, University of Copenhagen, Denmark
6. Picarro Inc, Santa Clara, CA 95054 USA

This chapter is going to be resubmitted in a slightly modified version, as M. Winther et al.:
Continuous measurements of nitrous oxide isotopomers during incubation experiments.

Abstract

Nitrous oxide (N_2O) is an important and strong greenhouse gas in the atmosphere and part of the climate on Earth. N_2O is produced by microbes during nitrification and denitrification in terrestrial and aquatic ecosystems. The main sinks for N_2O are turnover by denitrification and photolysis and photo-oxidation in the stratosphere. In the linear $\text{N}=\text{N}=\text{O}$ molecule ^{15}N substitution is possible in two distinct positions, central and terminal. The respective molecules, $^{14}\text{N}^{15}\text{N}^{16}\text{O}$ and $^{15}\text{N}^{14}\text{N}^{16}\text{O}$, are called isotopomers. It has been demonstrated that N_2O produced by nitrifying or denitrifying microbes exhibits a different relative abundance of the isotopomers. Therefore, measurements of the site preference (difference in the abundance of the two isotopomers) in N_2O can be used to determine the source of N_2O i.e. nitrification or denitrification. Recent instrument development allows for continuous position dependent $\delta^{15}\text{N}$ measurements at N_2O concentrations relevant for studies of atmospheric chemistry. We present results from continuous incubation experiments with denitrifying bacteria, *Pseudomonas fluorescens* (producing and reducing N_2O) and *Pseudomonas chlororaphis* (only producing N_2O). The continuous analysis of N_2O isotopomers reveal the transient pattern (KNO_3 to N_2O and N_2 , respectively), which can be compared to previous reported site preference (SP) values. We find bulk isotopic fractionation of $-5.6\text{‰} \pm 0.9$ for *P. chlororaphis*. For *P. fluorescens*, the bulk isotopic fractionation during production of N_2O is $-42.7\text{‰} \pm 7.3$ and $9.0\text{‰} \pm 4.2$ during N_2O reduction. The values for *P. fluorescens* are in line with earlier findings, whereas the values for *P. chlororaphis* are larger than previously published $\delta^{15}\text{N}^{\text{bulk}}$ measurements from production. A new first order approximation method for calculations of the SP isotope effect on denitrifying production and reduction using a Rayleigh model is applied. The calculations of the SP isotopic fractionation from the measurements of *P. chlororaphis* result in values of $-3.7\text{‰} \pm 1.8$. For *P. fluorescens*, the calculations result in SP values of $-7.1\text{‰} \pm 5.0$ during production of N_2O and $1.9\text{‰} \pm 2.5$ during reduction of N_2O . The slightly increased isotopic fractionation during reduction is believed to be due to diffusive isotopic fractionation and kinetic isotope effect. In summary, we implemented continuous measurements of N_2O isotopomers during incubation of denitrifying bacteria and believe that similar experiments will lead to a better understanding of denitrifying bacteria and N_2O turnover in soils and sediments and ultimately hands-on knowledge on the biotic mechanisms behind greenhouse gas exchange of the Globe.

6.1 Introduction

The atmospheric concentration of nitrous oxide (N_2O) has increased from approximately 271 ppb before the industrialization to 324 ppb in 2011 (Ciais et al., 2013). This increase has resulted in (1) N_2O being the third most important greenhouse gas, e.g. N_2O has the third highest contribution to the radiative forcing of the naturally occurring greenhouse gases (Hartmann et al., 2013), and (2) an increased production of nitrogen oxides (NO_x) in the stratosphere and thereby an increased ozone-depletion. (Forster et al., 2007; Kim and Craig, 1993)

Ice core records show that N_2O concentrations positively correlate with northern hemispheric temperature variations, e.g. during the last glacial-interglacial termination as well as over the rapid climate variations occurring during the glacial period, known as Dansgaard-Oeschger events (D-O events) (Schilt et al., 2010). However, occasionally (e.g. D-O event 15 and 17) the N_2O concentration increases long before the onset of the dramatic temperature change Schilt et al. (2010), providing a potential early warning for rapid climate change. Isotopomers of N_2O provide information on the sources i.e. whether N_2O originates predominantly from nitrification or denitrification processes (Pérez et al., 2000; Perez et al., 2001; Park et al., 2011). As the conditions/ circumstances leading to emissions from the two processes differ both for the marine and terrestrial sources measuring isotopomers will potentially improve our understanding of the climate conditions leading to early release of N_2O over some rapid climatic changes.

The N_2O molecule has an asymmetric linear structure ($\text{N}=\text{N}=\text{O}$) where the position of the ^{15}N can be discriminated. The position in the N_2O molecule are named $^{15}\text{N}^\alpha$ and $^{15}\text{N}^\beta$ or short α and β for $^{14}\text{N}^{15}\text{N}^{16}\text{O}$ and $^{15}\text{N}^{14}\text{N}^{16}\text{O}$, respectively (Yoshida and Toyoda, 2000). The two isotopomers cannot be distinguished directly by isotope ratio mass spectrometry, if using the fragmented ions. A distinction is furthermore possible using mid-infrared spectroscopy because the rotational and vibrational conditions are different for the two isotopomers providing spectral regions where absorptions of the two isotopomers do not overlap (Waechter et al., 2008; Mohn et al., 2010, 2012; Köster et al., 2013b; Heil et al., 2014). For isotopomer measurements at low N_2O concentration (low ppm range), a joint instrument development was executed, applying cavity ring down spectroscopy (CRDS) to enable continuous measurements of the isotopomer abundances and yielding values for $^{15}\text{N}^\alpha$ and $^{15}\text{N}^\beta$.

The isotopic composition of a sample is usually reported as delta values which represents the deviation of the elemental isotope ratio R in the sample from a reference material (equation 6.1, where ^{14}N is short for $^{14}\text{N}^{14}\text{N}^{16}\text{O}$). Delta values can be calculated for bulk N_2O as well

as for $\delta^{15}\text{N}^\alpha$ and $\delta^{15}\text{N}^\beta$. The reference material used is atmospheric nitrogen.

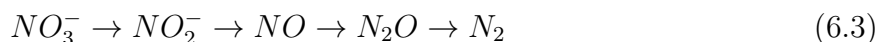
$$\delta^{15}\text{N} = \frac{R_{\text{Sample}}}{R_{\text{Std}}} - 1 \quad \text{where} \quad R = \frac{[^{15}\text{N}]}{[^{14}\text{N}]} \quad (6.1)$$

The N_2O bulk isotopic composition calculates as the average of $\delta^{15}\text{N}^\alpha$ and $\delta^{15}\text{N}^\beta$ (Eq. 6.2) while the site preference (SP) is defined as their difference (Eq. 6.2) (Brenninkmeijer and Röckmann, 1999; Toyoda et al., 2002).

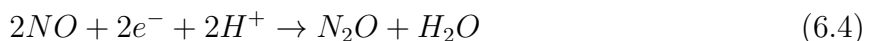
$$SP = \delta^{15}\text{N}^\alpha - \delta^{15}\text{N}^\beta \quad , \quad \delta^{15}\text{N}^{\text{bulk}} = \frac{\delta^{15}\text{N}^\alpha + \delta^{15}\text{N}^\beta}{2} \quad (6.2)$$

There are multiple natural and anthropogenic sources of N_2O . The primary anthropogenic sources of N_2O are organic and inorganic N fertilizers used for agriculture. The natural sources are primarily nitrification and denitrification in terrestrial and aquatic ecosystems. (Mosier et al., 1998; Olivier et al., 1998).

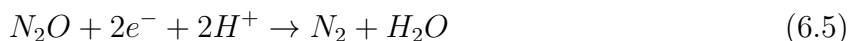
Denitrification is a stepwise biological reduction process in which denitrifying bacteria ultimately produce nitrogen (N_2). Under anaerobic conditions the denitrifying bacteria use nitrate (NO_3^-) instead of oxygen as an electron acceptor in the respiration of organic matter. Through multiple anaerobic reactions N_2 is produced as the end product of the complete denitrifying process (reaction 6.3) (Firestone and Davidson, 1989).



Each of these anaerobic reactions is carried out by a genuine enzyme, i.e., the production of N_2O is caused by the reaction between nitric oxide (NO) and the enzyme nitric oxide reductase (NOR). The NOR enzyme works as a catalyst in the reduction of NO as shown in equation 6.4. (Wrage et al., 2001; Tosha and Shiro, 2013)



The cleavage of the covalent $\text{N} = \text{O}$ bond of N_2O leading to N_2 and H_2O is the result of N_2O reduction during bacterial denitrification (6.5). According to kinetic isotope theory, the cleavage of N_2O is expected to have an increased fractionation effect on $^{15}\text{N}^\beta$, due to the stronger ^{15}N -O bond compared to the ^{14}N -O (Popp et al., 2002), diffusion into the cell (Tilsner et al., 2003), and enzymatic reduction (Wrage et al., 2004). N_2O reduction during bacterial denitrification is therefore expected to lead to an increase in SP.



Reactions with different enzymes typically result in specific isotopic fractionation. The isotopic fractionation of the intermediately produced N_2O during denitrification is a consequence of multiple reaction steps i.e., the isotopic fractionation is determined as product-to-substrate fractionation. Two species of denitrifying bacteria with slightly different enzymes

potentially leads to different fractionation. In this study, we compared the fractionation of N_2O by two contrasting denitrifying bacteria; *Pseudomonas fluorescens* producing and reducing N_2O , and *Pseudomonas chlororaphis* producing but not reducing N_2O . We hypothesized that these contrasting denitrifying bacteria show differences in isotopic fractionation and SP during N_2O production and reduction.

6.2 Method

Our objective was to perform continuous position dependent $\delta^{15}\text{N}$ measurements of two different bacterial cultures during incubation experiments. Using two denitrifying bacterial cultures we determined the isotopic fractionation and SP during production and reduction of N_2O , respectively.

6.2.1 Instrumentation

Bacterial production of N_2O was continuously measured by mid-infrared cavity ringdown spectroscopy using a prototype of the Picarro G5101-i analyzer (in the following named G5101i-CIC) (Picarro, Santa Clara, California, USA). The measurements are non-destructive and are therefore suitable for incubation experiments. The CRDS instrument measures the ^{14}N , $^{15}\text{N}^\alpha$ and $^{15}\text{N}^\beta$ absorption features of N_2O in the wavelength region between 2187.4 cm^{-1} and 2188 cm^{-1} (Balslev-Clausen, 2011). The typical precision of the instrument over 10 minutes averaging is $< 0.3\text{ ppb}$ for the N_2O mixing ratio and $< 0.4\text{ ‰}$ for each of the delta values of the isotopomers for concentrations in the range of 200 ppb - 2000 ppb.

Measurements are made by placing the sample delivery system of the G5101i-CIC in a closed loop with a microbial incubation glass chamber (Fig. 6.1). Circulation is provided by a "leak-reduced" diaphragm pump installed downstream from the analyzer. The pump (KNF N84.4 ANE) has been sealed using vacuum sealant (Celvaseal high vacuum leak sealant, Myers vacuum repair service, Inc., Kittanning, PA 16201, USA). A low leak rate is prerequisite for accurate measurements in a closed loop experiment. Before the analyzer, a Nafion unit and an "Ascarite" trap is installed. The Nafion unit removes H_2O vapor whereas the Ascarite trap chemically removes CO_2 by $\text{Mg}(\text{ClO}_4)_2$. Both gases are removed to exclude potential spectral interference with N_2O in the cavity of the analyzer. Underneath the glass chamber a magnetic stirrer is installed. The stirrer serves two purposes 1) ensure a complete mixing of the bacterial solution and the added nutrient, i.e. potassium nitrate (KNO_3^-), and 2) facilitate gas exchange.

In addition to the measuring mode, the system can be flushed with N_2 (not shown in

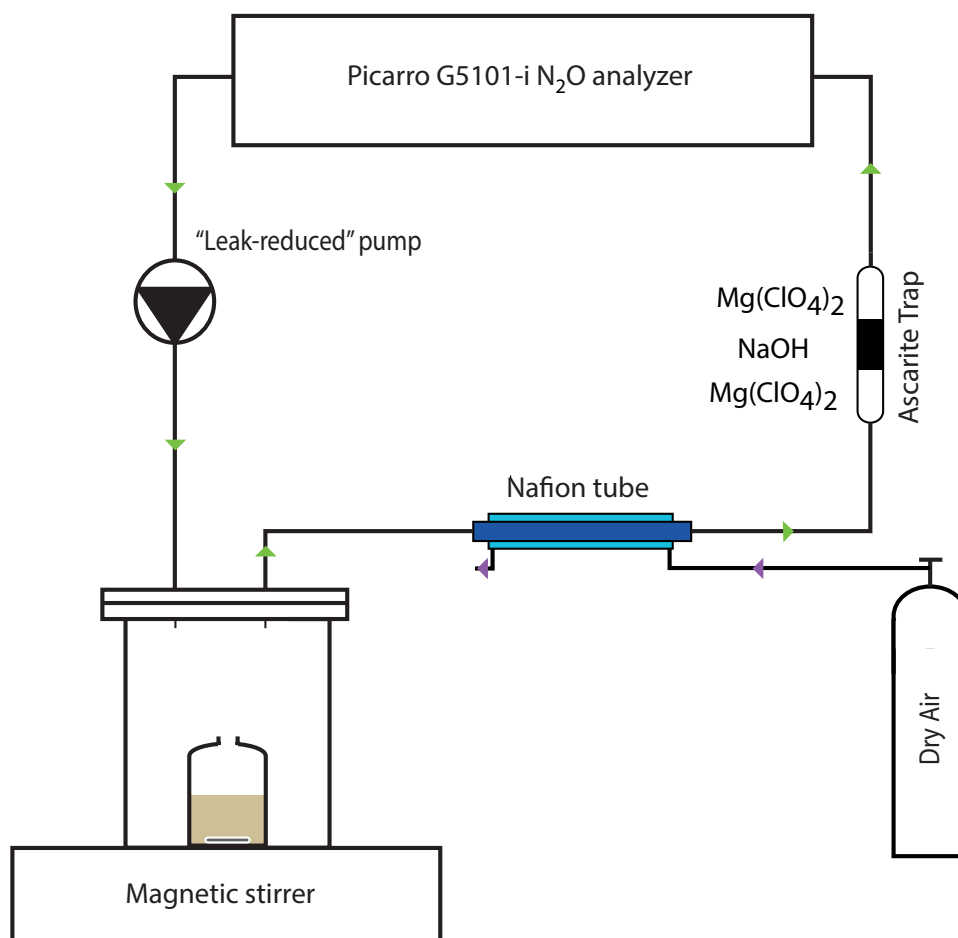


Figure 6.1: *Simplified schematic of the incubation setup. The green and the purple arrows show the flow direction of the measuring gas and the purge gas, respectively.*

Fig. 6.1). The flushing mode is used to obtain an anaerobic starting point of the incubation experiment free of N_2O . The flushing procedure is fully automated to ensure reproducibility. The entire incubation setup is flushed with N_2 for 310 seconds at a high flow rate. The resulting overpressure in the incubator is released prior to switching back to the closed loop position.

6.2.2 Correction of CRDS concentration dependence

Isotopomer measurements made with the G5101i-CIC have a N_2O concentration dependence and need to be corrected. A concentration dependent correction is required because there is a $1/\text{concentration}$ dependence, caused by small offsets in the measurement of the $^{14}N^{15}N^{16}O$ and $^{15}N^{14}N^{16}O$ peaks. These offsets are caused by baseline ripple created by optical cavity etalons. An etalon is an optical effect in which a beam of light undergoes multiple reflections between two reflecting surfaces, and whose resulting optical transmission or reflection is

periodic in wavelength. The ripples are not always constant in phase, which means that the ripples can shift spectrally, which can cause the offset to drift over time. The result is a concentration dependent error to δ of the form $\pm 1/\text{concentration}$. Because baseline ripple effects become more dominant as N_2O concentration decreases, the "relative" error is largest at low concentrations. Fig. 6.2 shows results from seven dilution experiments where

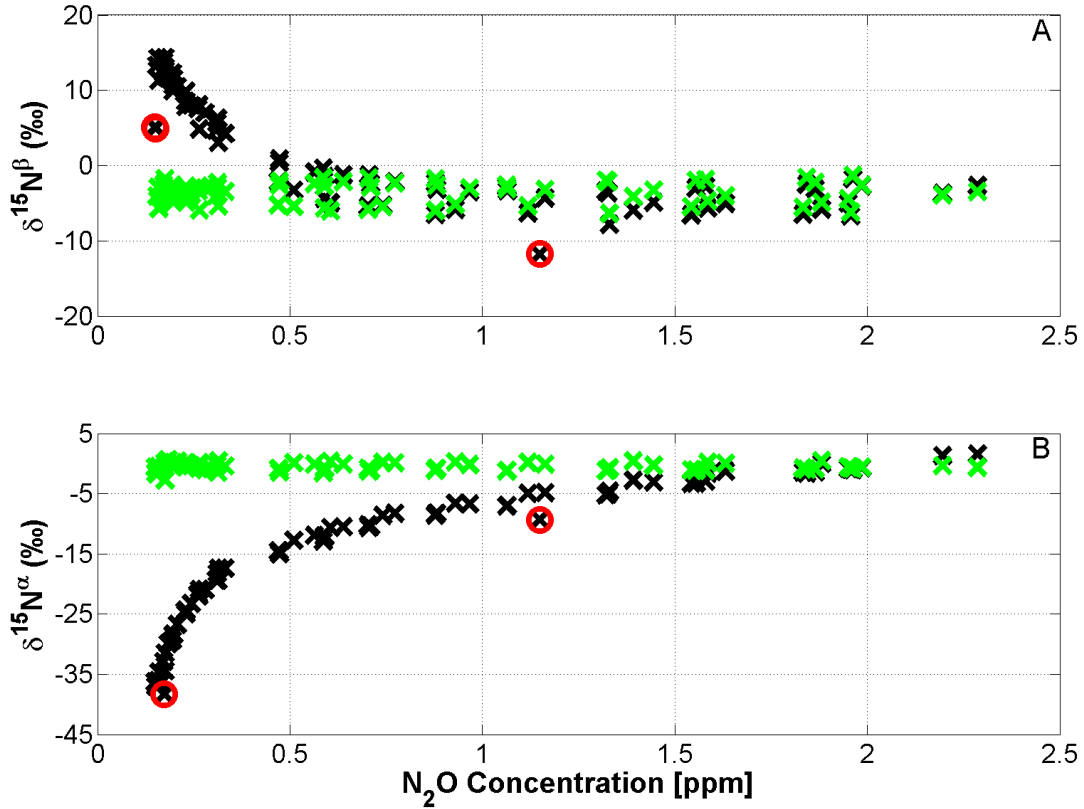


Figure 6.2: *The concentration-dependent correction (CDC) for (A) $\delta^{15}\text{N}^\alpha$ and (B) $\delta^{15}\text{N}^\beta$ respectively. In both Figures, the raw data are presented in black, the CDC data is plotted in green, and the outliers are marked with red circles.*

we gradually mixed a pure N_2O gas with a N_2/O_2 mixture (20.1 % O_2 and 79.9 % N_2 , purity 99.999 %). Measurements were performed in a 60 minutes stepwise (18 steps) sequence of both increasing and decreasing concentrations (fig. 6.2).

We chose to fit the raw data with a cubic spline smoothing function (CSS-function) (Brumback and Rice, 1998). The best fit of these CSS-functions are found using a smoothing parameter of $p = 0.999$ in a regression analysis. Four outliers were identified to be outside the 2σ boundary and were removed from the data set (the red circles in fig. 6.2). After these outliers were removed the best fit was found again and the concentration dependent correction was applied as shown with the green profiles in Fig. 6.2. Over the course of the

experiments, no further instrumental drift was observed.

6.2.3 Calibration gases

Working standards for N₂O bacterial incubations are CIC-MPI-1 and CIC-MPI-2. The two standard gases were prepared based on two standard gases provided by J. Kaiser at University of East Anglia (UEA), Norwich, United Kingdom. These standard gases, MPI-1 and MPI-2, are pure N₂O gases with different isotopic composition (Kaiser, 2002). In our laboratory, each of the standard gases was diluted with a N₂/O₂ mixture (20.1 % O₂ and 79.9 % N₂, purity 99.999 %) resulting in the two new standard gases, CIC-MPI-1 and CIC-MPI-2. Both CIC-standard gases were measured at four different laboratories to ensure consistent isotopic values according to an international standard reference. The gases were measured at Tokyo Institute of Technology in Japan, at Institute for Marine and Atmospheric research Utrecht in The Netherlands (IMAU), at the Centre for Ice and Climate in Copenhagen, Denmark (CIC), and originally at University of East Anglia in Norwich, United Kingdom (UEA). At Tokyo-Tech, three GC/IRMS measurements of each CIC-MPI gas resulted in an average $\delta^{15}\text{N}^\alpha = 1.44 \text{ ‰} \pm 0.09$ and an average $\delta^{15}\text{N}^\beta = 1.24 \text{ ‰} \pm 0.35$ for CIC-MPI-1, and for CIC-MPI-2 the measurements resulted in average $\delta^{15}\text{N}^\alpha = 12.79 \text{ ‰} \pm 0.22$ and $\delta^{15}\text{N}^\beta = -15.41 \text{ ‰} \pm 0.24$. At IMAU 22 GC/IRMS measurements of each CIC-MPI gas resulted for CIC-MPI-1 in $\delta^{15}\text{N}^\alpha = 2.31 \text{ ‰} \pm 0.25$ and $\delta^{15}\text{N}^\beta = -0.15 \text{ ‰} \pm 0.33$, and for CIC-MPI-2 in $\delta^{15}\text{N}^\alpha = 11.80 \text{ ‰} \pm 0.37$ and $\delta^{15}\text{N}^\beta = -15.16 \text{ ‰} \pm 0.46$. At CIC each CIC-MPI gas was continuously measured over two hours. The average results for CIC-MPI-1 was $\delta^{15}\text{N}^\alpha = 0.29 \text{ ‰} \pm 2.44$ and $\delta^{15}\text{N}^\beta = 4.95 \text{ ‰} \pm 2.37$, and for CIC-MPI-2 in $\delta^{15}\text{N}^\alpha = 12.58 \text{ ‰} \pm 2.51$ and $\delta^{15}\text{N}^\beta = -12.89 \text{ ‰} \pm 2.35$. All measurements were performed relative to our standard

Table 6.1: *Measurements of standard gas CIC-MPI-1 and CIC-MPI-2, diluted MPI-1 and MPI-2 gases respectively. The listed values are mean-values and combined standard deviations (σ) of measurements performed at Tokyo-Tech, IMAU, and CIC.*

Reference gas	[N ₂ O] (ppb)	$\delta^{15}\text{N}^{bulk}$ (‰)	$\delta^{15}\text{N}^\alpha$ (‰)	$\delta^{15}\text{N}^\beta$ (‰)
CIC-MPI-I	1909.8 ± 29.3	1.32 ± 0.82	1.94 ± 0.87	0.70 ± 1.42
CIC-MPI-II	1857.9 ± 19.2	-1.43 ± 0.82	12.01 ± 1.06	-14.87 ± 1.13

gases anchored to atmospheric N₂. Our position dependent $\delta^{15}\text{N}$ measurements are reported to atmospheric N₂. An average of the concentrations and the isotopic compositions of the two new standard gases are specified (Table 6.1). The standard deviation (Table 6.1) that we see from our measurements are similar to those presented by Mohn et al. (2014).

6.2.4 Pure bacterial cultures

The two bacterial cultures used in this study are both gram-negative bacteria with the capability to denitrify, i.e. reduce nitrate to gaseous nitrogen. Isolates were obtained from an agricultural soil of sandy loam type (Roskilde Experimental Station) on 11 April 1983. One culture is a *Pseudomonas fluorescens*, bio-type D that reduces NO_3^- all the way to N_2 . The second culture, *Pseudomonas chlororaphis*, is only capable of reducing NO_3^- to N_2O (Christensen and Bonde, 1985), which means that the nitrous oxide reductase is absent or at least not active in this organism. The latter bacterium is contained in the American Type Culture Collection with accession number ATCC 43928 (Christensen and Tiedje, 1988). The cultures were grown anoxic in 50 ml serum bottles with 1/10 tryptic soy broth (Difco) added $0.1 \text{ g KNO}_3 \cdot \text{L}^{-1}$. After six days of growth at room temperature ($24 \text{ }^\circ\text{C}$), *P. chlororaphis* had reduced all N in NO_3^- into N_2O . The bacterial culture of *P. Fluorescens* was cultivated for six days at a slightly lower temperature ($15 \text{ }^\circ\text{C}$) to assure that the cultures were in a comparable phase of potential activity when assayed for gas production/reduction activity. The six days old cultures were used in the incubation experiment in which it is conditional for the denitrifying process that organic carbon is available, that the concentration of oxygen is low and that the concentration of NO_3^- is high (Wrage et al., 2001; Stuart Chapin III et al., 2002).

Bacterial incubation experiments

50 mL bacterial solution of *P. chlororaphis* or *P. fluorescens* was placed in a petri-dish in the 1000 mL incubation chamber. Hereafter, the setup was flushed with pure N_2 (purity 99.9999 %) to ensure anaerobic conditions. To ensure no N_2O gas exchange prior to the experiment, the bacterial solution was left for 90 minutes under constant magnetic stirring. Then the incubation chamber was opened and the bacterial solution was fed with 2.5 mL and 15 mL 0.45 mM KNO_3 for *P. chlororaphis* and *P. fluorescens*, respectively. The incubation experiment started by again flushing the setup with pure N_2 immediately after the addition of KNO_3 .

A total of seven replicate incubations of the full denitrifying bacteria (*P. fluorescens*) and five replicate incubations of the denitrifying bacteria with no active nitrous oxide reductase (*P. chlororaphis*) were assessed. All of the cultures were continuously measured from the moment KNO_3 was added to the bacterial incubations. The experiment with *P. fluorescens* was terminated when the N_2O concentration was below 0.2 ppm. For *P. chlororaphis*, we defined the end of the experiment when the N_2O concentration had reached a constant level for 200 minutes.

Continuous measurements of the bacterial production of N₂O from *P. chlororaphis* were performed for approximately 500 minutes for each replica. All five replicas were measured within one week, starting at the same hour of the day and after equally long cultivation prior to the measurements. The bacterial evolution, of N₂O production and reduction, from *P. fluorescens* was continuously measured for 1000 minutes on average. The seven replicas were measured in three one week measuring campaigns over the course of half a year, but always with an equally long cultivation prior to measurements.

The CIC-MPI gases are based on a N₂/O₂ mixture where the incubation measurements are based on N₂. This difference relates to the effect of oxygen on measurements of isotopomers as shown by Erler et al. (2015). A similar experiment (see supplementary) has been performed resulting in a constant offset correction of the presented data.

6.2.5 Determination of isotopic fractionation

The isotopic fractionation (ϵ) associated with production of N₂O is the consequence of multiple reactions all leading to different isotopic fractionations (Ostrom and Ostrom, 2011). Albeit Ostrom and Ostrom (2011) argue that the isotopic fractionation observed during reduction of NO₃⁻ to N₂O can be treated as a net isotope effect (η) with NO₃⁻ being the substrate and N₂O as the product. The observed changes in N₂O isotopic composition during our incubation experiment can therefore be analyzed in terms of Rayleigh fractionation. Rayleigh fractionation describes the changing isotopic composition in substrate and product of a unidirectional reaction, hence we use the Rayleigh fractionation both during production (NO₃⁻ to N₂O). The reduction of N₂O to N₂ is a one-step reaction and Rayleigh fractionation can therefore be used directly to determine the isotopic fractionation (Ostrom et al., 2007a). Mariotti et al. (1981) derived the equation for the isotope ratio of the substrate (Eq. 6.6) as:

$$\frac{R_s}{R_{s,0}} = f^{(\alpha_{p/s}-1)} \quad (6.6)$$

where $R_{s,0}$ is the initial isotope ratio of the substrate, R_s is the isotope ratio of the substrate at time t , $\alpha_{p/s}$ is the fractionation factor of the product versus the substrate, and f is the unreacted fraction of substrate at time t . Mariotti et al. (1981) showed that the corresponding equation for the isotopic ratio of the accumulated product $R_{p,acc}$ derives as given in Eq. 6.7.

$$R_{p,acc} = R_{s,0} \cdot \left(\frac{1 - f^{\alpha_{p/s}}}{1 - f} \right) \quad (6.7)$$

For Rayleigh fractionation the fractionation factor in equation 6.6 is used to derive the isotopic fractionation, which calculates as $\epsilon = \alpha - 1$ (Mariotti et al., 1981). The isotopic

fractionation of the product derived from reduction of N_2O to N_2 is calculated using Eq. 6.7 and is valid for the bulk $^{15}\text{N} / ^{14}\text{N}$ isotope ratios of N_2O and for both of the isotopomers (Mariotti et al., 1981; Menyailo and Hungate, 2006; Ostrom et al., 2007b; Lewicka-Szczebak et al., 2014). The SP of N_2O , being the difference between the $\delta^{15}\text{N}^\alpha$ and $\delta^{15}\text{N}^\beta$, is not compatible to the Rayleigh equations. The isotopic fractionation for SP is derived using the relationship $\epsilon_{sp} = \epsilon_\alpha - \epsilon_\beta$ as stated by Ostrom et al. (2007b) and Well and Flessa (2009b). During production of N_2O we use Eq. 6.7 in calculation of the net fractionation factor, hence the net isotope effect, which calculates $\eta = \alpha - 1$ (Ostrom and Ostrom, 2011; Lewicka-Szczebak et al., 2014). The Rayleigh fractionation during production is valid for the bulk $^{15}\text{N} / ^{14}\text{N}$ isotope ratios of N_2O , since the bulk is a measure of the average abundance of the two isotopomers. We did not measure the isotopic composition of KNO_3 in our experiments. By definition when all KNO_3 has reacted to N_2O , its isotopic composition is identical to the initial composition of KNO_3 . The final isotopic values of N_2O for *P. chlororaphis* can therefore be used to estimate the initial composition of KNO_3 . The net isotope effect for SP is derived similarly to the isotope fractionation, hence $\eta_{sp} = \eta_\alpha - \eta_\beta$.

Modifications to the Rayleigh model

Ostrom and Ostrom (2011); Lewicka-Szczebak et al. (2014) showed that the described Rayleigh equation for the net isotope effect is applicable to the isotopomers during production of N_2O . Though the isotopomers are both direct products of the same denitrification process from the same batch of denitrifying bacteria and nitrate and nitric oxide. Hendriks et al. (2000) and Hino et al. (2010) argue that nitric oxide reductase being the primary enzyme in production of N_2O , and therefore the most important fractionation occurs in the last step prior to N_2O production. We therefore argue that a set of isotopomer modification factors are necessary in determination of the isotopomer net isotope effect during production of N_2O . The isotopomer modification factors (φ_α and φ_β) are shown in Eq. 6.8 and Eq. 6.9 for $\delta^{15}\text{N}^\alpha$ and $\delta^{15}\text{N}^\beta$, respectively. The two isotopomer modification factors allow for correction of each of the isotopomers from the isotopic ratio of the accumulated product of the bulk $R_{p,acc}^{bulk}$ (Eq. 6.7).

$$\varphi_\alpha = 1 + \left(\frac{\alpha_\beta - \alpha_\alpha}{2} \right) \quad (6.8)$$

$$\varphi_\beta = 1 - \left(\frac{\alpha_\beta - \alpha_\alpha}{2} \right) \quad (6.9)$$

The Rayleigh equation for the isotopic ratio of the accumulated product of $^{15}\text{N}^i$ ($R_{p,acc}^i$) is

therefore as presented in equation 6.10, where i can be α or β .

$$R_{p,acc}^i = R_{s,0} \cdot \left(\frac{1 - f^{\alpha_{p/s}}}{1 - f} \right) \cdot \left(1 \pm \left(\frac{\alpha_\beta - \alpha_\alpha}{2} \right) \right) = R_{p,acc}^{bulk} \cdot \varphi_i \quad (6.10)$$

Equation 6.10 is valid and final for *P. chlororaphis*. For *P. fluorescens*, both immediate reduction and an uptake reduction take place simultaneously with N₂O production due to the pre-experimental cultivation leading to activation of all enzymes in the bacterial solution. Part of the freshly produced N₂O is therefore immediately reduced to N₂. This reduction is fractionating with fractionation factor α_α^R , α_β^R , and α_{bulk}^R , respectively for each of the isotopomers and the bulk. The isotope imprint of the reduction on the remaining N₂O depends on the ratio between reduction rate and production rate. We therefore define a parameter for the ratio between reduction rate and production rate, which from here on is referred to as the reduction correction parameter (γ). Assuming γ is constant (for one experiment cf. Fig. 6.3B) results in the following first order approximation of the accumulated product including the isotope imprint of the reduction on the remaining N₂O ($R_{p,r,acc}^\alpha$).

$$R_{p,r,acc}^\alpha = R_{p,acc}^\alpha \cdot \frac{(1 - \alpha_\alpha^R \cdot \gamma)}{1 - \gamma} \quad (6.11)$$

Equation 6.11 is presented for ¹⁵N^α, though similar equations is used for both ¹⁵N^β and ¹⁵N^{bulk}. For any calculated ratio the values are given in ‰ using the delta-notation (equation 6.1).

In this study we present calculations of both the net isotope effect (η) during production of N₂O and the isotopic fractionation (ϵ) during reduction of N₂O to N₂. In the following both quantities (η and ϵ) will be referred to as the isotopic fractionation.

Fitting procedure

We determine the respective isotopic fractionation during production and reduction of N₂O for each of the bacterial strains assuming a Rayleigh type process. The best fit (highest R²) is found using an iterative approach between the measured data and the Rayleigh fractionation model for the accumulated product.

For *P. chlororaphis* (being a pure producer of N₂O) we use Eq. 6.10 as the Rayleigh fractionation model, with the production section being straight forward. We fit the Rayleigh fractionation model (Eq. eq:Riso) to the measured data. The highest R² values are iteratively found, using the extremes of the unreacted fraction parameter as $f_{start} = 1-1/n$ and $f_{end} = 0+1/n$, where n is the length of the sample, and by iterative calculations of the the fractionation factor during production of N₂O (between $\alpha = 0$ and $\alpha = 1$).

For *P. fluorescens* Eq. 6.11 and Eq. 6.7 is used as the Rayleigh fractionation model during production of N₂O and reduction of N₂O, respectively. We defined the section of production as being from the start of the measurements until the net production (net emission) rate turns negative. From the calculations of the net production rates (see Fig. 6.3) we believe that N₂O production continues after the point of maximum concentration. However, at one point NO₃⁻, NO₂⁻ and NO are fully consumed and *P. fluorescens* is forced to exclusively reduce N₂O. We defined the start of the section where *P. fluorescens* is only reducing N₂O to the point where both $\delta^{15}\text{N}^\alpha$ and $\delta^{15}\text{N}^\beta$ start decreasing (assumption based on reduction of $\delta^{15}\text{N}^\alpha$, $\delta^{15}\text{N}^\beta$, $\delta^{15}\text{N}^{bulk}$, and concentration). Between the end of the net production and the start of the exclusive reduction, no Rayleigh model can be fitted.

The fractionation factors resulting in the highest R² values are picked as the correct fractionation factor for each specific evolution. In the calculations of the N₂O production from *P. fluorescens* the fractionation factor during N₂O reduction is required. We therefore first fit the Rayleigh fractionation model (Eq. 6.7) to the measured N₂O reduction data. The highest R² values are iteratively found, using the extremes of the unreacted fraction parameter as $f_{start} = 1 - 1/n$ (where n is the length of the sample) and $f_{end} = 0$, and iterative calculations of the fractionation factor during reduction of N₂O (between $1 < \alpha < 2$). Secondly we fitted the Rayleigh fractionation model (Eq. 6.11) to the measured N₂O production data. Here the highest R² values are iteratively found using the fractionation factor during N₂O reduction (from calculations above), by iterative calculations of the 1) extremes of the unreacted fraction parameter (f_{start} and f_{end}) where $1 < f_{end} < 0$, $f_{start} < f_{end}$, and $f_{start} = 1 - f_{end} \cdot \frac{[N_2O]_{start}}{[N_2O]_{end}}$, 2) the reduction correction parameter (γ) (between $0 \leq \gamma \leq 1$), 3) the fractionation factor during production of N₂O (between $0 < \alpha < 1$).¹

Nitric oxide accumulation in the headspace can not be excluded from any of the presented N₂O production experiments. The effect of accumulation of nitric oxide in the headspace is assumed to be included in the offset from 0 in f_{end} and from 1 in f_{start} (Table 6.2 and Table 6.3 for *P. chlororaphis* and for *P. fluorescens*, respectively), hence no further adjustment is taken.

¹The intended procedure for finding f_{start} and f_{end} during production is an iterative determination for both, with $1 < f_{start} < f_{end} < 0$ as the only boundary conditions. During reduction the intention is that $f_{start} = 1$ and $f_{end} = 0$. I recently discovered that the implemented procedure is as line out above instead. This is an error and will need to be changed for the final publication. However, I repeated one experiment with the correct boundary conditions and found only a small change to the results currently in the manuscript. I expect that this is the case for all experiments.

6.3 Results

The evolution of N_2O concentration over time from the two bacterial strains shows two very distinctive patterns with both an increasing and decreasing N_2O concentration characteristic for *P. fluorescens* and an increasing N_2O concentration followed by a stabilization characteristic for *P. chlororaphis* (Fig. 6.3A) as has previously been described by Christensen and Tiedje (1988). These distinctive characteristics are only vaguely seen in the respective dynamics of the SP for the two bacterial strains (Fig. 6.4, 6.5, 6.6 and 6.7).

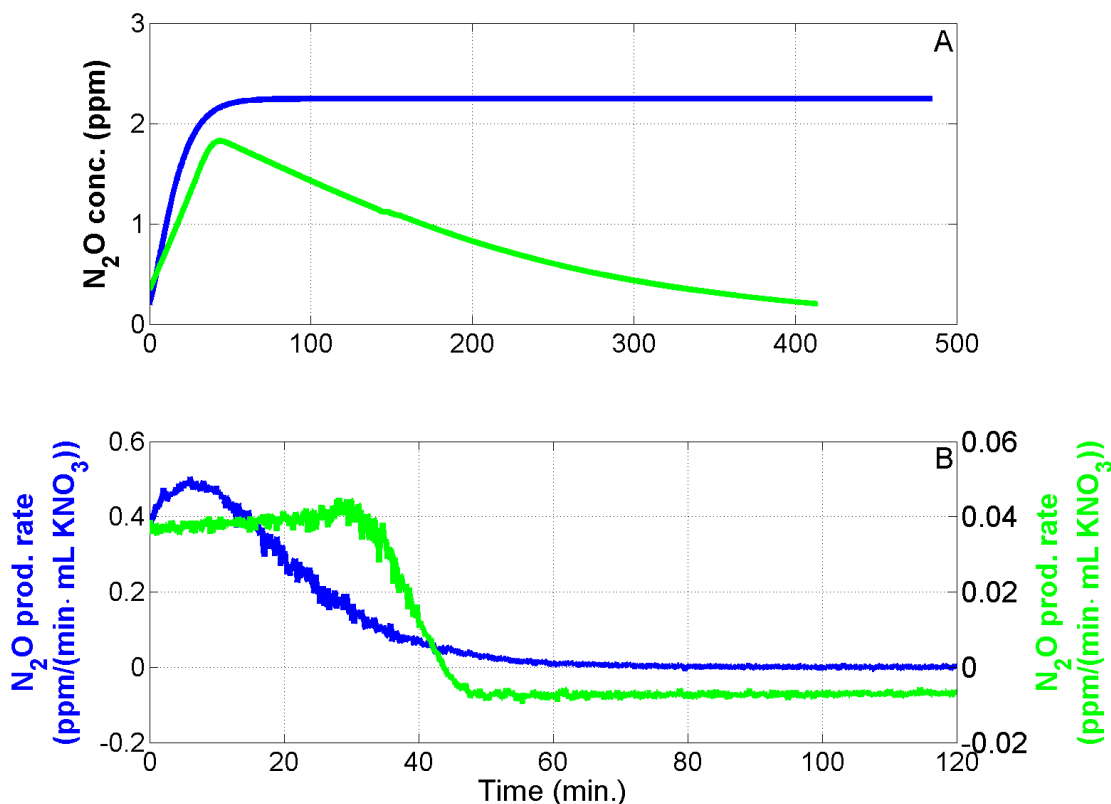


Figure 6.3: Continuous measurements of (A) N_2O concentrations and (B) the net N_2O production rate from experiments with *P. fluorescens* (green) and *P. chlororaphis* (blue), respectively. Only the first 120 minutes of the net N_2O production. Note that the scaling of the two horizontal axis differs.

6.3.1 Pseudomonas chlororaphis

Paralleling the increase in N_2O concentration (Fig. 6.3A), we also find an increase in $\delta^{15}N^\alpha$, $\delta^{15}N^\beta$ and $\delta^{15}N^{bulk}$ over time (Fig. 6.4 and 6.5). The final product of *P. chlororaphis* is assumed purely being N_2O ; this is a unidirectional transfer of nitrogen from KNO_3 to N_2O

and thereby a Rayleigh process although multiple fractionations are involved. Figure 6.4 and 6.5 shows the best fit Rayleigh profile for $\delta^{15}\text{N}^\alpha$ and $\delta^{15}\text{N}^\beta$ respectively

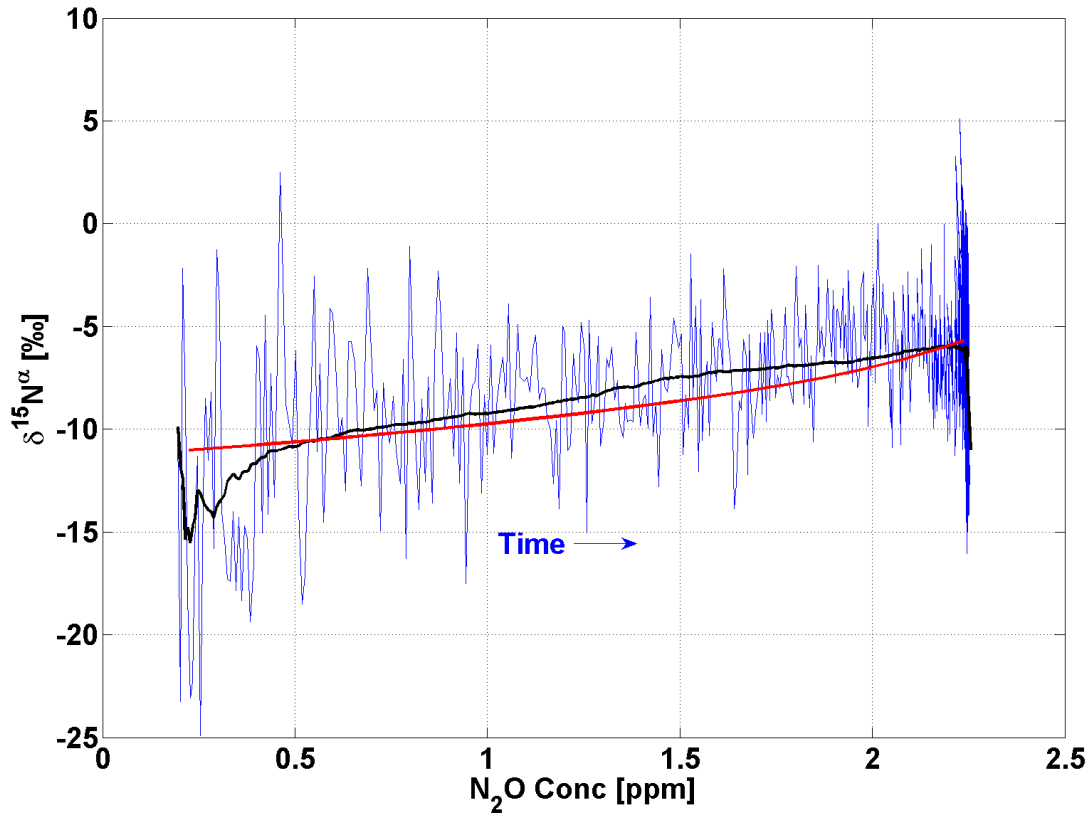


Figure 6.4: $\delta^{15}\text{N}^\alpha$ as a function of N_2O concentration as produced by *P. chlororaphis* and the modeled Rayleigh type distillation. High resolution CRDS data (blue line) and five minutes running average (black line). The red curve is the modeled Rayleigh type distillation curve for the production of N_2O . The blue arrow indicates the direction of time during production of N_2O .

The modeled Rayleigh distillation profiles were found to match the production of N_2O from *P. chlororaphis* to a relatively high degree. The average coefficient of determination (R^2) between data and fitted Rayleigh curves are 0.709, 0.654, and 0.767 for $\delta^{15}\text{N}^\alpha$, $\delta^{15}\text{N}^\beta$ and $\delta^{15}\text{N}^{bulk}$ respectively. The calculations of the isotopic fractionation for the fractionation of $\delta^{15}\text{N}^\alpha$ give a mean value of $-8.8 \text{‰} \pm 1.4$. For $\delta^{15}\text{N}^\beta$ the mean isotopic fractionation was found to be $-2.2 \text{‰} \pm 1.1$ (Table 6.2). These values leads to a mean SP value of $-3.7 \text{‰} \pm 1.8$ and a $\delta^{15}\text{N}^{bulk}$ isotopic fractionation of $-5.6 \text{‰} \pm 0.9$.

6.3.2 Pseudomonas fluorescens

Continuous measurements of the evolution of N_2O produced and consumed by the denitrifying bacteria *P. fluorescens* are presented in Fig. 6.6 and 6.7 for $\delta^{15}\text{N}^\alpha$ and $\delta^{15}\text{N}^\beta$,

Table 6.2: Isotopic fractionation, extremes of the unreacted fraction parameter (f_{start} and f_{end}), and production rate (k_p) for the production of N_2O from *P. chlororaphis*.

Replica #	ϵ_α (‰)	ϵ_β (‰)	ϵ_{bulk} (‰)	ϵ_{SP} (‰)	f_{start}	f_{end}	k_p (ppm/min)
1	-9.0	-3.0	-6.0	-6.0	0.9762	0.0238	0.1511
2	-6.3	-2.3	-4.3	-4.0	0.9778	0.0222	0.2014
3	-7.3	-3.6	-5.5	-3.7	0.9778	0.0222	0.1329
4	-6.0	-5.1	-5.6	-0.9	0.9783	0.0217	0.1247
5	-8.7	-4.9	-6.8	-3.8	0.9783	0.0217	0.0882
Mean	-7.5	-3.8	-5.6	-3.7	0.978	0.022	0.140
σ	1.4	1.2	0.9	1.8	$9e^{-4}$	$9e^{-4}$	0.041

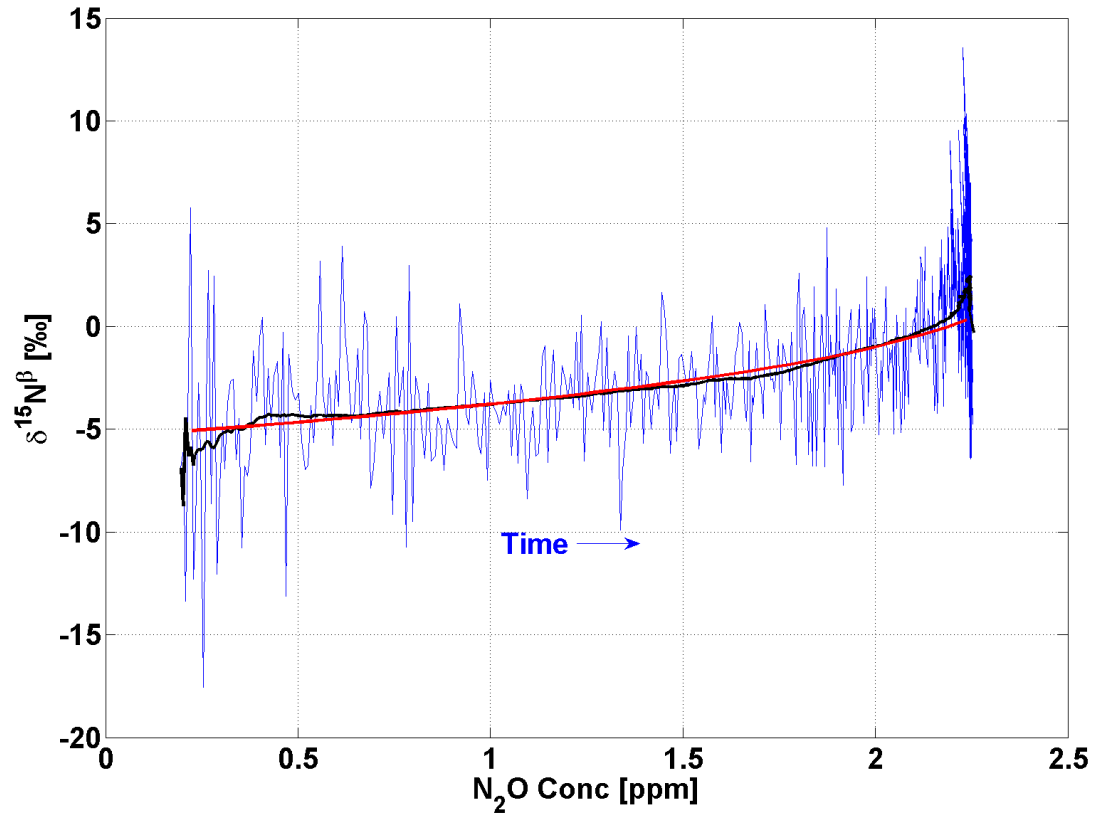


Figure 6.5: $\delta^{15}N^\beta$ as a function of N_2O concentration as produced by *P. chlororaphis* and the modeled Rayleigh type distillation. High resolution CRDS data (blue line) and five minutes running average (black line). The red curve is the modeled Rayleigh type distillation curve for the production of N_2O . The blue arrow indicates the direction of time during production of N_2O .

respectively. The correlation coefficient of the fitted apparent Rayleigh model for the pro-

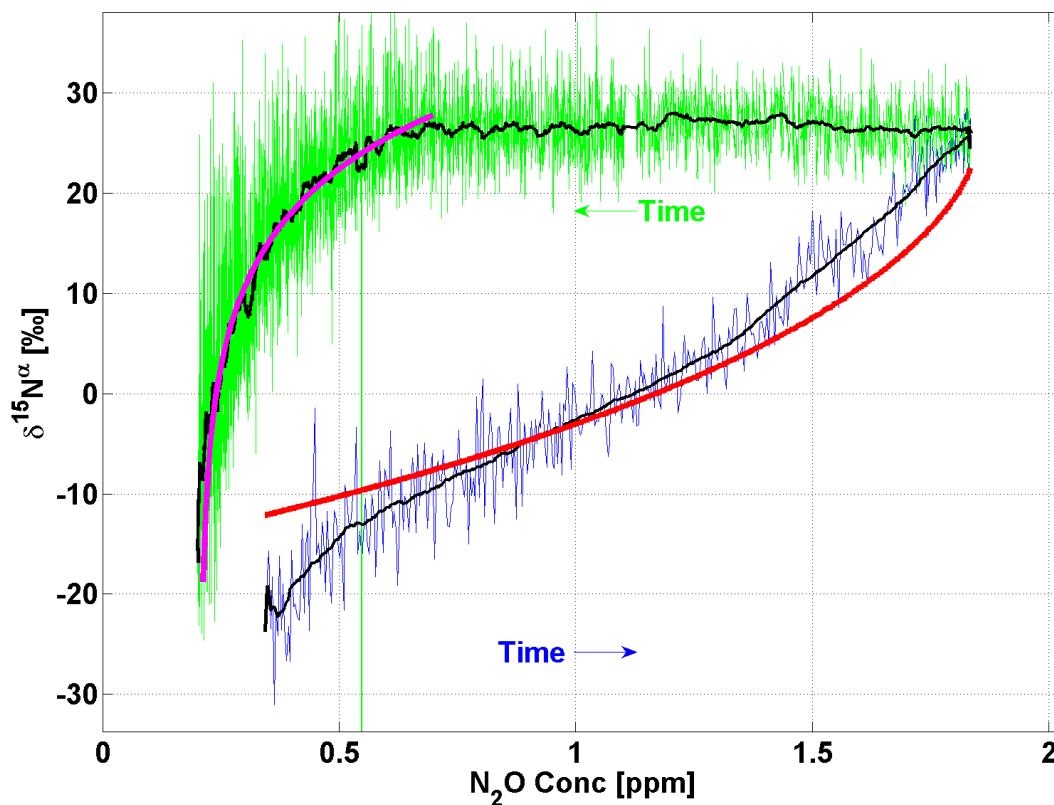


Figure 6.6: $\delta^{15}\text{N}^\alpha$ as a function of N_2O concentration as produced by *P. fluorescens* and the modeled Rayleigh type distillation. High resolution CRDS data (blue line) and five minutes running average (black line). The red and magenta curve is the modeled Rayleigh type distillation curve for the production and reduction of N_2O , respectively. The blue arrow indicates the direction of time during production of N_2O whereas the green arrow indicates the direction of time during reduction of N_2O .

duction matches the continuously measured $\delta^{15}\text{N}^\alpha$ data by 94.1 % on average using the R^2 method for the seven replicates of *P. fluorescens* incubations. Equivalent R^2 average for $\delta^{15}\text{N}^\beta$ are 88.7 %, whereas the average for $\delta^{15}\text{N}^{bulk}$ are found to be 94.8 %. The R^2 found for the reduction part is 91.3 % for $\delta^{15}\text{N}^\alpha$, 76.3 % for $\delta^{15}\text{N}^\beta$, and 91.7 % for $\delta^{15}\text{N}^{bulk}$ on average for the seven replicates. The fractionation during both the production and the reduction are therefore following the apparent Rayleigh type distillation to a large degree. The isotopic fractionation calculated using these models are therefore a good representation for the fractionation caused by the *P. fluorescens* bacteria on the N_2O .

The resulting isotopic fractionation is presented in Table 6.3 for the production part and in Table 6.4 for the reduction part together with the calculated isotopic fractionation for the

Table 6.3: Isotopic fractionation, reduction correction parameter (γ), extremes of the unreacted fraction parameter (f_{start} and f_{end}), and production rate (k_p) for the production of N_2O from *P. fluorescens*.

Replica #	ϵ_α (‰)	ϵ_β (‰)	ϵ_{bulk} (‰)	ϵ_{SP} (‰)	γ	f_{start}	f_{end}	k_p (ppm/min)
1	-41.4	-34.1	-37.8	-7.3	0.009	0.812	0.0011	0.0133
2	-34.0	-29.4	-31.7	-4.6	0.607	0.908	0.0004	0.0350
3	-44.1	-31.1	-37.6	-13.0	0.171	0.899	0.0010	0.0308
4	-55.6	-45.7	-50.7	-9.9	0.048	0.915	0.0009	0.0160
5	-54.1	-49.2	-51.7	-4.9	0.119	0.805	0.0012	0.0064
6	-51.1	-39.2	-45.2	-11.9	0.237	0.893	0.0011	0.0045
7	-42.9	-44.5	-43.7	1.6	0.194	0.931	0.0007	0.0244
Mean	-46.2	-39.0	-42.6	-7.1	0.198	0.880	0.001	0.019
σ	7.8	7.7	7.3	5.0	0.198	0.051	$2.8e^{-4}$	0.012

Table 6.4: Isotopic fractionation, extremes of the unreacted fraction parameter (f_{start} and f_{end}), and reduction rate (k_r) for the reduction of N_2O from *P. fluorescens*.

Replica #	ϵ_α (‰)	ϵ_β (‰)	ϵ_{bulk} (‰)	ϵ_{SP} (‰)	f_{start}	f_{end}	k_r (ppm/min)
1	10.1	8.1	8.5	2.0	0.9899	0	-0.0010
2	3.5	4.5	3.6	-1.0	0.9911	0	-0.0027
3	12.0	8.2	9.5	3.8	0.9916	0	-0.0022
4	4.6	6.3	5.1	-1.7	0.9915	0	-0.0027
5	17.1	12.5	14.2	4.6	0.9873	0	-0.0014
6	17.1	13.2	14.4	3.9	0.9937	0	-0.0019
7	9.9	8.4	7.4	1.5	0.9917	0	-0.0017
Mean	10.6	8.7	9.0	1.9	0.991	0	-0.002
σ	5.4	3.1	4.2	2.5	$2.0e^{-3}$	0	$6.4e^{-4}$

SP. During production of N_2O , the mean isotopic fractionation for SP was found to be $\epsilon_{SP} = -7.1 \text{ ‰} \pm 5.0$ while the $\epsilon_{bulk} = -42.7 \text{ ‰} \pm 7.3$ for the bulk, hence there is a difference of 3.4 ‰ and 37.1 ‰ for ϵ_{SP} and ϵ_{bulk} , respectively, to *P. chlororaphis*. During reduction of N_2O the mean isotopic fractionation for SP was found to be $\epsilon_{SP} = 1.9 \text{ ‰} \pm 2.5$ and $\epsilon_{bulk} = 9.0 \text{ ‰} \pm 4.2$ for the bulk.

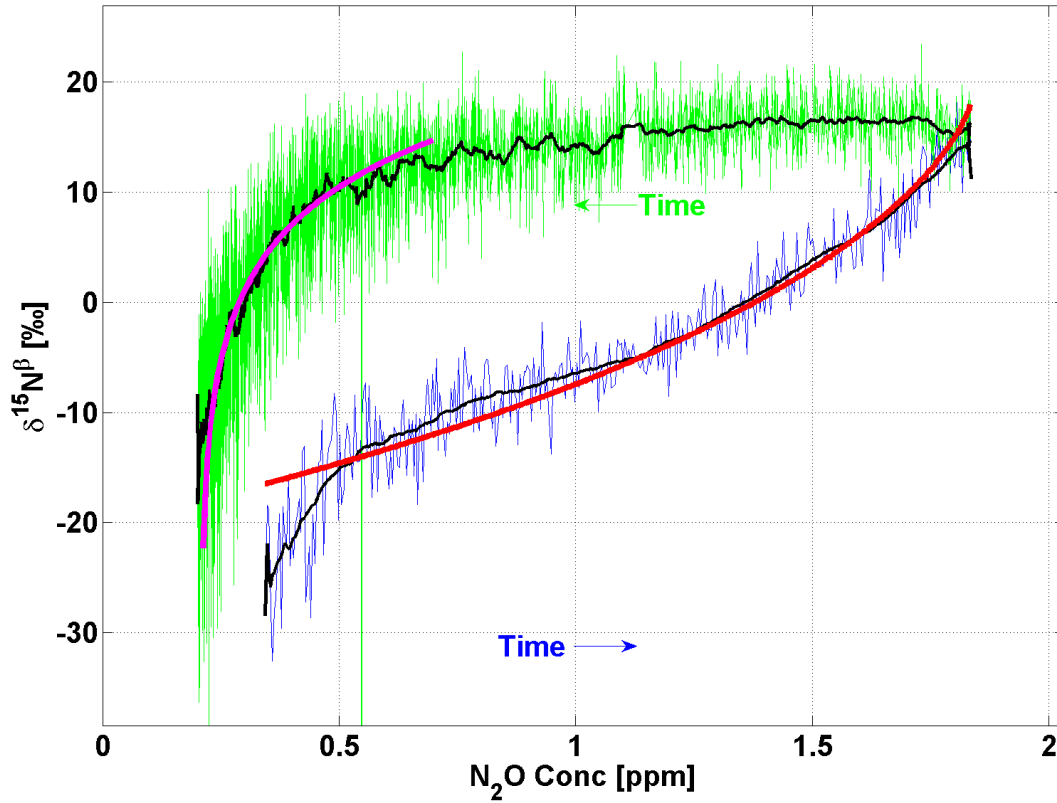


Figure 6.7: $\delta^{15}N^{\beta}$ as a function of N_2O concentration as produced by *P. fluorescens* and the modeled Rayleigh type distillation. High resolution CRDS data (blue line) and five minutes running average (black line). The red and magenta curve is the modeled Rayleigh type distillation curve for the production and reduction of N_2O , respectively. The blue arrow indicates the direction of time during production of N_2O whereas the green arrow indicates the direction of time during reduction of N_2O .

6.4 Discussion

The two bacteria investigated are denitrifiers, i.e. functionally similar but with *P. chlororaphis* lacking the ability to reduce N_2O to N_2 . Both denitrifiers were cultivated under anaerobic conditions leading to active nitric oxide reductase (both cultures) and nitrous oxide reductase (*P. chlororaphis*). This leads to a pre-experimental expectation that when fed the same amount of nitrate the maximum N_2O concentration and the N_2O production rate should be lower for *P. fluorescens* than for *P. chlororaphis*.

In Fig. 6.3, an example of the N_2O evolution by the two bacterial strains is plotted as the concentration of N_2O and the production rate versus time. Starting at time zero and moving with the profiles forward in time, the concentration of N_2O produced by *P. chlororaphis* has a higher production rate and reaches a higher level in concentration than that produced

by *P. fluorescens* even though *P. fluorescens* received six times more substrate than *P. chlororaphis*. These observations indicate that the nitrous oxide reductase consumes N₂O from a very early stage of the N₂O turnover, likely because the cultures were grown under anaerobic conditions leaving both N₂O-producing and -consuming enzymes active from the beginning of the experiment.

N₂O produced by the two denitrifying bacteria differs in the bulk isotopic fractionation whereas the SP isotopic fractionation are averaging to similar values. From the presented experiments we have found that the difference in isotopic fractionation between *P. chlororaphis* and *P. fluorescens* on average is 36.6 ‰ and 0.1 ‰ for ϵ_{bulk} and ϵ_{SP} respectively (Fig. 6.8). We therefore find that the isotopic fractionation is significantly increased for the isotopomers produced by *P. fluorescens* than for those produced by *P. chlororaphis*, since the Rayleigh model is calculated as product-to-substrate fractionation. Sutka and Ostrom (2006) conclude that a difference in the nitrite reductase does not have an effect on the SP during denitrification. This conclusion is based on measurements of two denitrifiers (*P. chlororaphis* (ATCC 43928) and *P. aureofaciens* (ATCC 13985)) possessing cd1-type nitrite reductase and Cu-containing nitrite reductase, respectively. We conclude the same for the two denitrifying cultures presented in this work (*P. fluorescens* and *P. chlororaphis*) since the difference in isotopic fractionation between the two bacteria species is on the bulk. Toyoda et al. (2005) present contrasting results for ϵ_{SP} of *P. fluorescens* (ATCC 13525) of 23 ‰. The result may, however, not be comparable to ours as Toyoda et al. (2005) suspect an abiological reaction within the incubation flask to be responsible for N₂O production in the incubation experiment.

The observed difference in the isotopic fractionation during production of N₂O could originate from 1) a difference in the production rate (Mariotti et al., 1982), or 2) a difference in the nitric oxide reductase enzymes. 1) The production rates in our experiments (Table 6.3 and 6.2) show an isotopic fractionation dependent on the production rate similar to the one observed by Mariotti et al. (1982). Our experiments show a production rate 10 times higher for *P. chlororaphis* than for *P. fluorescens*, which cf. Mariotti et al. (1982) would account for only approximately a 10 ‰ offset. We therefore believe that a change in production rate does not account for the 37.1 ‰ difference in isotopic fractionation. 2) Nitric oxide reductase is the primary enzyme in a chain of catalytic reactions leading to the production of N₂O (Hino et al., 2010; Hendriks et al., 2000). The catalytic cycle involving production of N₂O from NO has yet to be completely understood with respect to the formation of the N-N double bond, the complexity of the structural information of nitric oxide reductase, the proton transfer pathway into nitric oxide reductase (Tosha and Shiro, 2013), and the very short

lifetime of the intermediate states of the molecules (Collman et al., 2008). We hypothesized that the difference in the bulk observed during incubation of our two bacterial species was due to different nitric oxide reductases produced by the two species. To test this hypothesis, we compared the DNA sequences of the *norB* and *norC* genes coding for the large and small subunit, respectively, of nitric oxide reductase from three different strains of *P. fluorescens* (strains NCIMB 11764 [Genbank accession number CP010945], PA3G8 [742825335], and F113 [CP003150]) and *P. chlororaphis* (strains O6 [389686655], PA23 [749309655], and UFB2 [836582503]) as well as two closely related denitrifying species, *P. aeruginosa* and *P. stutzeri*. Our analysis revealed 1) a very high similarity of the two genes in *P. fluorescens* and *P. chlororaphis* and 2) that the intra-species variability of the two genes was similar to the inter-species variation. This led us to reject our hypothesis and conclude that differences in nitric oxide enzymes produced by the two species were not responsible for the observed differences in the bulk.

We hypothesized that the difference in the bulk isotopic fractionation between the two bacteria originates from 1) a difference in production rates, and 2) mass-dependent fractionation associated with the nitrous oxide reductase in *P. fluorescens*. After production of N_2O molecules, the light molecules degas quickly out of the liquid phase and away from the nitrous oxide reductase. The heavy N_2O molecules are slower and react with the nitrous oxide reductase leading to a depletion of the heavy N_2O isotopes. As this is a diffusion driven process it is mass-dependent and a slight effect on SP is expected. This is also in line with the kinetic isotope effect theory which suggest a small offset towards higher ϵ_α and therefore higher ϵ_{SP} (Popp et al., 2002; Tilsner et al., 2003; Wrage et al., 2004; Well and Flessa, 2008).

6.4.1 Comparison to previous studies

Numerous publications have presented experiments with both in situ measurements of denitrifying bacterial production and reduction of N_2O during incubation of bacterial cultures and soil samples. In Fig. 6.8, we present a comparison between the results from this study and the results from a selection of the previously published results. The general understanding is that denitrification results in $SP \leq 10 \text{ ‰}$.

Applying different incubation techniques on soils with different properties showed SP during production of N_2O between -3 ‰ and 9 ‰ and between -0.9 ‰ and -8.2 ‰ during reduction (Lewicka-Szczebak et al., 2014, 2015; Well and Flessa, 2009b,a; Köster et al., 2013a). During production of N_2O in bacterial culture experiments involving *P. chlororaphis* (ATCC 43928) and *P. aureofaciens* (ATCC 13985), Sutka and Ostrom (2006) found SP values of -2.5 ‰

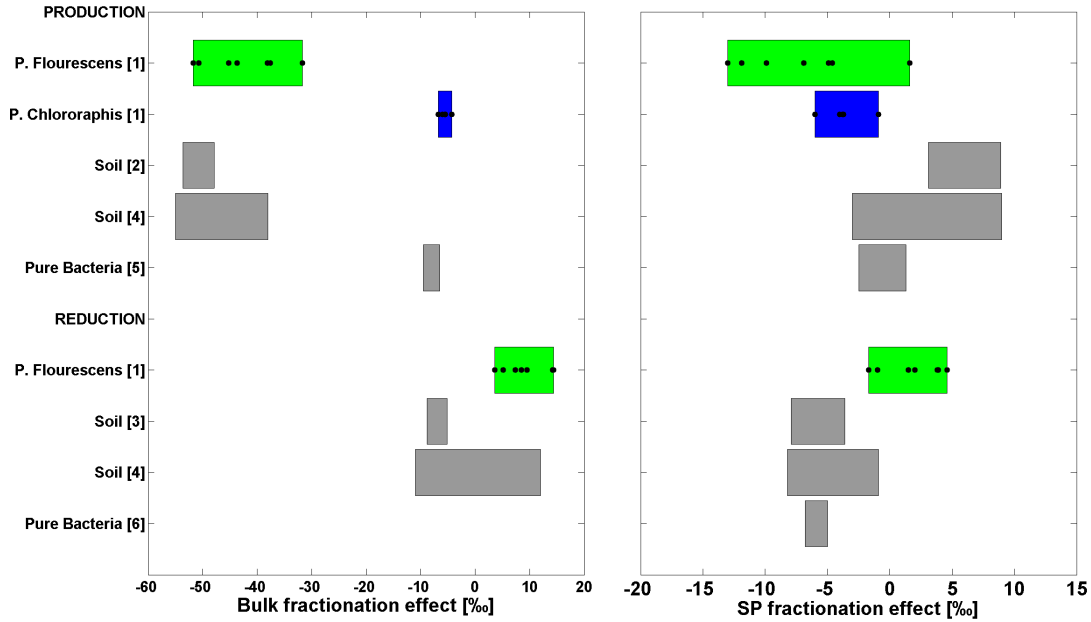


Figure 6.8: (A) Bulk and (B) SP isotopic fractionation calculated from the continuous measurements with *P. fluorescens* (green) and *P. chlororaphis* (blue) respectively. Both the production and reduction isotopic fractionations are shown and compared with previously presented results. [1] [This study], [2] [(Well and Flessa, 2009b)], [3] [(Well and Flessa, 2009a)], [4] [(Lewicka-Szczebak et al., 2014, 2015)], [5] [(Sutka and Ostrom, 2006)], [6] [(Ostrom et al., 2007b)].

and 1.3 ‰ and $\delta^{15}\text{N}^{\text{bulk}}$ values of between -7 ‰ and -10 ‰. Our results for N_2O SP and bulk isotopic fractionation from *P. chlororaphis* are in the same range as what has been reported previously.

A number of studies have investigated N_2O originating from denitrification in soils (e.g. (Well and Flessa, 2009a; Köster et al., 2013a; Lewicka-Szczebak et al., 2014, 2015)). The results are only partly in accord with our findings for specific bacteria strains. I.e. they find consistently negative isotopic fractionation for SP while we find slightly positive values on average. Ostrom et al. (2007b) investigated bacterial reduction of N_2O using *P. stutzeri* and *P. denitrificans*, and the SP isotopic fractionation resulting from this bacterial reduction of N_2O was between -6.8 ‰ and -5 ‰. However, they note that while for high net production (predominantly production of N_2O) SP is negative while with reduced net production that goes with an increasing rate of reduction the SP value increases, in line with our finding. This is also in agreement with kinetic isotope theory presented e.g. Popp et al. (2002), Tilsner et al. (2003), and Wrage et al. (2004).

6.5 Conclusions

We have presented successful continuous measurements of the denitrifying bacterial process using two different strains of bacteria: *P. fluorescens* which is a full denitrifier, and *P. chlororaphis* which is a denitrifier without nitrous oxide reductase activity. Assuming a Rayleigh type fractionation, modified for isotopomers and simultaneous reduction, we have calculated the isotopic fractionation during production and reduction of N₂O. The isotopic fractionation for *P. chlororaphis* is in line with previous results for both SP and bulk. For *P. fluorescens*, we find similar SP isotopic fractionation values during N₂O production, while we find slightly increased SP isotopic fractionation values during N₂O reduction. The bulk isotopic fractionation calculated for N₂O reduction is in line with previously presented results though for production we find an isotope depletion. We believe that, in our experiment, the bulk isotope depletion is due to mass-dependent fractionation.

6.6 Author contribution

MW and TB designed the experiments and MW carried out the measurements and analyzed data. SC prepared the bacteria prior to experiments. AP analyzed the bacterial DNA sequences. DBH and EC developed the G5101i-CIC analyzer. MW prepared the manuscript with contribution from all co-authors.

6.7 Acknowledgements

We thank Jan Kaiser for isotope specific gas samples used for our reference gases, Sakae Toyoda, Naohiro Yoshida, Carina van der Veen, and Thomas Röckmann for assistance on measurements of our reference gases. We want to thank Center for Permafrost (CENPERM DNRF100) and the Centre for Ice and Climate, funded by the Danish National Research Foundation for their support, and The Danish Agency for Science Technology and Innovation, for funding used in supporting this project. We want to thank Picarro Inc. and especially Eric Crosson, and Nabil Saad for the collaboration and guidance in the development of the N₂O isotope analyzer prototype used in this project.

6.8 Supporting material

6.8.1 Oxygen dependence

The gas matrix of the sample gas is of great importance when using spectroscopy based measuring techniques. When the mixing ratio of the gas matrix is changed, the line shape is also altered, leading to a change in the isotopic signature of the measured sample gas. For the CRDS analyzers, the isotopic signature of the N_2O isotopologues has a linear response to the oxygen availability in the gas matrix (Erler et al., 2015).

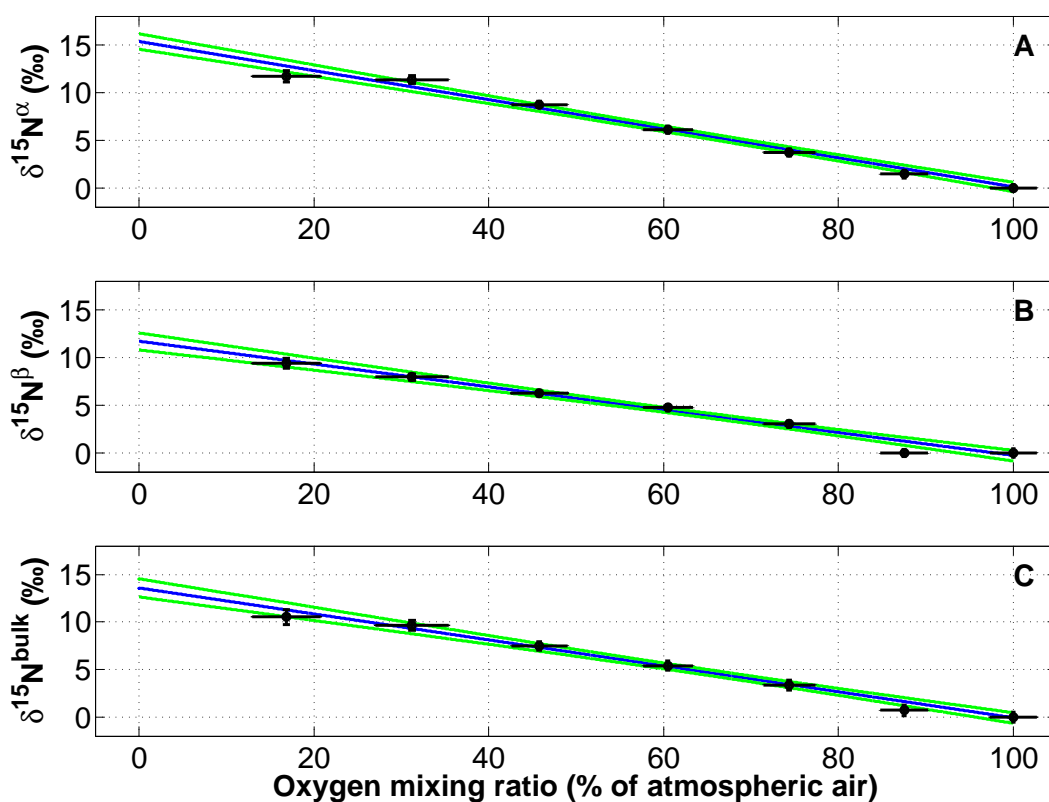


Figure S6.9: The effect of changing oxygen mixing ratio on the (A) $\delta^{15}N^\alpha$, (B) $\delta^{15}N^\beta$, and (C) $\delta^{15}N$. Black points represent mean values of the difference between the two dilution experiments performed with each of the two standard gas. In red the standard error of the measurements are shown for both the δ -value and the oxygen mixing ratio. The blue lines are mean values of the Monte Carlo simulation. The green lines are the $1-\sigma$ error-bar calculated using Monte Carlo simulation.

The presented bacterial experiments are performed under anaerobic conditions, where oxygen is not present. The effect of this lack of oxygen on the isotopic signal was quantified

by performing dilution experiments on the two CIC-MPI standard gases. Two stepwise dilution measurement with either pure synthetic air or N_2 was conducted for each of the standard gases. The N_2 was of purity 99.9999 % and the synthetic air was a N_2/O_2 mixture (20.1 % O_2 and 79.9 % N_2 , purity 99.999 %). The effect of a changing oxygen mixing ratio on the isotopic composition of N_2O is assessed from the difference between the two dilution experiments. Figure S6.9 show response of the isotope composition with respect to the Oxygen composition averaged for the two standard gases. This relation is calculated using a Monte Carlo algorithm applied to a linear relation model for the oxygen mixing ratio (OMR) (measured as percentage of the atmospheric concentration) and $\delta^{15}N^\alpha$, $\delta^{15}N^\beta$, and $\delta^{15}N$ respectively.

The linear relation model for the effect of Oxygen mixing ratio to the values of $\delta^{15}N^\alpha$, $\delta^{15}N^\beta$, and $\delta^{15}N$ are shown in equation 6.12, 6.13, and 6.14, respectively.

$$\delta^{15}N_{ODC}^\alpha = -0.1534 \cdot OMR + 15.269 \quad (6.12)$$

$$\delta^{15}N_{ODC}^\beta = -0.1210 \cdot OMR + 11.662 \quad (6.13)$$

$$\delta^{15}N_{ODC}^{bulk} = -0.1372 \cdot OMR + 13.465 \quad (6.14)$$

In the above $\delta^{15}N_{ODC}^\alpha$, $\delta^{15}N_{ODC}^\beta$, and $\delta^{15}N_{ODC}^{bulk}$ represent the offsets which are subtracted from the N_2O concentration corrected data.

The bacterial evolution experiments were performed under pure N_2 conditions. The reported values in the article, are derived by first applying the N_2O concentration correction and then subsequently applying the correction for the lack of Oxygen. With zero Oxygen this correction becomes a simple subtraction by the intercept values of the above linear models.

6.8.2 Pseudomonas chlororaphis

Figures of $\delta^{15}N^{\alpha}$ as a function of N_2O concentration and the modeled Rayleigh type distillation. High resolution CRDS data (blue line) and five minutes running average (black line). The red curve is the modeled Rayleigh type distillation curve for the production of N_2O . The blue arrow indicates the direction of time during production of N_2O .

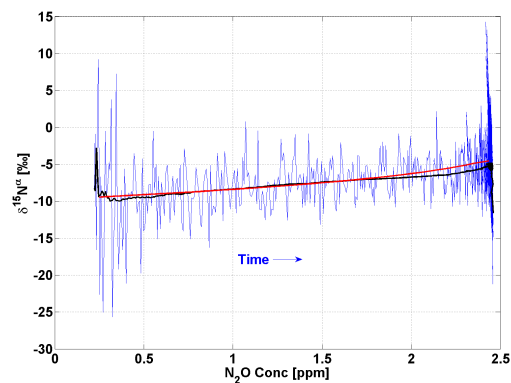


Figure S6.12: *Replica # 3*

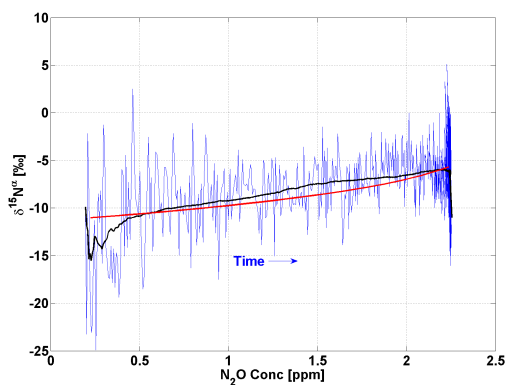


Figure S6.10: *Replica # 1*

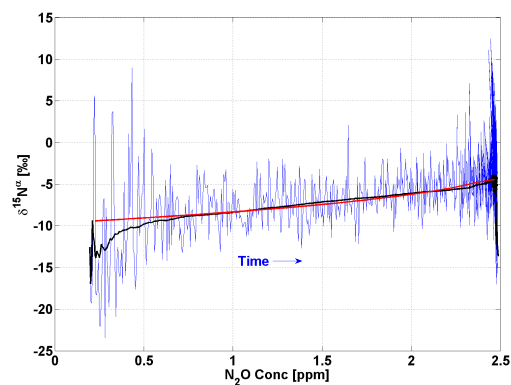


Figure S6.13: *Replica # 4*

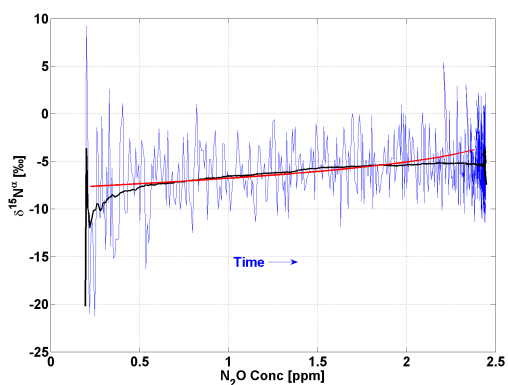


Figure S6.11: *Replica # 2*

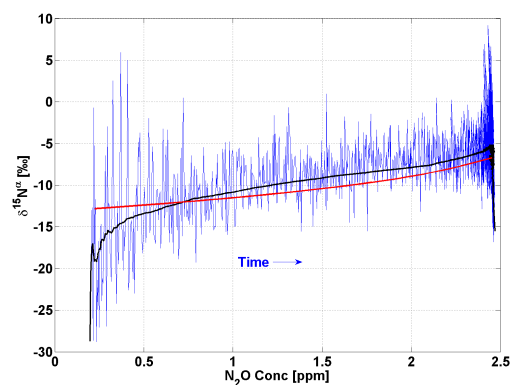


Figure S6.14: *Replica # 5*

Figures of $\delta^{15}N^{\beta}$ as a function of N_2O concentration and the modeled Rayleigh type distillation. High resolution CRDS data (blue line) and five minutes running average (black line). The red curve is the modeled Rayleigh type distillation curve for the production of N_2O . The blue arrow indicates the direction of time during production of N_2O .

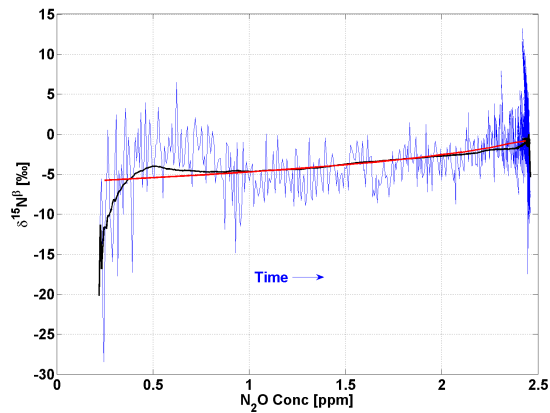


Figure S6.17: *Replica # 3*

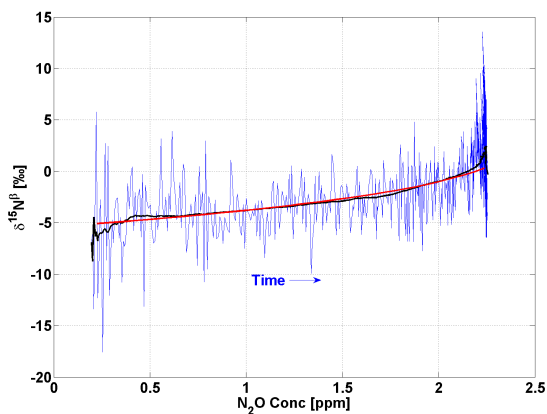


Figure S6.15: *Replica # 1*

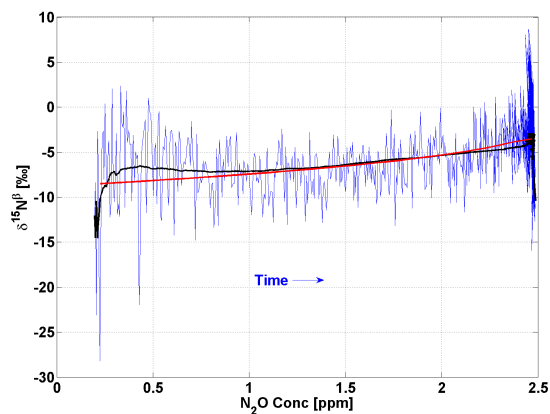


Figure S6.18: *Replica # 4*

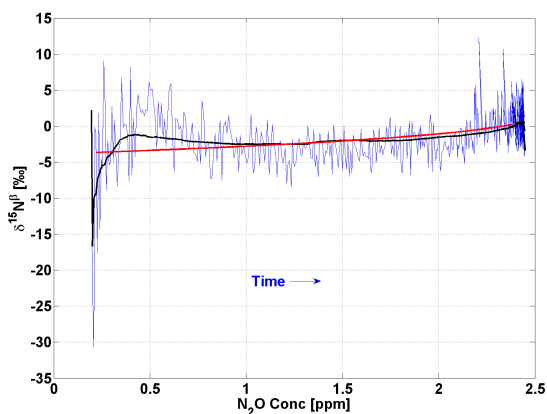


Figure S6.16: *Replica # 2*

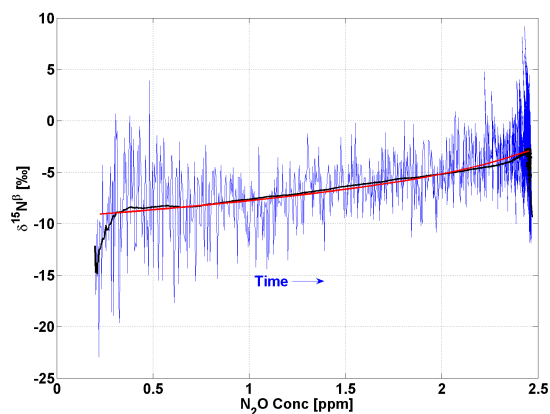


Figure S6.19: *Replica # 5*

Figures of $\delta^{15}N^{bulk}$ as a function of N_2O concentration and the modeled Rayleigh type distillation. High resolution CRDS data (blue line) and five minutes running average (black line). The red curve is the modeled Rayleigh type distillation curve for the production of N_2O . The blue arrow indicates the direction of time during production of N_2O .

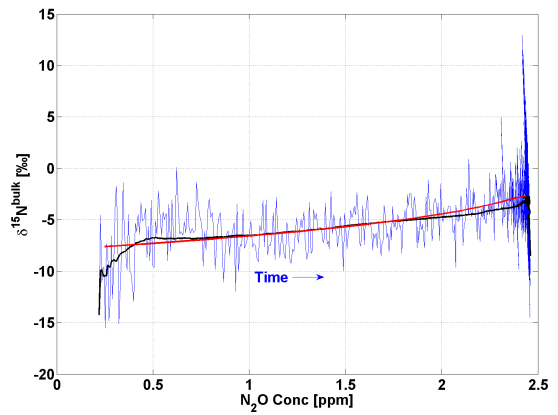


Figure S6.22: *Replica # 3*

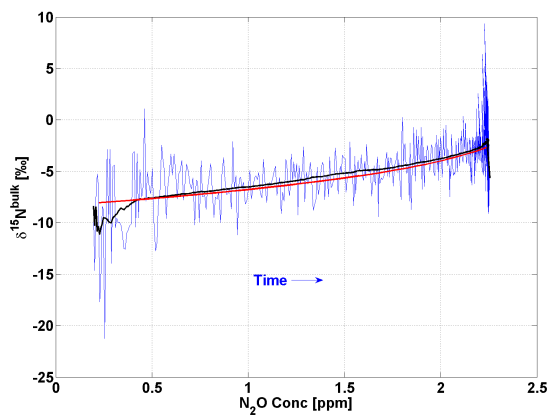


Figure S6.20: *Replica # 1*

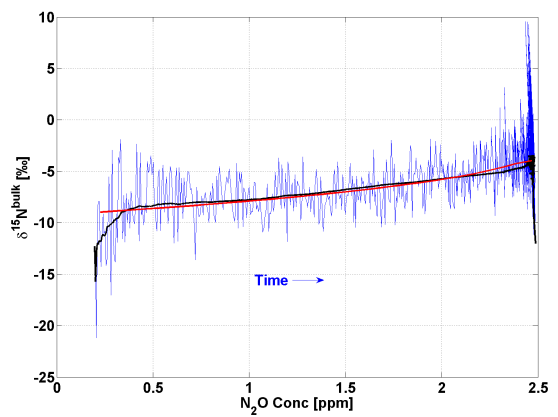


Figure S6.23: *Replica # 4*

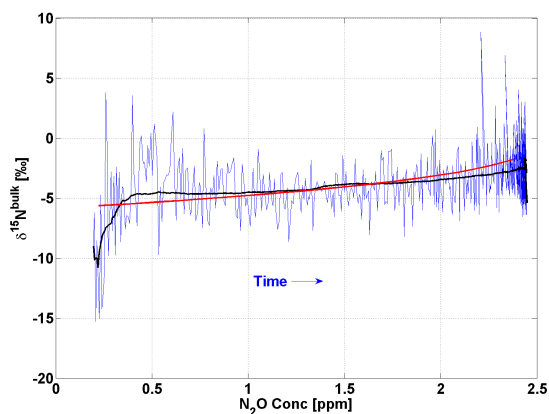


Figure S6.21: *Replica # 2*

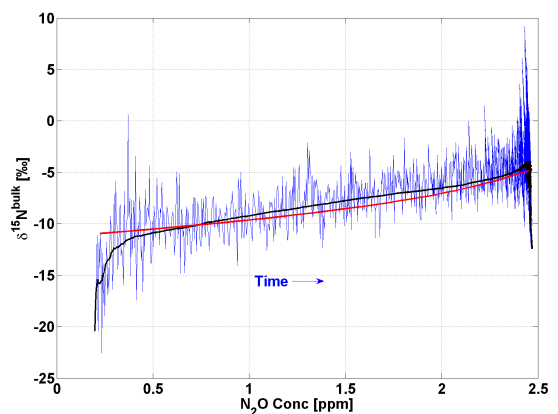


Figure S6.24: *Replica # 5*

6.8.3 Pseudomonas fluorescens

Figures of $\delta^{15}N^\alpha$ as a function of N_2O concentration and the modeled Rayleigh type distillation. High resolution CRDS data (blue line) and five minutes running average (black line). The red and magenta curve is the modeled Rayleigh type distillation curve for the production and reduction of N_2O , respectively. The blue arrow indicates the direction of time during production of N_2O whereas the green arrow indicates the direction of time during reduction of N_2O .

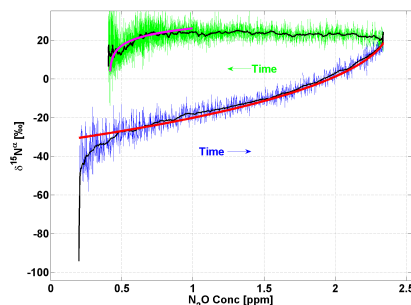


Figure S6.28: *Replica # 4*

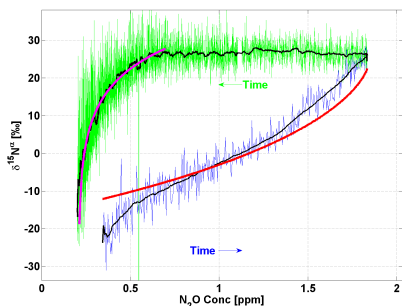


Figure S6.25: *Replica # 1*

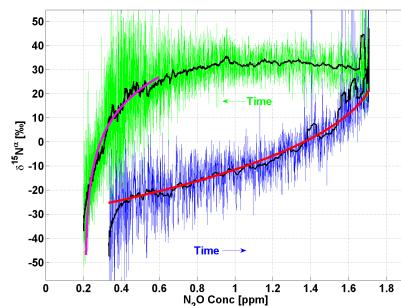


Figure S6.29: *Replica # 5*

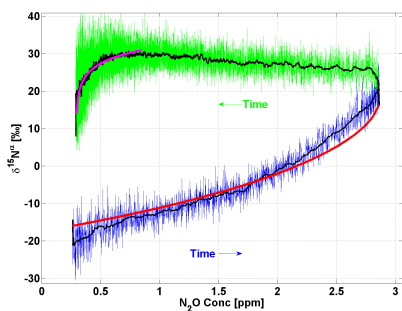


Figure S6.26: *Replica # 2*

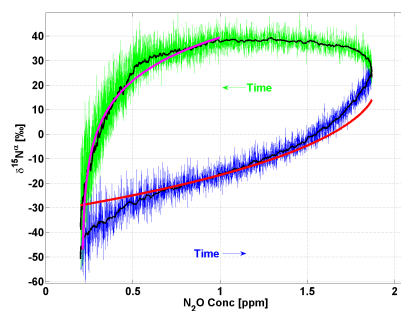


Figure S6.30: *Replica # 6*

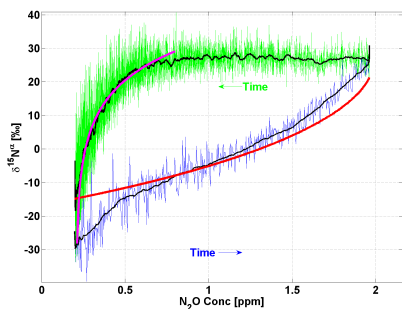


Figure S6.27: *Replica # 3*

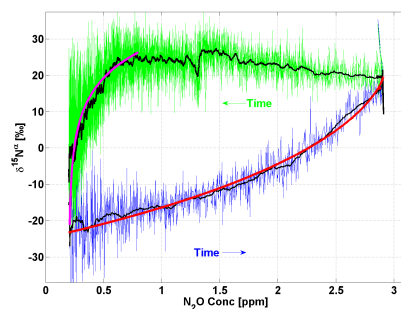


Figure S6.31: *Replica # 7*

Figures of $\delta^{15}N^{\beta}$ as a function of N_2O concentration and the modeled Rayleigh type distillation. High resolution CRDS data (blue line) and five minutes running average (black line). The red and magenta curve is the modeled Rayleigh type distillation curve for the production and reduction of N_2O , respectively. The blue arrow indicates the direction of time during production of N_2O whereas the green arrow indicates the direction of time during reduction of N_2O .

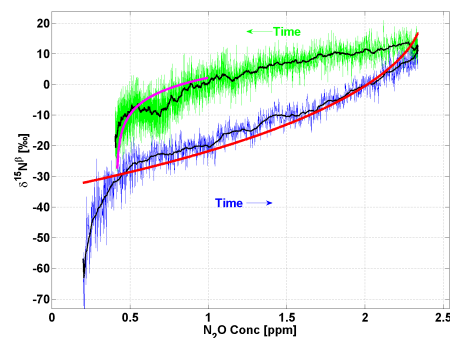


Figure S6.35: *Replica # 4*

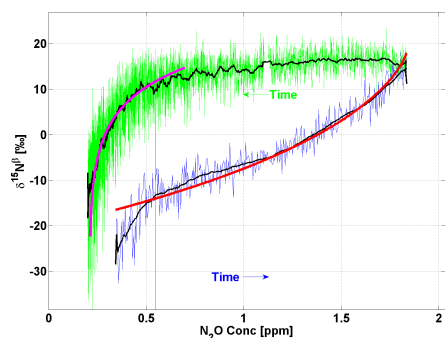


Figure S6.32: *Replica # 1*

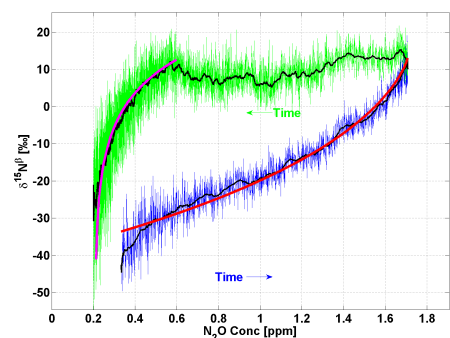


Figure S6.36: *Replica # 5*

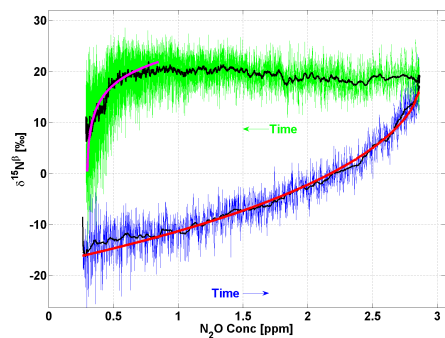


Figure S6.33: *Replica # 2*

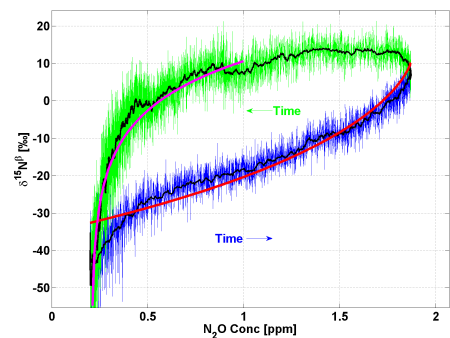


Figure S6.37: *Replica # 6*

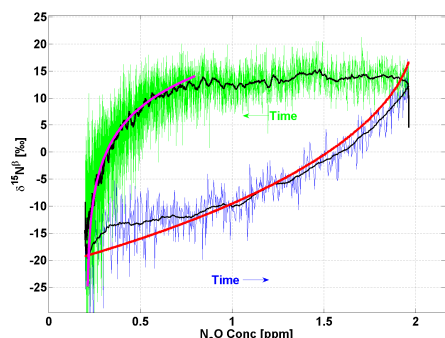


Figure S6.34: *Replica # 3*

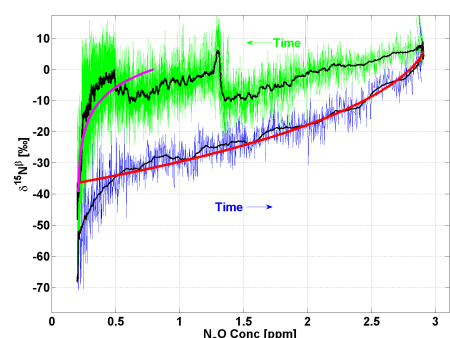


Figure S6.38: *Replica # 7*

Figures of $\delta^{15}N^{bulk}$ as a function of N_2O concentration and the modeled Rayleigh type distillation. High resolution CRDS data (blue line) and five minutes running average (black line). The red and magenta curve is the modeled Rayleigh type distillation curve for the production and reduction of N_2O , respectively. The blue arrow indicates the direction of time during production of N_2O whereas the green arrow indicates the direction of time during reduction of N_2O .

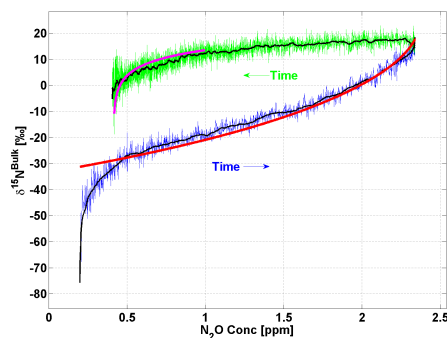


Figure S6.42: *Replica # 4*

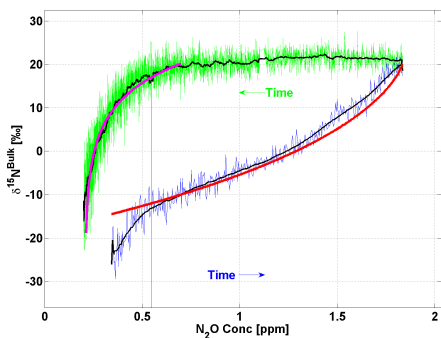


Figure S6.39: *Replica # 1*

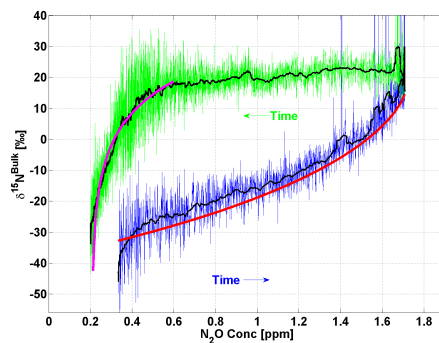


Figure S6.43: *Replica # 5*

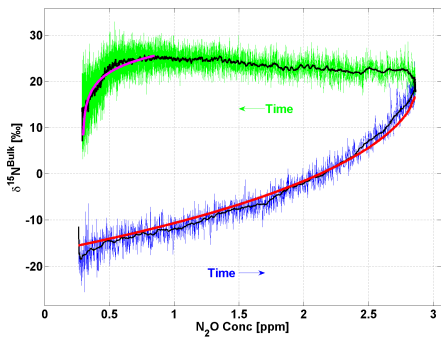


Figure S6.40: *Replica # 2*

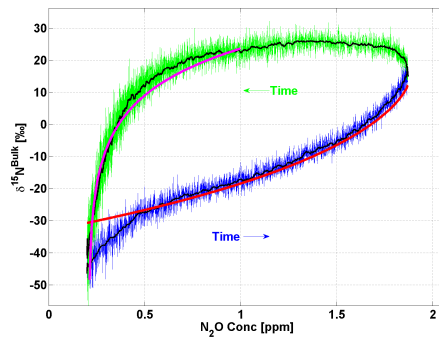


Figure S6.44: *Replica # 6*

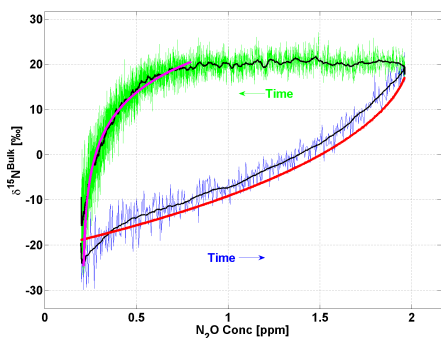


Figure S6.41: *Replica # 3*

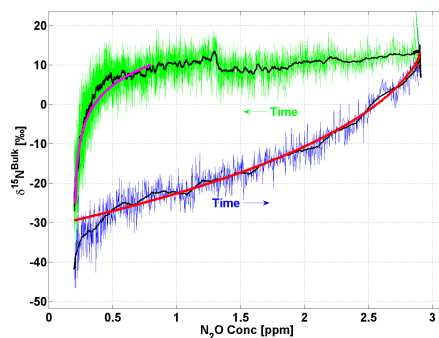


Figure S6.45: *Replica # 7*

Part III

Past atmosphere

Introduction - part III

The two major ice sheets on Earth, covering Antarctica and Greenland, have proven to play an important role as a climate archive. Kept within the ice sheets is information on the climatic history covering the past 800,000 years (EPICA Dome C) in Antarctica (e.g. Augustin et al. (2004); Lüthi et al. (2008); Loulergue et al. (2008)) and 130,000 years (NGRIP and NEEM) in Greenland (e.g. Andersen et al. (2004); Dahl-Jensen (2013)). The information stored in the ice cores (climate records) improve our understanding of past climates, which in turn improve the understanding of present day climate and the climatic responses, which can then assist in predictions of future climate scenarios, and therefore the impact on life on Earth.

In the following part (part III), the focus is on the past atmospheric signature of N_2O . This part starts with a short introduction to ice core history and science, followed by chapter 8 in which measurements of the isotopic signature of N_2O extracted from ice core samples is presented.

7.1 A short introduction to ice cores as climate archives

As snow precipitates in the accumulation zone of an ice sheet snow layers are formed year after year. Over time the snow layers accumulate on top of each other which results in compression of the underlying layers and eventually creation of ice layers. This continuous snow layer compression is known as firn densification. Ice is basically incompressible and compression of layers primarily take place in the firn (approximately the top 80-110 meter of the ice sheet), in which the pores are open and connected by channels between the ice crystals. In the transition between the firn and the ice we find the close-off zone. Densification models generally assume close-off when a density of 830 kg/m^3 has been reached. At this point all air channels are closed and the annual layers are thinned by horizontal

deformation. Before the close-off zone the air channels are connected and allows exchange of atmospheric air with the overlaying layers and the atmosphere. Once the air channels are closed (below the close-off depth) the ice becomes compressed to pure ice with a density of 917 kg/m^3 and the atmospheric gases are trapped within air bubbles. The trapped air is kept within the ice until it melts at the bedrock, hence the ice works as a unique continuously preserved climate archive. A consequence of open channels in the firn is that the gas age is significantly different than that of the surrounding ice and two age-scales are therefore required for one ice core. In the name of science, ice cores were and are drilled to access information on past temperature, atmospheric gas composition, chemical compounds, volcanic ash, dust, etc. (Langway Jr. et al., 1993; Mayewski et al., 1997; Kameda et al., 1994; Delmas, 1994; Reeh et al., 2005; Bender et al., 2006) (and references therein).

7.2 NEEM

The ice core samples used for the measurements presented in the following chapter are from the North Greenland Eemian ice core drilling (NEEM) project (Dahl-Jensen, 2013). The NEEM core was drilled in the northern hemisphere summer months from 2008 until 2012, in North Greenland at 77.45°N 51.06°W , and resulted in a 2542 meter long ice core. The scope of the NEEM project was to reach ice dating back to the previous interglacial, the Eemian period, which started approximately 130,000 years before present. The top 1419 m of the ice originates from the current interglacial period known as the Holocene. From 1419 m down to 2206.7 m, the ice originates from the glacial and has been dated back 108,000 years BP (BP being 1950 AD). The last 335.3 m was found to be folded and dating is therefore difficult, though measurements of stable isotopes have indicated the ice to stem from the Eemian and therefore are between 115,000 and 130,000 years old. (Dahl-Jensen, 2013)

Measurements of N₂O isotopomers from NEEM ice core

8.1 Introduction

Nitrous oxide (N₂O) is an important and strong atmospheric trace gas. The N₂O mixing ratio has increased by more than 50 ppb since the preindustrial atmosphere (Park et al., 2012). The large increase of N₂O is of great importance to life on Earth due to the long atmospheric lifetime (approximately 120 yrs (Montzka et al., 2011)), the ozone (O₃) depleting capacity of N₂O entering the stratosphere (Forster et al., 2007; Kim and Craig, 1993), and the effect of N₂O as a highly potent greenhouse gas (Hartmann et al., 2013). The isotopes of N₂O have proven to be an important tool in the determination of the origin of the N₂O molecule. The two primary natural sources of N₂O are bacterial nitrification and denitrification in the terrestrial and marine environment. The intramolecular distribution of the ¹⁵N isotope in the isotopomers of N₂O ($\delta^{15}\text{N}^\alpha$ (¹⁴N¹⁵N¹⁶O) and $\delta^{15}\text{N}^\beta$ (¹⁵N¹⁴N¹⁶O)) has been shown to be a tool for distinguishing the microbial sources of N₂O, e.g. nitrification and denitrification (Park et al., 2011). The intramolecular distribution is also called site preference (SP) and is defined as the difference between the isotopomers of N₂O ($\text{SP} = \delta^{15}\text{N}^\alpha - \delta^{15}\text{N}^\beta$) (Brenninkmeijer and Röckmann, 1999; Toyoda et al., 2002). Schilt et al. (2010) showed for the first time a complete (merged) ice core record of atmospheric N₂O concentrations going back to the last interglacial. The N₂O record showed variations in line with climate and considerable responses to the millennial timescale climatic variations during the glacial. The glacial variations are suggested to stem from changes in the sources, since the N₂O record showed variations similar to the methane record. Schilt et al. (2010) suggests that the differences found in the onset of the extreme temperature changes between the N₂O record and the other records occasionally (e.g. D-O event 15 and 17) lead to potential early warnings. Furthermore, Schilt et al. (2013) showed that the N₂O concentrations are related to different stadials during the glacial. This difference has the potential for further

verification by the use of the SP of N₂O.

To get a first impression of the SP of N₂O from the gas stored in the ice cores, we have performed the first preliminary measurements of the isotopic composition of N₂O from the NEEM ice core (Dahl-Jensen, 2013). We have performed measurements on four sections of the NEEM ice core namely the early-, mid-, and late Holocene, and also the glacial. In the following, we refer to the four periods as glacial (32.5 kyrs - 32 kyrs BP), early Holocene (10 kyrs - 9.5 kyrs BP), mid Holocene (5 kyrs - 4.5 kyrs BP), and late Holocene (0.5 - 0.2 kyrs BP). Measurements of m/z 30, m/z 31, m/z 44, m/z 45, and m/z 46 were performed using an isotope ratio mass spectrometry (IRMS) located at the Institute for Marine and Atmospheric Research Utrecht (IMAU), Utrecht University, The Netherlands. The measured masses were used to calculate the resulting delta-values $\delta^{15}N$ (N₂O), $\delta^{18}O$ (N₂O), and $\delta^{15}N$ (NO⁺ fragment)), as well as the isotopes of N₂O ($\delta^{15}N$, $\delta^{15}N^{\alpha}$, $\delta^{15}N^{\beta}$, $\delta^{17}O$, and $\delta^{18}O$) using the method described by Kaiser and Röckmann (2008).

8.2 Method

The presented trace gas measurements, extracted from the NEEM ice core, were performed using a dry extraction system developed by Sapart et al. (2011). The focus of the measurements was purely on the isotopomers of N₂O, and the setup was therefore adjusted accordingly. In the following subsections the gas extraction and measuring procedure is described. A more detailed description can be found in the original publication by Sapart et al. (2011).

8.2.1 Instrumentation

Measurements of the isotopomers of N₂O were performed in four steps, namely 1) preparation of the ice sample, 2) gas extraction, 3) IRMS measurements, 4) isotopomer calculation. An ice core consists of only approximately 100 mL STP/kg of gas, leaving the remaining approximately 900 mL STP/kg as ice (Delmas, 1994). Due to the low mixing ratio of N₂O in the atmosphere (both past and present), a relatively large amount of ice is needed to ensure the required gas volume. Sapart et al. (2011) stated that the preferred sample size for measurements of N₂O is found to be between 500 g and 700 g of ice. Fortunately this amount of ice is equivalent to one sample bag, and stacking of previously packed sample bags is therefore avoided. Preparation of the ice samples was performed in a working freezer at -30 °C. The ice sample is first divided into pieces approximately 15 cm long using a band saw. Then a thin (a few mm) layer is removed all around the sample by microtoming.

Microtoming is done to remove ice (and therefore gas) which has been exposed to surface contamination (e.g. drill-liquid). The cleaned sample pieces are weighted before they are placed in the extraction pot (see Fig. 8.1).

The extraction chamber is a 6 L stainless steel pot with a removable lid. The cleaned ice samples are placed in an "ice grater" inside the extraction pot. The ice grater is a perforated titanium nitride coated stainless steel cylinder of 22 cm in diameter and 15.8 cm high (inside the cylinder). The pot is sealed using a copper o-ring (conflat flange of 22 cm in diameter) and 12 bolts equally spaced to ensure the best possible seal. Once the pot is sealed, the ice grater is stuck between the top and bottom of the pot to hinder mechanical heat production, leaks, and mechanical methane (CH_4) production. The sealed pot is then carefully placed and mounted in a $-30\text{ }^\circ\text{C}$ freezer before the pot is connected to the extraction setup and evacuated to $1.2 \cdot 10^{-6}$ mbar. The evacuated extraction pot is then dismantled from the extraction setup, securely fixed to the shaking device, and left to be shaken back and forth while the ice samples are grated. The grating occurs for 30 minutes at 33 Hz, after which approximately 99 % of the ice has been grated to flakes no larger than 1-2 mm in diameter. (Sapart et al., 2011)

Once the ice has been grated, the pot is once again connected to the extraction setup, and the extraction line in front of the pot is evacuated. After evacuation of the pot the valve on top of the pot is opened and the gas flows into the evacuated line. From the pot, the gas flows through a H_2O vapor trap (T1) and a N_2O (and CO_2) trap (T2) before the rest of the gas is trapped in trap T3 due to the chemical features of the liquid nitrogen cooled Hayesep. Trap T1 is a U-shaped glass tube immersed in a dry-ice-alcohol ($-80\text{ }^\circ\text{C}$) filled dewar. Trap T2 is a U-shaped glass tube immersed in a liquid nitrogen (LN2) ($-196\text{ }^\circ\text{C}$) dewar. Trap T3 is a U-shaped glass tube filled with Hayesep D (mesh 80/100, Altech GmbH, Germany) and immersed in an LN2 filled dewar. After approximately 45 minutes all gas has been extracted from the pot and T2 is sealed off.

From T2 the sample is transferred (with He as carrier gas) to the fully automated N_2O IRMS setup (Röckmann et al., 2003). When the sample flows through the N_2O IRMS setup, the sample is cleaned from CO_2 using an ascarite trap (NaOH flakes reacting chemically with CO_2 , followed by $\text{Mg}(\text{ClO}_4)_2$ reacting with produced H_2O vapor). After the ascarite trap N_2O is trapped and concentrated in the precon (a U-shaped ss tube immersed in LN2 bath), followed by a cryofocus (a fused silica capillary cooled in an LN2 bath). After cryofocusing, N_2O is separated from any remaining chemical compounds by a GC column. Finally, the potentially abundant H_2O is removed through a nafion unit. The cleaned N_2O gas is then

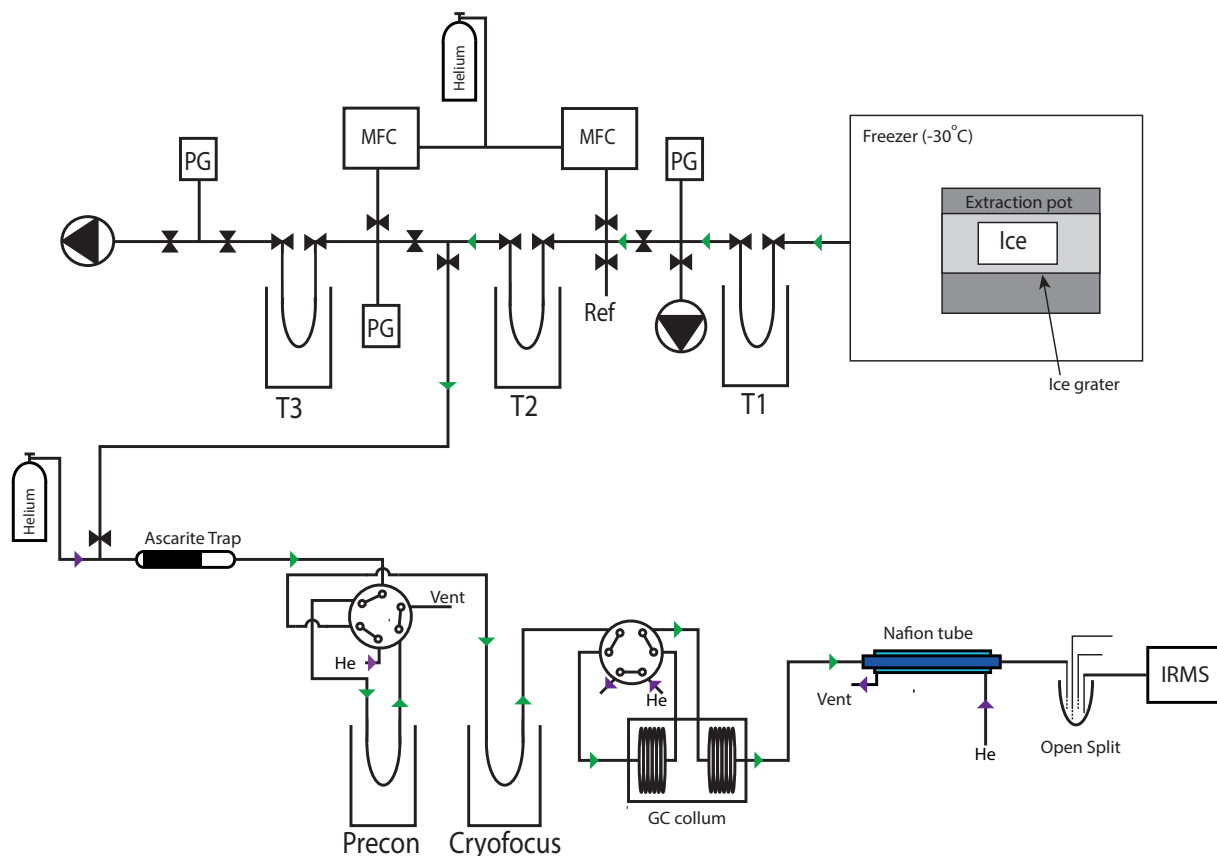


Figure 8.1: *Schematic Outline of the extraction and measuring setup. The green arrows indicate the flow of the sample gas. The purple arrows indicate the flow of helium (He) and overflow.*

transferred through an open split to the IRMS, where the sample is analyzed for m/z 30, 31, 44, 45, and 46. (Röckmann et al., 2003)

Brenninkmeijer and Röckmann (1999) describe how IRMS analysis of a pure N_2O gas can be analyzed for abundance of the isotopomers of N_2O . N_2O itself is being measured in the Faraday cups as mass 44 ($^{14}N^{14}N^{16}O$), mass 45 ($^{15}N^{14}N^{16}O$, $^{14}N^{15}N^{16}O$, $^{14}N^{14}N^{17}O$), and mass 46 ($^{14}N^{14}N^{18}O$, $^{14}N^{15}N^{17}O$, $^{15}N^{14}N^{17}O$, $^{15}N^{15}N^{16}O$). When bombarding the N_2O molecules with electrons (at an impact energy of approximately 70 eV), the molecules were found to dissociate into fragments (Brenninkmeijer and Röckmann, 1999), fragments which can be analyzed simultaneously together with the main N_2O molecules. For analysis of the isotopomers of N_2O , the important masses measured are mass 30 and 31. Mass 30 then represents the $^{14}N^{16}O$ fragment, whereas mass 31 represents the $^{15}N^{16}O$ and the $^{14}N^{17}O$ fragment. From these measurements only $\delta^{15}N$, $\delta^{15}N^\alpha$, and $\delta^{18}O$ can directly be calculated as shown by Kaiser and Röckmann (2008). Calculations of $\delta^{15}N^\beta$ are possible by comparison of $\delta^{15}N^\alpha$ and the $^{15}N / ^{14}N$ ratio as shown by Kaiser and Röckmann (2008). Finally, Kaiser

and Röckmann (2008) deduced the $\delta^{17}\text{O}$ from a series of equations involving all original ratios.

8.2.2 NEEM samples

The presented analysis consists of N_2O isotopomer measurements from 15 ice core samples from the NEEM ice core. The samples were chosen to represent four different geological time periods, the glacial (32 kyrs b2k), the early Holocene (10 kyrs - 9.5 kyrs b2k), the mid Holocene (5 kyrs - 4.5 kyrs b2k), and the late Holocene (0.5 - 0.2 kyrs b2k). Table 8.1 shows the pre-measurement information of the 15 samples. The ID number refers to the bag number given in Table 8.1, the sample depth was measured during the ice core drilling process, the gas age is estimated using the time scale constructed from the chronology GICC05modelext-NEEM-1 (Rasmussen et al., 2013), sample weight, gas pressure, and the approximate geological time period.

Table 8.1: *NEEM ice core data for samples used in the analysis.*

Ice ID #	Depth (m)	Gas age (year)	Weight (g)	Pressure (mbar)	Geological period
220	120.45	254.56	657	9.7	Late Holocene
237	129.8	298.15	636	10.2	Late Holocene
244	133.65	315.87	607	8.7	Late Holocene
259	141.9	354.87	666	10.4	Late Holocene
268	146.85	377.42	669	10.7	Late Holocene
284	155.65	419.27	627	9.7	Late Holocene
620	340.45	1355.28	637	9.2	Late Holocene
1538	845.35	4522.29	596	10.7	Mid Holocene
1560	857.45	4615.54	641	10.8	Mid Holocene
1582	869.55	4713.77	598	9.7	Mid Holocene
2366	1299.65	8998.63	681	8.7	Early Holocene
2372	1300.75	9048.21	681	8.3	Early Holocene
2412	1326.05	9405.63	662	7.4	Early Holocene
3094	1701.15	32343.51	632	7.1	Glacial
3096	1702.25	32436.93	652	7.3	Glacial

8.2.3 Correction of IRMS size dependence

To ensure stability and a high degree of accuracy of the NEEM samples, a working standard gas (NAT332) was measured both before and after each individual ice core sample was measured. The procedure for the working standard measurements was performed similarly to the ice core samples. While grated ice is still sitting in the extraction pot, the working standard is introduced to the pot and the line upstream from T2. The amount of working standard introduced was adjusted to cover the possible sample size range (measured as the area of the sample peak). The 15 samples were measured over three time periods. Due to a significant instrumental drift, each measurement required a distinctive evaluation of reference measurements. Fig. 8.2 shows the results from one measurement period (similar

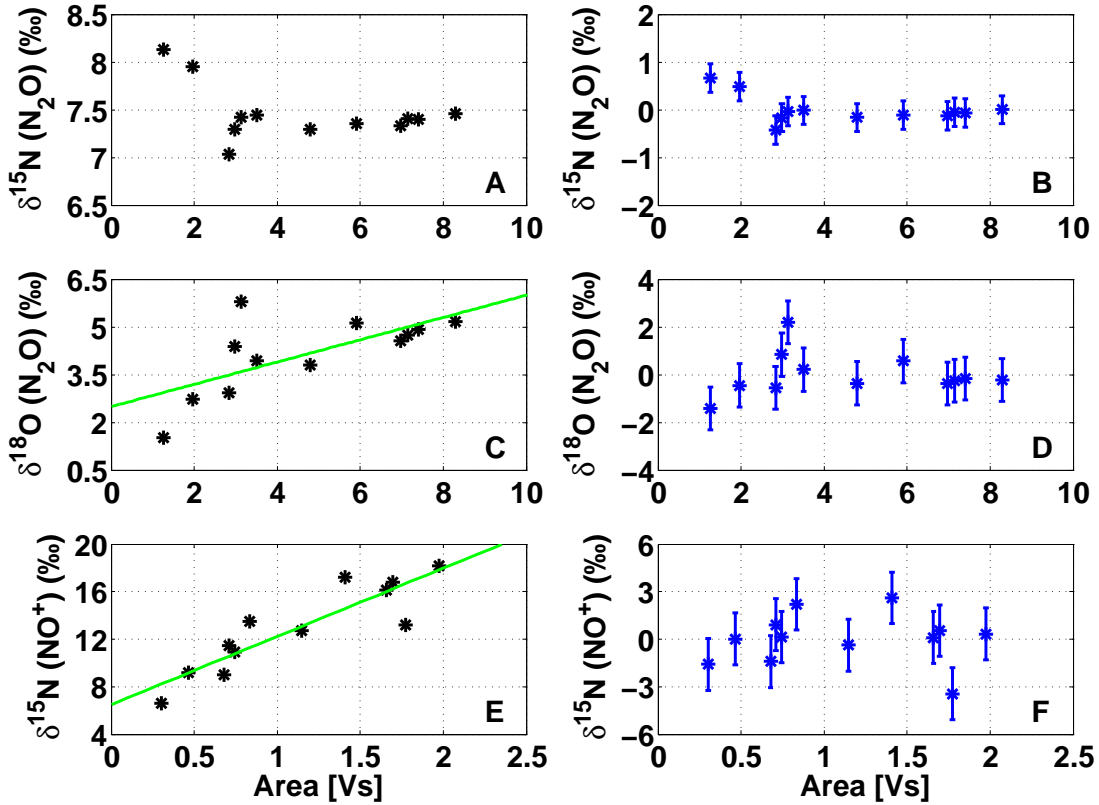


Figure 8.2: Working standard (NAT332) measurements for determination of sample size dependence. Raw IRMS measurements of $\delta^{15}\text{N}(\text{N}_2\text{O})$, $\delta^{18}\text{O}(\text{N}_2\text{O})$, and $\delta^{15}\text{N}(\text{NO}^+ \text{ fragment})$ are shown in black in subfigure A, C, and E, respectively. The size dependent correction (SDC) was applied to $\delta^{18}\text{O}(\text{N}_2\text{O})$, and $\delta^{15}\text{N}(\text{NO}^+ \text{ fragment})$. Subfigure B, D, and F show relation between measured values and reference for $\delta^{15}\text{N}(\text{N}_2\text{O})$, $\delta^{18}\text{O}(\text{N}_2\text{O})$, and $\delta^{15}\text{N}(\text{NO}^+ \text{ fragment})$, respectively.

figures for the two other periods are presented in the supporting material in section 8.8). A linear regression was fitted to the raw data. For the measurements of $\delta^{15}\text{N}(\text{N}_2\text{O})$, no

correction was applied since the measurements show no size dependence. Figure 8.2B, 8.2D, and 8.2F show the relation between the measured values and the reference measurements, as used in the further analysis. Data shown in Fig. 8.2D, and 8.2F are corrected for size dependence and calibrated with standard gas NAT332 simultaneously.

8.2.4 Isotopic calibration

The working standard (NAT332) was used for both calibration and for correction of IRMS size dependence. Measurements of NAT332 performed prior to the presented experiments have resulted in the "True" measurements as shown in Table 8.2. Measurements performed for the size dependent correction evaluation is presented as "Raw" NAT332 data (in Table 8.2), while the size dependent corrected measurements are shown as "SDC" data. The isotopic composition of all presented data is calculated as the offset to daily reference measurements and calibrated with the true NAT332 values. The daily reference measurements are always performed with identical volumes injected into the IRMS, therefore identical measurements are expected.

Table 8.2: *Isotopic composition of the working standard (NAT332) used for calibration of the ice samples. Calculated isotopic composition from both Raw measurements and SDC measurements, are presented together with the True isotopic composition.*

	$\delta^{15}\text{N}$ (‰)	$\delta^{15}\text{N}^{\alpha}$ (‰)	$\delta^{15}\text{N}^{\beta}$ (‰)	$\delta^{18}\text{O}$ (‰)	$\delta^{17}\text{O}$ (‰)
True	6.58	16.99	-3.80	45.81	24.42
Raw	5.81 ± 0.33	20.27 ± 4.87	-8.65 ± 5.22	41.89 ± 1.30	22.32 ± 0.66
SDC	6.58 ± 0.32	16.99 ± 2.18	-3.83 ± 2.38	45.81 ± 0.95	24.30 ± 0.48

For additional calibration, a second set of working standard gases were measured. The two standard gases are CIC-MPI-1 and CIC-MPI-2, which are based on pure N_2O gases (MPI-1 and MPI-2, respectively (see section 3.3)) with a known isotopic composition. The pure N_2O gases are mixed with a N_2/O_2 mixture (20.1 % O_2 and 79.9 % N_2 , purity 99.999 %) as described in section 3.3. In Table 8.3 the inter-laboratory mean value and combined standard deviation of the two standard gases, measured at three laboratories are shown. As described in section 3.3, the two standard gases were mixed and measured at the Centre for Ice and Climate in Copenhagen, Denmark (CIC), before they were measured at the laboratory at Tokyo Institute of Technology in Japan (Tokyo-Tech) and at the Institute for Marine and Atmospheric research Utrecht in The Netherlands (IMAU).

Table 8.3: *Inter-laboratory mean and combined standard deviation of CIC-MPI-1 and CIC-MPI-2, after measurements performed at Tokyo-Tech, IMAU, and CIC.*

Reference gas	[N ₂ O] (ppb)	$\delta^{15}\text{N}^{bulk}$ (‰)	$\delta^{15}\text{N}^{\alpha}$ (‰)	$\delta^{15}\text{N}^{\beta}$ (‰)
CIC-MPI-I	1909.8 ± 29.3	1.32 ± 0.82	1.94 ± 0.87	0.70 ± 1.42
CIC-MPI-II	1857.9 ± 19.2	-1.43 ± 0.82	12.01 ± 1.06	-14.87 ± 1.13

8.2.5 Statistical correction

After applying the size dependent correction to the measured NEEM-core samples the next step is correction for potential leaks. Unfortunately, we experienced some unexplainable issues with the Hayesep, which resulted in leaks while trapping gas from the extraction pot. For unknown reasons the issues were only unambiguously found while extracting gas from some of the ice core samples. The effect of leakage was not resolved by the SDC since only some samples were affected. We have corrected the samples based on investigations

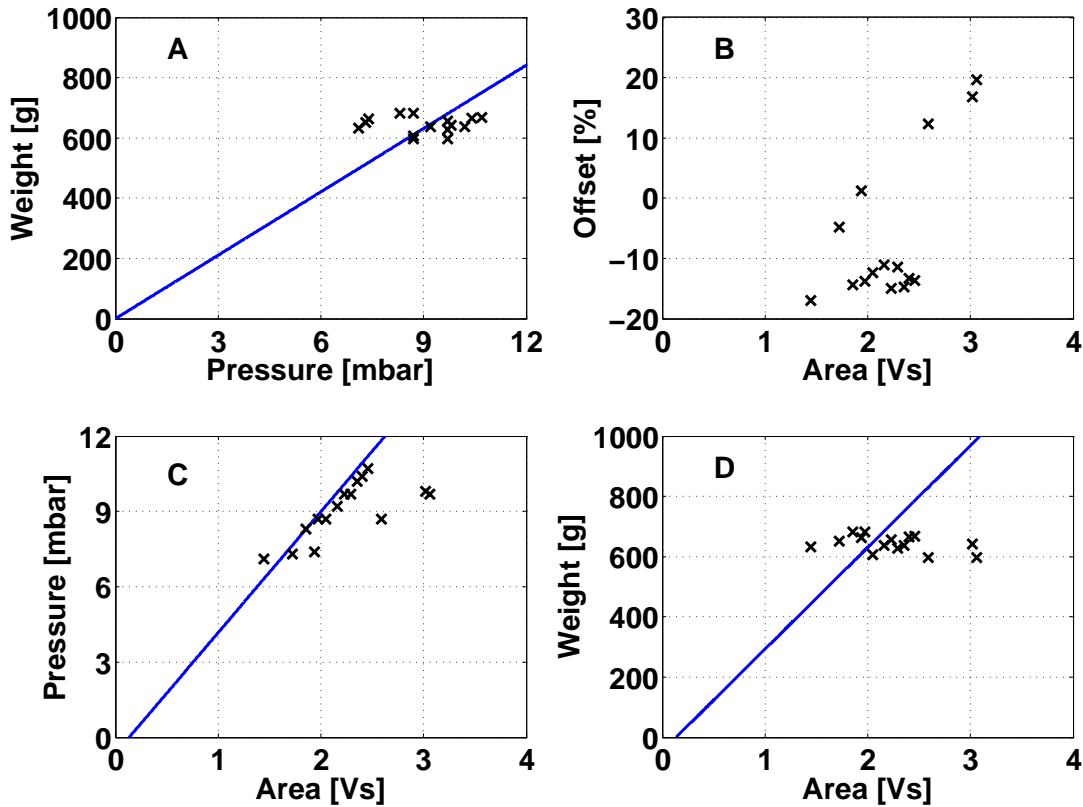


Figure 8.3: *Relationship between the sample weight, pressure, IRMS area, and concentration offset for the measured NEEM samples shown in black. The idealized relationships are plotted with the blue profiles.*

of the relationship between physical parameters measured before extraction and the results of IRMS measurements. The physical parameters measured during the extraction were the initial pressure released from the extraction pot (measured using the pressure gauge), and the ice sample weight (measured after preparation though before grating). Figure 8.3 shows the four interesting relationships between the measured ice weight, pressure, IRMS $\delta^{15}\text{N}$ area, and the estimated concentration offset.

The idealized relationships are based on theoretical calculations and all possible values within the range of the actual sample size, e.g. all possible sample weights. The idealized pressure (p) is calculated using the ideal gas law, using the mass of the sample calculated as 10 % of the ice weight, the molecular weight of dry air, the sample volume, room temperature ($24\text{ }^\circ\text{C} = 298.15\text{ K}$), and the ideal gas constant (R). The idealized area is calculated under the assumptions that the idealized ice weight can be converted to the ideal gas volume using the average density of ice being 0.92 g/mL and the gas volume being 100 mL/kg ice , hence 10 % of the ice volume (Delmas, 1994; Kameda et al., 1997). The ideal concentration

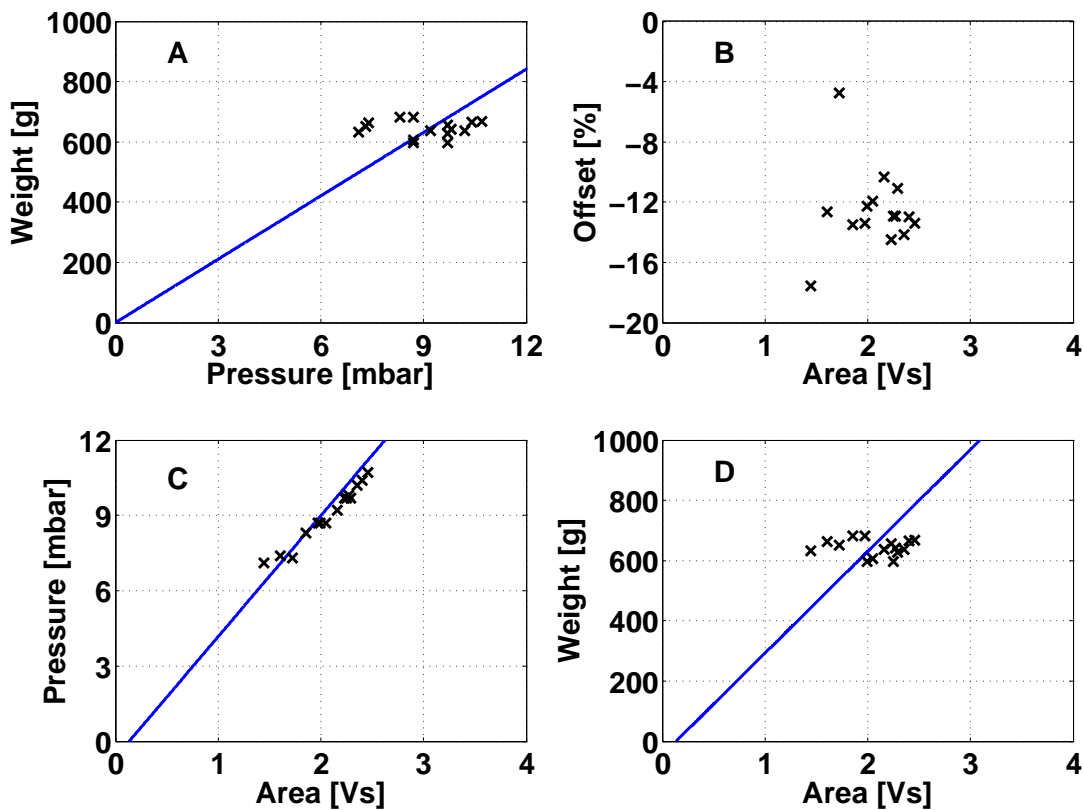


Figure 8.4: *Statistically corrected relationships between the sample weight, pressure, IRMS area, and concentration offset for the measured NEEM samples shown in black. The idealized relationships are plotted with the solid blue line.*

of N_2O is estimated from the calculated gas volume multiplied by a N_2O concentration of

239 ppb (the average of the records presented by Flückiger et al. (2004); Schilt et al. (2010, 2013)). From this, the resulting IRMS m/z 44 area is calculated using the linear relationship between N_2O -gas volume and IRMS m/z 44 area, measured using the working standard.

The described method allows for calibration of the isotopic N_2O composition, though the samples were not calibrated for N_2O concentration. The measured pressure and the IRMS $\delta^{15}N$ area allows for an approximated estimation of the N_2O concentration. For the following correction analysis, it is assumed that the estimated N_2O concentration has a constant offset to the actual concentration, within one standard deviation. The concentration offset is measured in percentage between the estimated N_2O concentration and the true concentration. The true concentration is assumed to be the N_2O concentration record (merged record from Dome C and NGRIP as shown in Fig. 8.6) as presented by Flückiger et al. (2002, 2004); Schilt et al. (2010, 2013).

Samples with a positive offset (see Fig. 8.3B) indicate an increased N_2O concentration compared to the reference record. An increased concentration is believed to be due to a leak somewhere in the extraction line, and therefore due to trapping of laboratory air. Measurements of the laboratory air combined with the calculated N_2O concentration offset are used to statistically correct both the IRMS m/z areas, and the resulting isotopic signature of the NEEM samples. Since a constant offset is expected, all samples are corrected to have the same average offset (that is all samples with an original positive offset). Fig. 8.4 shows the results of the statistical correction of the IRMS m/z 44 area, and the increased alignment of sample parameters as well as all four idealized relationships.

8.3 Results

The calibrated and corrected measurements of $\delta^{15}N$ (N_2O), $\delta^{18}O$ (N_2O), and $\delta^{15}N$ (NO^+ fragment) are used to calculate the isotopic composition of the N_2O gas extracted from the NEEM ice core samples, using the method described by Kaiser and Röckmann (2008). In addition to the corrections introduced above, a constant offset correction (6.48 ‰) was subtracted from the $\delta^{18}O$ (‰) values. We do this in order to homogenize our results to previous $\delta^{18}O$ values from Park et al. (2012) and Rosen (2014). The resulting isotopic composition given for the $\delta^{15}N$, $\delta^{15}N^\alpha$, $\delta^{15}N^\beta$, $\delta^{18}O$, and $\delta^{17}O$ values are shown in Table 8.4. The standard deviation (1σ) for each NEEM sample is taken as the standard deviation calculated from the size dependence correction analysis of the working standard (NAT332). The NEEM-samples are therefore divided into three groups each with different standard deviations.

Table 8.4: N_2O isotopic composition of the calibrated and corrected NEEM samples.

ID #	$\delta^{15}N$ (‰)	$\delta^{15}N^\alpha$ (‰)	$\delta^{15}N^\beta$ (‰)	$\delta^{18}O$ (‰)	$\delta^{17}O$ (‰)
220	9.49 ± 0.20	18.89 ± 1.48	0.09 ± 1.43	44.65 ± 0.57	26.99 ± 0.29
237	8.97 ± 0.20	17.32 ± 1.48	0.62 ± 1.43	46.39 ± 0.57	27.87 ± 0.29
244	9.21 ± 0.20	17.38 ± 1.48	1.03 ± 1.43	44.21 ± 0.57	26.77 ± 0.29
259	9.80 ± 0.20	16.51 ± 1.48	3.09 ± 1.43	42.73 ± 0.57	26.03 ± 0.29
268	8.76 ± 0.20	17.89 ± 1.48	-0.38 ± 1.43	45.05 ± 0.57	27.19 ± 0.29
284	10.00 ± 0.20	15.01 ± 1.48	4.99 ± 1.43	43.08 ± 0.57	26.20 ± 0.29
620	9.49 ± 1.02	18.70 ± 2.40	0.28 ± 2.78	49.67 ± 2.06	29.52 ± 1.04
1538	8.04 ± 0.12	17.23 ± 1.95	-1.14 ± 1.87	62.56 ± 0.63	36.01 ± 0.32
1560	8.70 ± 0.12	18.75 ± 1.95	-1.36 ± 1.87	61.29 ± 0.63	35.37 ± 0.32
1582	10.96 ± 0.12	17.95 ± 1.95	3.98 ± 1.87	52.58 ± 0.63	30.99 ± 0.32
2366	8.72 ± 0.20	13.61 ± 1.48	3.83 ± 1.43	46.24 ± 0.57	27.79 ± 0.29
2372	10.24 ± 0.20	16.55 ± 1.48	3.93 ± 1.43	42.61 ± 0.57	25.96 ± 0.29
2412	11.05 ± 0.12	18.14 ± 1.95	3.96 ± 1.87	49.59 ± 0.63	29.48 ± 0.32
3094	8.72 ± 1.02	12.10 ± 2.40	5.33 ± 2.78	45.63 ± 2.06	27.48 ± 1.04
3096	6.71 ± 1.02	9.61 ± 2.40	3.81 ± 2.78	51.60 ± 2.06	30.49 ± 1.04

Figure 8.5 shows the isotopic composition of N_2O from the 15 NEEM samples as SP, $\delta^{15}N$, and $\delta^{18}O$ records covering the past 35,000 years before the year 2000 (b2k). The samples were clustered around four geological time periods, late Holocene, mid Holocene, early Holocene, and the glacial. During each time period the samples agreed to a relatively high degree, with only samples from the mid Holocene being inconsistent (see discussion in section 8.4). During the late Holocene, the average isotopic composition of N_2O is calculated to be $15.59 \text{‰} \pm 3.66$, $9.37 \text{‰} \pm 0.48$, and $44.36 \text{‰} \pm 1.35$ for SP, $\delta^{15}N$, and $\delta^{18}O$, respectively. For the mid Holocene samples, the calculated composition is $17.48 \text{‰} \pm 3.74$, $9.24 \text{‰} \pm 1.26$, and $58.81 \text{‰} \pm 4.48$ for SP, $\delta^{15}N$, and $\delta^{18}O$, respectively. The early Holocene average isotopic composition of N_2O was found to be $12.19 \text{‰} \pm 2.93$ for SP, $10.00 \text{‰} \pm 0.98$ for $\delta^{15}N$, and $46.15 \text{‰} \pm 2.91$ for $\delta^{18}O$. Finally, the average isotopic composition during the glacial was found to be $6.29 \text{‰} \pm 3.70$, $7.71 \text{‰} \pm 1.43$, and $48.62 \text{‰} \pm 3.63$ for SP, $\delta^{15}N$, and $\delta^{18}O$, respectively.

Figure 8.6 shows the measured N_2O concentration from 1) the NGRIP ice core merged with the Dome C N_2O record, and 2) the Talos Dome N_2O record for the past 120 kyrs before present, as presented by Flückiger et al. (2002, 2004) and Schilt et al. (2010, 2013).

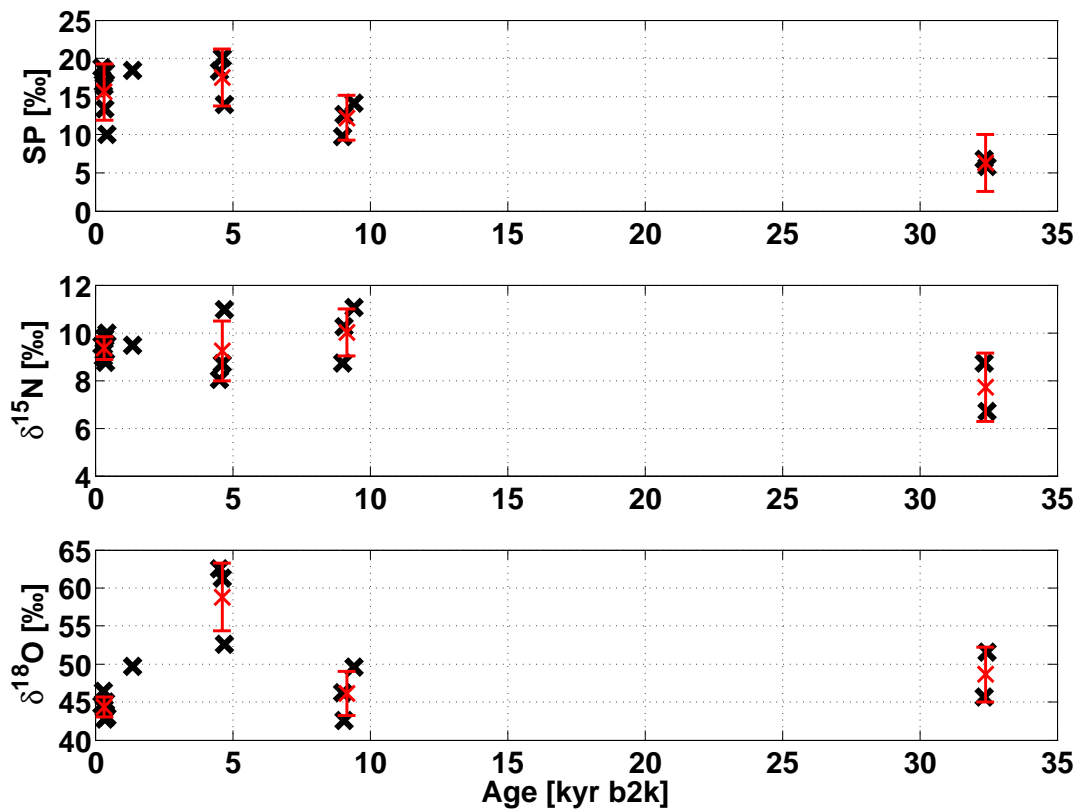


Figure 8.5: *The isotopic signature, of the 15 NEEM samples plotted for SP, $\delta^{15}\text{N}\text{-N}_2\text{O}$, and $\delta^{18}\text{O}\text{-N}_2\text{O}$ versus age. The calibrated and corrected data is plotted in black with the mean value and standard deviation of each section plotted in red.*

On top of these records the estimated N_2O concentrations and SDC corrected from the 15 NEEM samples are plotted. The performed measurements were not calibrated for N_2O concentration and the presented concentrations are therefore only estimated concentration.

8.4 Discussion

8.4.1 Determination of possible source

The past atmospheric records of N_2O have been analyzed a number of times for variations in concentrations, rather than the isotopic composition of N_2O . Schilt et al. (2013) discuss how changing N_2O concentrations during Heinrich stadials are found to be extremely low, and that this could be coupled to the shut-off of the Atlantic meridional overturning circulation (AMOC). The coupling is based on studies by Schmittner and Galbraith (2008)

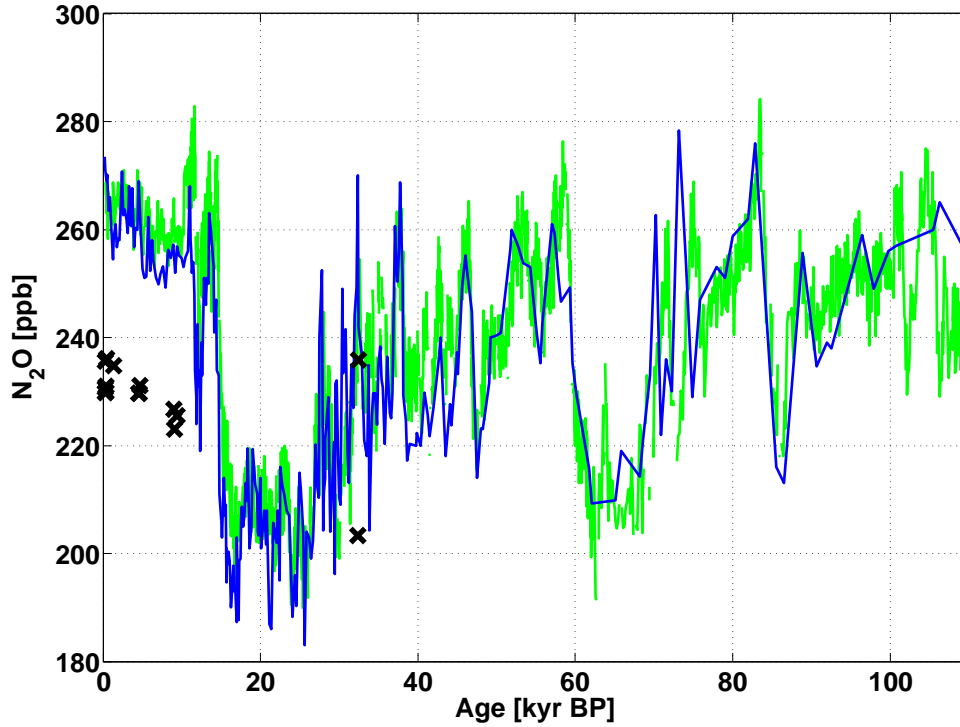


Figure 8.6: *The corrected N_2O concentration measurements shown with black crosses. Previously published data is presented in 1) green as a merged record of the Dome C (Flückiger et al., 2002) and NGRIP records (Flückiger et al., 2004; Schilt et al., 2010, 2013), and 2) the Talos Dome record in blue (Schilt et al., 2010).*

and Goldstein (2003), in which model studies have shown a high correlation between the atmospheric concentration of N_2O and the intensity of the AMOC during a number of the glacial stadials. In addition, Schilt et al. (2013) compare the N_2O concentration record from NGRIP with $\delta^{13}C$ marine sediment records (Shackleton et al., 2000; Elliot et al., 2002) and show a high correlation between the extremely low N_2O concentrations and decreased strength of the AMOC for the most recent Heinrich stadials (e.g. H1-H5).

The possible influence of the intensity of the AMOC on the sources of N_2O can further be investigated by looking at the isotopic composition of N_2O as shown by Dore et al. (1998), Pérez et al. (2000), Schilt et al. (2014) and others. Generally speaking, marine sources emit N_2O enriched in both $\delta^{15}N-N_2O$ and $\delta^{18}O-N_2O$ compared to that from terrestrial sources. Fig. 8.7 shows the relationship between $\delta^{15}N-N_2O$ and $\delta^{18}O-N_2O$ from marine and terrestrial sources with the blue and green rectangles, respectively. The isotopic signature of the 15 NEEM samples are plotted on top, in Fig. 8.7, clearly indicating that the measured N_2O samples originate from marine environments.

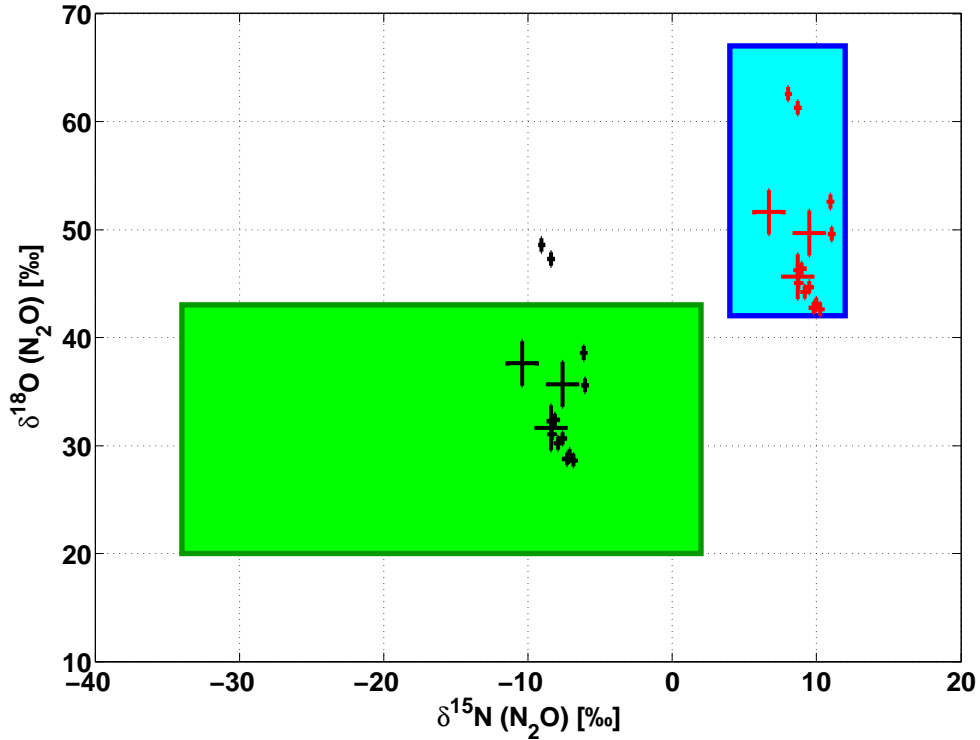


Figure 8.7: *The isotopic signature of the relationship between $\delta^{15}\text{N-N}_2\text{O}$ and $\delta^{18}\text{O-N}_2\text{O}$. The green rectangle represents the possible relationship for terrestrial sources (Schilt et al., 2014). The blue rectangle represents the relationship for marine sources (Schilt et al., 2014). Red crosses are the 15 NEEM samples with the respective error-bars for $\delta^{15}\text{N-N}_2\text{O}$ and $\delta^{18}\text{O-N}_2\text{O}$. Black dots are the 15 NEEM samples corrected for stratospheric shift with the respective error-bars for $\delta^{15}\text{N-N}_2\text{O}$ and $\delta^{18}\text{O-N}_2\text{O}$.*

Previous studies have shown no evidence that the natural N_2O production ratio between marine and terrestrial sources should have changed during the past 16 kyr BP (Schilt et al., 2014). It can therefore be assumed that marine ecosystems should contribute 37 % of the emitted N_2O while terrestrial ecosystems are responsible for 63 % (see Chapter 1). This would imply that the clear marine signal of $\delta^{15}\text{N-N}_2\text{O}$ and $\delta^{18}\text{O-N}_2\text{O}$ has been fractionated in the stratosphere prior to trapping in the ice. Röckmann et al. (2001) showed how UV photolysis in the stratosphere leads to an isotopic fractionation of N_2O and therefore an isotopic enrichment of both $\delta^{15}\text{N-N}_2\text{O}$ and $\delta^{18}\text{O-N}_2\text{O}$. The resulting stratospheric fractionation constants were furthermore found to be $17.1 \text{ ‰} \pm 1.6$ for $\delta^{15}\text{N}$, and $14.0 \text{ ‰} \pm 2.0$ for $\delta^{18}\text{O} (\text{N}_2\text{O})$. Assuming a similar stratospheric fractionation constant for all of the presented NEEM samples results in a depleted isotopic signature with terrestrial ecosystems being the

primary source region for the samples.

The site preference has been established as a reliable tracer to distinguish microbial N₂O production pathways from soils and pure bacterial solutions, hence nitrification or denitrification. Park et al. (2011) (and references therein) show that N₂O produced as a byproduct during nitrification (NH₄⁺ reduced to NO₃⁻) is enriched in $\delta^{15}\text{N}^\alpha$ and therefore in SP. On the other hand, N₂O emitted during denitrification (NO₃⁻ ultimately oxidized to N₂) is enriched in $\delta^{15}\text{N}^\beta$ and therefore depleted SP. N₂O produced during denitrification is known to have SP values in the range of -20 ‰ to 2 ‰ whereas N₂O emitted during nitrification has SP values from 11 ‰ to 40 ‰ (Park et al. (2011) and others). The 15 NEEM samples were all increased in SP, with average SP values at 15.59 ‰ ± 3.66, 17.48 ‰ ± 3.74, 12.19 ‰ ± 2.93, and 6.29 ‰ ± 3.70 for the late Holocene, mid Holocene, early Holocene, and glacial period, respectively. The SP values suggests nitrification as the primary source but with a significant amount originating from denitrification. Though Röckmann et al. (2001) showed that the stratospheric sink fractionates the two isotopomers differently (see Chapter 1). Assuming similar stratospheric fractionation constants for all the presented NEEM samples, would it result in depletion of SP by 8.4 ‰. The average SP for the four time periods would then be 7.19 ‰ ± 3.66, 9.08 ‰ ± 3.74, 3.79 ‰ ± 2.93, and -2.11 ‰ ± 3.70 for the late Holocene, mid Holocene, early Holocene, and glacial period, respectively. Then the isotopic signature from denitrifying bacterial production would have a larger impact on the Holocene, while the glacial N₂O would almost purely be produced by denitrifying bacterial production.

Based on published literature, the best estimate for the primary source of the N₂O extracted from the NEEM core, is nitrifying bacterial production in marine environments. Taking the stratospheric fractionation into account results in a depletion of the isotopic signatures, which changes the primary source region to terrestrial ecosystems with a mixture of nitrification and denitrification during the Holocene and denitrification being the primary source of N₂O during the glacial. This estimate is based on only a relatively small number of measurements and additional studies of the isotopic signature of N₂O produced from marine nitrification and denitrification are still missing, therefore it is assumed that only marine and terrestrial production leads to similar SP.

8.4.2 Stability of isotopic composition

The measurements presented in this study, have been calibrated to atmospheric N₂ (for $\delta^{15}\text{N}$, $\delta^{15}\text{N}^\alpha$, and $\delta^{15}\text{N}^\beta$) and VSMOW (for $\delta^{17}\text{O}$ and $\delta^{18}\text{O}$). A check of the stability of the

method used can be done by comparison of the 15 NEEM samples to the N_2O isotopic measurements from Taylor glacier as presented by Schilt et al. (2014), and to the Siple dome N_2O data from Rosen (2014). Firn air samples from Law Dome and air samples from Cape Grim presented by Park et al. (2012), are used for comparing to present day isotopic composition. Figure 8.8 shows a comparison between the five data sets for SP, $\delta^{15}N$, and $\delta^{18}O$ versus age in subfigure A, B, and C respectively.

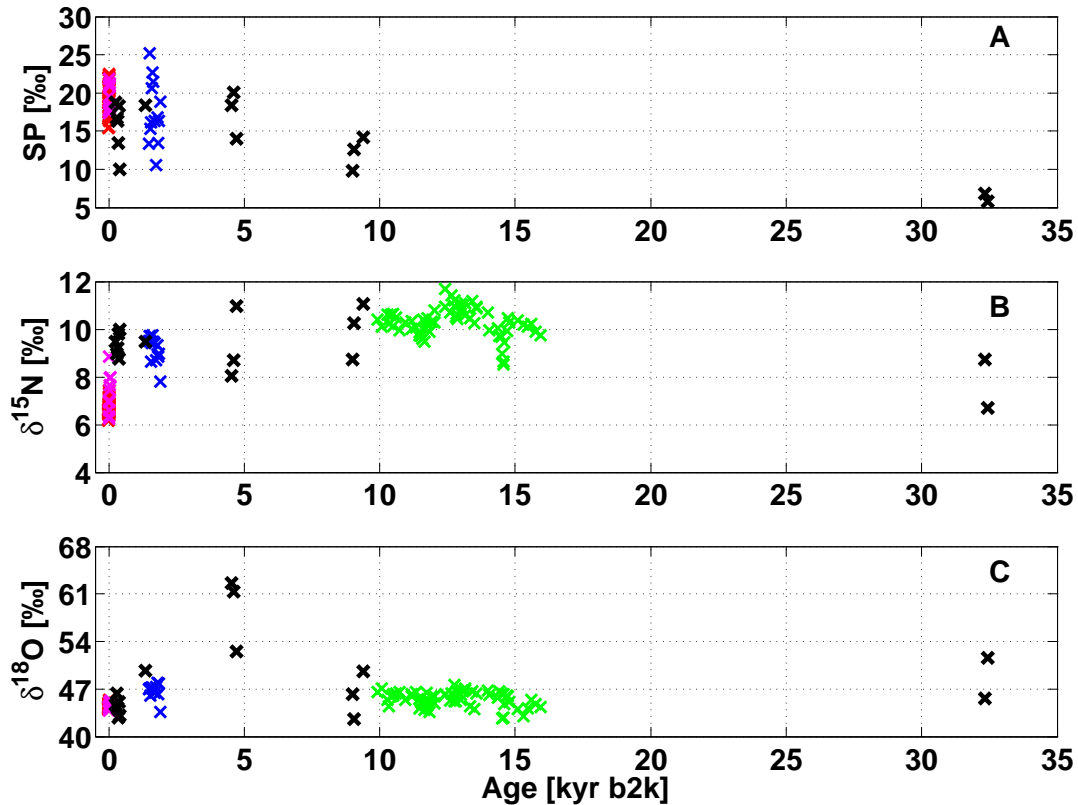


Figure 8.8: The isotopic signature, of the 15 NEEM samples plotted for SP, $\delta^{15}N-N_2O$, and $\delta^{18}O-N_2O$ versus age in black. Taylor glacier N_2O data from Schilt et al. (2014) is in green. Siple Dome N_2O data from Rosen (2014) is in blue. Air samples from Cape Grim (Park et al., 2012) are in red. Firn air samples from Law Dome (Park et al., 2012) are in pink. Age zero is set to year 2000 (b2k), hence the timescale is years before year 2000 (b2k).

The presented data is generally in agreement with previously published data from Park et al. (2012); Schilt et al. (2014); Rosen (2014). Some variations are observed though, especially in the signal from SP and $\delta^{18}O-N_2O$. The $\delta^{15}N-N_2O$ signal (Fig. 8.8B) of the NEEM samples is more or less constant (within the standard deviation) during the Holocene. The results from the glacial samples are slightly depleted compared to the Holocene samples. The glacial data is more similar to the samples from Park et al. (2012), and also to the present day situation.

The $\delta^{18}\text{O-N}_2\text{O}$ samples (Fig. 8.8C) are constant (within one standard deviation) and in agreement with the reference data (published values from (Park et al., 2012; Schilt et al., 2014; Rosen, 2014)) from the late Holocene, early Holocene, and glacial. The $\delta^{18}\text{O-N}_2\text{O}$ samples from the mid Holocene (4.6 kyrs b2k) are significantly increased, with a discrepancy in of +10 ‰. With the data available, this discrepancy can not be resolved, though it is hypothesized to be a true signal, since no corresponding signal is found in the SP record or in the $\delta^{15}\text{N-N}_2\text{O}$ record.

From the SP record (Fig. 8.8A), the presented late and mid Holocene NEEM samples are in agreement with the reference records. Interestingly, it is, seen that there seems to be a general downward slope with a decreasing SP enrichment, going back in time from the mid Holocene with an SP of $17.48 \text{ ‰} \pm 3.74$ to the glacial with an SP of $6.29 \text{ ‰} \pm 3.70$. This implies that the primary source of N_2O has changed during the past 35 kyrs, with a decreasing production originating from denitrifying bacterial and an increasing production from nitrifying bacterial. A change in the primary microbial production pathways is one hypothesis for this SP depletion over the past 35 kyrs. Another hypothesis is that since N_2O produced in the oceans primarily originates from bacterial production in the southern hemisphere 40-60 °S latitude band, equatorial upwelling zone, and in the tropical coastal upwelling zones (Nevison et al., 1995), the depleted SP values in the glacial could be a signal of a change in source region caused by a change in the AMOC during Greenland Interstadial GI-5.2. Though a change in AMOC as a response to GI-5.2 would result in a relatively short change in the source, which would imply the decreased SP around year 9000 b2k to have a different origin. Based on the available data we therefore hypothesize that the sources of N_2O have changed from the glacial and into the Holocene though additional measurements are required to improve the discussion of the changed microbial source.

8.5 Conclusion

Measurements of the isotopic composition of N_2O have successfully been performed for 15 samples from the NEEM ice core. The samples were selected to represent four different geological time periods, namely the glacial (32 kyrs BP), the early Holocene (10 kyrs - 9.5 kyrs BP), the mid Holocene (5 kyrs - 4.5 kyrs BP), and the late Holocene (0.5 - 0.2 kyrs BP). The calculation of the isotopic composition resulted in similar values of site preference and $\delta^{15}\text{N}$, while the $\delta^{18}\text{O}$ values are slightly more enriched compared to previously published isotopic N_2O compositions from ice cores. The general isotopic composition leans towards the primary sources originating from nitrifying bacterial production in marine environments.

The results do furthermore raise questions about the evolution of the primary source of N_2O from 35 kyrs b2k until the present day marine nitrifying bacteria being the primary source.

8.6 Author contribution

MW performed ice preparation, measurements, analyzed the data, and prepared the manuscript. TR and CS designed the setup and experiment. CV and MP assisted in technical issues with IRMS.

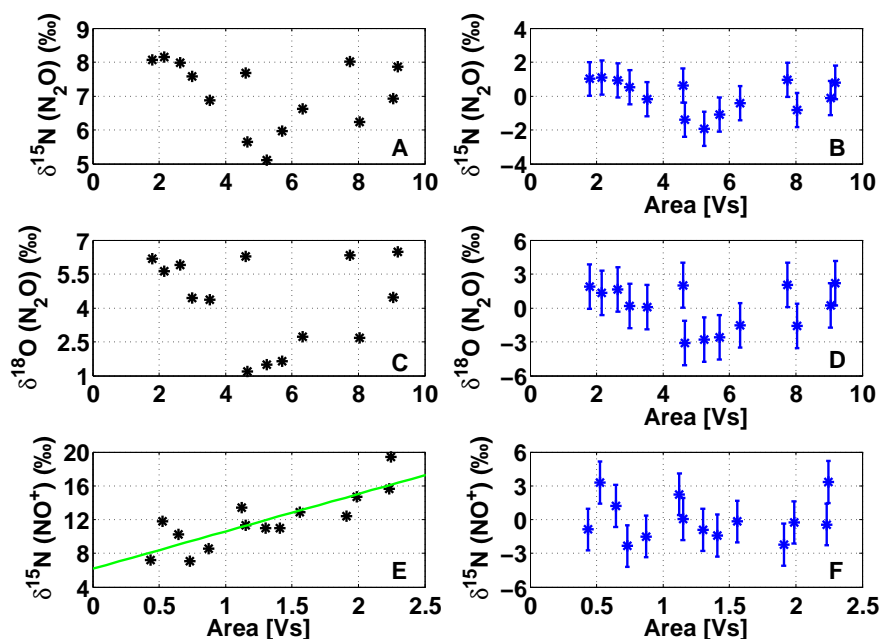
8.7 Acknowledgements

We want to thank the NEEM community for logistics, drilling, science, etc. NEEM is directed and organized by the Center of Ice and Climate at the Niels Bohr Institute and US NSF, Office of Polar Programs. It is supported by funding agencies and institutions in Belgium (FNRS-CFB and FWO), Canada (NRCan/GSC), China (CAS), Denmark (FIST), France (IPEV, CNRS/INSU, CEA and ANR), Germany (AWI), Iceland (RannIs), Japan (NIPR), Korea (KOPRI), The Netherlands (NWO/ALW), Sweden (VR), Switzerland (SNF), United Kingdom (NERC) and the USA (US NSF, Office of Polar Programs).

8.8 Supporting material

Size Dependence Correction

Figures: Working standard (NAT332) measurements for determination of sample size dependence. Raw IRMS measurements of $\delta^{15}\text{N}$ (N_2O), $\delta^{18}\text{O}$ (N_2O), and $\delta^{15}\text{N}$ (NO^+ fragment) are shown in black in sub-figures A, C, and E, respectively. The size dependent corrected (SDC) data is shown in blue in sub-figures B, D, and F for $\delta^{15}\text{N}$ (N_2O), $\delta^{18}\text{O}$ (N_2O), and $\delta^{15}\text{N}$ (NO^+ fragment), respectively. Only data with a visible dependence has been corrected.



Measured IRMS sample area

Figure S8.9: Size Dependence Correction.

Figure: Working standard (NAT332) measurements of different volumes. Black points are actual measurements. Blue line is the linear relationship, which is also shown with the equation.

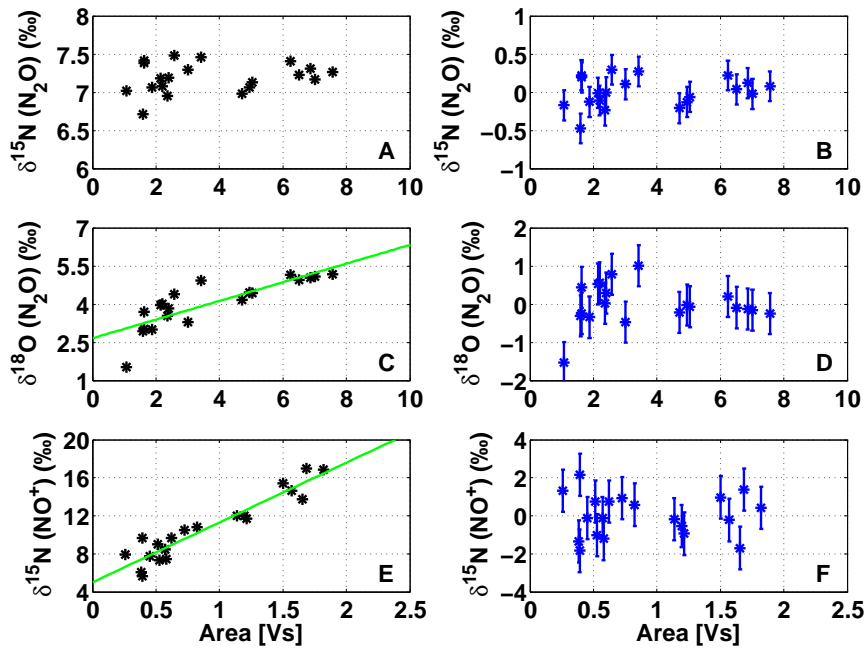


Figure S8.10: *Size Dependence Correction.*

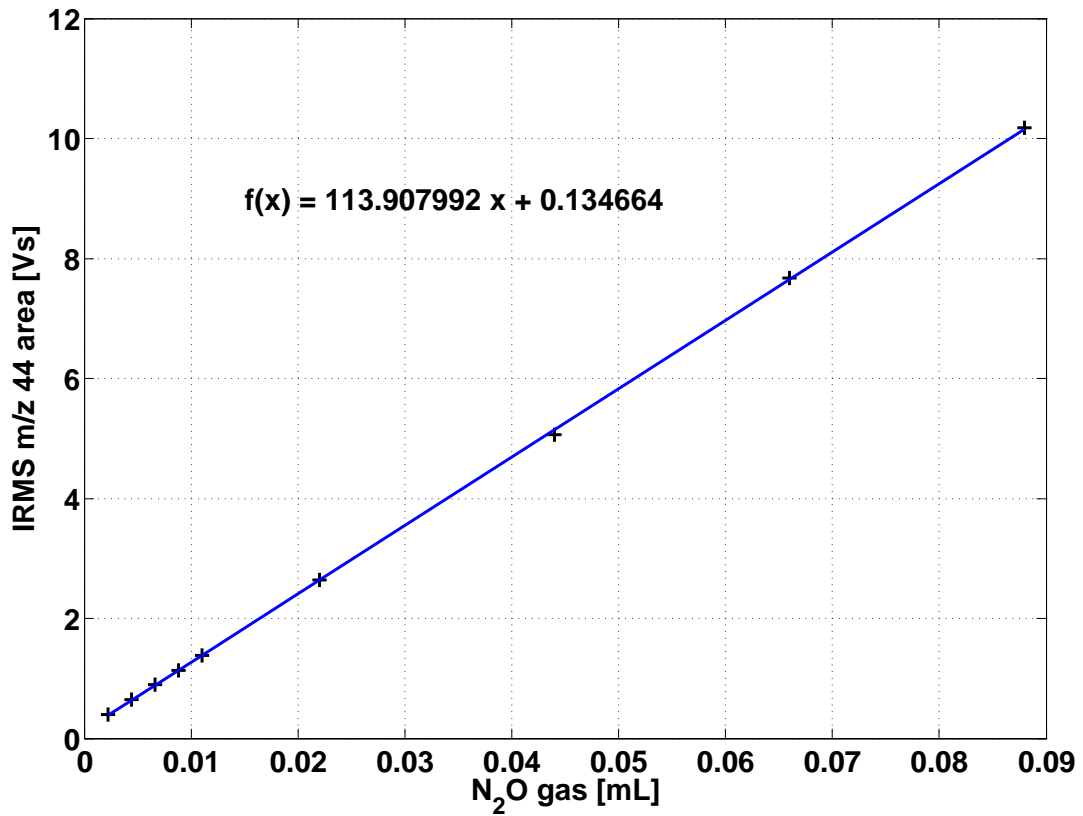


Figure S8.11: *IRMS area size calculation.*

Part IV

Present atmosphere

Introduction - part IV

In this part of the PhD thesis, two field studies are presented. The two studies have the overall purpose to investigate N_2O emissions from different environments to the present atmosphere. The presented work originates from experiments designed with equal contributions from the collaborators, while experiment execution and manuscript preparation was performed with varied contribution as described in the author contribution sections.

The first study was carried out on Disko island, Greenland, in July and August 2013, in collaboration between the Centre for Ice and Climate (CIC) Niels Bohr Institute, University of Copenhagen Denmark, the Section of terrestrial ecology, department of biology, University of Copenhagen Denmark, and the Center for Permafrost, Department of Geosciences and natural management, University of Copenhagen Denmark. The preliminary results were first presented in the M.Sc. of C. E. Kjærsgaard 2014. In chapter 10 a draft of the manuscript is presented. We investigated the N_2O produced and emitted from thawing permafrost on a dry to wet transition slope, and discuss the potential relation between nitrite production found simultaneously as N_2O consumption and hypothesize that the natural nitrogen processes in the Arctic may lead to reduction of atmospheric N_2O , due to high denitrification rates despite relatively low NO_3^- concentrations.

The second study was performed on a drained organic field at Roholte, Sjælland Denmark in collaboration between the Centre for Ice and Climate (CIC) Niels Bohr Institute, University of Copenhagen Denmark, and the Section of terrestrial ecology, department of biology, University of Copenhagen Denmark. The preliminary results were presented in the M.Sc. by A. Lee 2015. In chapter 11 the manuscript of a joint publication is presented. We investigated the temporally changing emission of N_2O from a drained organic soil toposequence and discuss the influence of the changing interface. Furthermore we demonstrate the significance of the site preference in the interpretation of the likely N_2O producing microbial activity cycle.

Fast production of nitrate in the Arctic leads to lower emission of greenhouse gas N₂O

Søren Christensen¹, Christian Emil Kjærsgaard¹, Mette Vestergård¹, Malte Winther², David Balslev-Harder^{2,3}, Thomas Blunier², and Bo Elberling⁴

1. Section for Terrestrial Ecology, Department of Biology, University of Copenhagen, Denmark
2. Centre for Ice and Climate, Niels Bohr Institute, University of Copenhagen, Denmark
3. DFM - Danish National Metrology Institute, Kgs. Lyngby, Denmark
4. Center for Permafrost, Department of Geosciences and Natural Resource Management, University of Copenhagen, Denmark

The following chapter is a draft of a manuscript in preparation for publication. The manuscript will be submitted as S. Christensen et al.: Fast production of nitrate in the Arctic leads to lower emission of greenhouse gas N₂O.

Abstract

In natural unfertilized systems nitrous oxide (N_2O) production depends on nitrification. Nitrifying bacteria can produce N_2O directly during NH_4^+ oxidation or by reducing NO_2^- . Subsequently, the end product of nitrification, NO_3^- , can also be reduced to N_2O by denitrification. Large N_2O production has been observed in the Arctic when permafrost thaws. There is an apparent discrepancy between occasional high N_2O production and low or even absent nitrification in the Arctic tundra. We hypothesize that N_2O is a product of denitrification rather than nitrification and that the production is governed by the nitrification rate in a moist arctic fen site. Here we show - quite surprisingly - that high nitrification leads to N_2O consumption in moss-covered sites where N_2O derives from denitrification. We therefore conclude that nitrate production in such sites where nitrate levels are low may lead to reduced emission of greenhouse gas N_2O . This is in contrast to the effect of opening nitrogen cycles in temperate and tropical areas where nitrification prevails and N_2O is produced in relation to N transformations. We thus demonstrate that natural nitrogen processes in the Arctic may reduce greenhouse gases and thereby global warming. This is the first clear demonstration that N_2O is produced by denitrification rather than nitrification in the Arctic and the first presentation of a close coupling between N_2O consumption and NO_3^- production in soil. The predictive capability of earth system models - basis of IPCC predictions of global change - improves when including such detailed understanding of belowground microbial processes.

10.1 Introduction

N_2O exchange activity is considered to be very low in polar/sub-polar regions of the Globe due to low production and availability of nitrate (Limpens et al., 2006). Only an insignificant part of the global N_2O production activity takes place in the Arctic (IPCC, 2013). In contrast to this marked N_2O production was observed at thawing of permafrost soil at fen sites, up to 6-7 mg $\text{N}_2\text{O-N m}^{-2} \text{ d}^{-1}$ (Elberling et al., 2010; Marushchak et al., 2011).

Two microbial processes can result in N_2O formation, i.e. nitrification, the conversion of NH_4^+ to NO_3^- , and denitrification, where NO_3^- produced by nitrification is converted to N_2O (Firestone and Davidson, 1989; Gruber and Galloway, 2008). Hence, in both cases, N_2O formation requires active nitrification. In natural ecosystems nitrification tends to decrease from Equator towards the Arctic. In wet tropical areas net nitrification is of the same magnitude as net N mineralization (Hedin et al., 2003; Weintraub et al., 2015). Nitrification is also high in temperate forests even though often masked by nitrate immobilization (Stark and Hart, 1997). In boreal forests nitrification is low (Limpens et al., 2006), increasing during succession to about 5 % of N-mineralization (Kielland et al., 2006). In Arctic non-acidic tundra (Hobbie and Gough, 2002) nitrification rates are very low or even nil (Hart and Gunther, 1989). If denitrification produces the N_2O , oxidized nitrogen needs to be supplied by water flow from other areas or locally by nitrification.

We ask how N_2O release/absorption occur in an arctic fen, how this relates to the soil environment and which microbial processes are involved.

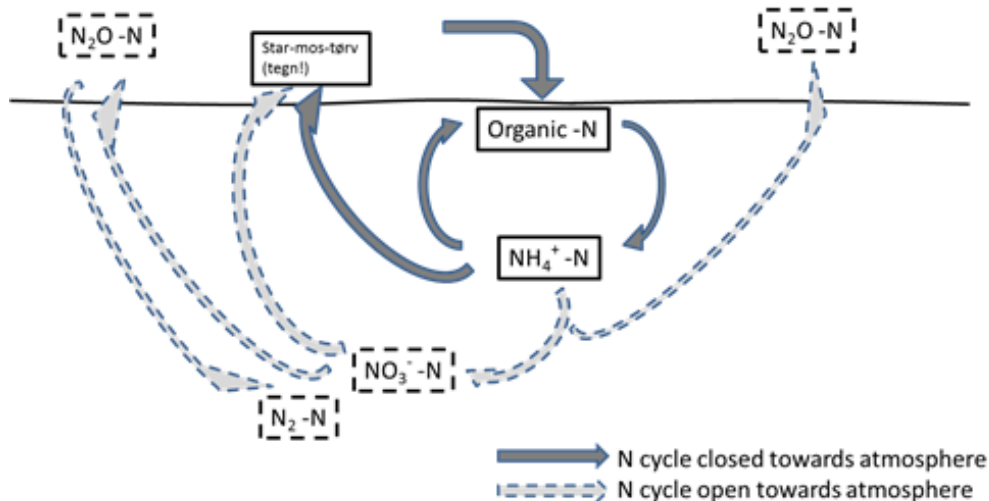


Figure 10.1: *Two types of nitrogen cycle without and with nitrification. The nitrogen cycle with nitrification can be open towards the atmosphere whereas the nitrogen cycle without nitrification is not open.*

10.2 Experiment

We characterize N₂O production in an arctic fen combining our knowledge of water-borne nitrate transport with measurement of N₂O emission and $\delta^{15}\text{N}$ site preference, which indicates whether nitrification or denitrification govern N₂O formation, with assessment of potential nitrification and denitrification activity.

Table 10.1: Six sites in arctic meadow. * frequency of samples with NO₃⁻. ** average NO₃⁻ in these samples. # Sedge-wintergreen. ## Sedge-moss

Vegetation	Depth	Water, % of sample		pH		Soil water NO ₃ ⁻		Soil water NH ₄ ⁺	
		avg.	s.e.	avg.	s.e.	*	**	avg.	s.e.
	cm	%	%			No	ppm N	ppm N	ppm N
Birch	0-8	38.4	6.5	5.3	0.2				
	8-18	24.4	2.5	5.7	0.1	0.1	0.11	2.42	0.61
	18-28	11.1	1.2	6.0	0.2				
Willow	0-8	76.1	1.8	6.0	0.1				
	8-18	70.0	5.0	5.9	0.1	0.2	0.07	0.83	0.14
	18-28	58.1	5.9	5.7	0.1				
S-W#	0-8	79.4	1.1	6.0	0.1				
	8-18	72.1	2.2	6.1	0.1	0.3	0.02	0.80	0.21
	18-28	41.9	4.2	5.4	0.2				
S-M##	0-8	85.3	1.1	6.5	0.2				
	8-18	51.4	10.0	5.4	0.1	0.3	0.20	0.78	0.13
	18-28	28.4	1.1	5.3	0.1				
Moss	0-8	88.5	1.4	5.4	0.1				
	8-18	76.5	8.3	5.3	0.0	0.2	0.09	1.39	0.35
	18-28	68.5	8.7	5.5	0.1				
Peat	0-8	91.7	1.7	6.4	0.0				
	8-18	88.2	2.9	5.7	0.1	0.0	-	0.32	0.05
	18-28	90.0	0.9	5.8	0.1				

We selected a downslope site to cover a moisture gradient with the associated differences in vegetation. The area is located in Blæsedalen on Disko Island, Greenland, a young

non-acidic tundra (Yano et al., 2013). Moving downslope in the upper layer organic matter content increases and volume weight decreases (Table S10.2) whereas soil moisture increases (Table 10.1). Seven weeks after the first day of fully thawed soil (7 June 2013) measurements were performed during the 3-week period 20 July - 10 August where seasonal soil temperature peaked at 8.5 °C average in 10 cm depth. During the following 7-week period soil temperature decreased being zero at 28 September. Soil moisture (Table 10.1) and organic matter (Table S10.2) decreased whereas bulk density increased (Table S10.2) down through the profiles. Ammonium concentration in profile water averaged 0.3-2.4 $\mu\text{g N mL}^{-1}$ over the six sites whereas nitrate was below detection limit in more than 70 % of samples with concentrations in soil water of 0.02-0.2 ppm where detected (Table 10.1). This is in accordance with reports from other non-acidic tundra sites where ammonium dominates the inorganic nitrogen pools (Hobbie and Gough, 2002; Nordin et al., 2004; Yano et al., 2013). We measured N_2O exchange at the soil surface with the closed chamber technique (see supporting material 10.5). The horizontal and vertical distribution of soil water nitrate and soil air N_2O was assessed. In the down-sloping landscape where direction of water flow was obvious the spatial distribution of nitrate will indicate if marked water-borne transport of nitrate occur.

We further assess, whether N_2O is generated via nitrification or denitrification from measurements of the three most abundant isotopic N_2O compositions, namely $^{14}\text{N}^{15}\text{N}^{16}\text{O}$ ($^{15}\text{N}^\alpha$), $^{15}\text{N}^{14}\text{N}^{16}\text{O}$ ($^{15}\text{N}^\beta$), and $^{14}\text{N}_2^{16}\text{O}$, and the site preference of the intramolecular distribution of the isotope ratio ($\text{SP} = \delta^{15}\text{N}^\alpha - \delta^{15}\text{N}^\beta$) (Brenninkmeijer and Röckmann, 1999; Yoshida and Toyoda, 2000). Both isotopomers and N_2O concentration are directly measured using a prototype of the Picarro G5101- isotope N_2O analyser which is based on mid-infrared cavity ringdown spectroscopy (CRDS) (Chapter 6). We finally measured the potential for nitrification and denitrification in the soil profile down the slope (Fig. S10.8).

10.3 Results and Discussion

N_2O exchange was close to nil at 17 out of 18 sampling locations on July 23. However, during early August the number of locations with either N_2O uptake- or emission increased (Fig S10.5). At low NO_3^- availability, active denitrifying bacteria use N_2O as an alternative electron acceptor; hence, N_2O uptake signifies low local NO_3^- availability. The increase in N_2O turnover reflects time with soil temperature above zero (Fig S10.9). N_2O exchange activity is considered to be very low in polar/subpolar regions of the Globe due to low

production and availability of nitrate (Limpens et al., 2006). Most of the N_2O on the Globe is produced in wet tropical forests, in temperate agricultural areas and in the oceans whereas insignificant production takes place in the Arctic (IPCC, 2013). N_2O exchange has been observed in permafrost areas, however, with release as well as uptake in soil below larch (Koide et al., 2010) and a release of $0.2 \text{ mg N}_2\text{O-N m}^{-2} \text{ d}^{-1}$ from a fen core (Elberling et al., 2010) and generally low N_2O uptake from vegetated fens ($0-0.06 \text{ mg N}_2\text{O-N m}^{-2} \text{ d}^{-1}$) (Marushchak et al., 2011) in accordance with our results (Fig. 10.2A). The N_2O exchange activity in August occurred at the lower three sites of the catena series, and here N_2O absorption rates in the moss-covered sites were twice as high as the highest rates of N_2O emission from the peat site (Fig. 10.2A).

For the first time we provide evidence to identify which process is responsible for N_2O release from the Arctic. Measurement of the position of the heavy isotope ^{15}N (which contributes 0.36 % of the nitrogen of the Globe) in the N_2O molecule can identify the process that forms N_2O (Pérez et al., 2000; Perez et al., 2001). All our sites show negative SP values indicating that denitrification is the dominant process of N_2O formation (Fig. 10.2B). The relatively high rates of net N_2O consumption parallel to the low availability of NO_3^- shows that N_2O is used as electron acceptor by denitrifying bacteria in the lack of NO_3^- .

The NO_3^- can be supplied either by horizontal water transport or by nitrification. Since NO_3^- did not occur at a higher frequency in the upper sites of the slope (Table 10.1) NO_3^- is probably not transported downhill by horizontal water flow. Moreover, NO_3^- mainly occurs in the upper soil layer (Fig. S10.8), which suggest that NO_3^- is produced locally and not imported from below by upward water flow.

Since flow of nitrate in the soil is not prevalent nitrification must be the mechanism supplying NO_3^- at the sites of N_2O turnover by denitrification. Nitrification potential is clearly highest in two of the lower sites of the slope covered with moss (Fig. 10.2C). The moss covered areas are the main sites of both nitrification and N_2O consumption. It is very surprising that high nitrification, the process that produces the NO_3^- substrate for denitrification, leads to N_2O consumption, as denitrifiers consume N_2O , when NO_3^- availability is low. Since N fixation is also high at moss-covered sites in the arctic (Solheim et al., 2006) the high nitrification in our moss-covered sites is likely fed by N-fixation. This actually means that the N_2 uptake from the atmosphere is followed by an N_2O uptake from the atmosphere due to the induced increase in nitrification and denitrification in the soil of these moss-covered sites.

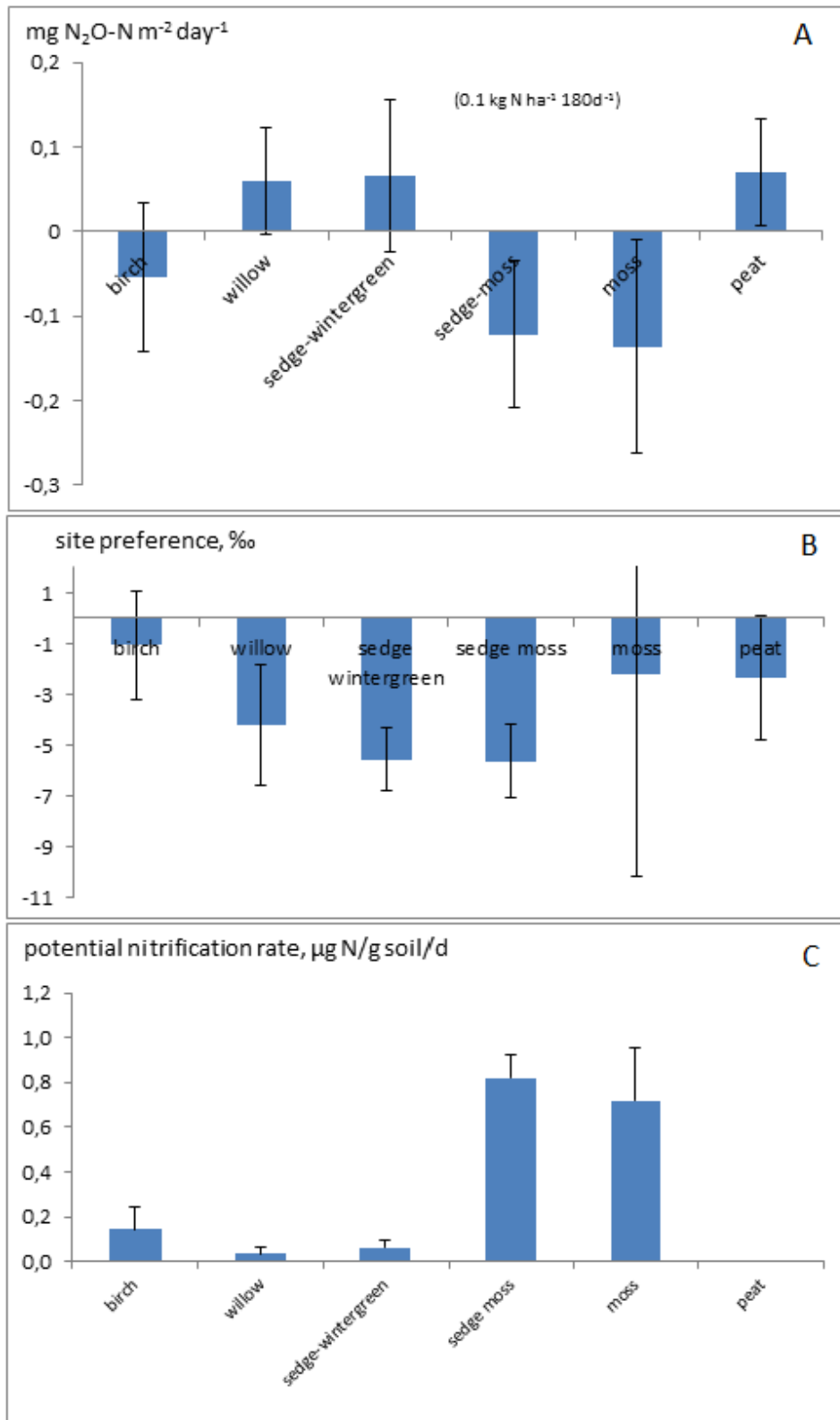


Figure 10.2: A) N₂O emission: Six sites along the catena series from dry to wet. Three sites (willow, sedge-wintergreen, peat) tend to produce N₂O, one site is neutral (birch) and two sites (moss-covered) consume N₂O. B) site preference: difference in abundance of the isotopomers. C) Potential nitrification rate: Nitrification higher in moss covered sites than in any other sites. Moss covered sites are expected to have high nitrogen fixation suggesting that the high nitrification stimulating N₂O turnover was again stimulated by high inputs of ammonium.

Potential nitrification activity (ammonium oxidation rate with unlimited substrate availability) correlated closely with N_2O exchange (Fig. 10.3). It is a paradox that N_2O consumption correlates positively with nitrate production (nitrification). A likely explanation for this relationship between nitrification and N_2O consumption may be that steady nitrification activity constantly supplies some NO_3^- and thereby maintains an activity of denitrifying populations in moss covered sites. These denitrifiers then reduce NO_3^- to a level where N_2O will be a relevant electron acceptor in their respiration.

N-fixation is high in cold moss-covered sites as reviewed by Vitousek et al. (2013) and also specifically in the arctic as apparent in the review of Solheim et al. (2006) and also found in the boreal zone (Rousk et al., 2014). Our results therefore suggest that the opening of the nitrogen cycle via N-fixation and nitrification in northern cold regions of the Globe may lead to N_2O absorption from the atmosphere, quite opposite to the effect of open N-cycles in the tropics where wet mature tropical forests have high nitrification (Weintraub et al., 2015) coupled to high N_2O releases (Hedin et al., 2003; Houlton et al., 2006).

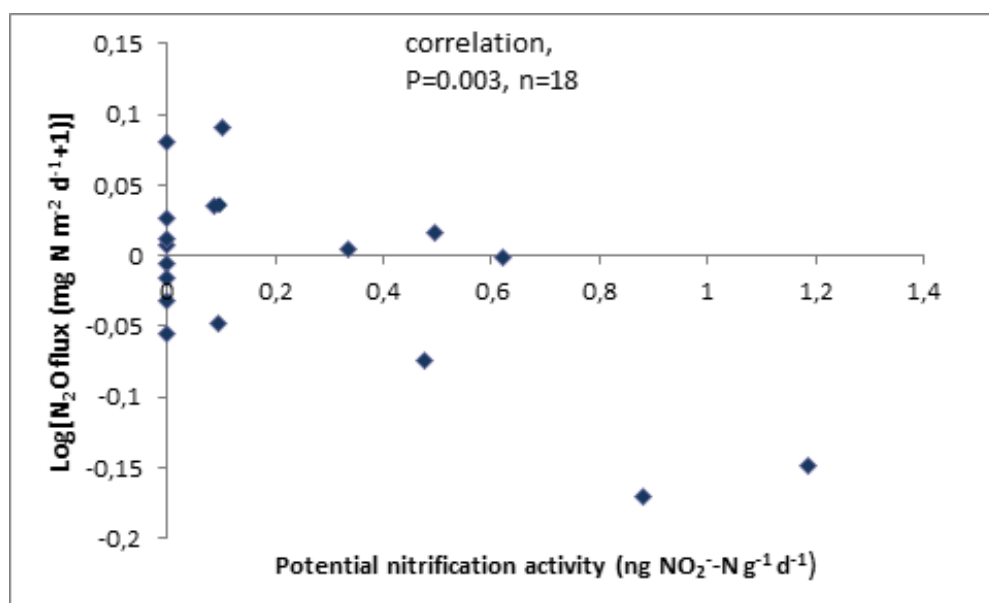


Figure 10.3: *Correlation of N_2O flux and nitrification activity. Where nitrification activity is highest there is marked N_2O consumption, whereas lower nitrification potential is coupled with smaller emission of N_2O or no activity. This suggests that opening the nitrogen cycle via nitrification actually reduce the emission of N_2O .*

The global N_2O budget (IPCC, 2013) has been updated by inclusion of N_2O sinks, estimated at $< 0.1 Tg N_2O-N yr^{-1}$ for the Globe (Syakila and Kroeze, 2011) with areal uptake rates of $0.2-7 \mu g N m^{-2} h^{-1}$ with the highest values suggested for temperate and high latitudes (Syakila et al., 2010). If just 10 % of the Taiga biome that covers $1.7 \cdot 10^7 km^2$ has a sink

activity similar to the moss-covered tundra of the present study for 180 days a year this sink alone corresponds to $0.05 \text{ Tg N}_2\text{O-N yr}^{-1}$. This is more than half of the current estimate of the global N_2O sink from moss-covered Taiga alone. Potentially, the current estimate of the global N_2O sink of $< 0.1 \text{ Tg N yr}^{-1}$ 1a may therefore need considerable adjustment upwards. Future work is needed to reveal if that is the case.

10.4 Author contribution

The experiments were designed by SC, CEK, MW, and BE. Field experiments were carried out by CEK, MW, and SC. Soil measurements and gas measurements using GC was performed by CEK. MW performed large volume gas extraction, measurements on the CRDS G5101i-CIC analyzer, calibration and correction of CRDS data. SC prepared the manuscript with contribution from MW and MV, while all co-authors contributed to the final manuscript.

10.5 Supporting material

10.5.1 Materials and Methods

N₂O flux measurements

A plastic tube 10 cm / 11.6 cm inner/outer diameter of 15 cm length and tapered at the one end was hammered 9 cm into the ground so 6 cm with 0.5 l air was above the soil surface when covered with a lid. When sampling N₂O exchange a 6 mm thick plastic lid was sealed on the plastic ring over a 5-mm thick foam rubber seal with a metal clamp fitting into a groove at the upper end of the plastic ring. Eight ml gas samples were collected 0 min and 30 min after sealing and stored in 5.3 ml Exetainers (LabCo, Lampeter, UK). One ml gas from the Exetainers was analyzed on a gas chromatograph with ECD.

N₂O in soil air

Nylon tubing of (6 mm outer diameter and 3 mm inner diameter) was inserted at different soil depths between 15 and 95 cm. The tubes were plugged at both ends and had four 1.5-mm holes on the side. Three replicate tubes were inserted at each topographic position with a distance of 2-5 m perpendicular to the direction of elevation/declination. A gas volume similar to the volume inside the tubes was removed before sampling 8 ml air, which were treated in the same way as described under N₂O flux measurement.

N₂O isotopomer measurements

Additionally 600 mL gas was collected from each of the 18 flux chambers 30 minutes after closure at one occasion. Gas extraction of this volume can not be performed using a syringe, due to large contamination risks and a gas extraction technique was therefore developed. A 600 mL sampling bag (SupelTM-Inert Multi-Layer Foil bag, Sigma-Aldrich, USA) was connected to the flux chamber via a syringe and placed inside a sealed box (5 L volume). Gas was extracted from the chamber into the sampling bag by gradually evacuating the box, hence outside the sampling bag. A gradual decreasing pressure outside the bag creates under-pressure inside the box, hence the sampling bag expands and gas is extracted from the flux chamber into the sampling bag. The sampling bags were transported directly to the laboratory and measured within 6 hours after extraction to prevent leakage. The large gas samples were continuously measured for 25 minutes (24 cc min⁻¹) using the G5101i-CIC analyzer. Measurements of both standard gases (CIC-MPI-1 and CIC-MPI-2) were performed before and after the samples were measured, and all samples were therefore

calibrated and measured against atmospheric N_2 (section 3.3). Furthermore was the samples corrected for the CRDS concentration dependence using the method described in section 3.1.

Potential denitrification

Two g soil (fresh wt.) in 117 ml glass flasks were added 5 ml liquid with 1 mM glucose and 1 mM KNO_3 . Flasks were sealed with a butyl rubber stopper, headspace evacuated and refilled with N_2 and 10 % of the atmosphere replaced with C_2H_2 . Flasks were mounted on a shaker and N_2O concentration in the headspace assessed after two hours on a gas chromatograph with ECD.

Potential nitrification

Twenty g soil (fresh wt.) in 250 ml glass flasks were added 100 ml liquid with 0.5 mM $(NH_4)_2SO_4$ and 10 mM $KClO_3$ to inhibit oxidation of NO_2^- to NO_3^- by nitrifying bacteria. Flasks were mounted on a shaker and 10 ml sample removed after 15 min and four hours later. Soil particles were removed by centrifugation and 2 ml sample added to 50 ml volumetric flasks with 45 ml water. One ml diazotation reagent (0.5 g sulphanilamide in 100 ml 2.4 N HCl) was added. Five min later 1 ml coupling reagent (0.3 g N(1 naphthyl)-ethylenediaminehydrochloride in 100 ml 0.12 N HCl) was added. 20 min later flask is filled to 50 ml and the absorption measured on a spectrophotometer at 540 nm. Rate of NO_2^- production was expressed as N in NO_2^- g^{-1} soil (dry wt.) h^{-1} .

The site



Figure S10.4: *The site, overview*

10.5.2 Results

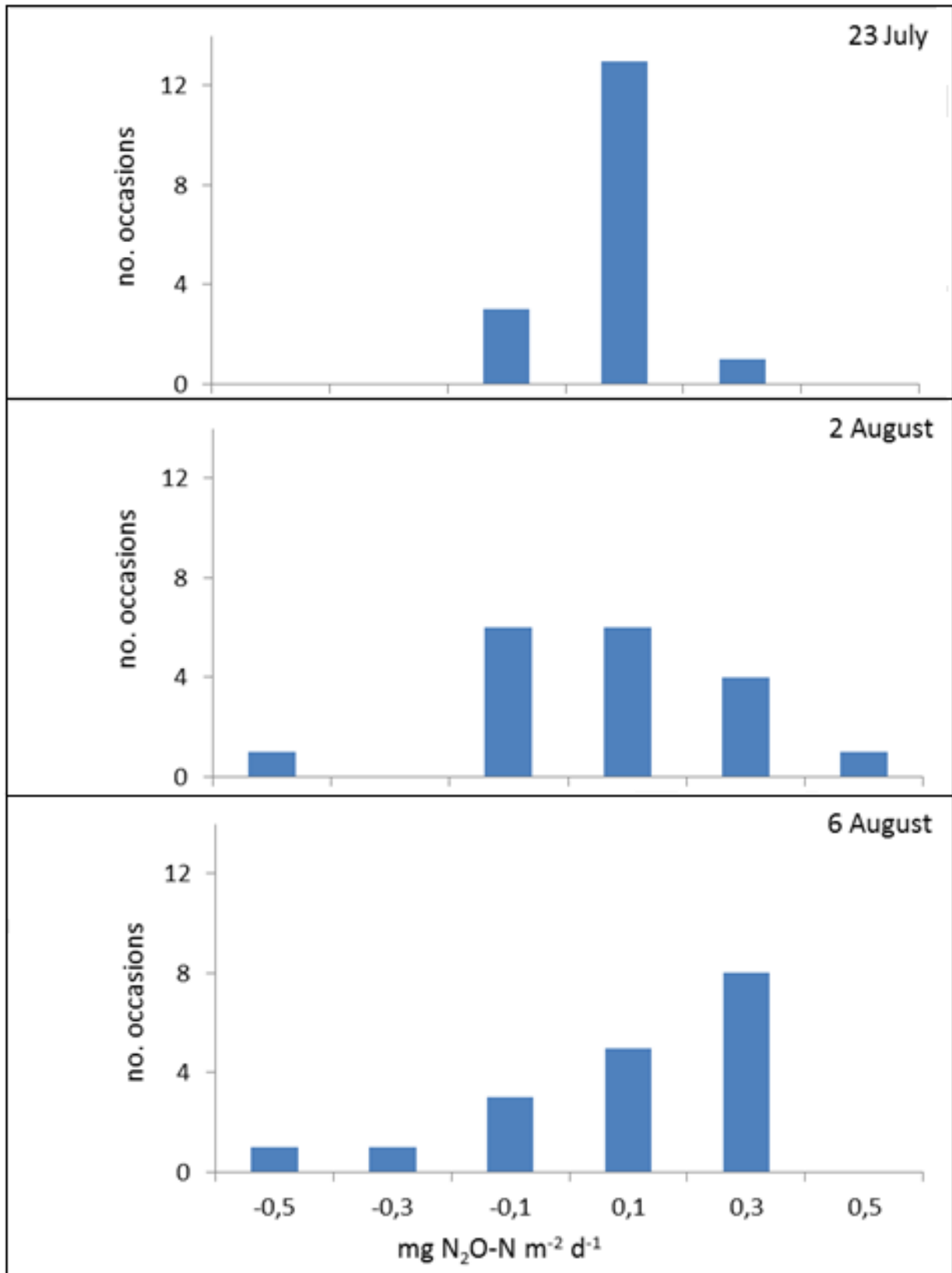


Figure S10.5: Frequency diagram of N₂O emission, for three sampling dates.

Table S10.2: The soil series downslope, botany and physics. * Sedge-wintergreen. ** Sedge-moss.

	Vegetation	Depth (cm)	SOM, % dry wt avg (s.e)	bulk density g cm ⁻³ avg (s.e)
Birch	Crowberry (<i>Empetrum nigrum</i> ssp <i>hermaphroditum</i>)	0-8	28.8 (9.9)	0.41 (0.05)
	Dwarf birch (<i>Betula nana</i>)	8-18	13.1 (1.6)	0.9 (0.06)
	Arctic bell heather (<i>Cassiope tetragona</i>), Arctic wintergreen (<i>Pyrola grandiflora</i>)	18-28	6.7 (0.1)	1.18 (0.02)
Willow	Arctic willow (<i>Salix arctica</i>)	0-8	72.8 (9)	0.06 (9.01)
	Gray willow (<i>Salix glauca</i>)	8-18	50.1 (12.2)	0.23 (0.09)
	peat moss (<i>Sphagnum</i> sp.), sheet moss (<i>Bryophyta</i> sp.)	18-28	33.5 (6.9)	0.38 (0.09)
S-W*	Alpine sedge (<i>Carex rariflora</i>)	0-8	55 (1.3)	0.21 (0.11)
	Common cottonsedge (<i>Eriophorum angustifolium</i>)	8-18	33.9 (0.8)	1.08 (0.45)
	Arctic wintergreen (<i>Pyrola grandiflora</i>)	18-28	11.6 (0.4)	1.3 (0.14)
S-M**	Alpine sedge (<i>Carex rariflora</i>)	0-8	55.9 (1.7)	0.09 (0.03)
	Island purslane (<i>koenigia islandica</i>)	8-18	18.4 (4.8)	0.64 (0.06)
	sheet moss (<i>Bryophyta</i> sp.)	18-28	7 (0.5)	1.23 (0.08)
Moss	sheet moss (<i>Bryophyta</i> sp.)	0-8	50.1 (4.2)	0.04 (0.01)
		8-18	41.1 (3.7)	0.11 (0.02)
		18-28	28.7 (6.5)	0.37 (0.1)
Peat	peat moss (<i>Sphagnum</i> sp.)	0-8	87.6 (2.8)	0.04 (0.01)
		8-18	84.4 (1.5)	0.07 (0)
		18-28	65.8 (7)	0.09 (0.01)

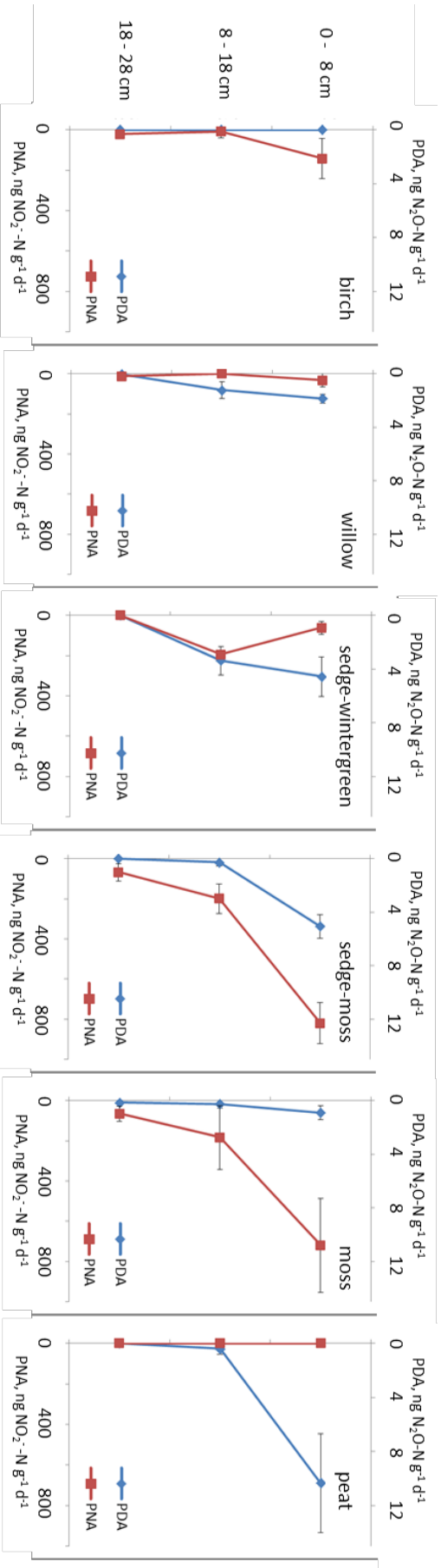


Figure S10.6: Potential denitrification and potential nitrification in the profiles of the six sites. Soil was sampled on the 25-31 July, 2013.

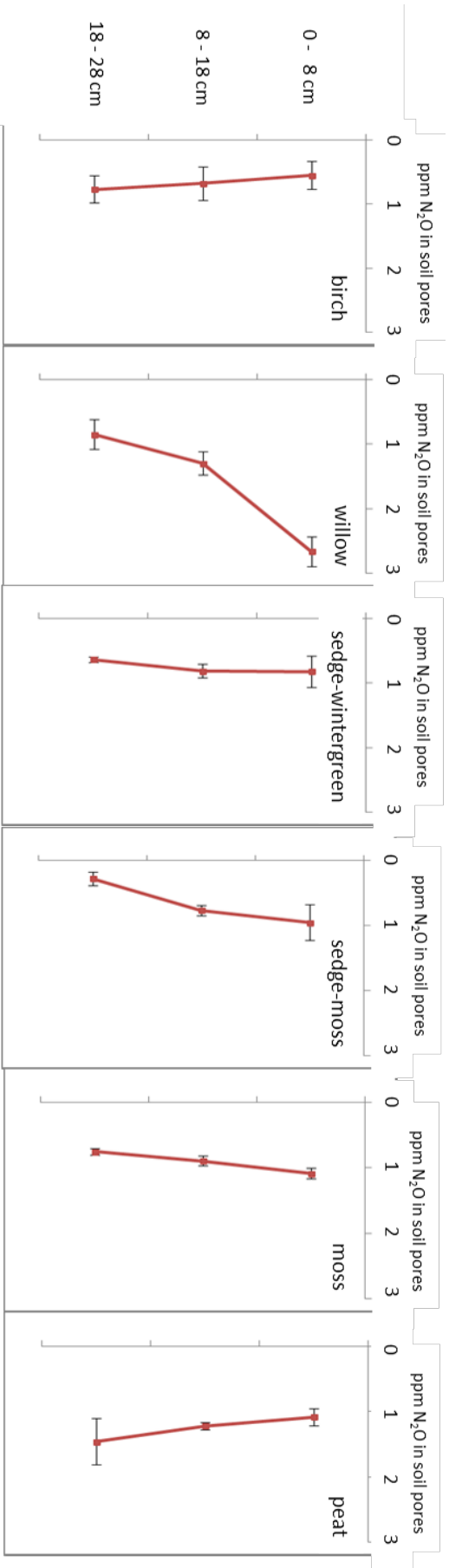


Figure S10.7: Average N_2O concentration ($\mu\text{L L}^{-1}$) in soil pores.

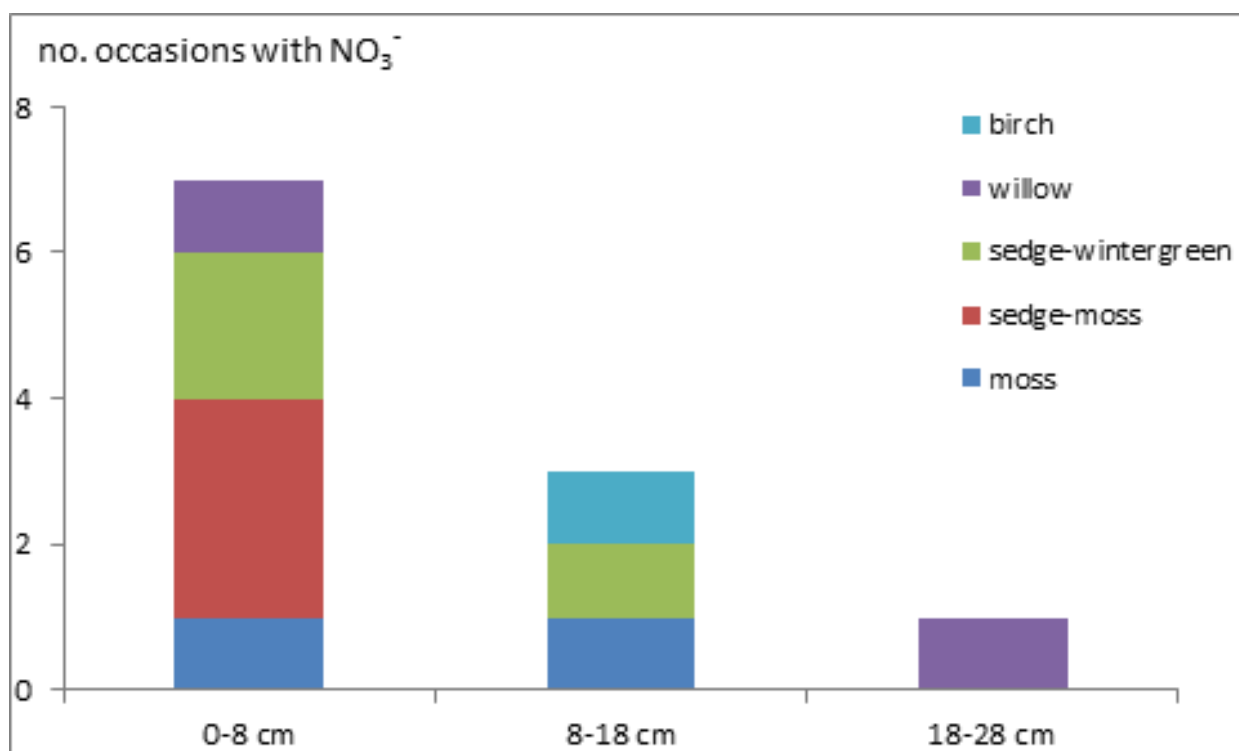


Figure S10.8: Occasions with measurable NO_3^- above zero with depth in the five of six profiles that had NO_3^- .

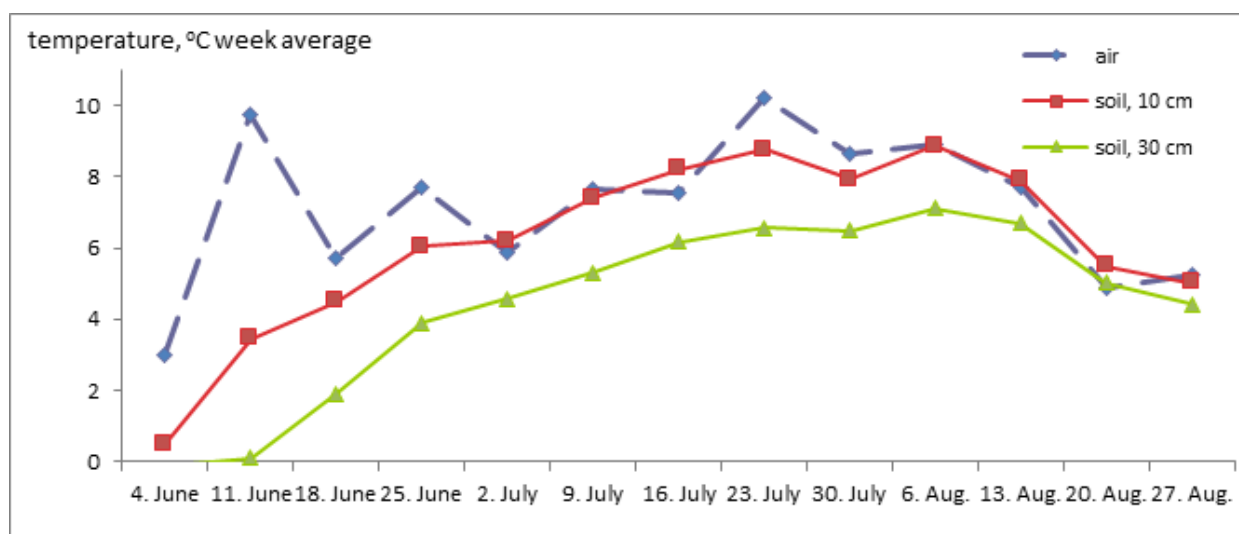


Figure S10.9: Development in temperature of soil and atmosphere during measuring period.

Huge N₂O emission from drained organic soil is related to seasonally mobile oxic-anoxic interface

Alexander Lee¹, Malte Winther², Anders Priemé³, Thomas Blunier², and Søren Christensen¹

1. Copenhagen University, Department of Biology, Section for Terrestrial Ecology, Universitetsparken 15, DK-2100 København Ø, Denmark
2. Copenhagen University, Niels Bohr Institute, Section for Ice and Climate, Juliane Mariesvej 30, DK-2100 København Ø, Denmark.
3. Copenhagen University, Department of Biology, Section for Microbiology, Universitetsparken 15, DK-2100 København Ø, Denmark.

This chapter has been published as A. Lee et al.: Huge N₂O emission from drained organic soil is related to seasonally mobile oxic-anoxic interface.,

Abstract

N_2O emission from soil is often regulated by the more or less sporadic occurrence of small anoxic volumes, which makes the process highly variable at the microscale. In a search for situations where variation in N_2O emission was at the mesoscale rather than at the microscale we selected a drained and nitrogen rich organic soil on a slope. In this situation, we expect a spatially more uniform distribution of anoxic volumes due to a widespread decomposition of soil organic matter at the increased oxygen availability upslope. We did find such gradients in N_2O emission at the mesoscale in the 10 meter range. Massive N_2O emissions occurred at an interface likely defined by oxic conditions upslope enhancing nitrate production from mineralized organic nitrogen and anoxic conditions downslope enhancing conversion of nitrate to N_2O primarily by denitrifying microorganisms. This N_2O -producing interface moved uphill in the wet season and downhill in the dry season so the mesoscale pattern also had a clear temporal component. One hectare soil encompassing such an interface emitted 73 kg N in N_2O annually, which makes it relevant to look for similar interface sites on slopes of drained organic soils elsewhere.

11.1 Introduction

Organic cultivated soils often show high emissions of N_2O . When organic soils are drained a massive subsidence and decomposition of soil organic matter may be initiated due to the easier access to oxygen for decomposing microorganisms. In eastern Finland, a drained fen lost 1 cm year^{-1} during 60 years (Nykanen et al., 2010) and an organic soil in Florida, US, lost 0.7 cm year^{-1} (Terry, 1980). A grazed grassland increased N_2O emission with 75 % after drainage (van Beek et al., 2010) and a forest site with alder increased N_2O emission nine times when drained (Von Arnold et al., 2005). Under such conditions decomposition of organic matter occurs widespread in the otherwise aerated soil matrix and implies large oxygen demands. This potentially creates anaerobic volumes in the aerated soil matrix, which can produce a large interface area between oxic and anoxic conditions per surface area. If the nitrogen mineralized from organic nitrogen or added as ammonium fertilizers is nitrified this environment has a huge nitrate input in the oxic parts of the soil volume leading to a large anoxic-oxic interface area with optimal conditions for N_2O production by denitrification. Large N_2O emission from drained organic soils have been observed previously, e.g. $23 \text{ kg N ha}^{-1} \text{ yr}^{-1}$ in a boreal site (Maljanen et al., 2004), $23 \text{ kg N ha}^{-1} \text{ yr}^{-1}$ in a Canadian soil (Rochette et al., 2010), $56 \text{ kg N ha}^{-1} \text{ yr}^{-1}$ in southern Germany (Flessa et al., 1998), and $97 \text{ kg N ha}^{-1} \text{ yr}^{-1}$ in Ohio, US (Elder and Lal, 2008).

Our aim was to investigate the importance of soil organic matter for N_2O emission. To achieve this we selected a toposequence in a Danish arable field with a gradual increase in soil organic matter downhill. We expected N_2O emission rates along the toposequence to peak at the interface between unsaturated uphill positions where nitrate (NO_3^-) is produced by nitrification following mineralization of organic N and saturated downhill positions where anoxic conditions abound and NO_3^- is reduced to N_2O . Moreover, we expected this interface to move uphill when precipitation is greater than evapotranspiration and downhill during dry periods. We also expected that uphill positions of low soil organic matter content will not have such a marked interface peak of N_2O emission due to a low oxygen demand for decomposition. Finally, we expected denitrification to be more important than nitrification for these N_2O releases due to the large decomposition of soil organic matter at the site.

11.2 Materials and Method

11.2.1 The site

A drained organic soil on a slope at Roholte, Sjælland, Denmark, stretching uphill 200-500 m from Orup Bæk (Faxe Kommune, municipal stream no. 11) was selected. The 300 m slope had an average declination of 3 % towards the 200 m of horizontal bottom along the stream. The slope and bottom are farmland grown with grass and maize, respectively. The lowest about 50 m of the slope and some 50 m of the bottom adjacent to the slope were studied. The upper two soil strata down to 40 cm depth have similar organic matter that increase down the slope from 15 % to 30 % loss on ignition. In the deeper soil layer, organic matter is virtually constant down the slope at 10-15 % ignition loss (Fig. 11.1). Soil pH from 0 to 35 cm depth was 6.0 ± 0.3 , and 5.5 ± 0.7 from 60 to 70 cm depth.

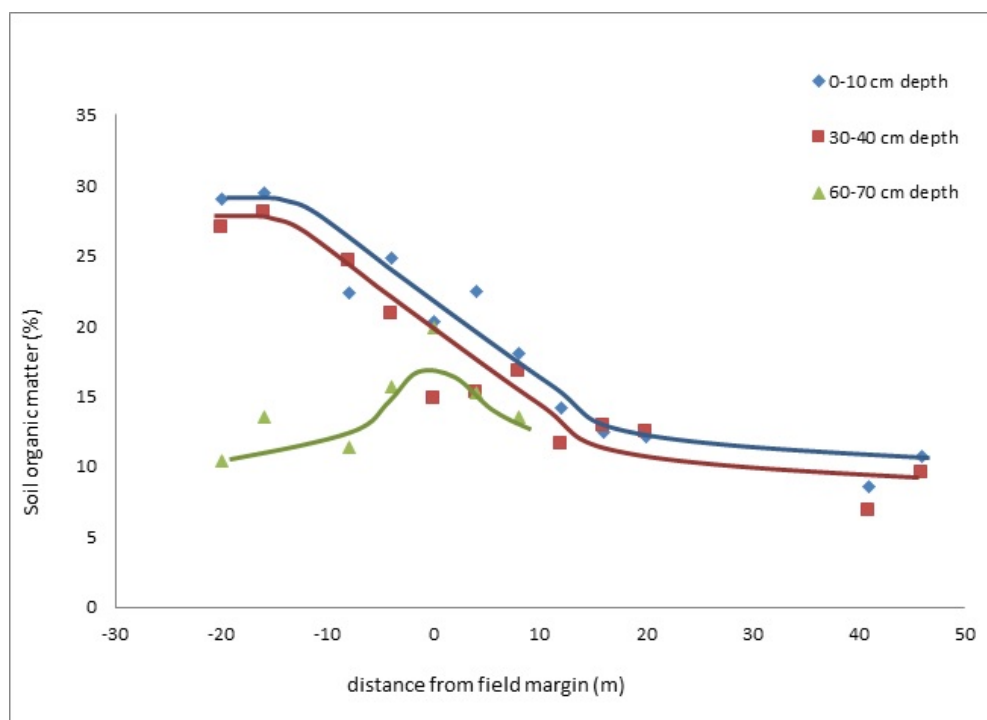


Figure 11.1: *Distribution of soil organic matter along the toposequence at different soil depths. Lines are fitted by eye.*

11.2.2 N₂O flux measurements

A plastic tube 10 cm / 11.6 cm inner/outer diameter of 15 cm length and tapered at the one end was hammered 9 cm into the ground so 6 cm with 0.5 l air was above the soil surface when covered with a lid. When sampling N₂O exchange a 6 mm thick plastic lid was sealed

on the plastic ring over a 5 mm thick foam rubber seal with a metal clamp fitting into a groove at the upper end of the plastic ring. Eight ml gas samples were collected 0 min and 30 min after sealing and stored in 5.3 ml Exetainers (LabCo, Lampeter, UK). One ml gas from the Exetainers was analyzed on a gas chromatograph with ECD.

N₂O in soil air

Nylon tubing of (6 mm outer diameter and 3 mm inner diameter) was inserted at different soil depths between 15 and 95 cm. The tubes were plugged at both ends and had four 1.5 mm holes on the side. Three replicate tubes were inserted at each topographic position with a distance of 2-5 m perpendicular to the direction of elevation/declination. A gas volume similar to the volume inside the tubes was removed before sampling 8 ml air, which were treated in the same way as described under N₂O flux measurement.

N₂O isotopomer measurements

Between 500 mL and 600 mL sample gas was collected in a 600 mL sampling bag (SupelTM-Inert Multi-Layer Foil bag, Sigma-Aldrich, USA) from the flux chamber. To prevent leak from the sampling bags, the isotopomers (¹⁴N¹⁵N¹⁶O ($\delta^{15}\text{N}^\alpha$) and ¹⁵N¹⁴N¹⁶O ($\delta^{15}\text{N}^\beta$)) and concentration of N₂O was measured using a Picarro G5131-i analyser within 6 hours of sampling. Measurements were performed continuously for 20 minutes (24 mL min⁻¹) or more to improve the statistical analysis. Park et al. (2011) state that the source of N₂O can be distinguished due to a difference in SP, e.g., denitrification leads to SP < 0 ‰ and nitrification leads to SP > 11 ‰.

11.2.3 Potential activity of processes forming N₂O

Soil was sampled at three positions along the toposequence (-20 m - 0 m; 0 m - 12 m, and 12 m - 46 m) and at two depths (0-10 cm and 30-40 cm) on 10 May 2014. Potential denitrification and potential nitrification were measured on these (four replicates per position and depth).

Potential denitrification

Two g soil (fresh wt.) in 117 ml glass flasks were added 5 ml liquid with 1 mM glucose and 1 mM KNO₃. Flasks were sealed with a butyl rubber stopper, headspace evacuated and refilled with N₂ and 10 % of the atmosphere replaced with C₂H₂. Flasks were mounted on a shaker and N₂O concentration in the headspace assessed after two hours on a gas chromatograph with ECD.

Potential nitrification

Twenty g soil (fresh wt.) in 250 ml glass flasks were added 100 ml liquid with 0.5 mM $(\text{NH}_4)_2\text{SO}_4$ and 10 mM KClO_3 to inhibit oxidation of NO_2^- to NO_3^- by nitrifying bacteria. Flasks were mounted on a shaker and 10 ml sample removed after 15 min and four hours later. Soil particles were removed by centrifugation and 2 ml sample added to 50 ml volumetric flasks with 45 ml water. One ml diazotation reagent (0.5 g sulphanilamide in 100 ml 2.4 N HCl) was added. Five min later 1 ml coupling reagent (0.3 g N(1 naphthyl) ethylenediaminehydrochloride in 100 ml 0.12 N HCl) was added. 20 min later flask is filled to 50 ml and the absorption measured on a spectrophotometer at 540 nm. Rate of NO_2^- production was expressed as N in $\text{NO}_2^- \text{ g}^{-1}$ soil (dry wt.) h^{-1} .

Activity in intact soil cores from various depths

4.5 cm diameter soil cores of 166 ± 11 g (average height 10 cm) were collected at five positions along the toposequence (-25 m, -20 m, -5 m, +4 m, +12 m) with up to three replicate cores per position. Samples were collected from six depths, 15, 30, 45, 60, 75, and 90 cm. The cores were left open for a few days to degas N_2O accumulated at depth before sealing in 1100 ml glass jars to quantify N_2O production.

Activity in soil \pm amended with acetylene

Soil sampled from the upper 20 cm at position -12 m (organic soil) and at position +12 m (mineral soil) 28 July 2014 was homogenized and 30 g dwt soil added to glass containers, packed to $0.45 \text{ g} / \text{cm}^3$ and left open for three weeks at 12°C . N_2O production by four replicate cores from each position was assessed at 12°C followed by addition of 10 % acetylene and a new measurement the following day.

11.3 Results

11.3.1 Field N_2O fluxes

Field N_2O fluxes from the nine dates indicate a seasonally "mobile" hot spot for N_2O emissions of varying intensity. Peak N_2O emission moved uphill when precipitation was greater than evapotranspiration, and downhill following dry periods (Fig. 11.3). In six of nine cases, we found a correlation between size of emission and relative position along the toposequence. This means that the emission rates at neighboring positions was likely to be low if the N_2O activity at the position is low, respectively high when the N_2O activity at

the position is high (Table 11.1). In other words, we do have a pattern of N_2O emission at the mesoscale of meters.

Annual N_2O emissions were estimated by summing up the N_2O release from the sections measured along the toposequence for each measurement date. Daily measured emissions were set to represent emissions for a period of half the time between two neighboring dates except for the day with emission rate above $1 \text{ kg N}_2\text{O-N ha}^{-1} \text{ d}^{-1}$ (3. Nov. 2013). The activity measured this day was only regarded as representing the day of measurement and the preceding and following day. These estimates revealed an annual emission of $73 \text{ kg N}_2\text{O-N ha}^{-1}$ (Table 11.1).

There was no correlation of daily flux rate with the precipitation in the preceding week or month. The NH_4^+ content in the soil is remarkably high particularly in the bottom section (Fig. 11.2). Nitrate content is also rather high in the bottom section decreasing to nil up the slope (Fig. 11.2). The NH_4^+ and NO_3^- content at 0-40 cm soil depth in one hectare covering the 80 m assessed on Fig. 11.2 and with the values on the slope stretching further

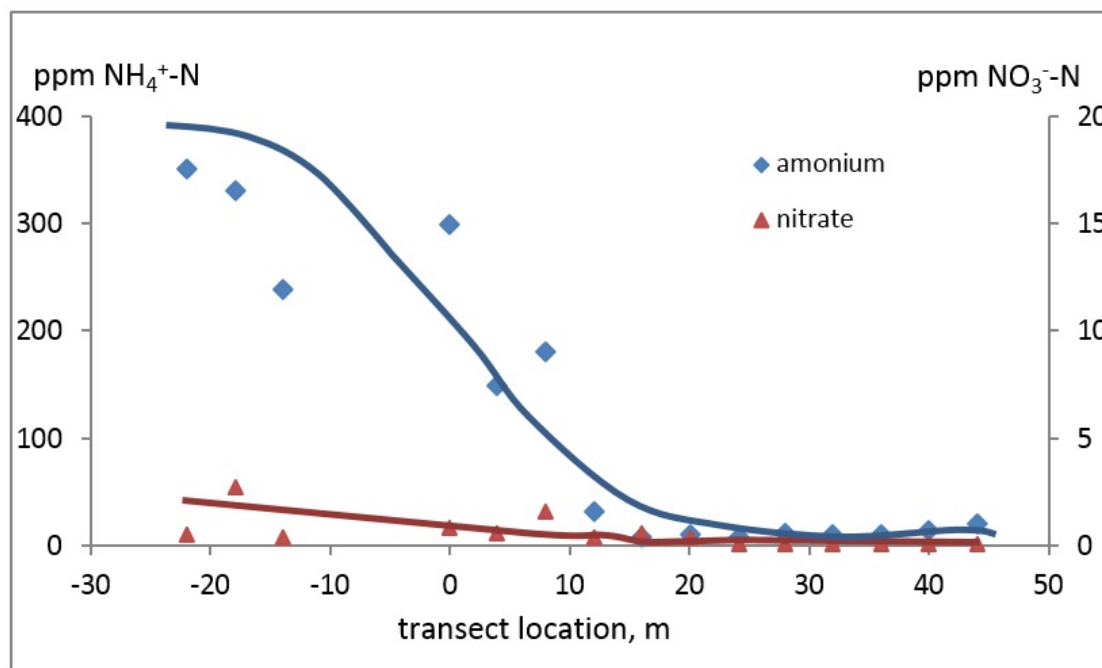


Figure 11.2: *Inorganic N along the toposequence measured at 0-20 cm soil depth on 15 Dec. 2015. Lines are fitted by eye.*

20 m uphill gives $201 \text{ kg NH}_4^+\text{-N ha}^{-1}$ and $0.7 \text{ kg NO}_3^-\text{-N ha}^{-1}$ or $202 \text{ kg inorganic N ha}^{-1}$. The organic matter content in one hectare covering the 80 m assessed on Fig. 11.1 and with the values on the slope stretching further 20 m uphill gives $465 \text{ t organic matter ha}^{-1}$. With 60 % C in soil organic matter and a C/N (wt/wt) ratio of 11 this corresponds to $25 \text{ t organic N ha}^{-1}$.

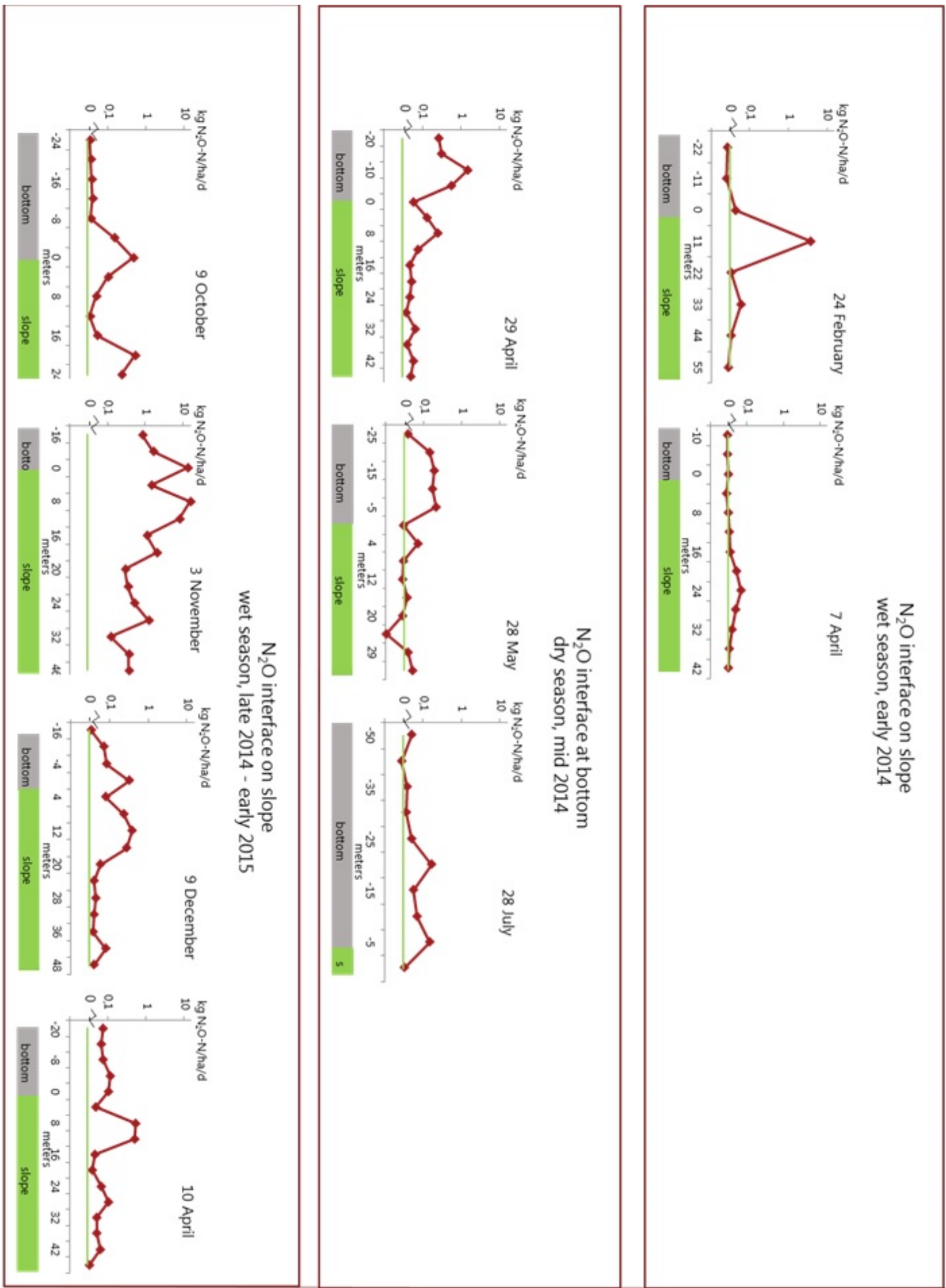


Figure 11.3: Seasonal variation in N₂O emission along toposequence on drained organic soil.

Table 11.1: Cumulated N₂O emission rates. When rates measured neighboring locations are both likely to be high or low, respectively then neighbor rates correlate strongly with each other, and P will be low. Table shows that in six out of nine measurement occasions rates correlated with neighbor rates at the 4-6 m scale - the distance between points along transect; *** P < 0.001, * P < 0.05, n.s. P > 0.05. Cumulated N₂O emission We made a conservative estimate of cumulated flux by letting the three daily rates of above 1 kg N ha⁻¹

Spatial correlation of N ₂ O fluxes			Quantification of N ₂ O emissions					
Day	Pearson coeff.	P	Part of topose- quence assessed (m)	Position of max N ₂ O emission (m)	N ₂ O emission (kg N ₂ O-N ha ⁻¹ d ⁻¹)	Interval, (d)	Cumulated N ₂ O emission (kg N ha ⁻¹ period ⁻¹)	
24-Feb-14	0.362	n.s.	-22 ± 60	11	0.605	27	16.3	
07-Apr-14	0.719	***	-10 ± 42	24	0.066	33	2.2	
29-Apr-14	0.592	***	-20 ± 47	-10	0.402	24	9.6	
28-May-14	0.484	*	-25 ± 34	-5	0.107	46	4.9	
28-Jul-14	0.184	n.s.	-50 ± 5	-20	0.073	69	5.0	
09-Oct-14	0.451	*	-24 ± 24	20	0.172	60	10.3	
03-Nov-14	0.426	*	-16 ± 46	8	3.641	3	10.9	
09-Dec-14	0.454	*	-16 ± 48	12	0.147	87	12.8	
10-Apr-15	0.101	n.s.	-20 ± 48	8	0.17	80	13.6	
sum						427	85.7	
sum						365	73.0	

11.3.2 Soil air N₂O

The soil air N₂O content suggests that N₂O production occurs down to 95 cm soil depth. The very high N₂O production at 3 November 2014 (Fig. 11.3) apparently occurred at a slightly more shallow depth between 35 and 75 cm (Fig. 11.4). N₂O production of incubated soil cores from May 28 2013 (Fig. 11.5) supported the N₂O production activity at depth indicated from the soil air analysis (Fig. 11.4). These data show that N₂O production increase with depth (Fig. 11.5). A three-way ANOVA with five positions on the toposequence and six soil depths as fixed factors and core as random factor showed N₂O production to increase with depth (P=0.0051).

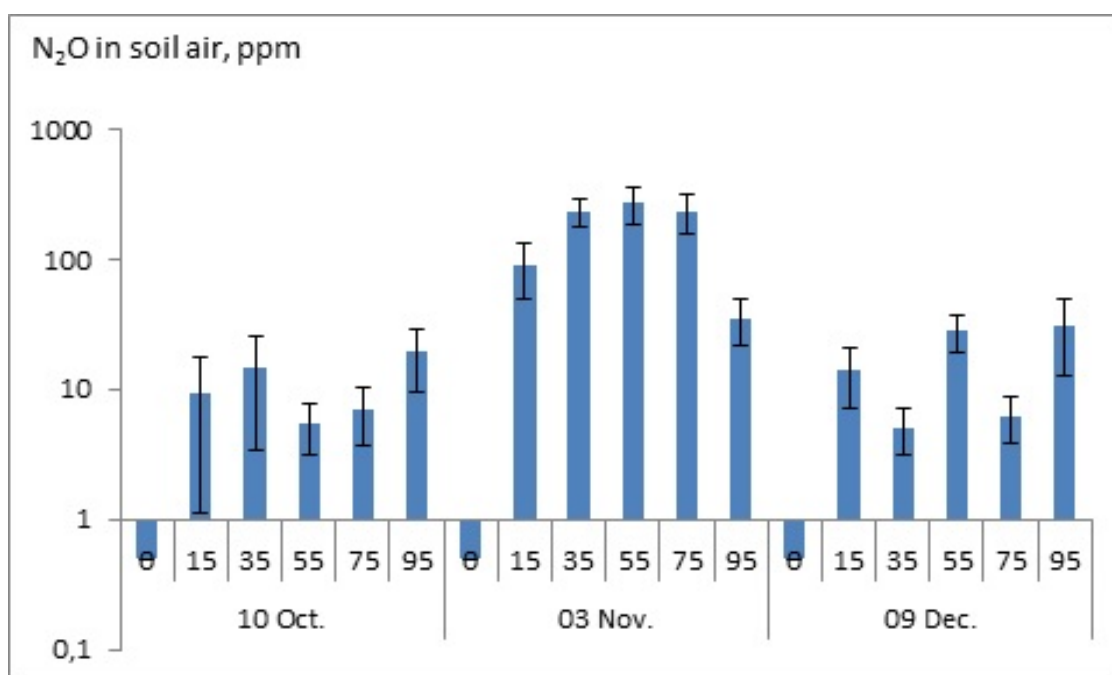


Figure 11.4: N₂O concentration in soil air collected at five soil depths and 20 cm above the soil surface ("0") on three days. Position -16m, 0m and +20m along toposequence were sampled with three replicate profiles per position and day.

11.3.3 N₂O isotopomer site preference

The isotopomers of N₂O cumulating in a flux chamber at the soil surface were assessed at ten locations along the toposequence on 15 December 2015. At the ten locations, N₂O increased above the ambient 0.33 ppm during 20 min of sealing. The site preference (SP = $\delta^{15}\text{N}^{\alpha} - \delta^{15}\text{N}^{\beta}$ (Park et al., 2011)) of the enclosed N₂O decreased with increasing emission of N₂O (P=0.0013, Pearson Coefficient 0.86 Fig. 11.6). At the three sites out of ten with lowest N₂O emission, we found nitrification to dominate the N₂O production (SP > 40, Fig.

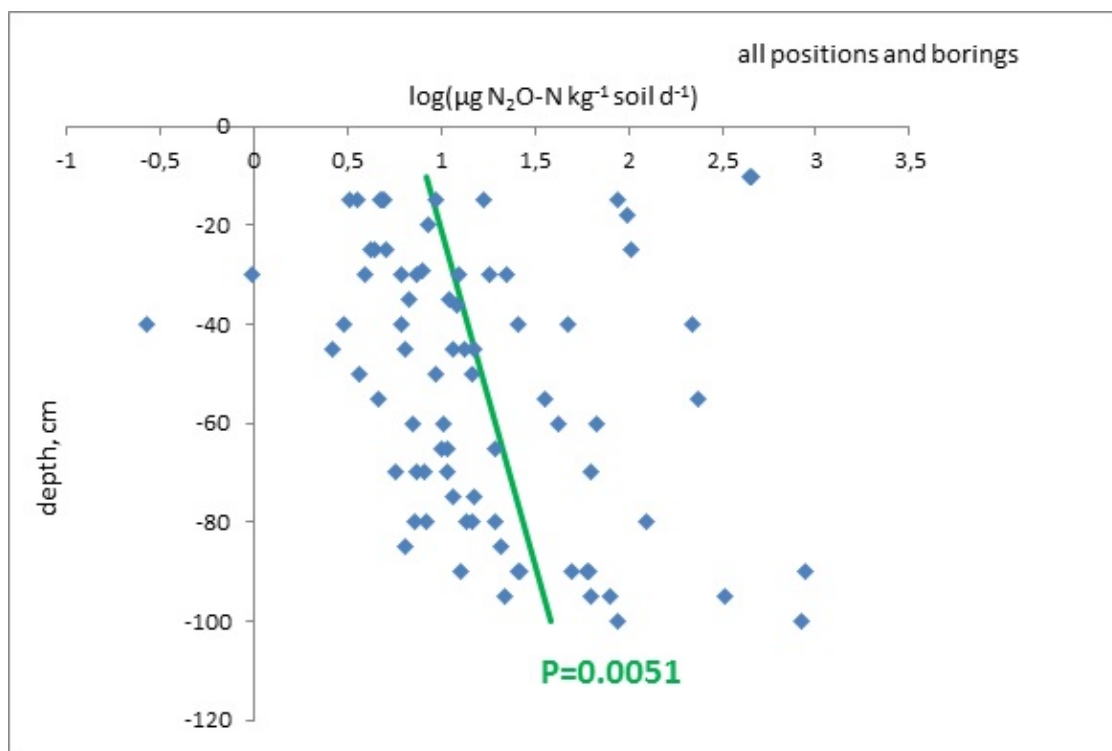


Figure 11.5: N_2O production in intact soil cores sampled at different depths May 28 2013 ($R^2=0.097$; $n = 79$).

11.6). At the highest N_2O emission assessed, the site preference was 3.5 (Fig. 11.6), which corresponds to 1/3 of the N_2O from nitrification with a site preference of 11 and 2/3 of the N_2O from denitrification with a site preference of -1. This is a conservative estimate in the favor of nitrification as N_2O source, since site preference of nitrifying bacteria can be well above 11 (Park et al., 2011). Moreover, even the highest N_2O release encountered at the time of SP assessment ranged among the lowest activities encountered in this study (Fig. 11.6 vs. Table 11.2). We therefore suggest that denitrification is the major N_2O -producing activity at this site.

Table 11.2: Effect of acetylene amendment on N_2O production in soil samples (measured in $ng\ N_2O-N\ cm^{-3}\ h^{-1}$) expressed on a relative scale setting N_2O production without acetylene to 1. Assessment was made on soil sampled 28 July 2014. Data are average \pm standard error of the mean.

	Acetylene added	Relative N_2O production
Mineral soil	No	1 ± 0
	Yes	0.47 ± 0.14
Organic soil	No	1 ± 0
	Yes	0.42 ± 0.33

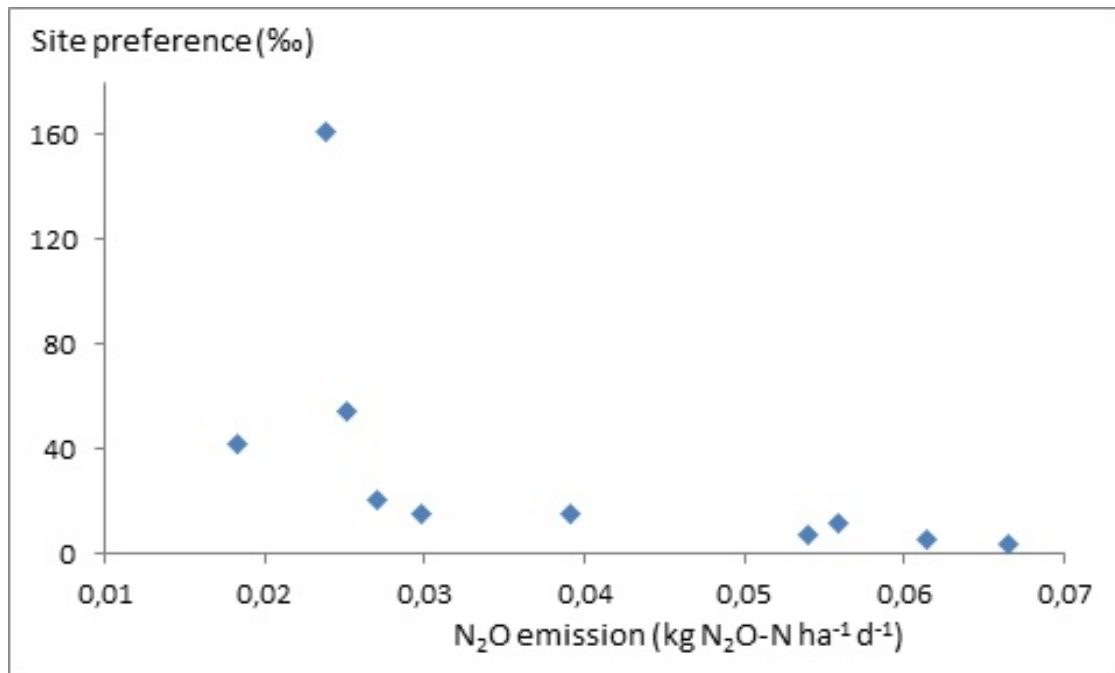


Figure 11.6: *Isotopomer site preference of N₂O emitted along the toposequence. N₂O emission and the corresponding site preference of the N₂O cumulated in flux chambers were assessed 15 December 2015.*

11.3.4 Coupling of nitrification and denitrification

Acetylene reduced N₂O production (Table 11.2) and potential denitrification rates were positively correlated with potential nitrification rates (Fig. 11.7, P=0.0054). The activity of both processes was highest in locations at the bottom as expected for a summer sampling (Fig. 11.3). There was no effect of soil depth on the relationship between the two processes.

11.4 Discussion

11.4.1 Field fluxes

The very large N₂O fluxes recorded are in accordance with the literature giving high values for organic soils (Flessa et al., 1998; Maljanen et al., 2004; Elder and Lal, 2008; Rochette et al., 2010). These large fluxes are often related to drainage, which increased N₂O emission from grazed grassland in The Netherlands from 51 to 90 g N-N₂O ha⁻¹ d⁻¹ or a 75 % increase (van Beek et al., 2010) with higher activity when groundwater is deeper (40 cm) than at more shallow depth (18 cm) (van Beek et al., 2011).

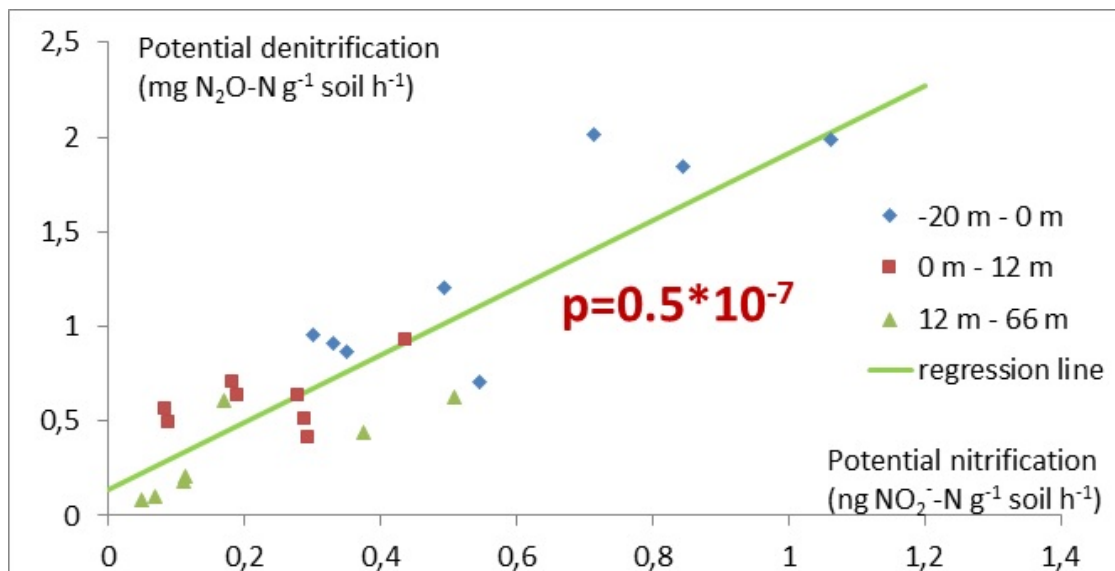


Figure 11.7: *Relation between potential denitrification and potential nitrification ($R^2=0.75$, $n=24$).*

Field fluxes from the nine sampling dates indicate a mobile interface of high N₂O production at a certain position along the toposequence. This suggests that soil volumes with spatially mixed oxic and anoxic conditions occur at this interface. Emissions are based on nitrate produced by nitrification in the aerated volumes that then may diffuse to the anoxic volumes where N₂O is produced by denitrification of the inflowing nitrate. This indicates that N₂O emissions are the result of stable physical constraints on a landscape scale and not of local conditions along the toposequence as often seen when spatial variability in N₂O production mainly occur at the small scale (Groffman, 2012; Hénault et al., 2012) and even down to centimeter scale (e.g. Christensen et al. (1990a)), which most often is due to build-up of small anoxic volumes in an otherwise aerobic soil (Christensen et al., 1990b). The position of the high N₂O emission along the toposequence changes between dates, which may be explained by changing ground water levels while access to nitrate may explain seasonal fluctuations in emissions size.

The active interface is located where soil water content is sufficient for small respiration-driven anoxic soil volumes to be formed but not so high that the major part of the soil volume gets anoxic. In this situation with many smaller anoxic soil volumes the interface area between oxic and anoxic conditions will be maximized. Since N₂O is formed by denitrification the negative effect of acetylene in soil from the bottom as well as soil from the slope suggests that NO₃⁻ production by nitrification is inhibited by acetylene and indicates a fast consumption of NO₃⁻ by denitrification as soon as it is produced by nitrification. The

same conclusion is drawn from the close relationship between potential denitrification and potential nitrification (Fig. 11.7, $P=0.0054$). At our site where N_2O is produced by denitrification, which is built on nitrification activity delivering the NO_3^- , the N_2O production depends on the interface area because the two processes are anaerobic and aerobic, respectively. One may only speculate about the size of the anaerobic volumes in this situation. Anaerobic volumes far below one ml (Parkin, 1987) or up to 9 ml (Christensen et al., 1990b) have been shown to be very active in N_2O emission from denitrifying bacteria. Taken together the results from Table 11.2 and Fig. 11.7 shows that denitrification strongly depends on nitrification activity. Even at moderate rates of N_2O production ($0.2 - 0.4 \text{ kg N ha}^{-1} \text{ d}^{-1}$, Table 11.2) the emission of N_2O requires about half of the available NO_3^- pool (0.7 kg N ha^{-1} , Fig. 11.2) each day which again suggests a fast turnover of the NO_3^- pool.

The extreme N_2O emission we found on November 3 2014 covered much of the annual emission in accordance with van Beek et al. (2011) who found that a single day of measurement may be responsible for 25-50 % of the total annual emission. We only let the emission measured this day represent three days so the estimate of annual emission can therefore be considered conservative and still show a quite extraordinary annual emission of $73 \text{ kg } N_2O\text{-N ha}^{-1}$. There was no correlation of daily flux rate with the precipitation in the preceding period in contrast to the results of Elder and Lal (2008) and Maljanen et al. (2004) who both found N_2O flux to correlate with rain events. This may in part be due to the location of considerable N_2O production at deeper soil depth at our site.

The N_2O emission requires a considerable rate of nitrate input. The size of the inorganic N pool (202 kg N ha^{-1}) is almost three times the annual N_2O emission ($73 \text{ kg N ha}^{-1} \text{ yr}^{-1}$) and corresponds to 0.8 percent of the 25 t organic N ha^{-1} in the upper 40 cm profile. Annual rates of N mineralization reported in drained organic soils are of the same order of magnitude as the inorganic N pool we found, being $250\text{-}571 \text{ kg N ha}^{-1} \text{ yr}^{-1}$ in a Canadian site (Rochette et al., 2010), $466 \text{ kg N ha}^{-1} \text{ yr}^{-1}$ in Florida (Terry, 1980) and $480 \text{ kg N ha}^{-1} \text{ yr}^{-1}$ in the Netherlands (Schothorst, 1977). Considering that the elevation of the soil surface in the organic bottom is reduced by about one meter since drainage in 1962 annual loss of organic matter in the area must be well above the one percent required to produce an amount of inorganic N as we measured in a year. We may therefore conclude that the supply of inorganic nitrogen by decomposing soil organic matter due to drainage far exceeds the amount leaving the soil surface in N_2O .

11.4.2 Soil air N₂O

It is very difficult to reveal N₂O transforming processes in the soil based on the N₂O concentration down the profile because the physical processes diffusion and convective flow are involved on top of the biological production and consumption processes Clough et al. (2005). Characterization of vertical profiles of N₂O concentration in the soil can reveal, however, the relative changes in net production of N₂O with depth. Our data suggests that N₂O is produced at considerable soil depth down to one meter in the profile. A significant part of the very high N₂O production at 3 November 2014 apparently occurred at a depth between 35 and 75 cm, i.e. just above the depth of standing water. This is in agreement with Van Beek et al. (2004) and Yano et al. (2014) who found maximal N-gas production just above the groundwater level.

11.4.3 Microbial processes producing N₂O

Under field conditions, it is difficult to unravel if nitrification or denitrification produces the N₂O emitted, not the least because the two processes are often closely linked in space and time as we have evidenced to be the case in our work. However, an assessment of N₂O SP may help differentiate the contributions of the two processes. (Yoshida and Toyoda, 2000) described how intermolecular position of the ¹⁵N isotope in the N₂O molecule can be used to track if the origin of the N₂O is biological or chemical. Our assessment of SP suggest denitrification to be the process mainly responsible for the N₂O release. This is in accordance with several authors who found that N₂O from soil mainly originate in reduction of NO₂⁻ performed by denitrifying or by nitrifying bacteria (Opdyke et al., 2009; Ostrom et al., 2010; Smemo et al., 2011; Yano et al., 2014; Zou et al., 2014; Wolf et al., 2015; Wu et al., 2016). The opposite, N₂O originating in autotrophic NH₄⁺ oxidation has also been found (Kato et al., 2013; Yamamoto et al., 2014; Zhang et al., 2016). It has also been described how denitrification dominated N₂O production in soil but that nitrification gained importance after amending with manure (Köster et al., 2011, 2015). The dominance of NO₂⁻ reduction as the N₂O forming process allows us to evaluate how the processes nitrification and denitrification are coupled at this site, see below.

11.4.4 Coupling of nitrification and denitrification

Since acetylene reduced N₂O emission and N₂O is mainly produced by denitrification this suggests a close coupling of denitrification with nitrification. The same conclusion is drawn from the very close correlation of potential denitrification with potential nitrification. These

results strongly indicate that denitrification depends on nitrification activity as shown before (e.g. Stehfest and Bouwman (2006)). At this location, the available NO_3^- pool should be renewed in about two days just to satisfy the N_2O production. This conclusion is in accordance with Petersen et al. (1991) who were among the first to demonstrate how denitrification coupled to nitrate production by nitrification in a mixed oxic-anoxic environment can result in denitrification of the major part (70 %) of the ammonium produced, a mechanism that was also evidenced by Bergstrom et al. (1994) and by Abbasi and Adams (1998).

11.5 Conclusion

We conclude that the high N_2O emission along a toposequence on a drained organic soil occur in an interface position on the slope with seasonal movements up- or downhill. Contrary to our expectations an interface of high N_2O production may also be located where organic matter content is rather low. This suggests that more emphasis should be devoted to N_2O emission on such locations.

11.6 Author contribution

The experiments were designed by SC, AL, MW, and TB. Field experiments were carried out by AL, MW, and SC. Soil measurements and gas measurements using GC was performed by AL. MW performed large volume gas extraction, measurements on the CRDS G5101i-CIC analyzer, data calibration and correction. SC prepared manuscript with contribution from AL and MW. Manuscript was finalized with contribution from all co-authors.

Conclusions and Outlook

This thesis presents experiments highlighting the spatial and temporal evolution of N₂O from pure bacterial species (Part II), from the past atmosphere (Part III), and from the present atmosphere (Part IV). The spatial evolution is investigated via measurements of the $\delta^{18}\text{O-N}_2\text{O}$ and the isotopomers of N₂O (SP and $\delta^{15}\text{N}^{bulk}$).

Continuous measurements of incubated nitrifying and denitrifying bacterial species revealed distinct isotopic features of N₂O. The experiments with nitrifying bacterial species *Nitrosomonas mobilis* were hypothesized to reveal NH₃ oxidation and NO₂⁻ reduction as cyclic reactions appearing as two distinct levels of isotopic N₂O composition separated by a transition period. The two distinct levels of SP that were discovered, were found to be in line with previous findings, and were used to distinguish the two N₂O producing reactions. Both $\delta^{18}\text{O-N}_2\text{O}$ and $\delta^{15}\text{N}^{bulk}$ experienced a significant depletion from the first experiment to the second experiment, which is hypothesized to be due to mass-dependent fractionation during the reduction of N₂O to N₂. Unfortunately the experiment lacks information of the initial isotopic composition of the gas-matrix. Information of the initial $\delta^{18}\text{O-O}_2$ composition has the potential to partly explain the strongly depleted $\delta^{18}\text{O-N}_2\text{O}$ values measured during the second experiment.

Continuous measurements of two denitrifying bacterial species resulted in two distinct evolutions of the resulting N₂O and of the isotopomers of N₂O. Incubation experiments with *Pseudomonas chlororaphis* showed isotopic fractionation in line with previous results for both SP and $\delta^{15}\text{N}^{bulk}$. Incubation experiments with *Pseudomonas fluorescens* showed SP isotopic fractionation in line with previous results during production, while the SP isotopic fractionation during reduction was slightly increased. The $\delta^{15}\text{N}^{bulk}$ isotopic fractionation during reduction was in line with previous results, whereas the $\delta^{15}\text{N}^{bulk}$ isotopic fractionation during production was found to be depleted because of mass-dependent fractionation. To further improve the understanding of the different processes involved in production of N₂O during denitrification, additional experiments with denitrifying bacteria are necessary. The additional experiments should focus on full denitrifying bacterial cultures, and use acetylene (or similar) to block reduction of nitrous oxide reductase and thereby hinder reduction of N₂O to N₂.

Continuous incubation investigations with bacterial cultures would be improved by measurements of NH₃ and/or NO₂⁻ in the liquid phase and of gaseous NO and N₂. For the presented incubation setup, modifications could be made relatively easily to perform discrete measurements on a regular basis. These measurements would potentially provide additional

information of the specific reactions and of the continuously changing mass balance and thereby contribute significantly to the microbial evolution of N_2O .

The evolution of N_2O has been investigated through measurements of samples from the NEEM ice core and from present day ecosystems in Greenland (arctic ecosystem) and in Denmark (temperate ecosystem). Using measurements of the SP, $\delta^{15}\text{N}^{bulk}$, and $\delta^{18}\text{O}-\text{N}_2\text{O}$ under the assumption that nitrification and denitrification are, and were, the predominant sources of N_2O in both aquatic and terrestrial ecosystems has lead to investigations of the past and present atmospheric N_2O .

The atmospheric isotopic composition of N_2O was measured from 15 samples of the NEEM ice core covering four sections of the past 35,000 years before year 2000. The measurements resulted in relatively constant signatures of $\delta^{15}\text{N}^{bulk}$ for all samples. The SP signature was found to be relatively stable throughout the Holocene, while the glacial SP signal was found to be significantly depleted and therefore indicating a shift in the dominant microbial community towards the denitrifying bacterial species. Measurements of the $\delta^{15}\text{N}^{bulk}$ combined with measurements of the $\delta^{18}\text{O}-\text{N}_2\text{O}$ indicated that N_2O has originated from aquatic ecosystems over the past 35,000 years. Although applying a correction for the stratospheric fractionation effect, as described by Röckmann et al. (2001), resulted in a depletion of all the isotopes, and therefore shifting the primary source region to terrestrial ecosystems during both the Holocene and the glacial. The SP suggested that N_2O during the Holocene is produced from both nitrification and denitrification, while denitrifying bacterial production dominates the N_2O production during the glacial. Unfortunately only a small number of measurements were performed, which resulted in a limited verification for the different features discovered. Additional measurements of the isotopic composition of N_2O trapped in the ice cores are therefore necessary for verification of the hypothesis resulting from the presented measurements.

Present day terrestrial ecosystem emissions of N_2O were investigated on two occasions, once on Disko island in Greenland and once at a drained organic slope on Sjælland in Denmark. From field measurements at Disko island, we found high nitrification potential in moss covered soils, which in contrast showed net consumption of N_2O . Measurements of the isotopic composition of N_2O extracted resulted in SP values indicating denitrification as the primary microbial source. We therefore hypothesize that denitrification dominates these sites and that this specific ecosystem favored nitrous oxide reductase leading to a net consumption of N_2O from the atmosphere, hence we discovered a potential greenhouse gas reducing ecosystem in the arctic using the isotopomers of N_2O .

Field measurements from the drained organic soil on a slope were performed to investigate the microbial productivity over a toposequence on a mesoscale. The measurements resulted in a clear distinction with a massive emission on an interface defined by oxic and ammonium rich ecosystems resulting in high nitrification upslope, while the ecosystem downslope was anoxic and nitrate rich resulting in denitrifying bacterial N_2O emission. We found the interface to be moving up and down the slope depending on the conditions and resulting in a clear temporal component of the N_2O producing ecosystem.

Investigations presented in this thesis have shown 1) continuous incubation experiments highlighting the evolution of the isotopic composition of N_2O , which have the potential to reveal new aspects of the microbial production and reduction of N_2O . 2) Measurements of the isotopic composition of N_2O from the NEEM ice core indicated a potential change in the primary microbial community responsible for emission of N_2O from the glacial into the Holocene. A change, which if verified through additional measurements, that has the possible potential to lead to an improved understanding of the changes causing the dramatic climatic changes. 3) Measurements of the isotopic composition of N_2O extracted from arctic moss covered soils give the first indication of an ecosystem leading to general consumption of N_2O . 4) Gas extraction measurements from present day ecosystems furthermore show the great advantage and potential of both continuous and discrete N_2O isotope measurements.

Bibliography

Bibliography

- Abbasi, M. K. and Adams, W. a. (1998). Loss of nitrogen in compacted grassland soil by simultaneous nitrification and denitrification. *Plant and Soil*, 200(2):265–277.
- Andersen, K. K., Azuma, N., Barnola, J.-M., Bigler, M., Biscaye, P., Caillon, N., Chappellaz, J., Clausen, H. B., Dahl-Jensen, D., Fischer, H., Flückiger, J., Fritzsche, D., Fujii, Y., Goto-Azuma, K., Grønvold, K., Gundestrup, N. S., Hansson, M., Huber, C., Hvidberg, C. S., Johnsen, S. J., Jonsell, U., Jouzel, J., Kipfstuhl, S., Landais, A., Leuenberger, M., Lorrain, R., Masson-Delmotte, V., Miller, H., Motoyama, H., Narita, H., Popp, T., Rasmussen, S. O., Raynaud, D., Rothlisberger, R., Ruth, U., Samyn, D., Schwander, J., Shoji, H., Siggard-Andersen, M.-L., Steffensen, J. P., Stocker, T., Sveinbjörnsdóttir, A. E., Svensson, A., Takata, M., Tison, J.-L., Thorsteinsson, T., Watanabe, O., Wilhelms, F., and White, J. W. C. (2004). High-resolution record of Northern Hemisphere climate extending into the last interglacial period. *Nature*, 431(7005):147–51.
- Augustin, L., Barbante, C., Barnes, P., Barnola, J., Bigler, M., Castellano, E., Cattani, O., Chappellaz, J., Dahl-Jensen, D., Delmonte, B., Dreyfus, G., Durand, G., Falourd, S., Fischer, H., Flückiger, J., Hansson, M., Huybrechts, P., Jugie, G., Johnsen, S., Jouzel, J., Kaufmann, P., Kipfstuhl, J., Lambert, F., Lipenkov, V., Littot, G., Longinelli, A., Lorrain, R., Maggi, V., Masson-Delmotte, V., Miller, H., Mulvaney, R., Oerlemans, J., Oerter, H., Orombelli, G., Parrenin, F., Peel, D., Petit, J.-R., Raynaud, D., Ritz, C., Ruth, U., Schwander, J., Siegenthaler, U., Souchez, R., Stauffer, B., Steffensen, J., Stenni, B., Stocker, T., Tabacco, I., Udisti, R., Van De Wal, R., Van Den Broeke, M., Weiss, J., Wilhelms, F., Winther, J.-G., Wolff, E., and Zucchelli, M. (2004). Eight glacial cycles from an Antarctic ice core. *Nature*, 429(6992):623–8.

- Balslev-Clausen, D. M. (2011). *Application of cavity ring down spectroscopy to isotopic bio- geo- & climate-sciences & the development of a mid-infrared CRDS analyzer for continuous measurements of N₂O isotopomers*. PhD thesis, University of Copenhagen.
- Beaumont, H., Hommes, N., Sayavedra-Soto, L., Arp, D., Arciero, D., Hooper, A., Westerhoff, H., and Van Spanning, R. (2002). Nitrite reductase of *Nitrosomonas europaea* is not essential for production of gaseous nitrogen oxides and confers tolerance to nitrite. *Journal of Bacteriology*, 184(9):2557–2560.
- Beaumont, H., Lens, S., Reijnders, W., Westerhoff, H., and Van Spanning, R. (2004). Expression of nitrite reductase in *Nitrosomonas europaea* involves NsrR, a novel nitrite-sensitive transcription repressor. *Molecular Microbiology*, 54(1):148–158.
- Belser, L. (1979). Population Ecology of Nitrifying Bacteria. *Annual review of Microbiology*, 33:309–333.
- Bender, M. L., Floch, G., Chappellaz, J., Suwa, M., Barnola, J. M., Blunier, T., Dreyfus, G., Jouzel, J., and Parrenin, F. (2006). Gas age-ice age differences and the chronology of the Vostok ice core, 0-100 ka. *Journal of Geophysical Research Atmospheres*, 111(21):1–10.
- Bergstrom, D. W., Tenuta, M., and Beauchamp, E. G. (1994). Increase in nitrous oxide production in soil induced by ammonium and organic carbon. *Biology and Fertility of Soils*, 18(1):1–6.
- Bremner, J. (1997). Sources of nitrous oxide in soils. *Nutrient Cycling in Agroecosystems*, 49:7–16.
- Brenninkmeijer, C. A. M. and Röckmann, T. (1999). Mass spectrometry of the intramolecular nitrogen isotope distribution of environmental nitrous oxide using fragment-ion analysis. *Rapid communications in mass spectrometry : RCM*, 13(20):2028–33.
- Brumback, B. a. and Rice, J. a. (1998). Smoothing spline models for the analysis of nested and crossed samples of curves. *Journal of the American Statistical Association*, 93(443):961–994.
- Cardenas, L. M., Chadwick, D., Scholefield, D., Fychan, R., Marley, C. L., Jones, R., Bol, R., Well, R., and Vallejo, a. (2007). The effect of diet manipulation on nitrous oxide and methane emissions from manure application to incubated grassland soils. *Atmospheric Environment*, 41(33):7096–7107.

- Casciotti, K., Böhlke, J., McIlvin, M., Mroczkowski, S., and Hannon, J. (2007). Oxygen isotopes in nitrite: Analysis, calibration, and equilibration. *Analytical Chemistry*, 79(6):2427–2436.
- Casciotti, K. L., Sigman, D. M., Hastings, M. G., Böhlke, J. K., and Hilkert, A. (2002). Measurement of the oxygen isotopic composition of nitrate in seawater and freshwater using the denitrifier method. *Analytical Chemistry*, 74(19):4905–4912.
- Chandran, K., Stein, L. Y., Klotz, M. G., and van Loosdrecht, M. C. M. (2011). Nitrous oxide production by lithotrophic ammonia-oxidizing bacteria and implications for engineered nitrogen-removal systems. *Biochemical Society transactions*, 39(6):1832–7.
- Christensen, S. and Bonde, G. J. (1985). Seasonal variation in numbers and activity of denitrifier bacteria in soil. Taxonomy and physiological groups among isolates. *Danish Journal of Plant and Soil Science*, 89:367–372.
- Christensen, S., Simkins, S., and Tiedje, J. (1990a). Spatial Variation in Denitrification: Dependency of Activity Centers on the Soil Environment. *Soil Science Society of America Journal*, 54:1608.
- Christensen, S., Simkins, S., and Tiedje, J. (1990b). Temporal patterns of soil denitrification: their stability and causes. *Soil Science Society of America Journal*, 54(6):1614–1618.
- Christensen, S. and Tiedje, J. M. (1988). Sub-parts-per-billion nitrate method: Use of an N₂O-producing denitrifier to convert NO₃⁻ or ¹⁵NO₃⁻ to N₂O. *Applied and environmental microbiology*, 54(6):1409–1413.
- Ciais, P., Sabine, C., Bala, B., Bopp, L., Brovkin, V., Canadell, J., Chhabra, A., DeFries, R., Galloway, J., Heimann, M., Jones, C., Le Quéré, C., Myneni, R., Piao, S., and Thornton, P. (2013). 6: Carbon and Other Biogeochemical Cycles. In *Carbon and Other Biogeochemical Cycles. In: Climate Change 2013: The Physical Science Basis. Contribution of Working Group I to the Fifth Assessment Report of the Intergovernmental Panel on Climate Change [Stocker, T.F., Qin, D., Plattner, G.-K., Tignor,, pages 465–570. Cambridge University Press, Cambridge, United Kingdom and New York, NY, USA.*
- Clough, T. J., Sherlock, R. R., and Rolston, D. E. (2005). A review of the movement and fate of N₂O in the subsoil. *Nutrient Cycling in Agroecosystems*, 72(1):3–11.

- Collman, J. P., Yang, Y., Dey, A., Decréau, R. A., Ghosh, S., Ohta, T., and Solomon, E. I. (2008). A functional nitric oxide reductase model. *Proceedings of the National Academy of Sciences of the United States of America*, 105(41):15660–5.
- Crutzen, P. (1972). SST's - A Threat to the Earth's Ozone Shield. *Ambio*, 1(2):41–51.
- Crutzen, P. (1974). Estimates of possible variations in total ozone due to natural causes and human activities. *Ambio*, 3(6):201–210.
- Dahl-Jensen, D. (2013). Eemian interglacial reconstructed from a Greenland folded ice core. *Nature*, 493(7433):489–94.
- Delmas, R. (1994). Ice records of the past environment. *Science of the Total Environment, The*, 143(1):17–30.
- Dore, J. E., Popp, B. N., Karl, D. M., and Sansone, F. J. (1998). A large source of atmospheric nitrous oxide from subtropical North Pacific surface waters. *Nature*, 396(November):63–66.
- Elberling, B., Christiansen, H. H., and Hansen, B. U. (2010). High nitrous oxide production from thawing permafrost. *Nature Geoscience*, 3(5):332–335.
- Elder, J. W. and Lal, R. (2008). Tillage effects on gaseous emissions from an intensively farmed organic soil in North Central Ohio. *Soil and Tillage Research*, 98(1):45–55.
- Elliot, M., Labeyrie, L., and Duplessy, J.-C. (2002). Changes in North Atlantic deep-water formation associated with the Dansgaard-Oeschger temperature oscillations (60-10ka). *Quaternary Science Reviews*, 21(10):1153–1165.
- Erler, D. V., Duncan, T. M., Murray, R., Maher, D. T., Santos, I. R., Gatland, J. R., Mangion, P., and Eyre, B. D. (2015). Applying cavity ring-down spectroscopy for the measurement of dissolved nitrous oxide concentrations and bulk nitrogen isotopic composition in aquatic systems : Correcting for interferences and field application. *Limnology and Oceanography*, 13:391–401.
- Firestone, M. K. and Davidson, E. A. (1989). Microbiological basis of NO and N₂O production and consumption in soil. *Exchange of Trace Gases between Terrestrial Ecosystems and the Atmosphere*, pages 7–21.
- Flessa, H., Wild, H., Klemisch, M., and Pfadenhauer, J. (1998). Nitrous oxide and methane fluxes from organic soils under agriculture. *European Journal of Soil Science*, 49(2):327–335.

- Flückiger, J., Blunier, T., Stauffer, B., Chappellaz, J., Spahni, R., Kawamura, K., Schwander, J., Stocker, T. F., and Dahl-Jensen, D. (2004). N₂O and CH₄ variations during the last glacial epoch: Insight into global processes. *Global Biogeochemical Cycles*, 18(1).
- Flückiger, J., Monnin, E., Stauffer, B., Schwander, J., Stocker, T. F., Chappellaz, J., Raynaud, D., and Barnola, J.-M. (2002). High-resolution Holocene N₂O ice core record and its relationship with CH₄ and CO₂. *Global Biogeochemical Cycles*, 16(1):1010.
- Forster, P., Ramaswamy, V., Artaxo, P., Berntsen, T., Betts, R., Fahey, D., Lean, J. H. J., Lowe, D., Myhre, G., Prinn, J. N. R., Raga, G., Schulz, M., and Dorland, R. V. (2007). Climate Change 2007: The Physical Science Basis. Contribution of Working Group I to the Fourth Assessment Report of the Intergovernmental Panel on Climate Change, chapter Changes in Atmospheric Constituents and in Radiative Forcing. *Cambridge University Press, Cambridge, United Kingdom and New York, NY, USA.*, pages 130–217.
- Goldstein, B. (2003). A modeling study of oceanic nitrous oxide during the Younger Dryas cold period. *Geophysical Research Letters*, 30(2):1–4.
- Groffman, P. M. (2012). Terrestrial denitrification: challenges and opportunities. *Ecological Processes*, 1:1–11.
- Gruber, N. and Galloway, J. (2008). An Earth-system perspective of the global nitrogen cycle. *Nature*, 451(7176):293–6.
- Hart, S. and Gunther, A. (1989). In Situ Estimates of Annual Net Nitrogen Mineralization and Nitrification in a Subarctic Watershed. *Oecologia*, 80(2):284–288.
- Hartmann, D., Klein Tank, A., Rusticucci, M., Alexander, L., Brönnimann, S., Charabi, Y., Dentener, F., Dlugokencky, E., Easterling, D., Kaplan, A., Soden, B., Thorne, P., Wild, M., and Zhai, P. (2013). 2013: Observations: Atmosphere and Surface. In: *Climate Change 2013: The Physical Science Basis. Contribution of Working Group I to the Fifth Assessment Report of the Intergovernmental Panel on Climate Change*. Cambridge University Press, Cambridge, United Kingdom and New York, NY, USA.
- Hedin, L., Vitousek, P. M., and Matson, P. A. (2003). Nutrient losses over four million years of tropical forest development. *Wiley*, 84(9):2231–2255.
- Heil, J., Wolf, B., Brüggemann, N., Emmenegger, L., Tuzson, B., Vereecken, H., and Mohn, J. (2014). Site-specific ¹⁵N isotopic signatures of abiotically produced N₂O. *Geochimica et Cosmochimica Acta*, 139:72–82.

- Hellerstein, M. K. and Neese, R. A. (1999). Mass isotopomer distribution analysis at eight years: theoretical, analytic, and experimental considerations. *American Journal of Physiology - Endocrinology and Metabolism*, 276.
- Hénault, C., Gossel, a., Mary, B., Roussel, M., and LéOnard, J. (2012). Nitrous Oxide Emission by Agricultural Soils: A Review of Spatial and Temporal Variability for Mitigation. *Pedosphere*, 22(4):426–433.
- Hendriks, J., Oubrie, A., Castresana, J., Urbani, A., Gemeinhardt, S., and Saraste, M. (2000). Nitric oxide reductases in bacteria. *Biochimica et biophysica acta*, 1459(2-3):266–273.
- Hino, T., Matsumoto, Y., Nagano, S., Sugimoto, H., Fukumori, Y., Murata, T., Iwata, S., and Shiro, Y. (2010). Structural Basis of Biological N₂O Generation by Bacterial Nitric Oxide Reductase. *Science*, 330(6011):1666–1670.
- Hobbie, S. and Gough, L. (2002). Foliar and soil nutrients in tundra on glacial landscapes of contrasting ages in northern Alaska. *Oecologia*, 131:453–462.
- Houlton, B., Sigman, D., and Hedin, L. (2006). Isotopic evidence for large gaseous nitrogen losses from tropical rainforests. *Proceedings of the National Academy of Sciences*, 103(23):8745–8750.
- Hu, H. W., Chen, D., and He, J. Z. (2015). Microbial regulation of terrestrial nitrous oxide formation: Understanding the biological pathways for prediction of emission rates. *FEMS Microbiology Reviews*, 39(5):729–749.
- Igarashi, N., Moriyama, H., Fujiwara, T., Fukumuri, Y., and Tanaka, N. (1997). The 2.8 Å structure of hydroxylamine oxidoreductase from a nitrifying chemoautotrophic bacterium, *Nitrosomonas europaea*. *Nature*, 4(4):276–284.
- IPCC (2013). *Climate Change 2013: The physical Science Basis. Contribution of Working group I to the Fifth Assessment Report of the Intergovernmental Panel on Climate Change*. [Stocker, T.F., Qin, D., Plattner, G.K., Tignor, M., Allen, S.K., Boschung, J., Nauels, A., Xia, Y., Bex, V., and Midgley, P.M. (eds.)] Cambridge University Press, Cambridge, United Kingdom and New York, NY, USA.
- Johnston, H. (1972). Newly recognized vital nitrogen cycle. *Proceedings of the National Academy of Sciences of the United States of America*, 69(9):2369–2372.

- Kaiser, J. (2002). *Stable isotope investigations of atmospheric nitrous oxide*. PhD thesis, Johannes Gutenberg-Universität Mainz.
- Kaiser, J. and Röckmann, T. (2008). Correction of mass spectrometric isotope ratio measurements for isobaric isotopologues of O₂, CO, CO₂, N₂O and SO₂. *Rapid communications in mass spectrometry : RCM*, 22:3997–4008.
- Kaiser, J., Röckmann, T., and Brenninkmeijer, C. A. M. (2002). Temperature dependence of isotope fractionation in N₂O photolysis. *Physical Chemistry Chemical Physics*, 4(18):4420–4430.
- Kaiser, J., Röckmann, T., Brenninkmeijer, C. A. M., and Crutzen, P. J. (2003). Wavelength dependence of isotope fractionation in N₂O photolysis. *Atmospheric . . .*, 2(2):303–313.
- Kameda, T., Shoji, H., Kawada, K., Watanabe, O., and Clausen, H. (1997). An empirical relation between overburden pressure and firn density. *Annals of Glaciology*, 20:87–94.
- Kameda, T., Shoji, H., Kawada, K., Watanabe, O., and Clausen, H. B. (1994). An empirical relation between overburden pressure and firn density. *Annals of Glaciology*, 20(2):87–94.
- Kato, T., Toyoda, S., Yoshida, N., Tang, Y., and Wada, E. (2013). Isotopomer and isotopologue signatures of N₂O produced in alpine ecosystems on the Qinghai-Tibetan Plateau. *Rapid Communications in Mass Spectrometry*, 27(13):1517–1526.
- Kielland, K., Olson, K., Ruess, R., and Boone, R. (2006). Contribution of winter processes to soil nitrogen flux in taiga forest ecosystems. *Biogeochemistry*, 81:349–360.
- Kim, K. R. and Craig, H. (1993). Nitrogen-15 and oxygen-18 characteristics of nitrous oxide: A global perspective. *Science*, 262.
- Koide, T., Saito, H., Shiota, T., Iwahana, G., Lopez, M., Maximov, T., Hasegawa, S., and Hatano, R. (2010). Effects of changes in the soil environment associated with heavy precipitation on soil greenhouse gas fluxes in a Siberian larch forest near Yakutsk. *Soil Science and Plant Nutrition*, 56:645–662.
- Köster, J. R., Cárdenas, L., Senbayram, M., Bol, R., Well, R., Butler, M., Mühling, K. H., and Dittert, K. (2011). Rapid shift from denitrification to nitrification in soil after biogas residue application as indicated by nitrous oxide isotopomers. *Soil Biology and Biochemistry*, 43(8):1671–1677.

- Köster, J. R., Cárdenas, L. M., Bol, R., Lewicka-Szczebak, D., Senbayram, M., Well, R., Gieseemann, A., and Dittert, K. (2015). Anaerobic digestates lower N₂O emissions compared to cattle slurry by affecting rate and product stoichiometry of denitrification - An N₂O isotopomer case study. *Soil Biology and Biochemistry*, 84:65–74.
- Köster, J. R., Well, R., Dittert, K., Gieseemann, A., Lewicka-Szczebak, D., Mühling, K. H., Herrmann, A., Lammel, J., and Senbayram, M. (2013a). Soil denitrification potential and its influence on N₂O reduction and N₂O isotopomer ratios. *Rapid Communications in Mass Spectrometry*, 27(21):2363–2373.
- Köster, J. R., Well, R., Tuzson, B., Bol, R., Dittert, K., Gieseemann, A., Emmenegger, L., Manninen, A., Cárdenas, L., and Mohn, J. (2013b). Novel laser spectroscopic technique for continuous analysis of N₂O isotopomers - Application and intercomparison with isotope ratio mass spectrometry. *Rapid Communications in Mass Spectrometry*, 27(1):216–222.
- Langway Jr., C., Shoji, H., Mitani, A., and Clausen, H. (1993). Transformation process observations of polar firn to ice. *Annals of Glaciology*, 18:493–495.
- Leuenberger, M., Borella, S., Stocker, T., Saurer, M., Siegwolf, R., Schweingruber, F., and Matyssek, R. (1998). *Stable isotopes in tree rings as climate and stress indicators*. vdf Hochschulverlag AG an der ETH Zürich.
- Lewicka-Szczebak, D., Well, R., Bol, R., Gregory, A., Matthews, G., Misselbrook, T., Whalley, W., and Cardenas, L. (2015). Isotope fractionation factors controlling isotopocule signatures of soil-emitted N₂O produced by denitrification processes of various rates. *Rapid Communications in Mass Spectrometry*, 29(3):269–282.
- Lewicka-Szczebak, D., Well, R., Köster, J. R., Fuß, R., Senbayram, M., Dittert, K., and Flessa, H. (2014). Experimental determinations of isotopic fractionation factors associated with N₂O production and reduction during denitrification in soils. *Geochimica et Cosmochimica Acta*, 134:55–73.
- Limpens, J., Heijmans, M., and Berendse, F. (2006). The Nitrogen Cycle in Boreal Peatlands. In Wieder, R. and Vitt, D., editors, *Boreal Peatland Ecosystems*, volume 188, pages 195–230. Springer - Verlag Berlin Heidelberg.
- Loulergue, L., Parrenin, F., Blunier, T., Barnola, J.-M., Spahni, R., Schilt, a., Raisbeck, G., and Chappellaz, J. (2007). New constraints on the gas age-ice age difference along the EPICA ice cores, 0-50 kyr. *Climate of the Past*, 3:527–540.

- Loulergue, L., Schilt, A., Spahni, R., Masson-Delmotte, V., Blunier, T., Lemieux, B., Barnola, J.-M., Raynaud, D., Stocker, T. F., and Chappellaz, J. (2008). Orbital and millennial-scale features of atmospheric CH₄ over the past 800,000 years. *Nature*, 453(7193):383–386.
- Lüthi, D., Le Floch, M., Bereiter, B., Blunier, T., Barnola, J.-M., Siegenthaler, U., Raynaud, D., Jouzel, J., Fischer, H., Kawamura, K., and Stocker, T. F. (2008). High-resolution carbon dioxide concentration record 650,000–800,000 years before present. *Nature*, 453(7193):379–382.
- MacFarling Meure, C., Etheridge, D., Trudinger, C., Steele, P., Langenfelds, R., Van Ommen, T., Smith, a., and Elkins, J. (2006). Law Dome CO₂, CH₄ and N₂O ice core records extended to 2000 years BP. *Geophysical Research Letters*, 33(14):2000–2003.
- Maljanen, M., Komulainen, V. M., Hytönen, J., Martikainen, P. J., and Laine, J. (2004). Carbon dioxide, nitrous oxide and methane dynamics in boreal organic agricultural soils with different soil characteristics. *Soil Biology and Biochemistry*, 36(11):1801–1808.
- Mariotti, A., Germon, J. C., Hubert, P., Kaiser, P., Letolle, R., Tardieux, A., and Tardieux, P. (1981). Experimental determination of nitrogen kinetic isotope fractionation: some principles; illustration for the denitrification and nitrification processes. *Plant and soil*, 430(1981):413–430.
- Mariotti, A., Germon, J. C., and Leclerc, A. (1982). Nitrogen isotope fractionation associated with the NO₂⁻ to N₂O step of denitrification in soils. *Canadian journal of soil science*, 62(2):227–241.
- Marushchak, M. E., Pitkämäki, a., Koponen, H., Biasi, C., Seppälä, M., and Martikainen, P. J. (2011). Hot spots for nitrous oxide emissions found in different types of permafrost peatlands. *Global Change Biology*, 17(8):2601–2614.
- Mayewski, P. a., Meeker, L. D., Twickler, M. S., Lyons, W. B., and Prentice, M. (1997). Major features and forcing of high latitude northern hemisphere atmospheric circulation using a 110,000 year long glaciochemical series. *Journal of Geophysical Research*, 102(C12):26,345–26,366.
- McLinden, C., Prather, M., and Johnson, M. (2003). Global modeling of the isotopic analogues of N₂O: Stratospheric distributions, budgets, and the O-17-O-18 mass-independent anomaly. *Journal of Geophysical Research-atmospheres*, 108(D8):4233.

- Menyailo, O. V. and Hungate, B. A. (2006). Stable isotope discrimination during soil denitrification: Production and consumption of nitrous oxide. *Global Biogeochemical Cycles*, 20(3):n/a–n/a.
- Mohn, J., Guggenheim, C., Tuzson, B., Vollmer, M. K., Toyoda, S., Yoshida, N., and Emmenegger, L. (2010). A liquid nitrogen-free preconcentration unit for measurements of ambient N₂O isotopomers by QCLAS. *Atmospheric Measurement Techniques*, 3(3):609–618.
- Mohn, J., Tuzson, B., Manninen, A., Yoshida, N., Toyoda, S., Brand, W. a., and Emmenegger, L. (2012). Site selective real-time measurements of atmospheric N₂O isotopomers by laser spectroscopy. *Atmospheric Measurement Techniques*, 5(7):1601–1609.
- Mohn, J., Wolf, B., Toyoda, S., Lin, C. T., Liang, M. C., Brüggemann, N., Wissel, H., Steiker, A. E., Dyckmans, J., Szewc, L., Ostrom, N. E., Casciotti, K. L., Forbes, M., Giesemann, A., Well, R., Doucett, R. R., Yarnes, C. T., Ridley, A. R., Kaiser, J., and Yoshida, N. (2014). Interlaboratory assessment of nitrous oxide isotopomer analysis by isotope ratio mass spectrometry and laser spectroscopy: Current status and perspectives. *Rapid Communications in Mass Spectrometry*, 28(18):1995–2007.
- Montzka, S. a., Dlugokencky, E. J., and Butler, J. H. (2011). Non-CO₂ greenhouse gases and climate change. *Nature*, 476(7358):43–50.
- Mosier, A., Kroeze, C., and Nevison, C. (1998). Closing the global N₂O budget: nitrous oxide emissions through the agricultural nitrogen cycle. *Nutrient Cycling in Agroecosystems*, 52(2-3):225–248.
- Nevison, C., Weiss, R., and Erickson III, D. (1995). Global oceanic emissions of nitrous oxide. *Journal of Geophysical Research*, 100(8):15809 – 15820.
- NOAA (2016). https://www.esrl.noaa.gov/gmd/hats/insitu/cats/cats_conc.html.
- Nordin, A., Schmidt, I., and Shaver, G. (2004). Nitrogen uptake by arctic soil microbes and plants in relation to soil nitrogen supply. *Ecology*, 85(4):955–962.
- Nykanen, H., Alm, J., Lang, K., Silvola, J., and Martikainen, P. (2010). Emissions of CH₄, N₂O and CO₂ from a Virgin Fen and a Fen Drained for Grassland in Finland
 Author (s): Hannu Nykanen , Jukka Alm , Kristiina Lang , Jouko Silvola , Pertti J . Martikainen Source : Journal of Biogeography , Vol . 22 , No . 2 / 3 , Terres.
Interactions, 22(2):351–357.

- Olivier, J. G. J., Bouwman, A. F., Van der Hoek, K. W., and Berdowski, J. J. M. (1998). Global air emission inventories for anthropogenic sources of NO_x, NH₃, and N₂O in 1990. *Environmental Pollution*, 102:135–148.
- Opdyke, M. R., Ostrom, N. E., and Ostrom, P. H. (2009). Evidence for the predominance of denitrification as a source of N₂O in temperate agricultural soils based on isotopologue measurements. *Global Biogeochemical Cycles*, 23(4):1–10.
- Ostrom, N. E. and Ostrom, P. H. (2011). The isotopomers of Nitrous oxide: Analytical considerations and application to resolution of microbial production pathways. In Baskaran, M., editor, *Handbook of Environmental Isotope Geochemistry*, pages 453–476. Springer Berlin Heidelberg, Berlin, Heidelberg.
- Ostrom, N. E., Piit, A., Sutka, R., Ostrom, P. H., Grandy, a. S., Huizinga, K. M., and Robertson, G. P. (2007a). Isotopologue effects during N₂O reduction in soils and in pure cultures of denitrifiers. *Journal of Geophysical Research: Biogeosciences*, 112(2):1–12.
- Ostrom, N. E., Pitt, A., Sutka, R., Ostrom, P. H., Grandy, A. S., Huizinga, K. M., and Robertson, G. P. (2007b). Isotopologue effects during N₂O reduction in soils and in pure cultures of denitrifiers. *Journal of Geophysical Research*, 112(G2):G02005.
- Ostrom, N. E., Sutka, R., Ostrom, P. H., Grandy, a. S., Huizinga, K. M., Gandhi, H., von Fischer, J. C., and Robertson, G. P. (2010). Isotopologue data reveal bacterial denitrification as the primary source of N₂O during a high flux event following cultivation of a native temperate grassland. *Soil Biology and Biochemistry*, 42(3):499–506.
- Otte, S., Schalk, J., Kuenen, J. G., and Jetten, M. S. M. (1999). Hydroxylamine oxidation and subsequent nitrous oxide production by the heterotrophic ammonia oxidizer *Alcaligenes faecalis*. *Applied Microbiology and Biotechnology*, 51(2):255–261.
- Park, S., Croteau, P., Boering, K. a., Etheridge, D. M., Ferretti, D., Fraser, P. J., Kim, K.-R., Krummel, P. B., Langenfelds, R. L., van Ommen, T. D., Steele, L. P., and Trudinger, C. M. (2012). Trends and seasonal cycles in the isotopic composition of nitrous oxide since 1940. *Nature Geoscience*, 5(4):261–265.
- Park, S., Pérez, T., Boering, K. A., Trumbore, S. E., Gil, J., Marquina, S., and Tyler, S. C. (2011). Can N₂O stable isotopes and isotopomers be useful tools to characterize sources and microbial pathways of N₂O production and consumption in tropical soils? *Global Biogeochemical Cycles*, 25(1):GB1001.

- Parkin, T. B. (1987). Soil microsites as a source of denitrification variability. *Soil Science Society of America Journal*, 51:1194–1199.
- Peng, L., Ni, B., Erler, D., Ye, L., and Yuan, Z. (2014). The effect of dissolved oxygen on N₂O production by ammonia-oxidizing bacteria in an enriched nitrifying sludge. *Water Research*, 66:12–21.
- Pérez, T., Trumbore, S. C., Tyler, S. C., Davidson, E. A., Keller, M., and De Camargo, P. B. (2000). Isotopic variability of N₂O emissions from tropical forest soils. *Global Biogeochemical Cycles*, 14(2):525–535.
- Perez, T., Trumbore, S. E., Tyler, S. C., Matson, P. A., Ortiz-Monasterio, I., Rahn, T., and Griffith, D. W. T. (2001). Identifying the agricultural imprint on the global N₂O budget using stable isotopes. *Journal of Geophysical Research*, 106(D9):9869–9878.
- Petersen, S. O., Henriksen, K., and Blackburn, T. H. (1991). Coupled nitrification-denitrification associated with liquid manure in a gel-stabilized model system. *Biology and Fertility of Soils*, 12(1):19–27.
- Popp, B. N., Westley, M. B., Toyoda, S., Miwa, T., Dore, J. E., Yoshida, N., Rust, T. M., Sansone, F. J., Russ, M. E., Ostrom, N. E., and Ostrom, P. H. (2002). Nitrogen and oxygen isotopomeric constraints on the origins and sea-to-air flux of N₂O in the oligotrophic subtropical North Pacific gyre. *Global Biogeochemical Cycles*, 16(4):12–12–10.
- Rasmussen, S. O., Abbott, P. M., Blunier, T., Bourne, a. J., Brook, E., Buchardt, S. L., Buizert, C., Chappellaz, J., Clausen, H. B., Cook, E., Dahl-Jensen, D., Davies, S. M., Guillevic, M., Kipfstuhl, S., Laepple, T., Seierstad, I. K., Severinghaus, J. P., Steffensen, J. P., Stowasser, C., Svensson, a., Vallelonga, P., Vinther, B. M., Wilhelms, F., and Winstrup, M. (2013). A first chronology for the north greenland eemian ice drilling (NEEM) ice core. *Climate of the Past*, 9(6):2713–2730.
- Ravishankara, A., Daniel, J., and Portmann, R. (2009). Nitrous oxide (N₂O): The dominant ozone-depleting substance emitted in the 21st Century. *Science*, 326(2):123–125.
- Reeh, N., Fisher, D. a., Koerner, R. M., and Clausen, H. B. (2005). An empirical firn-densification model comprising ice lenses. *Annals of Glaciology*, 42(August 2005):101–106.

- Reutenauer, C. (2016). *Measuring the triple O₂ isotopic composition of air trapped in ice cores and quantifying the causes of $\delta^{18}\text{O}_{\text{atm}}$ millennial scale variations*. PhD thesis, University of Copenhagen, Denmark.
- Ritchie, G. a. F. and Nicholas, D. J. (1972). Identification of the sources of nitrous oxide produced by oxidative and reductive processes in *Nitrosomonas europaea*. *The Biochemical journal*, 126(5):1181–1191.
- Rochette, P., Tremblay, N., Fallon, E., Angers, D. a., Chantigny, M. H., MacDonald, J. D., Bertrand, N., and Parent, L. E. (2010). N₂O emissions from an irrigated and non-irrigated organic soil in eastern Canada as influenced by N fertilizer addition. *European Journal of Soil Science*, 61(2):186–196.
- Röckmann, T., Kaiser, J., Brenninkmeijer, C., Crowley, J., Borchers, R., Brand, W., and Crutzen, P. (2001). Isotopic enrichment of nitrous oxide ($^{15}\text{N}^{14}\text{NO}$, $^{14}\text{N}^{15}\text{NO}$, $^{14}\text{N}^{14}\text{N}^{18}\text{O}$) in the stratosphere and in the laboratory. *Journal of Geophysical Research*, 106(D10):10403–10410.
- Röckmann, T., Kaiser, J., Brenninkmeijer, C. a. M., and Brand, W. a. (2003). Gas chromatography/isotope-ratio mass spectrometry method for high-precision position-dependent ^{15}N and ^{18}O measurements of atmospheric nitrous oxide. *Rapid Communications in Mass Spectrometry*, 17(16):1897–1908.
- Rosen, J. L. (2014). *Augmenting and Interpreting Ice Core Gas Records*. PhD thesis, Oregon State University.
- Rousk, K., Jones, D., and DeLuca, T. (2014). Moss-nitrogen input to boreal forest soils: Tracking ^{15}N in a field experiment. *Soil Biology and Biochemistry*, 72:100–104.
- Sapart, C. J., Van Der Veen, C., Vigano, I., Brass, M., Van De Wal, R. S. W., Bock, M., Fischer, H., Sowers, T., Buizert, C., Sperlich, P., Blunier, T., Behrens, M., Schmitt, J., Seth, B., and Röckmann, T. (2011). Simultaneous stable isotope analysis of methane and nitrous oxide on ice core samples. *Atmospheric Measurement Techniques*, 4(12):2607–2618.
- Schilt, A., Baumgartner, M., Blunier, T., Schwander, J., Spahni, R., Fischer, H., and Stocker, T. F. (2009). Glacial-interglacial and millennial-scale variations in the atmospheric nitrous oxide concentration during the last 800,000 years. *Quaternary Science Reviews*, 29(1-2):182–192.

- Schilt, A., Baumgartner, M., Eicher, O., Chappellaz, J., Schwander, J., Fischer, H., and Stocker, T. F. (2013). The response of atmospheric nitrous oxide to climate variations during the last glacial period. *Geophysical Research Letters*, 40(9):1888–1893.
- Schilt, A., Baumgartner, M., Schwander, J., Buiron, D., Capron, E., Chappellaz, J., Loulergue, L., Schüpbach, S., Spahni, R., Fischer, H., and Stocker, T. F. (2010). Atmospheric nitrous oxide during the last 140.000years. *Earth and Planetary Science Letters*, 300(1-2):33–43.
- Schilt, A., Brook, E., Bauska, T., Baggenstos, D., Fischer, H., Joos, F., Petrenko, V., Schaefer, H., Schmitt, J., Severinghaus, J., Spahni, R., and Stocker, T. (2014). Isotopic constraints on marine and terrestrial N₂O emissions during the last deglaciation. *Nature*, 516(7530):234–237.
- Schimel, J. P., Firestone, M. K., and Killham, K. S. (1984). Identification of heterotrophic nitrification in a Sierran forest soil. *Applied and Environmental Microbiology*, 48(4):802–806.
- Schmittner, A. and Galbraith, E. D. (2008). Glacial greenhouse-gas fluctuations controlled by ocean circulation changes. *Nature*, 456(7220):373–376.
- Schothorst, C. J. (1977). Subsidence of low moor peat soils in the western Netherlands. *Geoderma*, 17:265–291.
- Schreiber, F., Wunderlin, P., Udert, K. M., and Wells, G. F. (2012). Nitric oxide and nitrous oxide turnover in natural and engineered microbial communities: Biological pathways, chemical reactions, and novel technologies. *Frontiers in Microbiology*, 3(OCT):1–24.
- Shackleton, N. J., Hall, M. a., and Vincent, E. (2000). Phase relationships between millennial-scale events 64,000- 24,000 years ago. *Paleoceanography*, 15(6):565–569.
- Shaw, L., Nicol, G., Smith, Z., Fear, J., Prosser, J., and Baggs, E. (2006). *Nitrosospira* spp. can produce nitrous oxide via a nitrifier denitrification pathway. *Environmental Microbiology*, 8(2):214–222.
- Sigman, D., Casciotti, K., Andreani, M., Barford, C., Galanter, M., and Böhlke, J. (2001). A bacterial method for the nitrogen isotopic analysis of nitrate in seawater and freshwater. *Analytical chemistry*, 73(17):4145–53.
- Smemo, K. a., Ostrom, N. E., Opdyke, M. R., Ostrom, P. H., Bohm, S., and Robertson, G. P. (2011). Improving process-based estimates of N₂O emissions from soil using temporally

- extensive chamber techniques and stable isotopes. *Nutrient Cycling in Agroecosystems*, 91(2):145–154.
- Solheim, B., Zielke, M., Bjerke, J., and Rozema, J. (2006). Effects of enhanced UV-B radiation on nitrogen fixation in arctic ecosystems. *Plant Ecology*, 182:109–118.
- Stark, J. and Hart, S. (1997). High rates of nitrification and nitrate turnover in undisturbed coniferous forests. *Nature*, 385:61–64.
- Stehfest, E. and Bouwman, L. (2006). N₂O and NO emission from agricultural fields and soils under natural vegetation: Summarizing available measurement data and modeling of global annual emissions. *Nutrient Cycling in Agroecosystems*, 74(3):207–228.
- Stein, L. Y. (2011). Surveying N₂O-producing pathways in bacteria. *Methods in Enzymology*, 486(C):131–152.
- Stein, L. Y. and Yung, Y. L. (2003). Production, isotopic composition, and atmospheric fate of biologically produced nitrous oxide. *Annual Review of Earth and Planetary Sciences*, 31(1):329–356.
- Stuart Chapin III, F., Matson, P. A., and Mooney, H. A. (2002). *Principles of terrestrial ecosystem ecology*. Springer-Verlag, New York.
- Sutka, R. L. and Ostrom, N. E. (2006). Distinguishing nitrous oxide production from nitrification and denitrification on the basis of isotopomer abundances. *Applied and environmental microbiology*, 72(1):638–644.
- Sutka, R. L., Ostrom, N. E., Ostrom, P. H., Gandhi, H., and Breznak, J. A. (2003). Nitrogen isotopomer site preference of N₂O produced by *Nitrosomonas europaea* and *Methylococcus capsulatus* Bath. *Rapid communications in mass spectrometry : RCM*, 17(7):738–45.
- Sutka, R. L., Ostrom, N. E., Ostrom, P. H., Gandhi, H., and Breznak, J. A. (2004). Nitrogen isotopomer site preference of N₂O produced by *Nitrosomonas europaea* and *Methylococcus capsulatus* Bath. *Rapid Communications in Mass Spectrometry*, 18(12):1411–1412.
- Syakila, A. and Kroeze, C. (2011). The global nitrous oxide budget revisited. *Greenhouse Gas Measurement and Management*, 1(1):17–26.

- Syakila, A., Kroeze, C., and Slomp, C. (2010). Neglecting sinks for N₂O at the earth's surface: does it matter? *Journal of Integrative Environmental Sciences*, 7(S1):79–87.
- Terry, R. E. (1980). Nitrogen Mineralization in Florida Histosols. *Soil Science Society of America Journal*, 44(4):747–750.
- Tilsner, J., Wrage, N., Lauf, J., and Gebauer, G. (2003). Emission of gaseous nitrogen oxides from an extensively managed grassland in NE Bavaria, Germany. II. Stable isotope natural abundance of N₂O. *Biogeochemistry*, 63(3):249–267.
- Tosha, T. and Shiro, Y. (2013). Crystal structures of nitric oxide reductases provide key insights into functional conversion of respiratory enzymes. *IUBMB Life*, 65(3):217–226.
- Toyoda, S., Mutobe, H., Yamagishi, H., Yoshida, N., and Tanji, Y. (2005). Fractionation of N₂O isotopomers during production by denitrifier. *Soil Biology and Biochemistry*, 37(8):1535–1545.
- Toyoda, S., Yamamoto, S., and Arai, S. (2008). Isotopomeric characterization of N₂O produced, consumed, and emitted by automobiles. *Rapid Communications in Mass Spectrometry*, 22:603–612.
- Toyoda, S. and Yoshida, N. (1999). Determination of nitrogen isotopomers of nitrous oxide on a modified isotope ratio mass spectrometer. *Analytical Chemistry*, 71(20):4711–4718.
- Toyoda, S., Yoshida, N., Miwa, T., Matsui, Y., Yamagishi, H., and Tsunogai, U. (2002). Production mechanism and global budget of N₂O inferred from its isotopomers in the western North Pacific. *Geophysical Research Letters*, 29(3):5–8.
- Van Beek, C. L., Hummelink, E. W. J., Velthof, G. L., and Oenema, O. (2004). Denitrification rates in relation to groundwater level in a peat soil under grassland. *Biology and Fertility of Soils*, 39(5):329–336.
- van Beek, C. L., Pleijter, M., Jacobs, C. M. J., Velthof, G. L., van Groenigen, J. W., and Kuikman, P. J. (2010). Emissions of N₂O from fertilized and grazed grassland on organic soil in relation to groundwater level. *Nutrient Cycling in Agroecosystems*, 86(3):331–340.
- van Beek, C. L., Pleijter, M., and Kuikman, P. J. (2011). Nitrous oxide emissions from fertilized and unfertilized grasslands on peat soil. *Nutrient Cycling in Agroecosystems*, 89(3):453–461.

- Veres, D., Bazin, L., Landais, a., Toyé Mahamadou Kele, H., Lemieux-Dudon, B., Parrenin, F., Martinerie, P., Blayo, E., Blunier, T., Capron, E., Chappellaz, J., Rasmussen, S. O., Severi, M., Svensson, a., Vinther, B., and Wolff, E. W. (2013). The Antarctic ice core chronology (AICC2012): An optimized multi-parameter and multi-site dating approach for the last 120 thousand years. *Climate of the Past*, 9(4):1733–1748.
- Vitousek, P., Menge, D., Reed, S., and Cleveland, C. (2013). Biological nitrogen fixation: rates, patterns and ecological controls in terrestrial ecosystems. *Philosophical Transactions of the Royal Society B-Biological Sciences*, 368.
- Von Arnold, K., Nilsson, M., Hå nell, B., Weslien, P., and Klemetsson, L. (2005). Fluxes of CO₂, CH₄ and N₂O from drained organic soils in deciduous forests. *Soil Biology and Biochemistry*, 37(6):1059–1071.
- Waechter, H., Mohn, J., Tuzson, B., Emmenegger, L., and Sigrist, M. W. (2008). Determination of N₂O isotopomers with quantum cascade laser based absorption spectroscopy. *Optics express*, 16(12):9239–9244.
- Weintraub, S., Taylor, P., Porder, S., Cleveland, C., Asner, G., and Townsend, A. (2015). Topographic controls on soil nitrogen availability in a lowland tropical forest. *Ecology*, 96(6):1561–1574.
- Well, R. and Flessa, H. (2008). Isotope fractionation factors of N₂O diffusion. *Rapid Communications in Mass Spectrometry*, 22:2621–2628.
- Well, R. and Flessa, H. (2009a). Isotopologue enrichment factors of N₂O reduction in soils. *Rapid Communications in Mass Spectrometry*, pages 2996–3002.
- Well, R. and Flessa, H. (2009b). Isotopologue signatures of N₂O produced by denitrification in soils. *Journal of Geophysical Research*, 114(G2):G02020.
- Wingen, L. M. and Finlayson-Pitts, B. J. (1998). An upper limit on the production of N₂O from the reaction of O(1D) With CO₂ in the presence of N₂. *Geophysical research letters*, 25(4):517–520.
- Wolf, B., Merbold, L., Decock, C., Tuzson, B., Harris, E., Six, J., Emmenegger, L., and Mohn, J. (2015). First on-line isotopic characterization of N₂O above intensively managed grassland. *Biogeosciences*, 12(8):2517–2531.

- Wrage, N., Lauf, J., del Prado, a., Pinto, M., Pietrzak, S., Yamulki, S., Oenema, O., and Gebauer, G. (2004). Distinguishing sources of N₂O in European grasslands by stable isotope analysis. *Rapid Communications in Mass Spectrometry*, 18(11):1201–1207.
- Wrage, N., Velthof, G. L., Beusichem, M. L. V., and Oenema, O. (2001). Role of nitrifier er denitrification in the production of nitrous oxide. *Soil Biology and Biochemistry*, 33:1723–1732.
- Wu, D., Köster, J. R., Cárdenas, L. M., Brüggemann, N., Lewicka-Szczebak, D., and Bol, R. (2016). N₂O source partitioning in soils using ¹⁵N site preference values corrected for the N₂O reduction effect. *Rapid Communications in Mass Spectrometry*, 30(5):620–626.
- Wunderlin, P., Lehmann, M., Siegrist, H., Tuzson, B., Joss, A., Emmenegger, L., and Mohn, J. (2013). Isotope Signatures of N₂O in a Mixed Microbial Population System: Constraints on N₂O Producing Pathways in Wastewater Treatment. *Environmental Science & Technology*, 47:1339–1348.
- Wunderlin, P., Mohn, J., Joss, A., Emmenegger, L., and Siegrist, H. (2012). Mechanisms of N₂O production in biological wastewater treatment under nitrifying and denitrifying conditions. *Water Research*, 46(4):1027–1037.
- Yamamoto, A., Uchida, Y., Akiyama, H., and Nakajima, Y. (2014). Continuous and unattended measurements of the site preference of nitrous oxide emitted from an agricultural soil using quantum cascade laser spectrometry with intercomparison with isotope ratio mass spectrometry. *Rapid Communications in Mass Spectrometry*, 28(13):1444–1452.
- Yano, M., Toyoda, S., Tokida, T., Hayashi, K., Hasegawa, T., Makabe, A., Koba, K., and Yoshida, N. (2014). Isotopomer analysis of production, consumption and soil-to-atmosphere emission processes of N₂O at the beginning of paddy field irrigation. *Soil Biology and Biochemistry*, 70:66–78.
- Yano, Y., Shaver, G., Rastetter, E., Giblin, A., and Laundre, J. (2013). Nitrogen dynamics in arctic tundra soils of varying age: Differential responses to fertilization and warming. *Oecologia*, 173:1575–1586.
- Ye, R., Toro-suarezb, I., Tiedje, J., and Averill, B. (1991). H₂18O Isotope Exchange Studies on the Mechanism of Reduction of Nitric Oxide and Nitrite to Nitrous Oxide by Denitrifying Bacteria. *The journal of biological chemistry*, 266(20):12848–12851.

- Yoshida, N. and Toyoda, S. (2000). Constraining the atmospheric N₂O budget from intramolecular site preference in N₂O isotopomers. *Nature*, 405(6784):330–4.
- Yung, Y. and Miller, C. (1997). Isotopic Fractionation of Stratospheric Nitrous Oxide. *Science*, 278(5344):1778–1780.
- Zhang, J., Müller, C., and Cai, Z. (2015). Heterotrophic nitrification of organic N and its contribution to nitrous oxide emissions in soils. *Soil Biology and Biochemistry*, 84:199–209.
- Zhang, W., Li, Y., Xu, C., Li, Q., Lin, W., Smith, P. M., Edenhofer, O., Montzka, S. a., Dlugokencky, E. J., Butler, J. H., Prinn, R., Smith, P., Metz, B., Lam, S. K., Well, R., Flessa, H., Lu, X., Ju, X. T., Römheld, V., Hu, H. W., Zhu, X., Burger, M., Doane, T. a., Horwath, W. R., Zhang, L. M., Baggs, E. M., Bouwman, a. F., Boumans, L. J. M., Batjes, N. H., Wrage, N., Velthof, G. L., Oenema, O., Laanbroek, H. J., Bateman, E. J., Baggs, E. M., Wunderlin, P., Palmer, K., Horn, M. a., Malone, J. P., Stevens, R. J., Laughlin, R. J., Mulvaney, R. L., Sparks, D. L., Park, S., Pérez, T., Ueda, S., Westley, M. B., Yamagishi, H., Popp, B. N., Yoshida, N., Ostrom, N. E., Decock, C., Six, J., Maeda, K., Sutka, R. L., Ostrom, N. E., Ostrom, P. H., Gandhi, H., Breznak, J. a., Zou, Y., Cai, Y. J., Ding, W. X., Zhang, X. L., Yu, H. Y., Wang, L. F., Wrage, N., Velth, G. L., Beusichem, M. L. V., Oenema, O., Cookson, W. R., Müller, C., O'Brien, P. a., Murphy, D. V., Grierson, P. F., Kool, D. M., Dolfing, J., Wrage, N., Groenigen, J. W. V., Park, S., Giblin, a. E., Jones, C. M., Pérez, T., Flanagan, L. B., Ehleringer, J. R., Pataki, D. E., Kool, D. M., Wrage, N., Oenema, O., Dolfing, J., Groenigen, J. W. V., Casciotti, K. L., Sigman, D. M., Hastings, M. G., Böhlke, J. K., Hikert, A., Szukics, U., Koehler, B., Bollmann, A., and Conrad, R. (2016). Isotope signatures of N₂O emitted from vegetable soil: Ammonia oxidation drives N₂O production in NH₄⁺-fertilized soil of North China. *Scientific Reports*, 6(April):29257.
- Zou, Y., Hirono, Y., Yanai, Y., Hattori, S., Toyoda, S., and Yoshida, N. (2014). Isotopomer analysis of nitrous oxide accumulated in soil cultivated with tea (*Camellia sinensis*) in Shizuoka, central Japan. *Soil Biology and Biochemistry*, 77:276–291.